Université de Montréal

Probing the Relationship Between Solutions, Gels, and Crystals by Using Salts of Bile Acids

Par

Puzhen Li

Département de chimie, Faculté des arts et des sciences

Thèse présentée en vue de l'obtention du grade de Philosophiae Doctor (Ph. D.) en chimie

Décembre, 2021

Université de Montréal

Département de chimie, Faculté des arts et des sciences

Cette thèse intitulée

Probing the Relationship Between Solutions, Gels, and Crystals by Using Salts of Bile Acids

Présente par

Puzhen Li

A été évaluée par un jury composé des personnes suivantes

Suzanne Giasson
Président-rapporteur

Julian X. X. Zhu
Directeur de recherche

James D. Wuest
Codirecteur

Christian Pellerin
Membre du jury

Cornelia Bohne
Examinatrice externe

Résumé

La gélification est un phénomène courant dans lequel une grande quantité de solvant est immobilisée dans un réseau constitué de relativement petites quantités de substrat. Avec des propriétés à la fois solides et liquides, un gel est un état unique. L'étude des propriétés et du mécanisme de la gélification attire l'attention des chercheurs du monde entier. Cependant, de nombreuses questions restent en suspens, telles que le processus d'auto-assemblage et les interactions moléculaires dans le système de gel, la relation entre les solutions, les gels et les cristaux et l'organisation moléculaire dans le réseau de gel. L'exploration de ces questions fournira des connaissances sur le mécanisme de gélification et contribuera à la conception et à la fabrication de nouveaux gels aux applications diverses.

Cette thèse décrit notre étude des gels et de leur relation avec les solutions et les cristaux à l'aide de sels biliaires, qui sont des molécules amphiphiles naturelles abondantes. La rigidité de la partie stéroïde et l'hydrophobie variable des sels biliaires facilitent l'étude du processus d'auto-assemblage. La recherche est présentée à travers trois articles publiés ou soumis au cours de mon programme de doctorat.

Le premier article explore les interactions moléculaires qui se produisent dans la formation d'hydrogels moléculaires fabriqués à partir de mélanges de désoxycholate de sodium et d'acide formique. La spectroscopie de résonance magnétique nucléaire fournit de nouvelles informations sur la transition gel-sol au niveau moléculaire, l'interaction entre les espèces libres/gélifiées et l'interaction des régions hydrophobes des sels biliaires avec le réseau de gel.

Le deuxième article résume notre exploration de la relation entre les gels et les cristaux, en particulier la façon dont les composants moléculaires sont organisés. Les sels d'ammonium d'acide lithocholique produisent différents modèles d'auto-assemblage, tels que des gels, des fibres et des cristaux, avec divers anions d'ammonium. L'organisation moléculaire de l’acide lithocholique dans différentes conditions est remarquablement cohérente, indiquant qu'il existe une relation intime entre la gélification et la cristallisation dans ce système. Les résultats ont également mis en lumière la question de longue date de l'agencement des molécules dans les fibres de gel.

Le troisième article décrit notre étude systématique de la gélification et de la cristallisation en utilisant une gamme plus large de sels biliaires. Généralement, avec l'augmentation de

l'hydrophobie des sels biliaires, la préférence pour la formation de solutions est progressivement remplacée par une tendance à produire des gels et finalement des cristaux. Une association bord à bord d'anions biliaires est également observée dans différents types de sels biliaires. Les résultats renforcent notre conclusion selon laquelle les structures moléculaires internes des fibres dans les gels et dans les cristaux sont étroitement liées.

Mots-clés: Acides biliaires, amines, hydrogel moléculaire, fibres, cristallisation, spectroscopie de résonnance magnétique nucléaire, organisation moléculaire.

Abstract

Gelation is a common phenomenon in which a large amount of solvent is immobilized in a network made up of relatively small amounts of substrate. With properties of both solid and liquid, a gel is a unique state. Gelation draws attention from researchers worldwide to study its properties and mechanism. However, many questions are still unraveled, such as the self-assembly process and molecular interactions in the gel system, the relationship between solutions, gels, and crystals, and the molecular organization in the gel network. Exploring these questions will provide knowledge about the mechanism of gelation and contribute to the design and fabrication of new gels for different applications.

This thesis describes our study of gels and their relationship with solutions and crystals using bile salts, which are abundant natural amphiphiles. The rigid steroid moiety and the variable hydrophobicity of the bile salts facilitate the study of the self-assembly process. The research is presented through three articles published or submitted during my Ph.D. program.

The first paper probes the molecular interactions that occur in the formation of molecular hydrogels made from mixtures of sodium deoxycholate and formic acid. Nuclear magnetic resonance spectroscopy provides new information about the gel-sol transition on the molecular level, the interaction between free/gelated species, and the interaction of hydrophobic regions of bile salts with the gel network.

The second paper summarizes our exploration of the relationship between gels and crystals, especially how the molecular components are organized. Ammonium salts of lithocholic acid produce different patterns of self-assembly, such as gels, fibers, and crystals, with various ammonium anions. The molecular organization of lithocholates under different conditions is remarkably consistent, indicating that there is an intimate relationship between gelation and crystallization in this system. The results also shed light on the long-existing question of how molecules are arranged in gel fibers.

The third paper describes our systematic study of gelation and crystallization using a broader range of bile salts. Generally, with increasing hydrophobicity of the bile salts, the preference to form solutions is gradually superseded by a trend to produce gels and finally crystals. An edge-to-edge association of bile anions is also observed in different kinds of bile salts. The results

strengthen our conclusion that the internal molecular structures of fibers in gels and in crystals are closely related.

Keywords: bile acids, amines, molecular hydrogels, fibers, crystallization, nuclear magnetic resonance spectroscopy, molecular organization.

Table of Contents

List of Figures

List of Tables

List of acronyms, abbreviations, and symbols

γ	specific free energy
γ_A	strain amplitude
h	Planck's constant
σ	supersaturation
δ	phase difference
ρ_{calc}	calculated density
τ_c	molecular correlation time
τ_A	shear-stress amplitude
μ	chemical potential
v	chain volume
Ω	volume of the growth units
3D	three-dimensional
Å	Ångström
a_0	headgroup area
a_i	activity of *i*
Azo	azobenzene
CA	cholic acid
CMC	critical micellar concentration
CMB	crystallographic mismatch branching
CD	cyclodextrin
CD	circular dichroism
CDCA	chenodeoxycholic acid
DBS	dibenzylidene-d-sorbitol
DCA	deoxycholic acid
DHL	dihydrolanosterol
FT-IR	Fourier transform-infrared
GoF	goodness-of-fit
G	Gibbs free energy

G*	complex shear modulus
G’	storage modulus
G”	loss modulus
GP-1	*N*-lauroyl-L-glutamic acid di-*n*-butylamide
HLB	Hydrophile-Lipophile Balance
IR	infrared spectroscopy
k	Boltzmann constant
lc	chain length
LCA	lithocholic acid
LMWG	low-molecular-weight gelator
NaDC	sodium deoxycholate
NaphC	naphthoylamine-substituted cholic acid
NMR	nuclear magnetic resonance
NOE	nuclear Overhauser effect
O/W	oil-in-water
PAA	polyacrylic acid
PAA	polyallylamine
PAGE	poly (allyl glycidyl ether)
PDL	poly-D-lysine
PEG	polyethylene glycol
PEI	polyethylenimine
PL	polylysine
PLL	poly-L-lysine
ppm	parts per million
PVA	polyvinyl alcohol
r	radius of the spherical nucleus
*r**	critical nucleus size
R_1	factor of agreement on the reflections observed
ROESY	rotating frame nuclear Overhauser effect spectroscopy
SA-CMB	small-angle crystallographic mismatch branching
SAXS	small-angle X-ray scattering

SANS	small-angle neutron scattering
SEM	scanning electron microscope
STD	saturation transfer difference
T	temperature
T_1	spin-lattice relaxation time
T_2	spin-spin relaxation time
TEM	transmission electron microscopy
TIP	transferable intermolecular potential
TMS	tetramethylsilane
UV-Vis	ultraviolet-visible spectroscopy
WA-CMB	wide-angle crystallographic mismatch branching
WAXS	wide-angle X-ray scattering
W/O	water-in-oil
wR_2	weighted agreement factor
XRD	X-ray diffraction
Z	number of molecules in the unit cell
Z'	number of molecules in the asymmetric unit

Acknowledgements

First and foremost, I want to thank my mother, Xuqing, for raising me and encouraging me to explore different cultures in the world by studying abroad.

I also want to thank Prof. Julian Zhu, who was the invited speaker when I was in the Master program at my previous university. He gave a fascinating presentation on the research of materials based on bile acid. That was the first time I realized the glamorous features of bile acids. That talk, along with his vivid explanation and gentle, patient way of communication, significantly contributed to my decision to pursue a Ph.D. at UdeM under his guidance. Despite all the challenges and setbacks during the program, I feel very proud of this decision.

Furthermore, I feel very grateful to have Prof. James D. Wuest as my co-supervisor. When he joined my committee, I was deeply frustrated by the messy results and buried in self-doubting and self-criticizing. Jim used his wisdom and kindness to help me see the value of my research and to reconstruct my confidence. Without his continuous, genuine support, it would be much harder for me to go through the mist of anxiety and uncertainty.

A huge thanks to Dr. Cedric Malveau and Dr. Thierry Maris for their great help in NMR and XRD, respectively. Without the full support from them and other collaborators, the research presented in this thesis will be impossible.

I want to thank my committee members, Prof. Suzanne Giasson and Prof. Christian Pellerin, for giving me valuable suggestions during the program. Thank all the jury members for taking the time to evaluate my thesis and offer advice.

It's my great pleasure to work with my incredible colleagues, including Prof. Chuanzhuang Zhao, Guillaume Beaudoin, Meng Zhang, Eric Habib, Frédéric Langlois, Kaojin Wang, Zhiyuan Ma, Alexander Cunningham, Yulin Zhang, Xuemin Liu, Xinzhen Fan, Alexy Sanseigne, Chetna Mohanty, Norbert Villeneuve, Johann Sosoe, Abdel Al Ahmad, and so on. Thanks so much for cheering me up and supporting me in many different ways! I also want to thank Dr. Le Goas Marine and Dr. Nicolas Macia for the instrument training.

In addition, I would like to thank my friends and families for helping me and encouraging me. Most importantly, I want to thank my wife, Qingchuan Zhao, for her unconditional love and

understanding! She supports me not only psychologically but sometimes financially as well. I feel fortunate to be her husband. We went to the same university for bachelor's, Master and Ph.D. degrees. I hope we can continue to grow together and support each other like this for many years.

Finally, I want to thank myself, Puzhen Li, for overcoming the difficulties all the way!

Chapter 1. Introduction

Crystals and gels are self-assembled structures composed of molecules. The present chapter will start by describing the "glue" that holds molecules together: intermolecular interactions (Part 1). This will be followed by the rules and theories governing the self-assembly in crystallization and gelation (Part 2). Part 3 will cover the main characterization methods for crystals and gels, and Part 4 will introduce bile acids and their derivatives as species that can undergo association. Part 5 will describe the content of the following chapters.

1.1 General notions of supramolecular chemistry and intermolecular interactions

The common view on the difference between crystallization and gelation is that crystallization involves the formation of highly ordered 3D patterns of molecules, whereas gelation yields a network of interconnected assemblies.[1] Despite the apparent differences, these two self-assembly processes share the same intermolecular interactions, including hydrogen bonding, van der Waals interactions, electrostatic interactions, π–π interactions, and other non-covalent bonds. In addition to these non-covalent interactions between structural units in crystals or gels, solvophobic effects induced by the presence of the poorly soluble functional groups or moieties in the molecular structure of the components can also contribute to the self-assembly process.

The structures of certain common gelators are shown in Figure 1.1 as examples to show the roles of intermolecular interactions in self-assembly, especially in gelation. Amphiphilic molecules that can be arranged head-to-tail are among the oldest gelators reported, and one of the examples is the lithium salt of 12-hydroxystearic acid (**a**).[2,3] From the molecular structure, we can see that several interactions can potentially be involved in the aggregation process:

Electrostatic interactions between charged groups

Hydrogen bonding between carboxylate groups and hydroxyl groups

van der Waals interactions between alkyl groups

Many gelators contain aryl groups. For example, 2,3-bis-n-decyloxyanthracene (**b**) can cause gelation of alcohol (methanol, ethanol and n-propanol) by associating, mainly driven by π– π interactions and van der Waals interactions.[4] Certain cholesteric derivatives such as dihydrolanosterol (DHL; **c**) are also effective gelators.[5–7] In addition to being able to form hydrogen bonds and other molecular interactions, cholesteric derivatives have rigid polycyclic structures that are thought to help form different domains in the micelle, facilitate the formation of higher-order structures,[8,9] or help reduce entropic losses upon aggregation.[10] Other interesting gelators include dibenzylidene-d-sorbitol (DBS; **d**), which has good gelation efficiency in organic solvents and water, owing to its potential to engage in π– π stacking, its ability to form hydrogen bonds,[11,12] and its high molecular rigidity.[10]

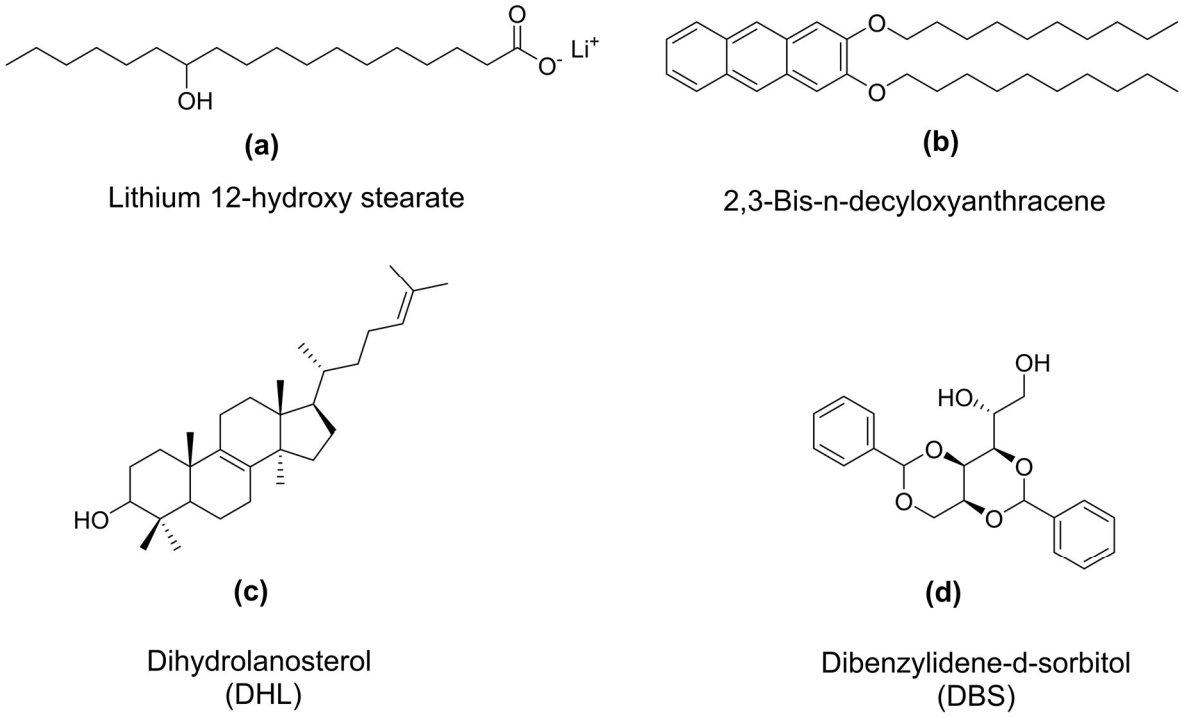

Figure 1.1. Structures of different molecular gelators.

Work described in this thesis mostly involves self-assembly that happens in an aqueous environment. Therefore, it is necessary to look in detail at the role of hydrogen bonding and hydrophobic effects on self-assembly. Hydrogen bonding is considered to be quasi-covalent due to sharing of a proton between two electronegative atoms (e.g., N, O, F). In ice (Figure 1.2a), the intermolecular O···H distance between hydrogen-bonded molecules of water is 0.176 nm, which

is larger than the covalent distance corresponding to O–H bonds (0.1 nm) but lower than the sum of the van der Waals radii of O and H (0.27 nm). Other hydrogen bonded structures are shown in Figure 1.2. The directionality of hydrogen bonds is also between that of van der Waals interactions and that of covalent bonds, as is the case of the binding energy w(σ): van der Waals interactions ≈ 1 kT < hydrogen bonds ≈ 10 kT < covalent bonds ≈ 100 kT at room temperature ($kT = 4.11 \times 10^{-21}$ J at 289 K) (Figure 1.3). The hydrogen-bonded angle (φ) X–H···X (X represents the electronegative atoms, e.g., N, O, F) is generally between 140° and 178°. The case of φ = 180° is statistically unlikely in hydrogen-bonded geometries.[13] Researchers continue to build interesting self-assembled structures or networks using hydrogen bonds, and more details will be discussed later in this chapter.[14–17]

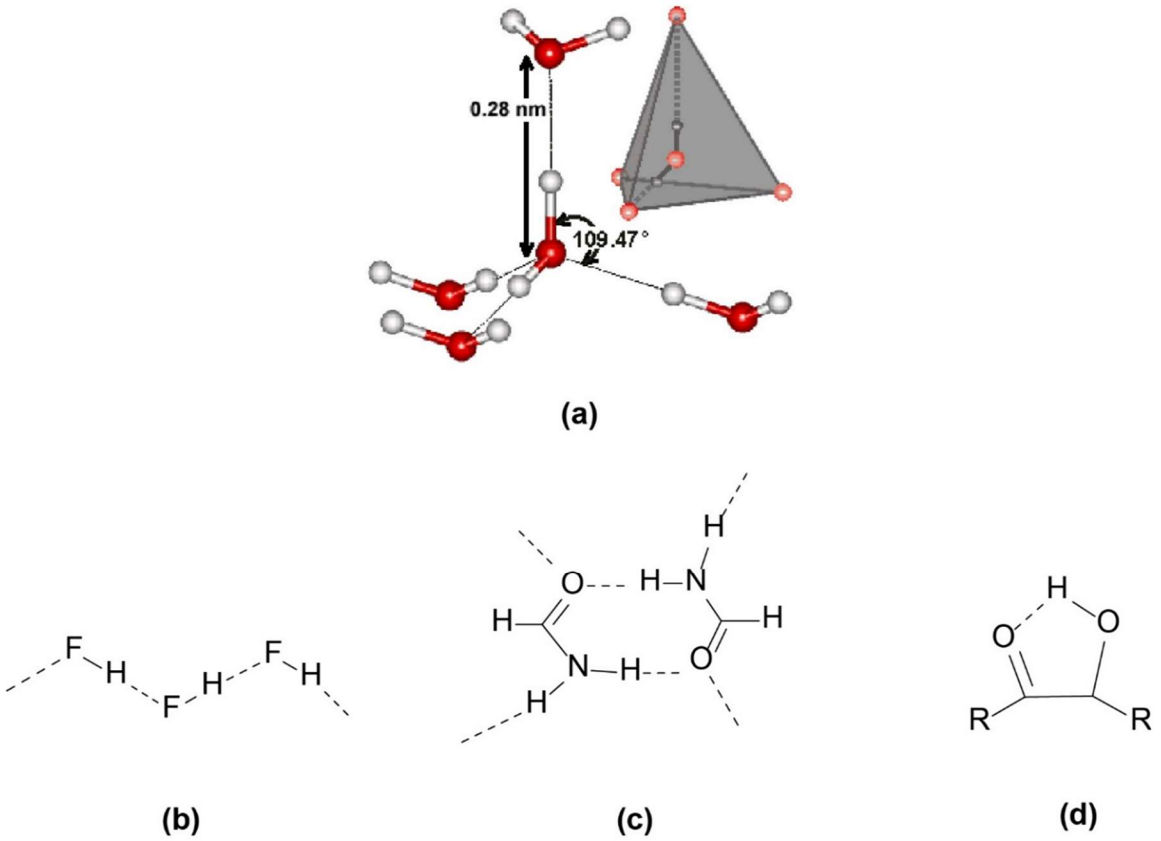

Figure 1.2. Examples of different hydrogen bonds and different hydrogen-bonded structures. (a) 3D structure in ice (modified from ref. [159] with permission). (b) 1D structure in HF. (c) 2D structure in formamide. (d) Intramolecular hydrogen bond. Figure partly adapted from ref. 20 with permission. Copyright (2011) Elsevier Inc.

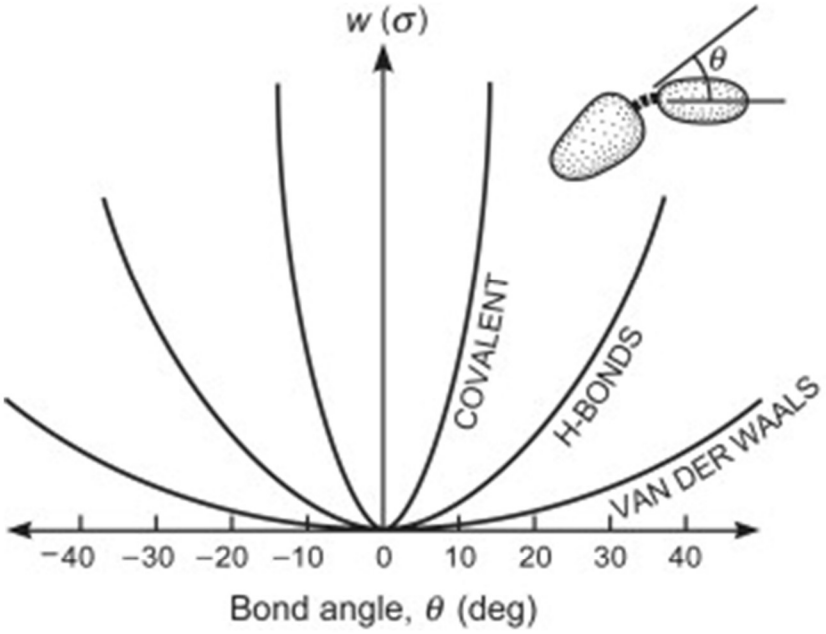

Figure 1.3. Illustrative diagram showing the orientational dependence of different types of bonds. The parameter w(σ) is the binding energy. Figure adapted from ref. 20 with permission. Copyright (2011) Elsevier Inc.

Another important aspect of hydrogen bonding is the hydrophobic effect, which is a vital driving force when self-assembly occurs in an aqueous environment. Water cannot form hydrogen bonds with hydrophobic moieties of molecules, such as alkyl chains. Moreover, molecules of water tend to contact each other and to form hydrogen bonds. To avoid breaking these hydrogen bonds when nonpolar molecules are added, the water molecules need to reorientate themselves and create a new arrangement that provides suitable cavities to include the foreign nonpolar species. Figure 1.4a shows a model water molecule called TIP5 (TIP: transferable intermolecular potential). The charges are distributed on tetrahedral arms: two positive hydrogen atoms and two virtual negative sites around the oxygen atom to represent its Lewis pairs.[18,19] The water molecules can form more ordered structures around the hydrophobic solutes, which is considered entropically unfavored for the water (Figure 1.4b). Therefore, energy is needed to transfer hydrocarbons from the bulk liquid to the water. The free energy of transfer increases in proportion to the surface areas of the foreign molecules or the portions that cannot engage in hydrogen bonding.[20]

A close relative of hydrophobic effects are hydrophobic interactions, which correspond to the tendency of hydrophobic molecules to show stronger attractions in water than in free space. Hydrophobic interactions are an entropic phenomenon rather than a bond. The interactions involve the rearrangement of hydrogen bond configurations when hydrophobic solutes come closer and share the solvation zone created by surrounding molecules of water. By comparing the structure of water at hydrophobic interfaces and at hydrophilic interfaces, we can see that at a hydrophobic interface, each water molecule needs to be more ordered to fully engage in hydrogen bonds. However, at a hydrophilic interface, molecules of water will need to be positionally ordered on the surface, but they are still free to adopt various orientations (Figure 1.4).

All these intermolecular interactions will link the individual molecules together in a process of modular construction that yields larger and more highly-ordered structures. The rules and driving force for the assembly process will be introduced in the next section.

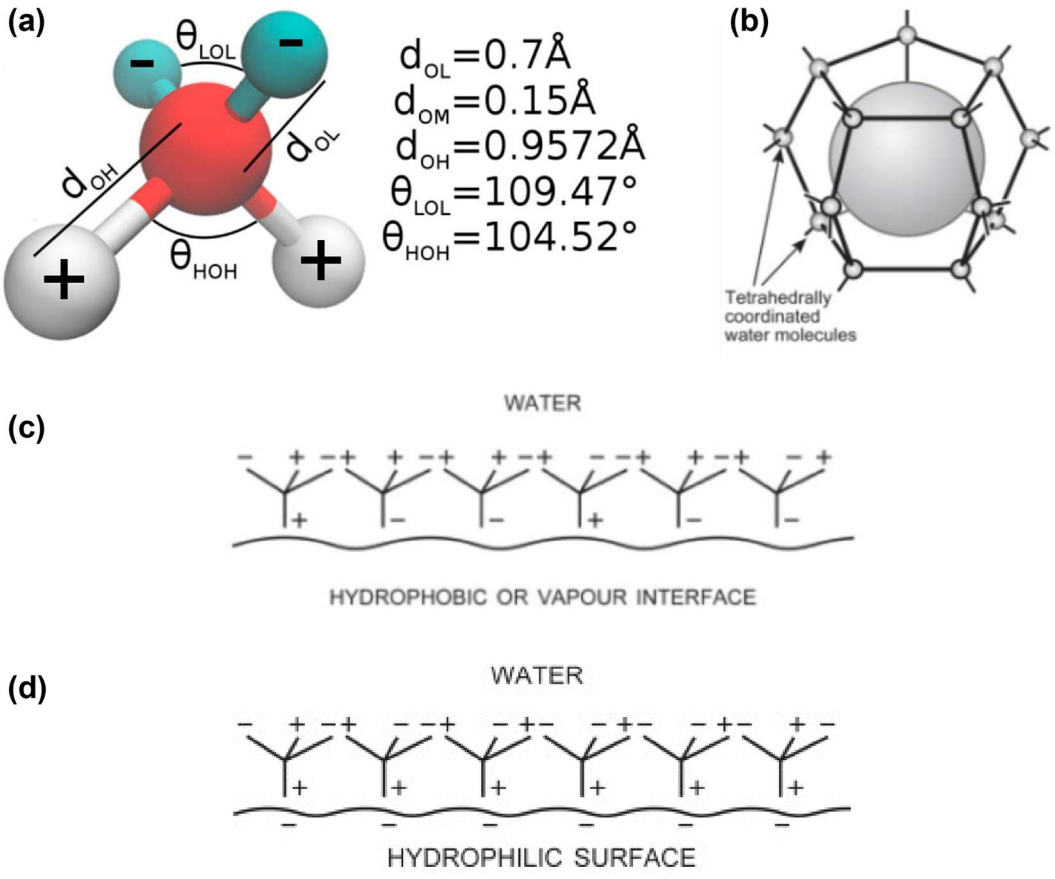

Figure 1.4. (a) Water molecule model TIP5 (TIP: transferable intermolecular potential) in which the charges are distributed on tetrahedral arms. Red: oxygen (O), white: hydrogen (H), and green: two virtual negative sites representing the oxygen's Lewis pairs (L). (b) An example of a water cage formed around a hydrophobic molecule. (c) Water structure at an extended hydrophobic or vapour surface. (d) Water structure at an extended hydrophilic electronegative surface. Reproduced from ref. 19, 20 with permission. Copyright (2018) AIP Publishing. Copyright (2011) Elsevier Inc.

1.2 Self-assembly and molecular arrangement: Gelation and crystallization

1.2.1 Phenomenon of gelation and behavior of molecules that can form gels

"Gelly-like" or "gel" states are widespread in nature, such as in the tissue of plants and animals. In 1861, Thomas Graham described the gelled state as follows: "*While the rigidity of the crystalline structure shuts out external impressions, the softness of the gelatinous colloid partakes of fluidity, and enables the colloid to become a medium for liquid diffusion, like water itself.*"[21] The definition of "gel" is still open for discussion, and researchers worldwide continue exploring and developing this area. Generally, a "gel" is usually a description for the solid-like system mainly comprising liquid. The self-supporting property of gels comes from the presence of interconnected structures that form an open network, which holds the gelled liquid within available spaces. Molecules in gels can generally be divided into two types: the gelators that form the network, and the solvent trapped in the network. In some cases, additives such as certain ions need to be included in the gel system to facilitate gelation. Commonly, these additives are considered as gel conditions, and the focus is still on the gelators and the solvents.

Based on the nature of the gelators involved, gels can be divided into polymeric gels and small-molecule gels. Gel networks in polymeric gels are usually dependent on the polymers, such as polyethylene glycol (PEG),[22] polyvinyl alcohol (PVA),[23] and polyacrylic acid (PAA),[24] chemically or physically crosslinked together. Polymeric gels arise because of association or entanglement of the polymer chains. In contrast, the fibrous or tubular structures that give rise to small-molecule gels are produced by aggregation of the individual molecular components to form larger self-assembled structures. In most cases, these low-molecular-weight gelators (LMWGs) are amphiphilic molecules that can form specific secondary or higher structures due to intermolecular interactions such as hydrogen bonding, hydrophobic interactions, van der Waals interactions, π– π interactions, and other effects. The characteristics of LMWGs, such as their flexibility, chirality, substituents, and many other properties, will potentially influence their interactions and packing patterns, leading to different morphologies and properties.

Amphiphiles are important members of the large family of LMWGs. The self-assembly pattern and gel properties of amphiphilic LMWGs are directly related to the structure of the gelator and polarity of the solvent. For head/tail(s) amphiphiles, namely those with hydrophilic heads and hydrophobic tails, the influences of structure (head structure,[25] tail length,[26] substitution group,[27] and head/tail orientation[28]) on the self-assembled structure have been widely examined. For these amphiphiles, it is relatively easy to calculate the packing parameter by considering the chain

volume *v*, the chain length *lc*, and the headgroup area a_0 (Figure 1.5a). The preferred packing geometry of head/tail(s) amphiphiles will change with the packing parameter (Figure 1.5b). The Hydrophile-lipophile balance (HLB) is generally in proportion to the packing parameter, showing the variation from oil-in-water (O/W) micelles to inverted water-in-oil (W/O) micelles (Figure 1.5b). A detailed analysis of different structures and "mesophases" formed by head/tail(s) surfactants in aqueous environment as a function of the packing parameter (v / ($a_0 l_c$)) is shown in Figure 1.5c.

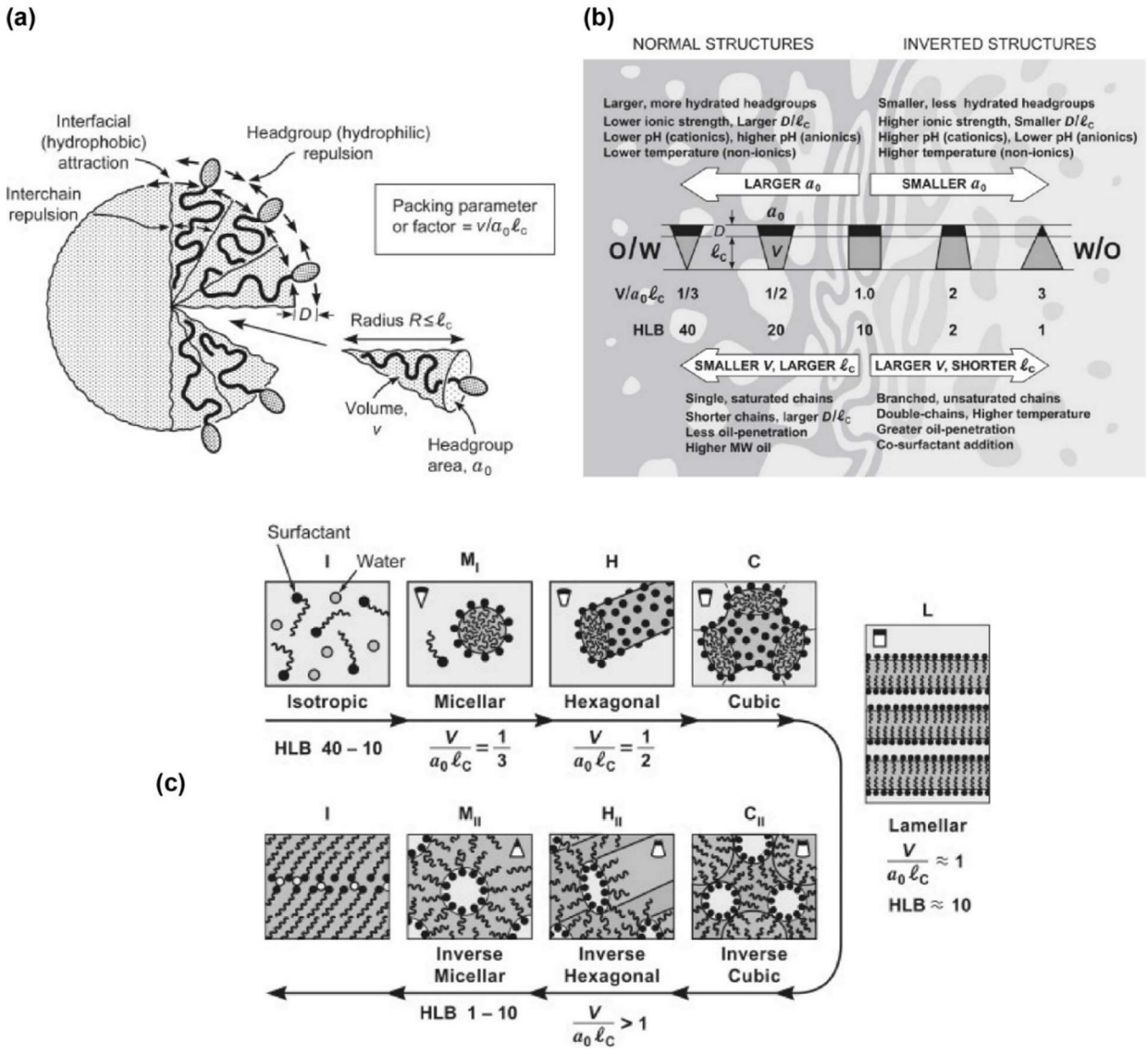

Figure 1.5. (a) The hydrocarbon interiors in micelles and the calculation of the packing parameter. (b) Changes in the preferred packing geometry of head/tail(s) amphiphiles as a function of the packing parameter under the effect of the chain volume v, the chain length lc, the headgroup area a_0, and the distance from the hydrocarbon-water interface to the location of the lateral repulsive forces between headgroups D. (c) Different structures and "mesophases" formed by head/tail(s) surfactants in aqueous media corresponding to the packing parameter (L: lamellar, M: micellar, H: hexagonal (cylindrical), C: cubic subscript I: normal structure; subscript II: inverted structure). Figures reproduced from the ref. 20 with permission. Copyright (2011) Elsevier Inc.

Amphiphiles with complex structures such as bile acids can have various functionalities, resulting in diverse patterns of self-assembly. The complexity of the structures of these amphiphiles also makes it hard to define a suitable packing parameter. To gain knowledge about these complicated amphiphiles, researchers continuously explore the influence of substituents,[29,30] the extent of protonation/deprotonation,[31] and the molecular structure[32,33] on the patterns of self-assembly.[34] More self-assembled structures derived from bile salts and their derivatives will be presented in Part 4 of this introductory chapter. Also, Chapters 2-4 show the results of our studies of how substituents, counterions, temperatures, and other factors exert an effect on the self-assembly of bile salts.

1.2.2 Introduction to theories of gelation and crystallization

This section will introduce theories of gelation and crystallization from a thermodynamic perspective. As the foundation of gelation and crystallization, the nucleation process is discussed first, including the driving forces of nucleation, the fundamental factors influencing nucleation, and different nucleation models. The second part of the section will focus on the relationship between gelation and crystallization, emphasizing the development of crystallite components such as fibers in the gel. Different fiber-branching patterns are compared in several respects, including crystallographic mismatch as a mechanism for branching, factors influencing the nature of fibers, and their relationship with macroscopic properties.

1.2.2.1 Nucleation

A crucial concept shared by gelation and crystallization is nucleation. Nucleation is defined as the formation of new thermodynamic phases from an old one caused by thermal fluctuations at the atomic level.[35] The driving force in nucleation is the difference in chemical potential ($\Delta\mu$) between the mother phase (μ_{mother}) and the ordered phase (μ_{crystal}) of a crystal.[36] Since $\Delta\mu = \mu_{mother} - \mu_{crystal}$, in the supersaturated system ($\Delta\mu$ >0), nucleation and crystalline phase growth proceed until the phase equilibrium is reached, at which $\Delta\mu = 0$, and $\mu_{mother}^{eq} = \mu_{crystal}$.

Therefore, the $\Delta\mu$ can be expressed as eq. 1

$$\Delta\mu = \mu_{mother} - \mu_{crystal} = \mu_{mother} - \mu_{mothe}^{eq} \qquad (1)$$

For the chemical species *i* crystallized from the solution, its chemical potential μ_i is related to the absolute temperature *T*, its activity a_i (or concentration C_i), and Boltzmann constant *k* as shown in eq. 2:

$$\mu_i = \mu_i^0 + kTlna_i \approx \mu_i^0 + kTlnC_i \qquad (2)$$

In eq. 2, μ_i^0 is the chemical potential in the standard state ($a_i = 1$). Based on eq. 1 and eq. 2, the thermodynamic driving force can be expressed as eq. 3:

$$\Delta\mu/kT = \ln\left(a_i/a_i^{eq}\right) \approx \ln\left(C_i/C_i^{eq}\right) \qquad (3)$$

An essential concept of supersaturation σ is introduced to these equations to describe the condition better:

$$\sigma = \left(a_i - a_i^{eq}\right)/a_i^{eq} \approx \left(C_i - C_i^{eq}\right)/C_i^{eq} \qquad (4)$$

Thus, eq. 3 can also be expressed as follows:

$$\Delta\mu/kT = \ln(1+\sigma) \cong \sigma \ \ (\sigma < 1) \qquad (5)$$

Nucleation processes are typically classified as homogenous and heterogeneous. Homogenous nucleation involves no foreign surface during the process. Usually, it requires large supersaturations σ, whereas the heterogeneous nucleation needs dust particles, the walls of the container, or other foreign solids as the substrate for the formation of nuclei at lower supersaturations.[35,37] In crystal nucleation, the nucleus needs to reach a size (critical nucleus size, *r**) above which the nucleus will be stable and can continue to grow. This stable nucleus size is smaller in a more highly supersaturated solution, facilitating crystal nucleation and the formation of more crystals.[38] Classical nucleation theory (eq. 6) explains the bulk free energy change ΔG during homogenous nucleation. In eq. 6, *r* is the radius of the spherical nucleus; Ω is the volume of the growth units; $4\pi r^3/3\Omega$ represents the number of growth units in a spherical cluster with radius *r*; σ is supersaturation (eq. 4); and γ_{cf} means the surface free energy between the crystal phase and fluid phase.

$$\Delta G_{homo} = \frac{-4\pi r^3}{3\Omega} kT\ ln(1+\sigma) + 4\pi r^2\gamma_{cf} \qquad (6)$$

We can see from eq. 6 that the first term $\frac{-4\pi r^3}{3\Omega} kT \ln(1+\sigma)$ will decrease ΔG, owing to the formation of a more stable crystalline phase with lower chemical potential than the mother phase

(See "Volume energy" in Figure 1.6). On the contrary, the second term $4\pi r^2\gamma_{cf}$ represents the increase in interfacial free energy accompanying the increased interface due to the new crystalline surface (Figure 1.6). Under the influence of these two opposed factors, ΔG reaches the maximum ΔG^*_{hom} at a critical nucleus radius $r^* = 2\,\gamma_{cf}/(kT\ln(1+\sigma))$, namely the nucleation barrier (eq. 7):

$$\Delta G^*_{homo} = \frac{16\pi\gamma^3_{cf}\Omega^2}{3[kT\ln(1+\sigma)]^2} \qquad (7)$$

Suitable foreign substrates will decrease the nucleation barrier for heterogeneous nucleation, resulting in the introduction of factor *f* in eq. 8 (Figure 1.6b):

$$\Delta G^*_{heter} = f\Delta G^*_{homo} \qquad (8)$$

Factor *f* is related to the structural match *m* between nuclei and substrate (eq. 9), *m* is defined on the basis of the surface free energy between substrate and fluid (γ_{sf}), substrate and crystal (γ_{sc}), and crystal and fluid (γ_{cf}), as well as the contact angle θ of the nucleus on the substrate (eq. 10, Figure 1.7a):

$$f(m) = \frac{1}{4}\times(2-3m+m^3) \qquad (9)$$

$$m = \frac{\gamma_{sf}-\gamma_{sc}}{\gamma_{cf}} \approx \cos\theta \quad (-1 \le m \le 1) \qquad (10)$$

In the -1 ≤ *m* ≤ 1 range, *f*(*m*) decreases (from 1 to 0) as m increases (Figure 1.7b). For a perfect match, $\gamma_{sc} \to 0$ and $m \to \gamma_{sf}/\gamma_{cf}$. If $\gamma_{sf} \approx \gamma_{cf}$, then $m \to 1, f \to 0$. This corresponds to the case when the new crystal is highly coherent with the substrate (Figure 1.7c). In other words, the crystallographic orientation {*hkl*} of the new phase is congruous with the strongest average interaction between the new phase and the substrate. If the structural match is poor, *m* will decrease (Figure 1.7d). If there is no correlation between the new phase and substrate, then $m \to -1$ ($f \to 1$). This case is equivalent to homogenous nucleation, as the substrate does not influence the nucleation.[39]

Eq. 5 can also be expressed as eq. 11, where ΔH_{diss} is the molar dissolution enthalpy of the nucleating phase and T_{eq} is the equilibrium dissociation temperature:

$$\Delta\mu/kT = \ln(1+\sigma) \cong \frac{\Delta H_{diss}}{kT_{eq}T}(T_{eq}-T) \qquad (11)$$

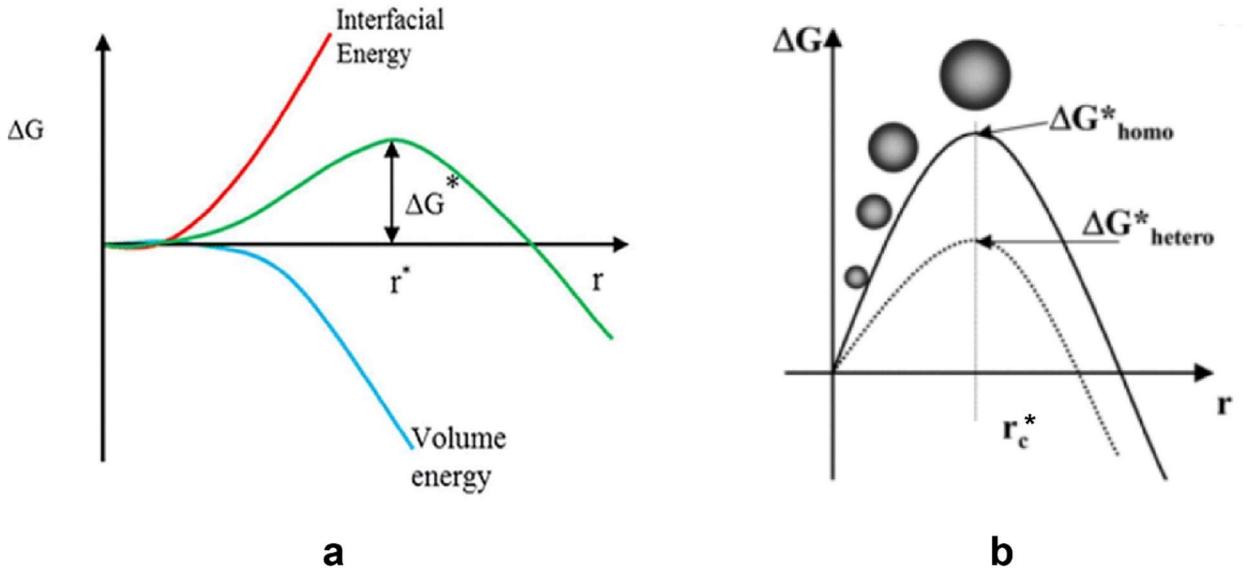

Figure 1.6. (a) Schematic representation showing the dependence of nucleation barrier Δ*G**on the radius r according to classical nucleation theory. (b) Comparison of homogenous and heterogeneous nucleation barrier Δ*G** as a function of the radius r, where r* is the critical nucleus size. Figures adapted from ref. [35,141] with permission. Copyright (2016) American Chemical Society. Copyright (2010) Wiley-VCH Verlag GmbH & Co. KGaA, Weinheim

Typically, the substrates in heterogeneous nucleation will be foreign bodies such as impurities or the walls of the container. However, there is a special "heterogeneous" nucleation where the substrate is the existing parent crystal surface. When θ is small, $\gamma_{sf} \approx \gamma_{cf}$ and eq. 10 can be rewritten as eq. 12. The newly introduced specific mismatch free energy $\gamma_{mis} = \gamma_{sc}$ is the energy Then we can calculate the ΔG^*_{mis}based on eq. 7 and eq. 8 (eq. 13):

$$m = \frac{\gamma_{sf}-\gamma_{sc}}{\gamma_{cf}} \approx 1 - \frac{\gamma_{mis}}{\gamma_{cf}} \quad (12)$$

$$\Delta G^*_{mis} = f\frac{16\pi\gamma_{cf}^3\Omega^2}{3[kT\ln(1+\sigma)]^2} \quad (13)$$

Crystallographic mismatch nucleation and growth describe the orientation deviation between the daughter crystal with the parent crystal. This process can be influenced by fundamental factors, including supersaturation σ, specific mismatch free energy γ_{mis}, and impurities. The importance of mismatched nucleation, especially in gel formation and how different factors can influence it, will be introduced in the following part.

1.2.2.2 Development of fibrous network in gels

Researchers have been trying for many years to build bridges between the study of supramolecular gel and crystals since both gelation and crystallization involve nucleation and the development of ordered aggregates, such as fibers in the gel system. The concept of "crystal network" was also introduced in the field of supramolecular gels, as a way to describe aggregates of associated crystallites.[36,40]

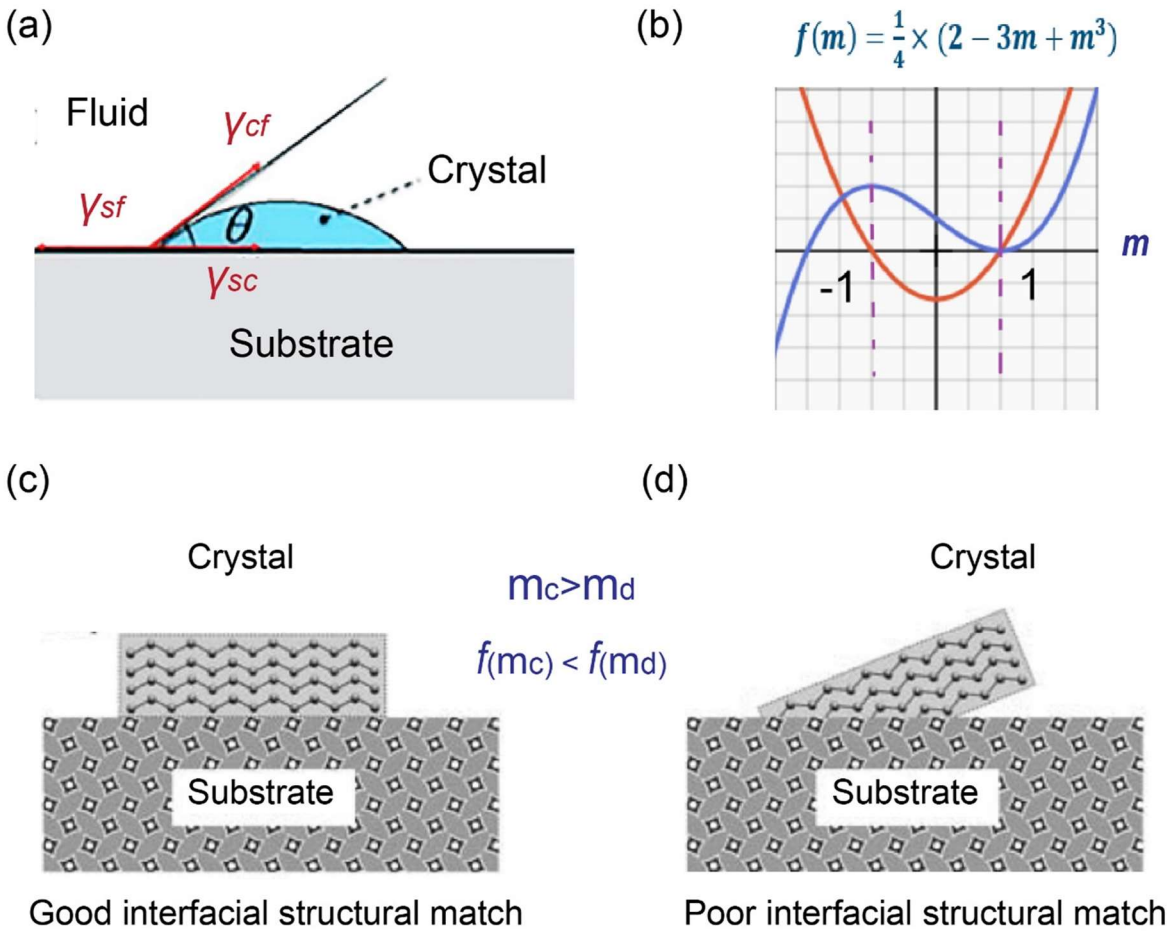

Figure 1.7. Illustration of (a) contact of crystal with the substrate and different types of surface free energy. (b) The plot of factor *f* as a function to *m* (blue line). The red line is the first derivative of f(m). The -1≤ m ≤1 range is within dashed lines. (c, d) Interfacial structural match between nuclei and substrate with good match (c) and poor match (d). Figures adapted from ref. [39,141] with permission. . Copyright (2010) (2013) Wiley-VCH Verlag GmbH & Co. KGaA, Weinheim.

The topological definition of a gel is a partly ordered structure in which junctions (nodes) are interconnected by edges, which usually correspond to fibers but can also be other entities. The junctions can be transient, resulting from temporary physical contact of the fibers, or permanent, which can be further divided into (1) fiber tip branching, (2) fiber side branching, and (3) fiber side merging (Figure 1.8). Usually, there will be a combination of different junctions in a gel system, and the division of the branch types is to facilitate analysis of the various possibilities.

Fiber side merging usually exists in cases where the gelator is polymeric. In typical cases, the polymer chain is stiffened but still has limited flexibility. The rigid parts contribute to the formation of nuclei by primary self-epitaxial nucleation. After this step, other stiffened chains will attach to the primary nucleus, and a similar process continues to create thicker fibers (Figure 1.8).

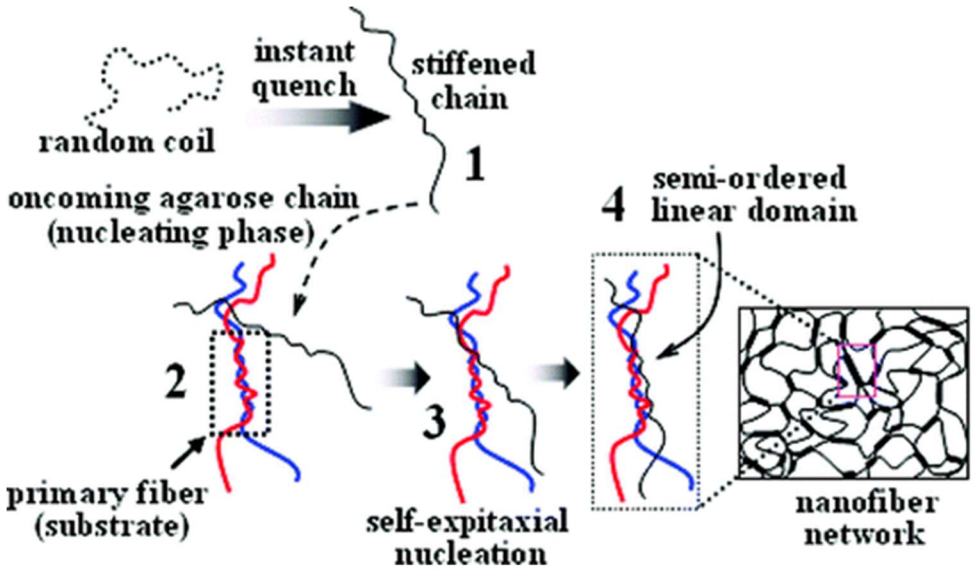

Figure 1.8. Schematic illustration of the side merging by self-epitaxial nucleation in a hydrogel network. Figure adapted with permission from ref. [160]. Copyright (2007) American Chemical Society.

The other two branchings (fiber tip branching and side branching) are commonly seen in the growth of small-molecule gels and are closely related. Since this thesis mainly focuses on the gelation and crystallization of small molecules, this section will specifically compare and discuss fiber tip branching and fiber side branching.

Fiber tip branching belongs to supersaturation-driven structural mismatch at the tip of the crystal or fibers, which usually happens at high supersaturation. It usually generates wide-angle crystallographic mismatch branching (WA-CMB) as a spherulitic pattern or open interconnected fiber network (Figure 1.9II). We can also clearly see the WA-CMB of N-lauroyl-L-glutamic acid di-*n*-butylamide (GP-1) from in *situ* microscope photos (Figure 1.9III).

When the supersaturation σ is relatively low, ΔG^*_{mis} will be large (eq. 13), creating difficulty for the crystallographic mismatch nucleation. In this case, for a needle crystal, the largest effective surface supersaturation appears around its side faces because the faces grow slowest in these directions. Consequently, crystallographic mismatch nucleation happens on the side faces of the crystal, defined as side branching. This pattern is also called "small-angle" crystallographic mismatch branching (SA-CMB). Both spherulitic and open interconnecting fiber networks can be generated in SA-CMB (Figure 1.9II). The *in situ* microscope photos also show the SA-CMB branching process of GP-1 (Figure 1.9III).

In some cases, the supersaturation σ is very low, making a high crystallographic mismatch nucleation barrier (ΔG^*_{mis}). The nucleation is mainly dominated by the ideal structural match and strong interactions between the newly nucleating phase and the parent crystals.[39,41,42] Fibers grown under this condition may have even fewer branches (Figure 1.10II-a).

Many factors can influence the crystallographic mismatch nucleation and growth.[39] This introduction will focus on several important factors.

Supersaturation σ can affect crystallographic mismatch nucleation by changing ΔG^*_{mis} (eq. 13). High σ will decrease ΔG^*_{mis}, facilitating crystallographic mismatch nucleation. The difference in σ is a crucial point differentiating tip branching (WA-CMB) and side branching (SA-CMB) (Figure 1.10I). Other conditions may also influence mismatch nucleation through σ; for example, slow surface integration will increase the supersaturation, making it easier for crystallographic mismatch nucleation to occur.

In addition, specific mismatch free energy γ_{mis} is in proportion to ΔG^*_{mis} (eq. 13). Crystallographic mismatch nucleation will be much easier on surfaces having low values of γ_{mis}.

Moreover, adsorbed impurities may perturb the interfacial structural match between the new layers and the substrates. This disturbance will lower m, promoting mismatch nucleation.

Thermal conditions such as the temperature difference (ΔT) between the starting and gelation temperature can also influences the outcomes.[43] This effect is also related to supersaturation σ, as shown in eq. 11. Larger values of ΔT will increase σ, making it easier for WA-CMB to occur (Figure 1.11I).

We have seen examples of distinct topological microstructures of fiber networks arising from tip and side branching. For a bulk gel, its mechanical properties and behaviour, including toughness, strength, and friction, are rooted in the entanglements and cross-links between fibers.[44] These topological microstructural differences can affect the entanglement and interpenetration of fibers, consequently influencing their macroscopic properties, as the example shown below.

In Figure 1.11, the gel system is 3 wt% GP-1 in propylene glycol (PG). The topological structure of the fiber network can be tuned from spherulitic (WA-CMB) to fibrillar (SA-CMB) by controlling the temperature (Figure 1.11I, eq. 11). The fibrillar network can interconnect and entangle. However, the spherulitic network is unable to interpenetrate and tends to form boundaries. Compared to the entanglement of fibrillar structures, the interactions at the boundary between spherulitic domains are weaker but may keep a certain degree of the interaction in displacements. Therefore, spherulitic networks tend to have lower elastic moduli (less rigid) but are more resistant to strain.

To sum up, different crystallographic mismatch nucleation patterns can lead to different topological microstructures of networks and macroscopic properties of the gel.

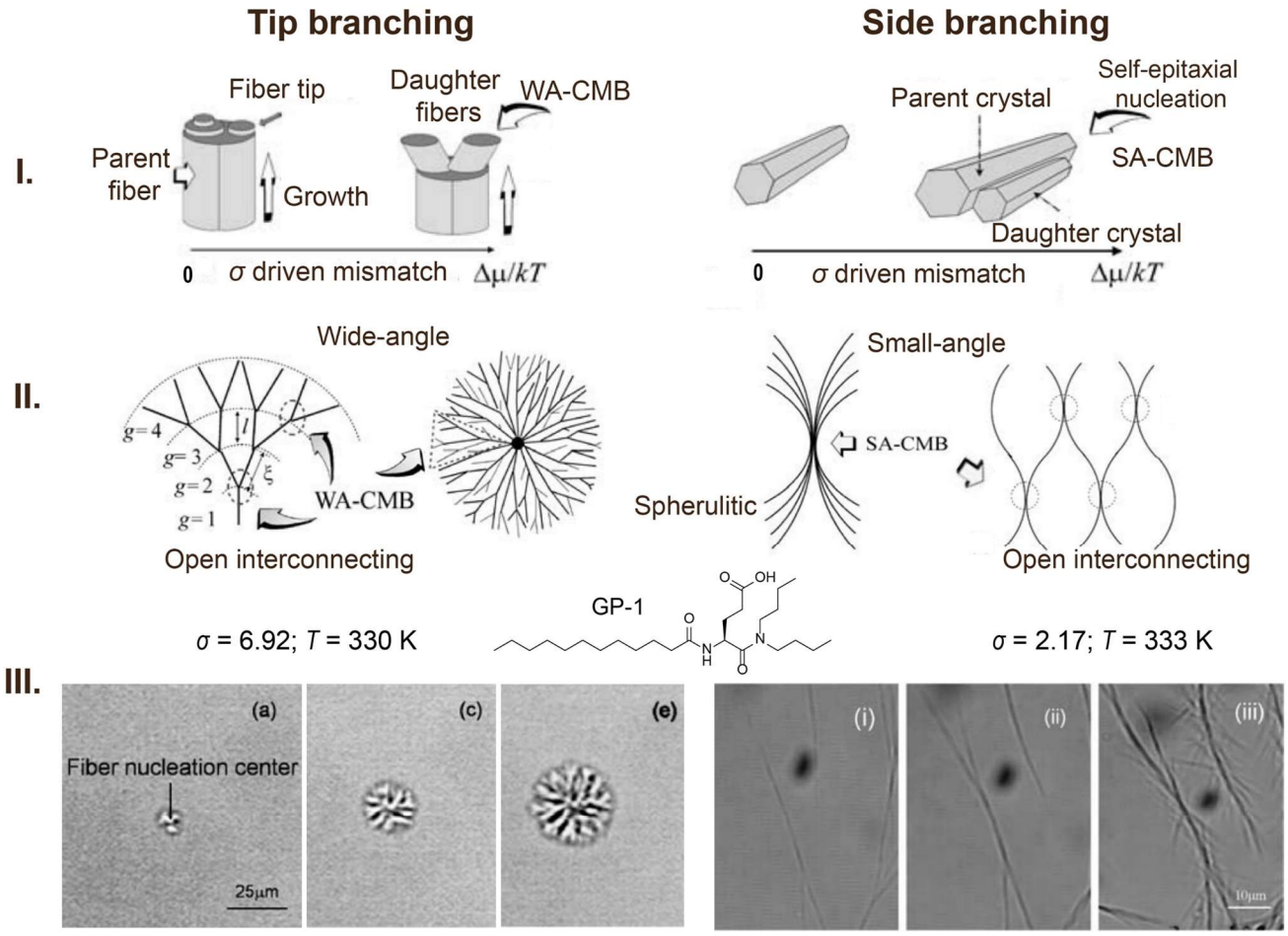

Figure 1.9. Comparison of fiber tip branching (left column) and fiber side branching (right column) on (I) nucleation and on (II) wide-angle/small-angle crystallographic mismatch branching (WA/SA-CMB). (III) *In situ* observation by optical microscopy showing the fiber network formation and branching process of *N*-lauroyl-L-glutamic acid di-*n*-butylamide (GP-1) in 1,2-propanediol. The left side of Figure III shows the WA-CMB pattern with (a) the formation of primary fibers initiating from a nucleation center. The formation of GP-1 fibers and the branching process is shown by the sequence (a), (c), (e), in which the time interval between two neighbouring photographs is 0.4 s (σ = 6.92, T = 330 K). The right side of Figure III shows the SA-CMB pattern, with the formation of GP-1 fibers and the branching process appearing in panels i–iii, in which the time interval between two neighbouring photographs is 0.2 s (σ = 2.17, T = 333 K). Figures adapted from ref. 39 with permission. Copyright (2005) Springer-Verlag Berlin Heidelberg.

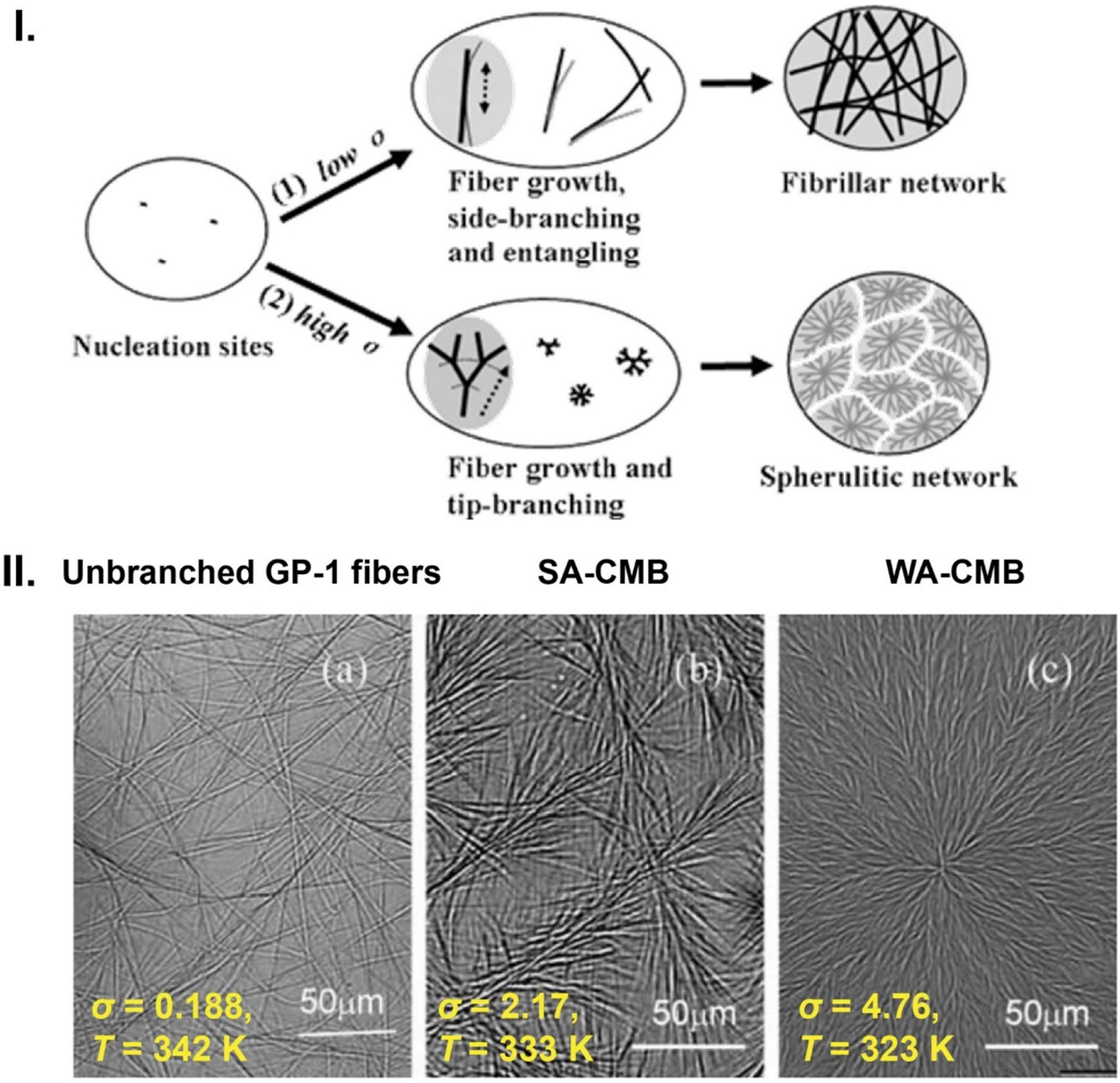

Figure 1.10. (I) Two branching models of the formation of a gel network, showing (1) side branching at a low supersaturation σ and (2) tip branching at high supersaturation σ. Dashed arrows denote the growth direction of fibers, and dotted lines mark the growth front surface of the spherulite. (II). Micrographs showing fibers and the evolution of the fiber network formed by GP-1in a 1,2-propanediol solution with increasing supersaturation. (a) Unbranched GP-1 fibers. (b) SA-CMB and GP-1 fiber network. (c) WA-CMB and GP-1 fiber network (σ and T listed in the images). Figure adapted from ref. 39, 42 with permission. Copyright (2005) Springer-Verlag Berlin Heidelberg. Copyright (2006) American Chemical Society.

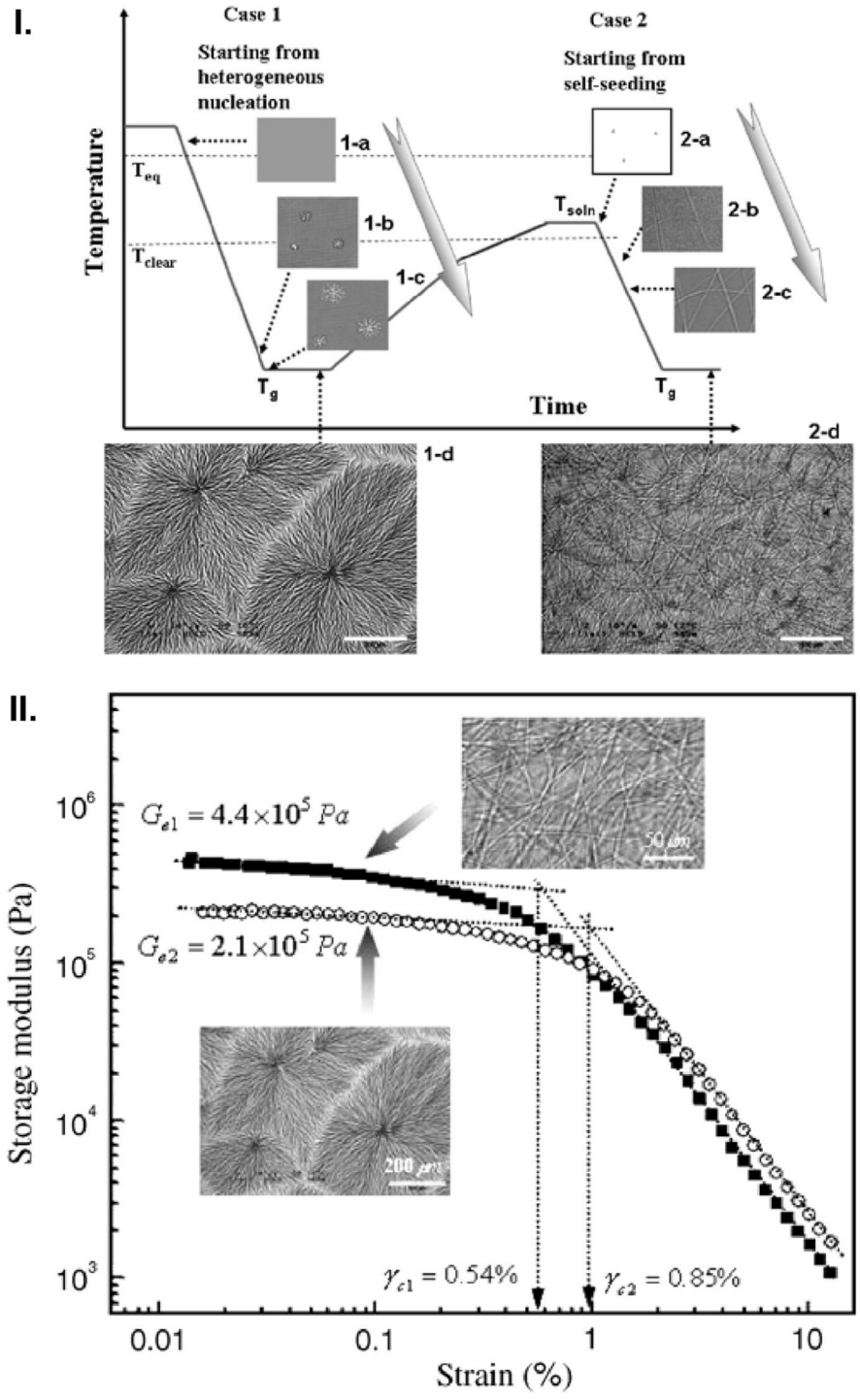

Figure 1.11. Characterizations of 3 wt % GP-1/PG gels. (I). Switching the gel network from spherulitic domains to a fibrillar network. (II). Strain sweep of the gels with the corresponding optical micrographs. G_e denotes the plateau value of the storage modulus, and γc denotes the critical strain. Figures adapted from ref. 42,43 with permission. Copyright (2006) American Chemical Society.

1.3 Characterization of gels and crystals

Gels have mechanical properties as bulk materials, which can be characterized using a rheometer or by direct observation (such as the inversion of vials containing the gel). There are many methods to study the microstructure of gels and the molecular interaction within them, including optical microscopy (with polarized light), transmission electron microscopy (TEM), scanning electron microscopy (SEM), nuclear magnetic resonance (NMR), and X-ray diffraction (XRD). The study of atomic and molecular structure in crystals is mainly based on XRD, and the technique also plays an important role in the characterization of gels.

1.3.1 Macroscopic characterization

1.3.1.1 Vial Inversion

Almost a hundred years ago, Jordon Lloyd made the following famous statement about gels: "The gel is easier to recognize than to define…if it looks like Jell-O, it must be a gel!"[45] Even now, the most direct way to check for gelation is to invert the vial and see whether the material will flow under the force of gravity. If the material can resist and keep its original shape, the self-supporting material is usually considered a gel. A similar test of gelation is the dropping ball method, in which a small metal ball is placed onto the surface of the gel and observed to remain in position or drop to the bottom.[46] Both vial inversion and the dropping ball method can provide visual assessment of gelation. However, these methods cannot provide quantitative results. Also, the results may change with conditions, like the size of the vial, sample mass, size/weight of the metal ball, waiting time, and others, making it quite challenging to compare the results from different labs.

1.3.1.2 Rheometry

Rheological methods study the response of objects to stress. The above-mentioned vial inversion tests the response of the material to gravity by "table-top" rheology,[47] but to get quantitative results, a rheometer is needed. Deformation is one of the most important properties in rheological studies. Deformation can be divided into flow (irreversible deformation) and elasticity (reversible deformation).[48] The measurements of flow properties are determined by the material's resistance to flow under shearing. Elasticity is evaluated from the deformation of material under stress. When materials can display both flow and elastic properties under shearing, they are called viscoelastics.

Figure 1.12 shows the definition of shear stress τ and shear strain γ in a two-plate model, in which the sample is placed between two plates and sheared with the movement of the upper plate. The stress plotted versus time will be a sinusoidal curve with shear-stress amplitude τ_A. A similar plot for strain will reveal the strain amplitude γ_A (Figure 1.12b). The difference in mechanical properties of the sample will be reflected in the time lag in the sinusoidal curves of the preset parameter (shear strain) and measuring result (shear stress). For extreme rigid samples, the phase difference $\delta = 0$ (ideally elastic deformation behaviour). Gel-like samples have $0 < \delta < 45°$, and fluid samples have $45° < \delta \leq 90°$ (Figure 1.12b). Complex shear modulus $G^* = \tau_A / \gamma_A$ is also introduced to describe the sample's entire viscoelastic behaviour. The vectors of G* on the *x*-axis and on the y-axis are the storage modulus G' (elastic portion) and the loss modulus G" (viscous portion) (Figure 1.12c). The viscous behaviour occurs owing to internal friction in the fluid. The deformation energy will dissipate and become unavailable for the sample. However, under force, the internal structure will be stretched and extended for elastic behaviour, storing the elastic portion of energy inside, which will become the driving force for the sample to recover its original shape. For gel studies, G' > G" is the criterion of gelation, indicating the formation of interconnected structures in the samples. The crossing point of G' and G" is also used to determine many gel properties, including the gel-sol transition temperature,[49] yield stress,[50] and recovery of the gel.[51] Figure 1.13 shows two different geometries of shearing rheometers and the determination of yield stress based on the G', G" data plot.

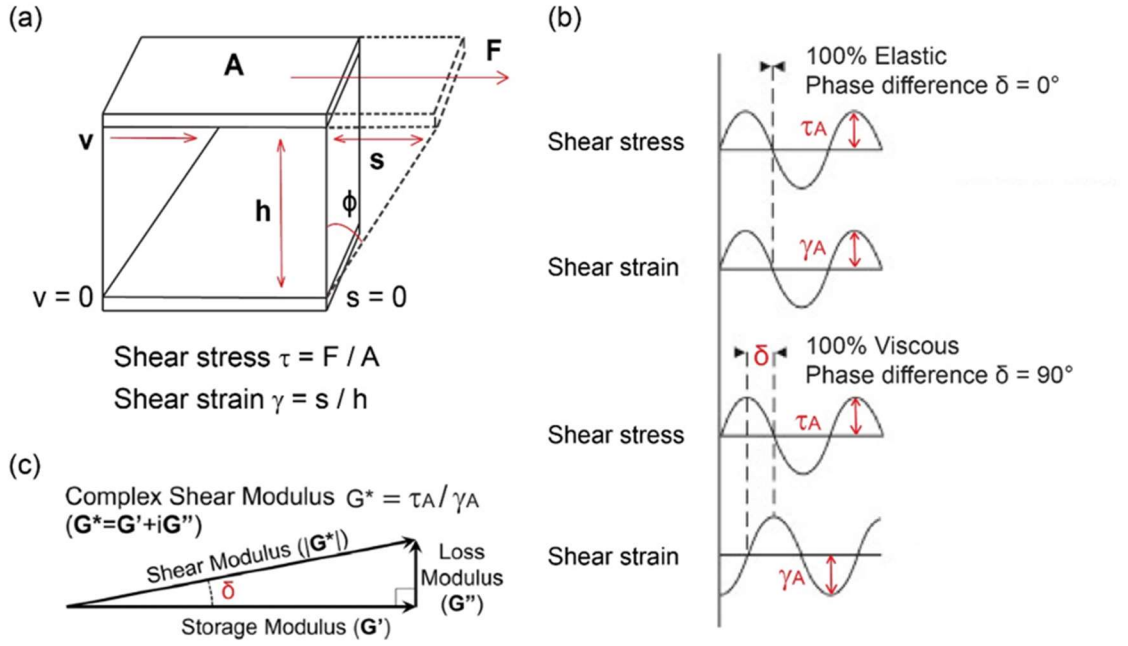

Figure 1.12. (a) Two-plate model of material between the movable upper plate and stationary bottom plate. The shear stress τ is defined using shear force F and shear area A. The shear strain γ is defined using deflection path s of the upper plate and the distance h between the plates. (b) Phase difference δ between preset shear strain and resulting shear stress for ideal elastic deformation behaviour and viscous flow behaviour. (c) Shear modulus G* is defined with shear-stress amplitude τ_A and strain amplitude γ_A. Projection of G* towards x-axis storage modulus G' is the elastic portion of the viscoelastic behaviour. Projection of G* on y-axis loss modulus is the viscous portion. Angle δ is the phase difference as in (b). Figures adapted from ref.. [161–163] with permissions. Copyright (2021) RSNA, (2016) Academic Press, (2018) Macmillan Publishers Limited, part of Springer Nature.

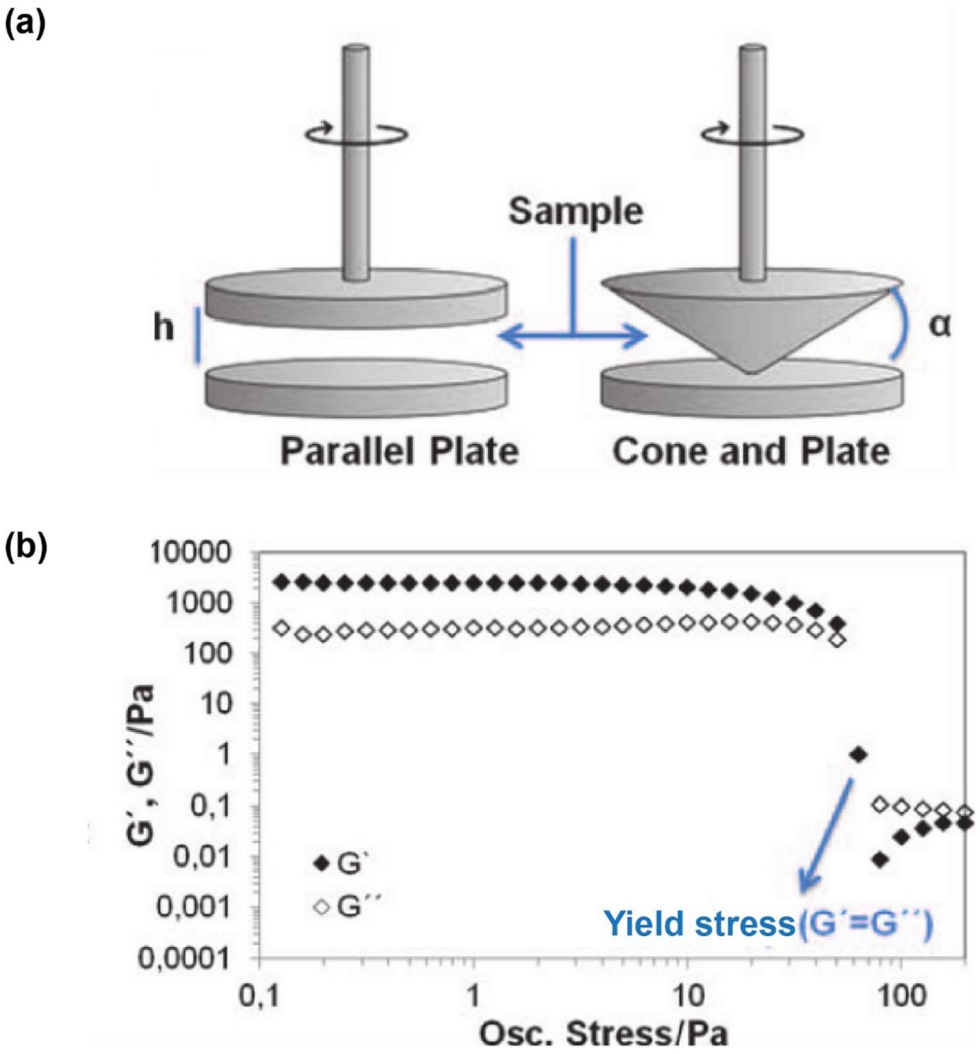

Figure 1.13. (a) Two different geometries of shearing rheometers. (b) Rheological data plot of the storage modulus G' and loss modulus G" with oscillation stress. Adapted from ref. [164] with permission. Copyright (2013) Royal Society of Chemistry.

1.3.2 Microscopic characterization

1.3.2.1 Microscopy

Optical microscopy, especially with polarized light, can provide images of the native structures of crystals and gel fibers (Figure 1.14).[52,53] However, given the wavelength of visible

light, the theoretical limit of resolution for an optical microscope is 0.2 μm. To analyze the nanoscale structures of gels or crystals, researchers need an electron microscope, including scanning electron microscopy (SEM) and transmission electron microscopy (TEM).

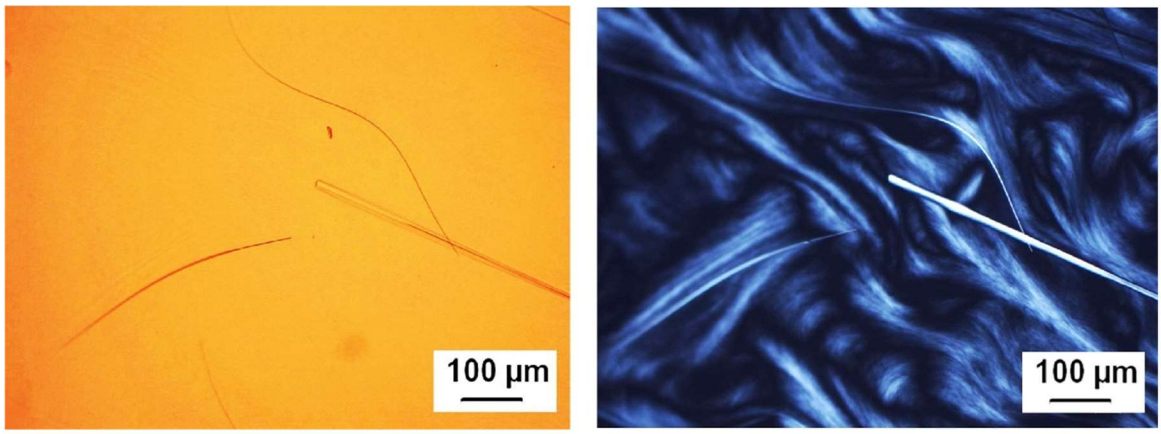

Figure 1.14. Optical microscopic images of *i*-$PrNH_3^+$ lithocholate crystal and fibers under normal light (left) and polarized light (right).

For both SEM and TEM, the sample need to be dried under vacuum before the measurement, and other treatments such as coating and stain are often necessary. The sample structures may change during all these pre-measurement procedures. For example, the gels may collapse, and crystals may break. In general, however, electron microscopy can still provide important nanoscale structural information for the samples. The fibrous structure in supramolecular gels is observed using SEM (Figure 1.15). The TEM images of lithium 12-hydroxystearate gel also clearly show different helical structures (Figure 1.16).

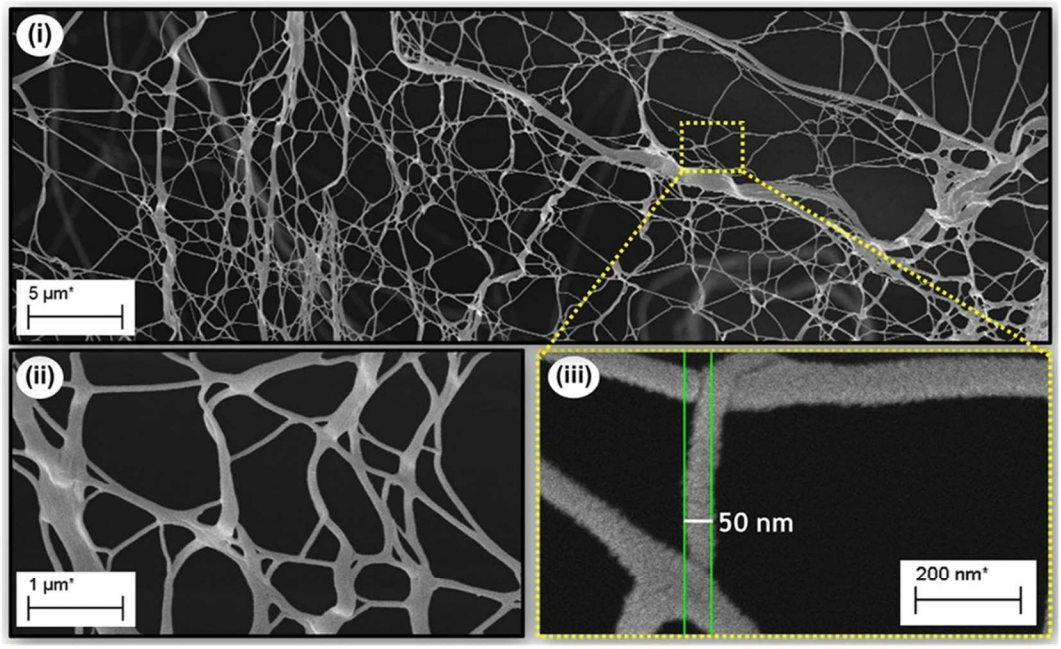

Figure 1.15. SEM micrograph of gold-coated chia seed fibers. at (i) 4,400X magnification. (ii) 30,000X magnification. (iii) 150,000X magnification, showing fiber diameter of ~50 nm. Figure adapted from ref. [165] with permission. Copyright (2018) Nature Publishing Group.

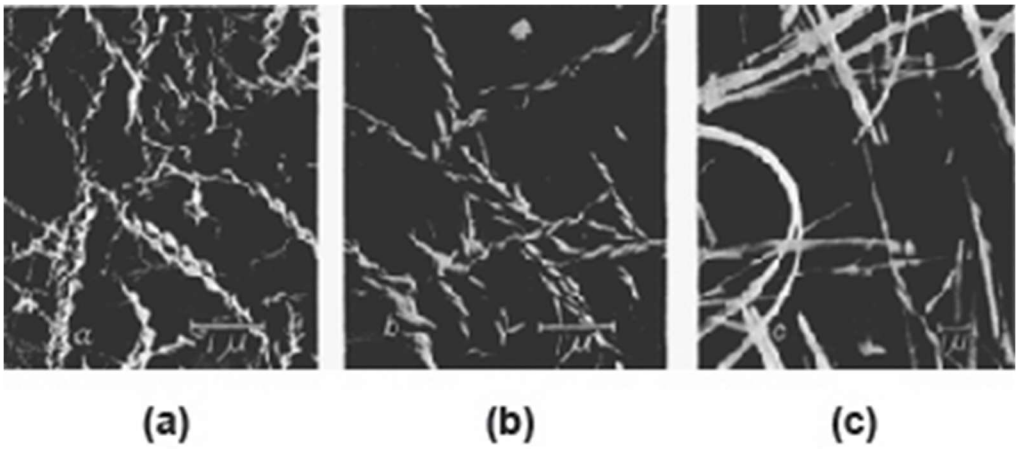

Figure 1.16. TEM images showing the effect of optical isomerism on the direction of the twist in fibrous aggregates of lithium 12-hydroxystearate. (a) D-form, right-handed twist. (b) L-form, left-handed twist. (c) DL-form, no twist. Figure adapted from ref. [166] with permission. Copyright (1965) ACS Publications.

1.3.2.2 Nuclear magnetic resonance (NMR)

Compared to TEM or SEM, NMR is a non-destructive characterization method, especially suitable for testing intact gels. NMR phenomena can be observed in nuclei having non-zero magnetic moments, such as ^{1}H, ^{13}C, ^{15}N, ^{19}F, and many others.[54] Generally, according to the quantum theory, the interaction of these nuclei with external magnetic field leads to a nuclear energy level diagram with discrete energy values (eigenstates). The total number of the possible eigenstates (energy levels) can be calculated from $2I + 1$ using the spin quantum number I. For the proton (^{1}H), $I = 1/2$, there are two eigenstates (spin states) for ^{1}H. The energy difference between these two spin states is $\Delta E = \gamma \hbar B_0 = h\nu_0$. In this equation, $\hbar$ is the reduced Planck's constant $\hbar = h/(2\pi)$; h is Planck's constant; γ is the magnetogyric ratio; B_0 is the strength of the magnetic field; and ν_0 is the Larmor frequency. The radiofrequency can match the energy difference between the spin states. Therefore, the nuclear spins can absorb specific radiofrequency (RF) to transit between energy states (resonance frequency). Besides, the different nuclei in the molecule may have different local magnetic fields B_{local} affected by the chemical environment. As a result, the resonance frequency can change, indicating different chemical environments. The comparison of the resonance frequency relative to a reference standard such as tetramethylsilane (TMS) in the magnetic field will give different positions, namely the chemical shift. The position of the peak is reflected as the chemical shift in the NMR spectra, and the peak width is related to the molecular reorientation rates and T_2 relaxation (spin-spin relaxation) time.

Based on these principles of NMR,[54] ^{1}H NMR spectroscopy is one of the most commonly used NMR techniques, and it can be used to study the immobilization of the gelators into the "solid-like" gel network. As small molecules are immobilized into the large gel network, their molecular reorientation rates decrease, and T_2 relaxation (spin-spin relaxation) decreases.[55] As a result, the peaks of these immobilized species will broaden and even merge with the baseline. The peak integration difference in conventional ^{1}H NMR can be used to study the mobile and solidified species (Figure 1.17). In the research in Figure 1.17, both the dendron and diamine will be visible in the solution state at 80 °C, whereas only the free diamine peaks can be seen after gelation at 40 °C.

In addition to ^{1}H NMR specroscopy, ^{13}C NMR spectroscopy can be used to study micelle formation and gel formation. For example, Yoshio and colleagues explored the aggregation patterns of sodium deoxycholate (NaDC) based on the ^{13}C NMR chemical shift.[56]

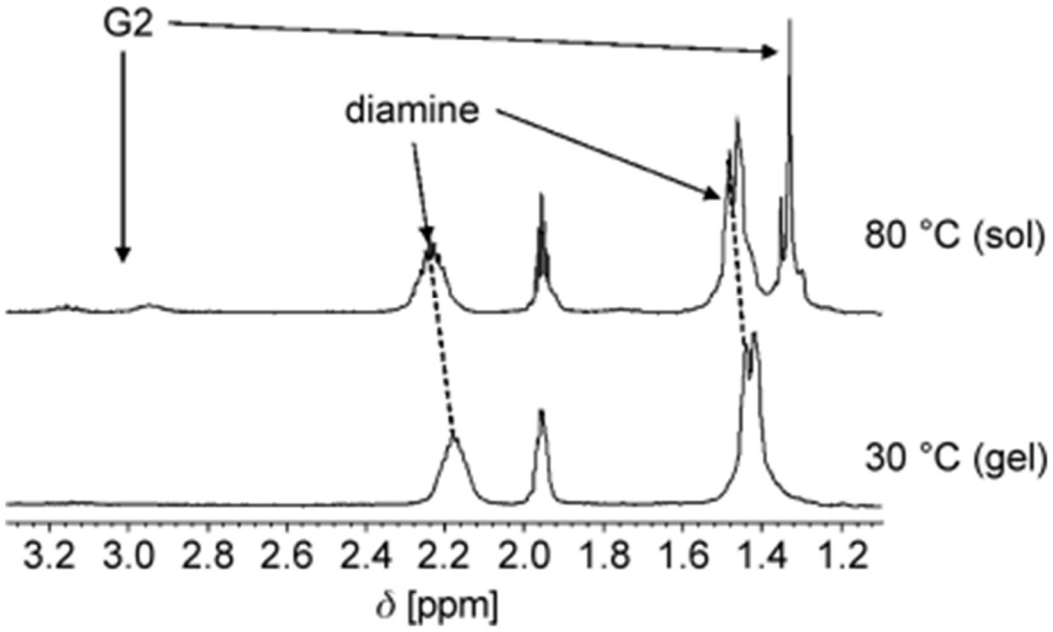

Figure 1.17. ^{1}H NMR spectra for the system G2-COOH/1, 4-CH, molar ratio1: 1.3. [dendron]= 18 mM, solvent = toluene at 80 °C (gel) and 30 °C (sol). Adapted from ref. [167] with permission. Copyright (2009) Wiley-VCH Verlag GmbH&Co. KGaA, Weinheim.

Nuclear Overhauser effect (NOE): NOE is the change of peak intensity of a nuclear spin (j) when irradiating its neighboring nuclear spin (i) with a specific pulse. It is caused by cross-relaxation and magnetization transfer between dipolar-coupled spins (i and j).[57–59] The cross-relaxation efficiency largely depends on the distance between the spins (r_{ij}) as the cross peak intensity $A_{NOE} \propto 1/r_{ij}^{6}$. The NOE experiment will provide distance information of two nuclear spins, specifically when the distance is less than 5 Å. This spatial relationship of two close nuclei can be easily seen in two-dimensional nuclear Overhauser effect spectroscopy (2D-NOESY) in terms of cross-peaks. For example, Tamesue and colleagues[60] designed a hydrogel system containing host polymer cyclodextrins (CDs) and guest polymer with azobenzene (Azo), which can change from gel to sol with UV irradiation (λ = 365 nm). They used NOESY spectra to study molecular changes during the gel-sol transition. In the gel system, the inner protons of the CD unit showed correlation peaks to those from the trans-azo group, suggesting the azo groups were inside

the CD unit for the gel state. However, after the UV irradiation (λ = 365 nm), there is no correlation between CD protons and the cis-azo in the sol state (Figure 1.18). 2D-NOESY can provide much insight into the threading/dethreading process in studies of self-assembly.

Saturation Transfer Difference (STD) NMR spectroscopy: The above application of NOE focuses on the influence of distance (r_{ij}) between nuclear spins. Another essential factor that contributes to NOE is the molecular correlation time (τ_c). Small molecules (molecular weight < 1000 Da) with short τ_c show positive NOE, while the large ones such as proteins show strong

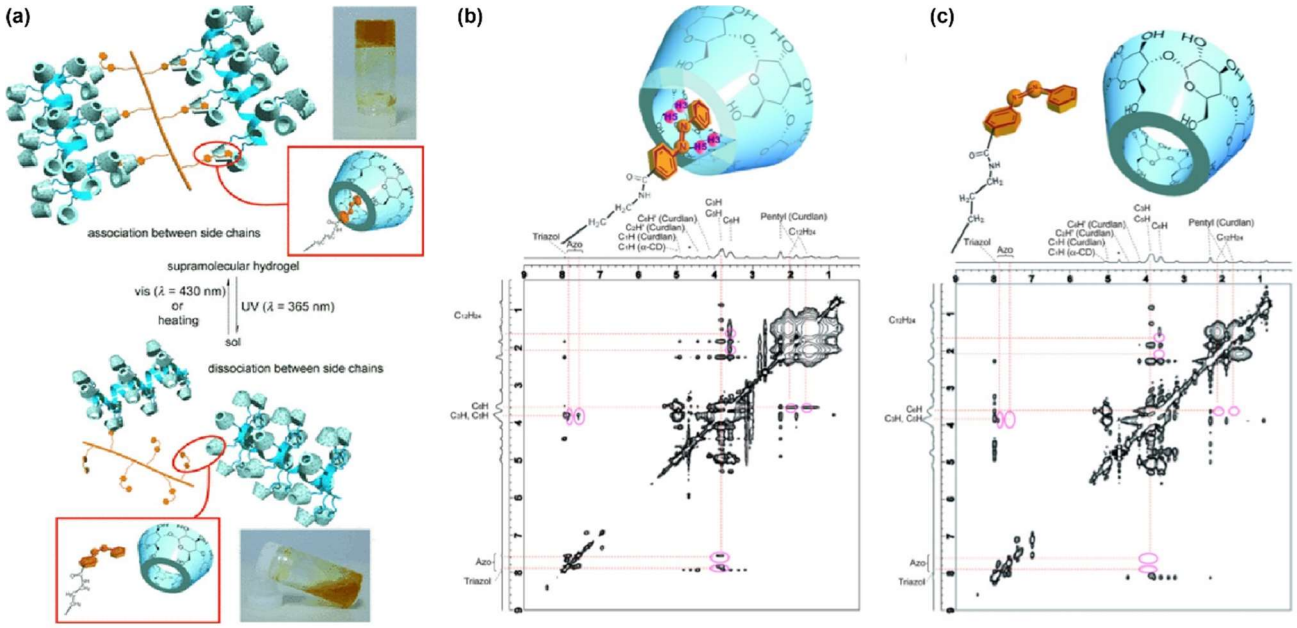

Figure 1.18. (a). Schematic illustration of the interactions of the α-CD unit (cylindrical shapes) with azobenzene moieties (yellow shapes) upon irradiation with UV (365 nm) and visible light (430 nm) or heating at 60 °C. 2D-NOESY spectra of CD/Azo groups in the polymers before (b) and after (c) UV irradiation (λ = 365nm) in D_2O. Figures adapted from ref. 60 with permission. Copyright (2010) Wiley-VCH Verlag GmbH & Co. KGaA, Weinheim.

negative NOE. If a small molecule irreversibly binds to a large molecule, it will behave as a part of it, exhibiting negative NOE as a result. Such a change in NOE behaviour is called transferred NOE. For a small molecule that interacts reversibly with the large molecule, the NOE is still positive, but the binding interaction can be revealed by saturation transfer difference (STD) NMR spectroscopy. [61,62]

STD NMR studies the dynamic, reversible interaction between small molecules and large ones, making it a powerful tool to explore the binding of ligands to target proteins.[63] The mechanism of STD NMR is shown in Figure 1.19. There are spectra from two conditions, and the binding information is in the difference spectra of these two conditions. The protons of the large protein receptor were irradiated with a radiofrequency pulse (on-resonance), leading to the selective saturation of the protein magnetization. The saturation will quickly spread across the protein via spin diffusion (^{1}H-^{1}H cross-relaxation, intramolecular NOE), transferring to the bound ligand as well (intermolecular NOE and chemical exchange). As a result, the peak intensity of the bound ligand will increase compared to that of the reference spectrum (off-resonance without saturation of the protein magnetization). So, the positive peak in the difference spectrum indicates the specific protein-ligand interaction. When the bound ligand dissociates from the protein to the solution, its saturation state can persevere since its longitudinal relaxation (T_1) rate is usually much slower than its dissociation rate. Hence, the protein can saturate newly bound ligands, and the population of saturated ligands (free and bound) will increase. What is worth noticing is that the difference in T_1 in different ligand protons may affect the STD-NMR results and need to be evaluated in some cases.[64] More details will be covered in Chapter 2.

The gel network-gelator relationship is analogous to the protein-ligand mentioned above: gelators will self-associate to create a large network which can be saturated with irradiation. Meanwhile, the gelator is involved in interacting with the network by association or dissociation. With the help of STD NMR, researchers have conducted many inspiring experiments, such as monitoring the incorporation of different additives to the fibrous gel network[65] and exploring the selective interaction of dopamine with the hydrogel. [66]

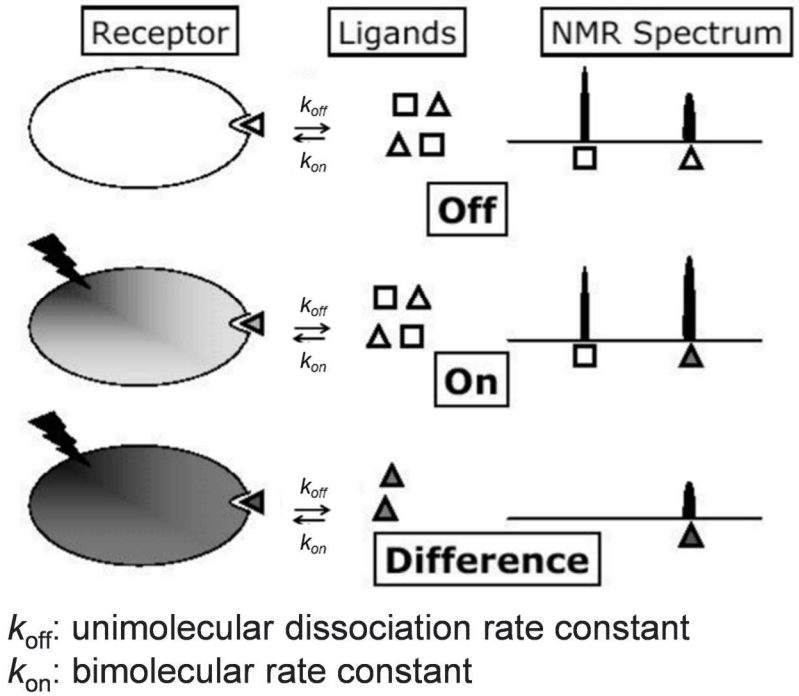

Figure 1.19. Schematic representation of the mechanism of saturation transfer difference (STD) NMR spectroscopy. Figure reproduced from ref. 63 with permission. Copyright (2005) Bentham Science Publishers Ltd.

In addition to the methods of ^{1}H NMR and ^{13}C NMR spectroscopy introduced above, including NOESY, and STD NMR, there are many other NMR techniques for studying self-assembly. Examples include diffusion-ordered NMR spectroscopy (DOSY), which can monitor the diffusion of species in the gel system,[67,68] high resolution magic angle spinning (HRMAS) NMR to study the role of solvent in gelation,[69] and rotating frame nuclear Overhauser effect spectroscopy (ROESY), in cases where NOE is weak.[70]

1.3.2.3 X-Ray/Neutron Scattering Methods

X-rays are electromagnetic radiation with a wavelength range from less than 0.1 Å to over 10 nm.[71,72] X-rays with a wavelength close to the interatomic distances in crystals can serve as a light source and generate diffraction patterns after interacting with the electron clouds of the atoms in the sample. These X-ray diffraction (XRD) patterns are the keys to revealing the spatial relationship and molecular arrangement in the crystalline samples. A similar principle also applies

to neutron scattering. The speed of neutrons is adjusted to achieve the wavelength (≈ 1 Å) comparable to atomic distances in the crystal. Elastic neutron scattering is based on the interaction with nuclei, not the electron cloud, making neutron scattering more sensitive to light atoms than the X-ray method. However, the intensity of neutrons is lower than that of X-rays. Therefore, it usually requires bigger crystal samples and longer data collection times.

For crystal samples of sufficient size (ideally 150-250 microns), single-crystal XRD can provide detailed information about molecular arrangement and structural parameters.[73] For gel samples, the molecular arrangement within a fiber might be ordered. However, the alignment of the fibers in gels is essentially random, unlike the highly ordered arrangements in crystals. Thus, gel samples will not show a well-defined diffraction pattern in XRD, making it difficult to directly get the packing patterns of molecules in gel samples. To study the molecular arrangement in the gels using XRD, two approaches are usually taken:

The first strategy is to obtain the crystals of the gelator under conditions similar to those that cause gelation. Single-crystal XRD analysis of gelator crystals provides a model that can help suggest what molecular arrangement is favored in the gel. With this method, Kim and colleagues got an insight into the molecular arrangement of hydrogelator cucurbit[7]uril (CB[7]) in fibrous structure from the single-crystal XRD of CB[7] needle crystals.[74] The CB[7] molecules form zigzagged columns owing to C-H ⋯ O hydrogen bonds. The water/hydronium ions between the columns will "glue" them together to form thicker units, followed by the bundling process that finally leads to the observed fibrous network (gel) (Figure 1.20).

Another method is to use small-angle X-ray scattering (SAXS), which detects the scattering intensity at small angles ($2\theta \leq 2°$) (Figure 1.21). In this case, the resolution is nanoscale instead of atomic scale as in wide-angle XRD (WAXS), and the technique provides parameters related to aggregation, such as shape, size, and surface-to-volume ratio. Experimental SAXS data from gel samples can be compared with the fit of the calculated model (helical, cylindrical, spherical, and so on) to get information about the shape and size of aggregates in the gel system. Likewise, small-angle neutron scattering (SANS) can be used to study gels. Draper and coworkers[75] used small-angle scattering techniques to study the packing of low-molecular-weight gelator 2NapFF with its selective deuterated analogs (Figure 1.22). Through comparing the experimental scattering results

and the fitting to models, they found that all three analogues pack into a cylinder model, with similar radii (4 nm to 4.3 nm), consistent with the cryo-TEM result (Figure 1.22).

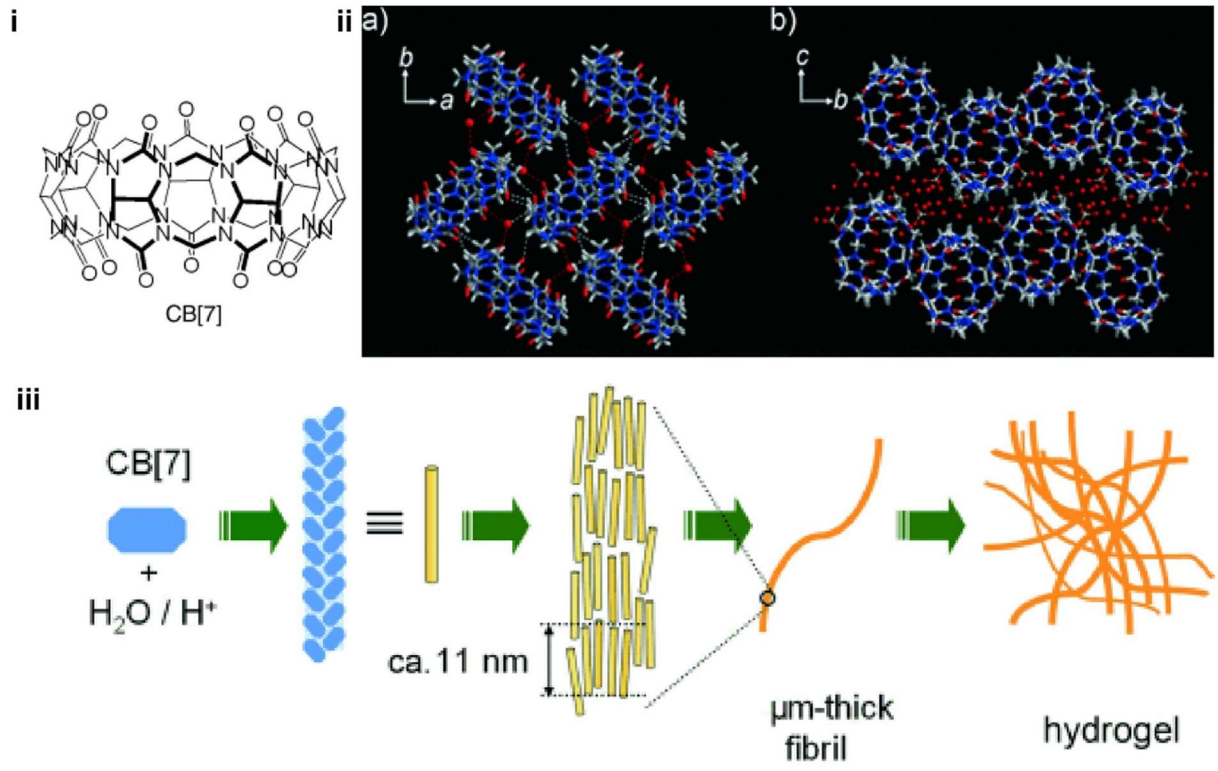

Figure 1.20. (i) Molecular structure of cucurbit[7]uril (CB[7]). (ii) X-ray crystal structure of CB[7]. Colour codes: gray C, blue N, red O, white H. Guest molecules of acetone are omitted for clarity. a) Organization of CB[7] molecules on the *ab*-plane. b) Packing in the *bc*-plane. (iii) Schematic representation of the hierarchical assembly of CB[7] gel. Figures reproduced from ref. 74 with permission. Copyright (2007) Wiley-VCH Verlag GmbH & Co. KGaA, Weinheim.

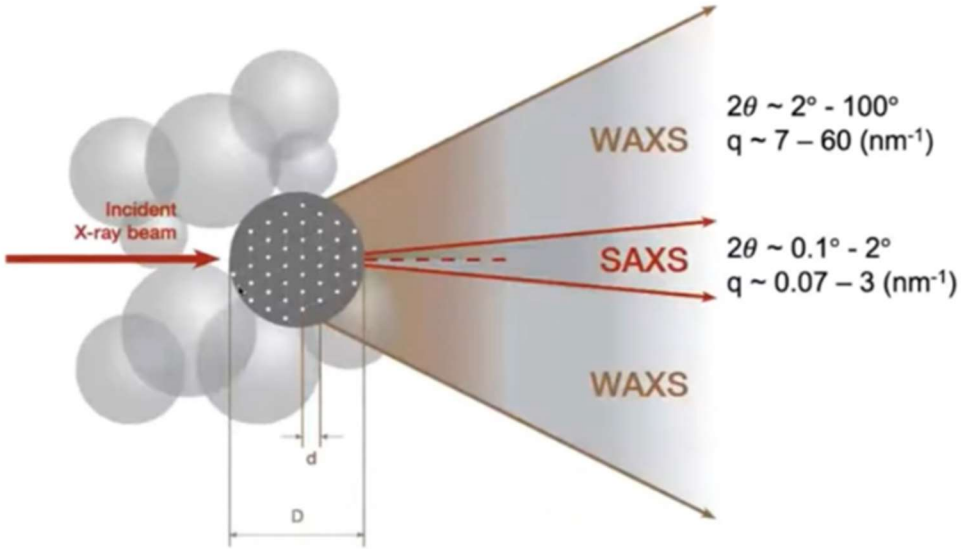

Figure 1.21. Schematic comparison of SAXS with WAXS. q value (momentum transfer in reciprocal-space) corresponds to a real-space distance (d). Figure from ref. [168]. Copyright (2013) Anton Paar GmbH, Austria.

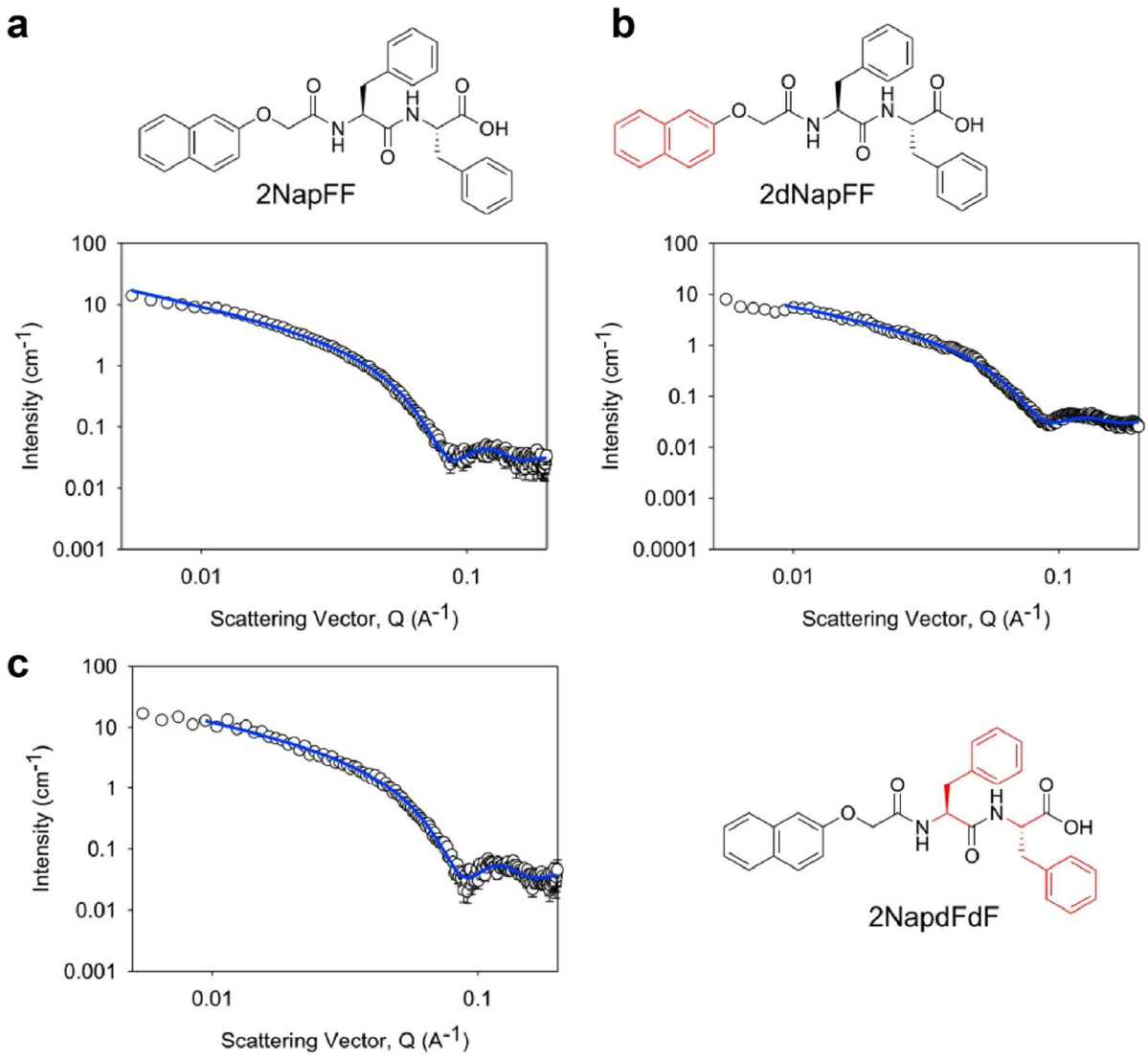

Figure 1.22. Comparison of SAXS data for (A) 2NapFF, (B) 2dNapFF, (C) 2NapdFdF at 10 mg/mL in D_2O (empty circle: data, blue lines: fit to a cylinder model, red: deuterated sections). Figure reproduced from ref. 75 with permission. Copyright (2020) Elsevier Inc.

1.3.2.4 Other spectroscopy methods

In addition to all the characterization methods introduced above, many other methods, including infrared spectroscopy (IR), fluorescence spectroscopy, and circular dichroism (CD) spectroscopy, can provide useful and interesting information about the structural changes and

intermolecular interactions that arise in gelation/crystallization. The fourth part of this introductory chapter will present specific examples of the use of these methods in the study of bile acids and their derivatives.

1.4 Bile acids and their derivatives: structures, properties, and applications

1.4.1 Structures of bile acids

Bile acids are amphiphilic molecules that widely exist in the digestive system of vertebrates and humans to facilitate the absorption of fat and other fat-soluble nutrients.[76,77] Owing to their natural abundance and biocompatibility, bile acids and their derivatives are promising for use as components of functional material, especially for medical applications. Bile acids have been used to design and prepare interesting materials useful as stimulus-responsive drug delivery nanocarriers,[78,79] dental materials,[80,81] gels,[82–86] and CO_2 absorbents.[32] The bile acid-based materials exhibit various physical and chemical properties, rooted in the structures and arrangement patterns of bile acids and their derivatives. This section will start with the structures of bile acids and their packing patterns, followed by several examples of bile acid derivatives.

Based on the biosynthetic routes, primary bile acids are synthesized from cholesterol in the liver. Secondary bile acids are converted from the primary bile acids by colonic bacteria in the intestine (Figure 1.23a).[87,88] Both primary and secondary bile acids are often conjugated with glycine or taurine, forming the conjugated bile acids.[87,89] Bile acids are steroid compounds with a rigid skeleton made of three six-membered rings and one five-membered ring. Cholic acid is the most hydrophilic among the non-conjugated bile acids; the hydrophobic methyl groups and the hydrophilic hydroxyl groups are arranged on the convex and concave sides, respectively, of the steroid skeleton, resulting in a “facial amphiphilicity” (Figure 1.23b). Bile acids with fewer hydroxyl groups may only have a hydrophilic “edge”. The rigidity of the steroid skeleton, the number and the position of the hydroxyl groups and the degree of protonation of the carboxylic acid group on the lateral chain affect hydrogen bonding and the structures resulting from self-assembly.

Bile acids are different from the simple head-tail amphiphiles, making it challenging to calculate the packing parameters (Figure 1.5 in part 2) for packing geometry prediction. Fortunately, in bile acids, the rigid polycyclic structure limits the number of accessible conformations; moreover, the position of hydroxyl groups and the directionality of hydrogen-bonds contribute additional "rigidity" into aggregates composed of bile acids. These structural features make bile acids uniquely interesting candidates for the study of molecular packing and morphology.

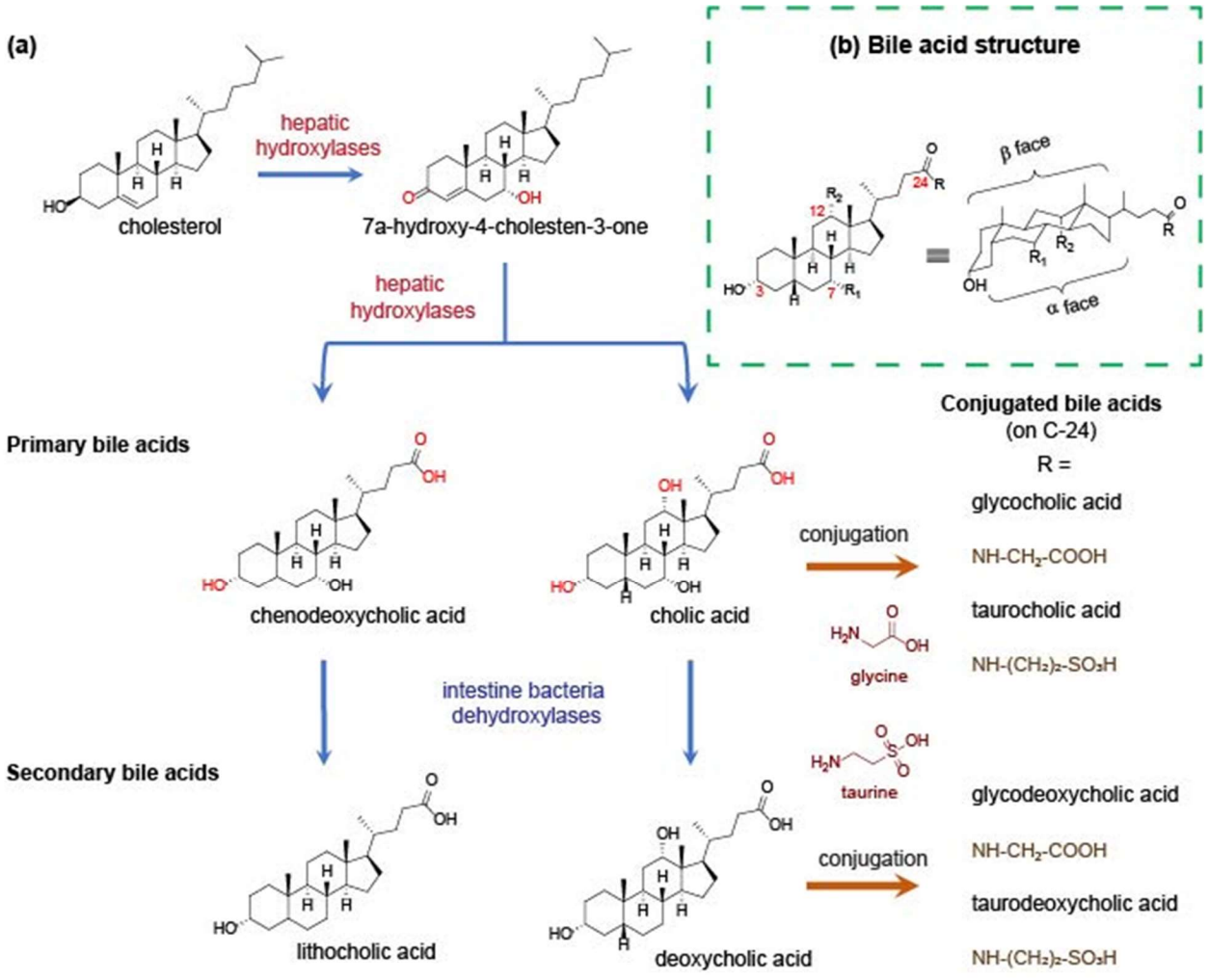

Figure 1.23. (a) The structures of bile acids and their biosynthetic pathways. (b) Structure of bile acids. The numbers indicate some specific carbon positions.

1.4.2 Micelles of bile salts

Bile acids usually exist as sodium salts in the gastrointestinal tract, known as bile salts. Bile salts form micelles in the body for the digestion of fats in food. The micellization of bile acids is a good starting point to explore bile acid self-assembly. The driving force of the micellization of bile salts is the formation of intermolecular hydrogen bonds and the creation of hydrophobic interactions.[90,91] Compared to classical amphiphiles, bile salts show a broader transition range instead of a single critical micellar concentration (CMC), indicating a continuous micellar aggregation phenomenon.[92–94] The CMC values measured for bile salts depend on temperature,[95,96] ionic strength,[93,96] the specific bile salt used,[93–99] and even the detection techniques used for the measurements.[93] At ambient temperature, the CMCs of trihydroxy bile salts are higher than those of the dihydroxy bile salts, and in the dihydroxyl bile acids, chenodeoxycholate shows slightly higher CMCs than deoxycholate salts.[28,93,97,98] For example, Norman et al. measured the first-stage association of bile salts based on the solubilization of 20-methylcholanthrene in aqueous solutions.[98] The CMCs of the sodium bile salts measured under their experimental conditions follow the order cholate (12 mM) > chenodeoxycholate (6 mM) > deoxycholate (5 mM) > lithocholate (1 mM), reflecting the influence of the number and position of hydroxyl groups on the association process of bile salts.[98,100] The stepwise micellization process, including primary and secondary bile acid micelles (Figure 1.24), has been studied by different techniques.[8,9,101,102] In the standard model, the primary micelles are formed through hydrophobic interaction of the convex faces. At higher concentrations, the primary micelles can form secondary micelles through hydrogen bonding. This model was further confirmed by Bohne et al. based on a study of the quenching of excited triplet probe molecules, depending on the state of association of bile salt aggregates.[102,103] The result revealed that the binding sites of primary aggregates are hydrophobic and well-protected, while the secondary micelles have binding sites that are relatively hydrophilic and more exposed to the aqueous solution. [102,103] Using fluorescence probe molecules was also a powerful way to help estimate and compare the different aggregation dynamics of bile acids.[8] Inspired by the previous investigation of how bile salt aggregates interact with probe molecules, Meier and colleagues used chiral selective guest molecules to explore the primary and secondary micellization process for cholate and deoxycholate and the interesting change of chiral selection during each step of this process. [9]

According to the primary/secondary micelles model, the initial aggregates are formed by the interaction of hydrophobic faces. A similar interaction pattern is also postulated in the disk-like model of bile acid aggregation (Figure 1.25C).[104] In addition to the models of primary/secondary micelles,[101] and disk-like micelles[104] discussed above, a helical micelle model was also proposed.[105–107] The structure of the helical micelle is similar to inverted micelles with nonpolar groups facing the aqueous environment (Figure 1.25D). This model is based on the small-angle X-ray scattering (SAXS) results, and it also assumes the coherence of the micellar structure with the helical crystalline structure reported for rubidium deoxycholate.[106,107] In sum, the micellar structures of bile salts have not been determined unambiguously and further work is needed. As a result, the aggregation of bile salts from preliminary stages to the formatiuon of higher-order assemblies continues to draw the attention of many researchers exploring various topics, including the self-association patterns of cholesterol derivatives and the role of bile acids in digestion.[108]

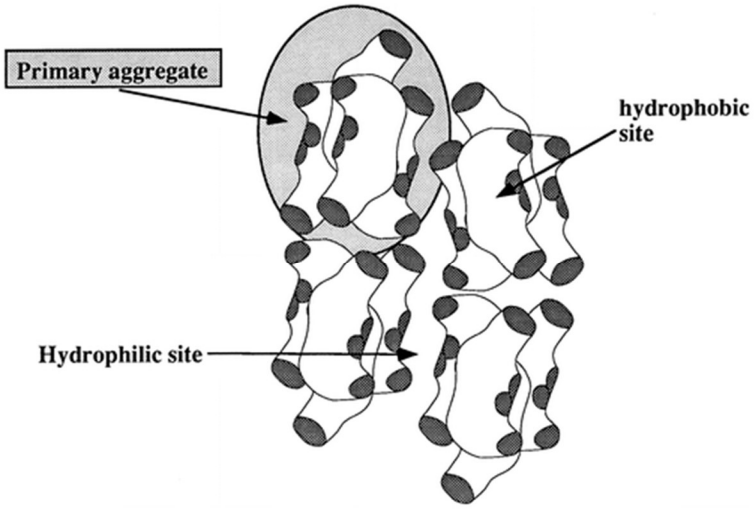

Figure 1.24. Schematic illustration of primary aggregation (in the circle) and secondary aggregation of bile salts. The dark areas correspond to the position of the hydroxyl and carboxyl groups, and the aggregation number of 4 and relative positioning of the bile salt monomers is arbitrary. Figure reproduced from ref. [103] with permission. Copyright (1996) American Chemical Society.

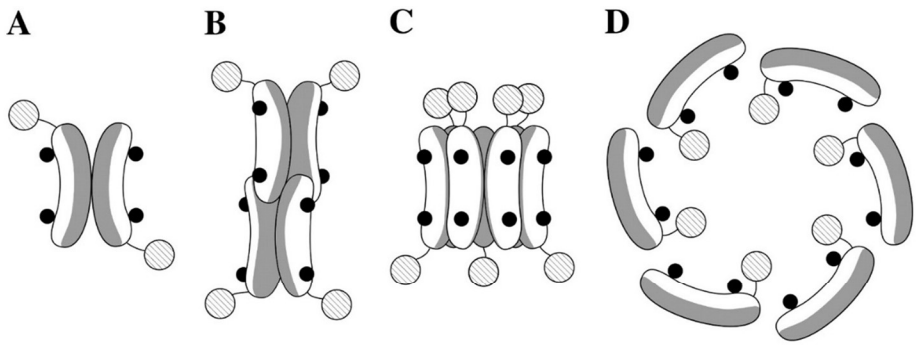

Figure 1.25. Schematic representation of different micellar models. (A, B) Different primary micelles. (C). Disk-like micelle. (D). Helical structure observed from the top. Figure reproduced from ref. [105] with permission. Copyright (2010) Elsevier Ltd.

1.4.3 Higher-order structures of bile salts

Forming higher-order structures involves intermolecular interactions such as hydrogen bonds, ionic interactions, and hydrophobic interactions as bridges to connect smaller subunits produced by initial aggregation of bile salts.

The influence of pH on behaviour of bile salts has been studied in different ways, especially for deoxycholate.[109–111] Lowering the pH of aqueous solutions of sodium deoxycholate (NaDC) decreases solubility, can increase the viscosity, and can even lead to gelation of the system. Previous work in our group explored the gelation of aqueous solutions of bile salts induced by exposure to CO_2.[32] Carbonic acid formed by the reaction of CO_2 with water can protonate some of the carboxylate groups in NaDC. Gelation then results from interconnecting micelles through hydrogen bonding between the protonated carboxylate groups, yielding a transparent gel. Higher CO_2 concentrations can produce fiber bundles, resulting in an opaque gel (Figure 1.26). The gradual protonation of the carboxylate groups in aqueous solutions of NaDC with CO_2 was also characterized using Fourier transform-infrared (FT-IR) spectroscopy. The aggregation of bile salts can be promoted with reduced repulsion among the charged heads at lower pH values or higher ionic strength. [112]

Because of the distribution of hydroxyl groups and methyl groups on the α and β faces of cholate, respectively, cholates can form a bilayer structure in which the molecules are organized in

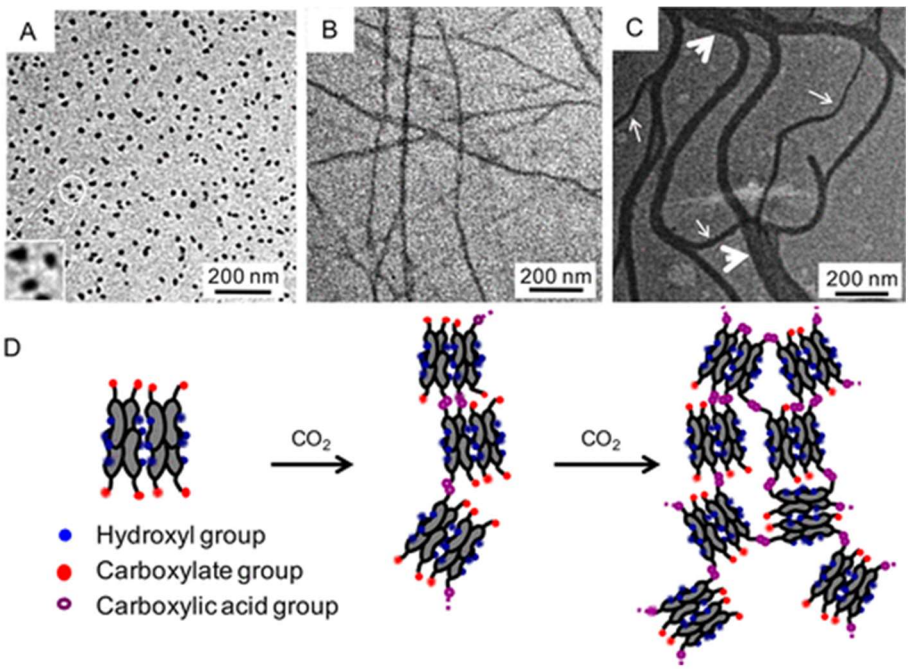

Figure 1.26. (A) TEM images of micelles in 10 mM aqueous solution of NaDC. (B) TEM image of fibers in an aqueous solution made by mixing of NaDC (10 mM) and CO_2 (4 mM). (C) TEM image of thick bundles of fibers in an aqueous mixture of NaDC (10 mM) and CO_2 (40 mM). (D) Schematic representation of the formation of hydrogels from aqueous solutions of NaDC and further aggregation with increasing contents of CO_2. Figures reproduced from ref. 32 with permission. Copyright (2019) American Chemical Society.

an α-face-to-α-face fashion.[113–115] More specifically, the hydroxyl group at the C-3 position of one cholate links the two hydroxyl groups (C-7 and C-12) in the other two molecules related by a 2-fold screw axis (Figure 1.27).[113–115] This bilayer structure was first discussed in the crystalline state of cholate and its derivatives.[113,114] In 2009, Qiao and colleagues obtained uniform, right-handed nanohelices of calcium cholate in an aqueous environment (Figure 1.27).[115] Based on the high-resolution TEM, SAXS, and FT-IR results, they proposed the possible molecular packing pattern as consisting of bilayer strips of cholate connected through metal-carboxyl coordination (Figure 1.27).[115] Other metal ions, such as Cu^{2+}, Co^{2+}, Zn^{2+}, Cd^{2+}, Hg^{2+}, and Ag^{+} can also form interesting structures or even generate hydrogels when mixed with bile salt solutions.[115–118] The metal ions play essential roles in connecting the bile salt aggregates together as a network.[115–117]

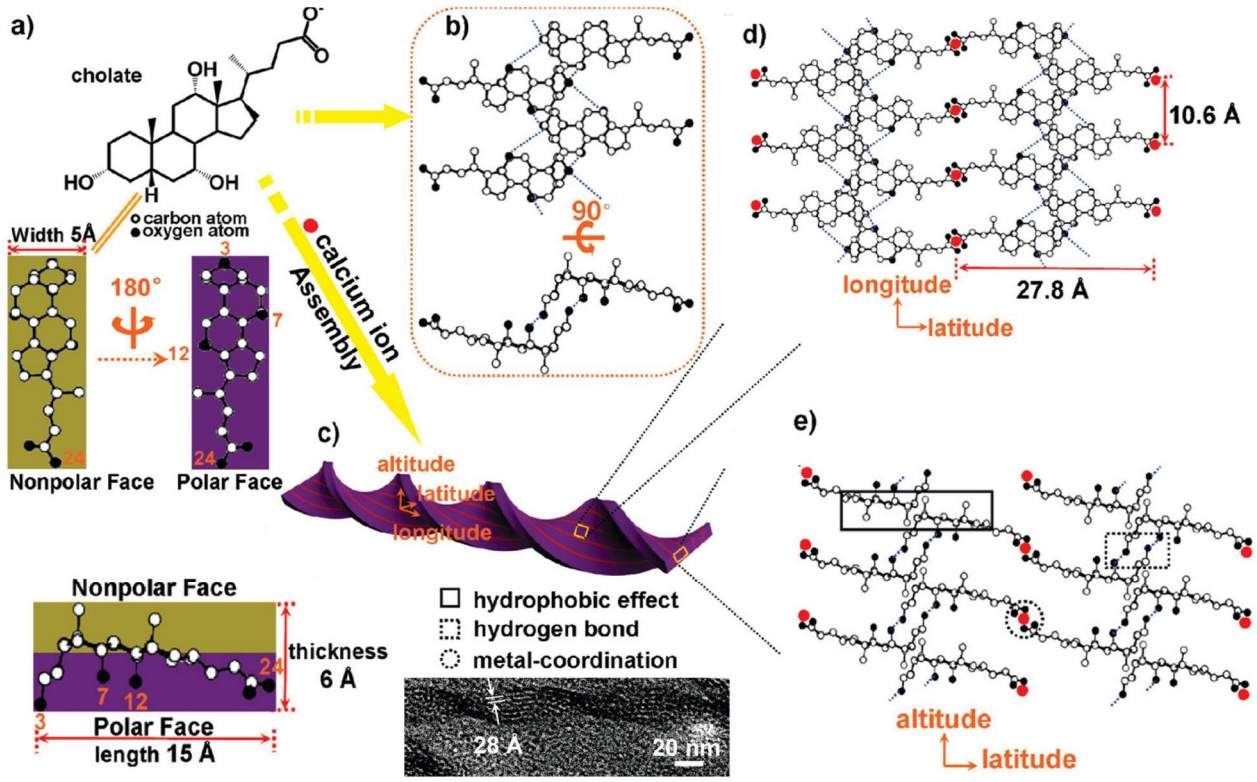

Figure 1.27. Schematic model of the nanohelix. (a) Molecular structure and backbone of cholate illustrating the facial amphiphilicity and molecular size. (b) The molecular aggregate as the minimum constitution unit of a bilayer type of cholate host framework (blue dotted lines: hydrogen -bonds). (c) TEM image of nanohelix and scheme of twisted nanoribbon composed of parallel, longitudinal strips. (d) Top view of the molecular model. (e) Corresponding cross-section view. Figures reproduced from ref. [115] with permission. Copyright (2009) American Chemical Society.

1.4.4 Functionalized bile acids

The previous examples are based on the self-assembly of natural bile salts. However, bile acids can be modified easily to give unnatural derivatives, and functionalization of bile acids has been carried out by many researchers.[30] The reactivity of the carboxyl group and hydroxyl groups makes them particularly easy to modify. Examples of functionalized bile salts are provided below.

Modifications of the carboxyl group or functionalization at C-24 of bile acids/salts were reported in studies involving both crystallization and the formation of gels. Sada et al. compared crystals of cholic acid with bishomocholic acid (compound **2** in Figure 1.28a) and achieved the

controlled expansion of a molecular cavity in the crystals using elongation of the side chain at C-24 (Figure 1.28b).[119] The C-24 functionalized bile acid gelators also show interesting stimuli-responsiveness. For example, a picolinic acid-conjugated bile acid derivative (compound **3** in Figure 1.28a) can form a gel in the presence of Cu^{2+} in organic and aqueous solvent mixtures.[120] The gel-sol transition of this system can be triggered by many factors such as the presence of additional reagents, heating, and sonication (Figure 1.28c). Another example is a phenanthroline-functionalized cholic acid (compound **4** in Figure 1.28a), which was an effective gelator for methanol-water; however, in the presence of Zn^{2+}, the white gel became a transparent liquid at room temperature.[121]

Modifications of the hydroxyl groups of bile acids usually start from the functionalization of hydroxyl on C-3, as it is more accessible. The example of naphthoylamine-substituted cholic acid (NaphC) in Figure 1.29 shows that its self-assembled structure changes from scrolls or tubules into ribbons by heating, and the transition from single-wall tubules to rolled sheets occurs with the addition of NaCl.[122] Zhao et al. functionalized C-3 with the β-NH_2 group to form crystals with higher guest inclusion with methanol than the previous bile acid in inclusion compounds.[123] The formation of larger channels in this C-3 functionalized bile acid crystal is related to the ammonium-carboxylate interaction and the rigidity of the bile acid moiety.[123] Other substitution groups on C-3 of bile acids such as *p-tert*-butylphenylamide,[124] phenylalanine,[125] and D-mannose[126] were also reported.

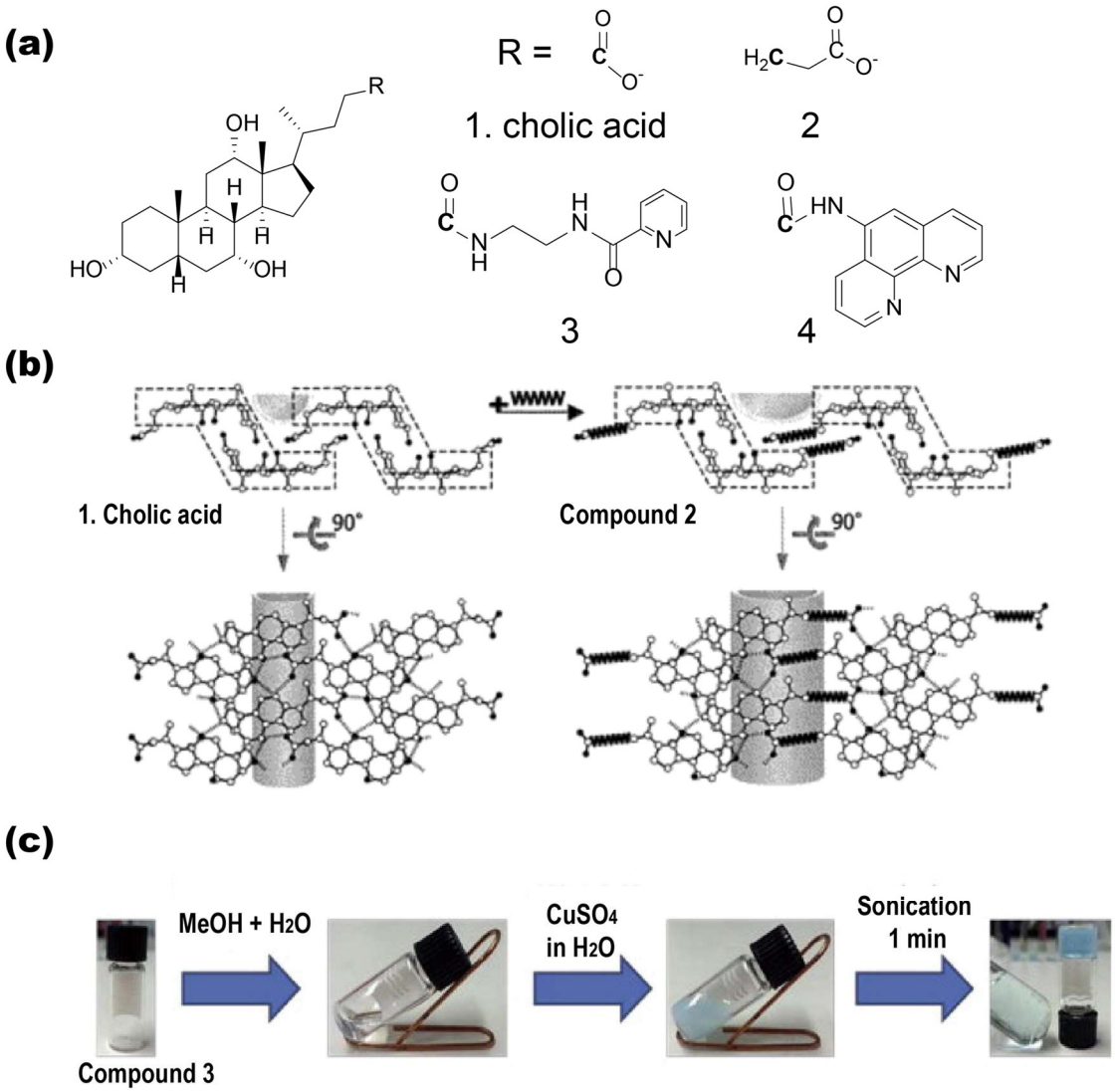

Figure 1.28. Examples of derivatives of bile acids functionalized at C-24. (a) Structures of cholic acid and its derivatives 2, 3, and 4 functionalized at C-24. (b) Schematic illustration of an expanded host cavity by elongation of the cholic acid. (c) Sonication-induced gelation caused by treating compound 3 with $CuSO_4$ (1:1) in aqueous MeOH (30%). Figures reproduced with permission from ref. [119] Copyright (2001) American Chemical Society and ref. [120] Copyright (2015) Elsevier Inc.

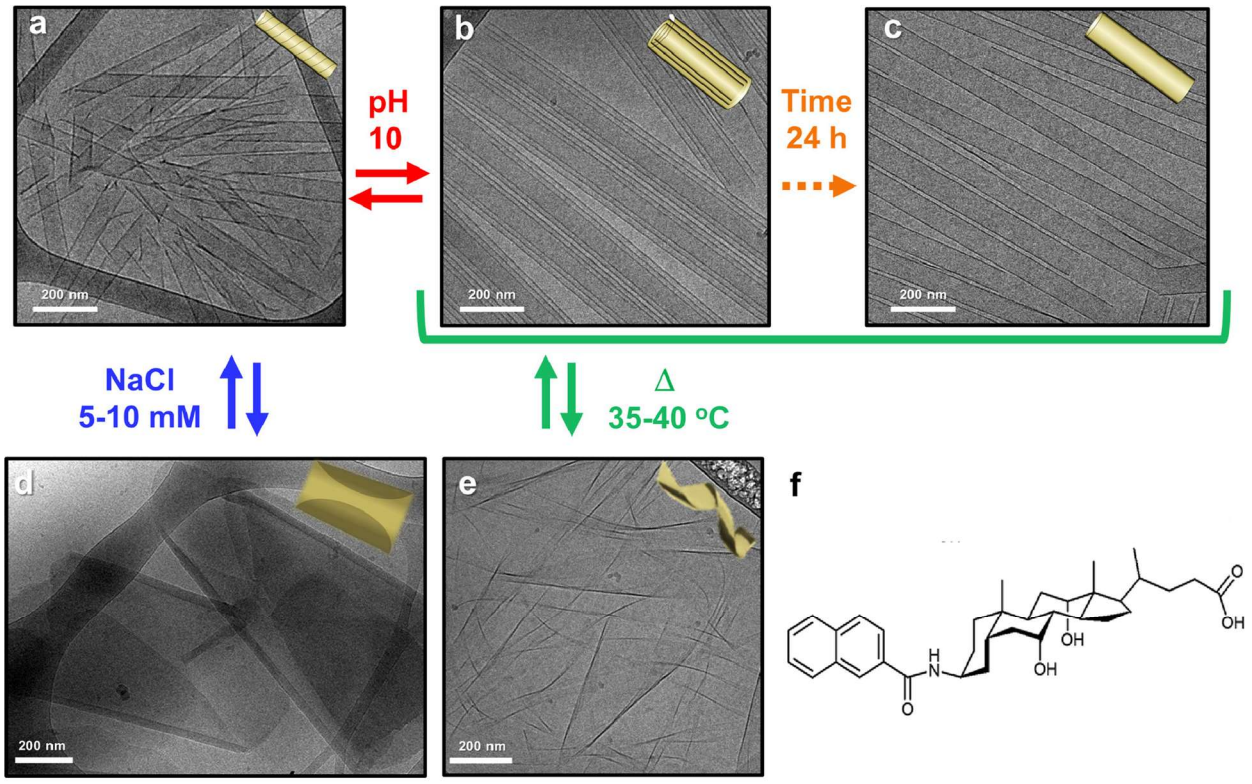

Figure 1.29. Multistimuli response of C-3-substituted derivative NaphC. Cryo-TEM micrographs showing the structures forming in a buffer solution at pH 8.5 (a), pH 12.3 (b) pH 12.3 after 24 h (c), pH 12.0 and NaCl 20 mM (d), and pH 12.3 and 55 °C (e). The arrows between the micrographs indicate the direction and the triggering parameters of the structural transitions. A schematic representation of the structures is in the top right of each micrograph. (f). Chemical structure of NaphC. Figures reproduced with permission from ref. 30 Copyright (2019) American Chemical Society and ref. [122] Copyright (2015) Royal Society of Chemistry.

Bile acids can be substituted at C-3 and C-24 by groups such as adamantyl and triethylamine.[127] They can also be substituted by grafting polymers at different positions. Figure 1.30 shows the grafting of poly(ethylene glycol) chains to different bile acids. These nonionic surfactants can form spherical aggregates potentially useful as drug carriers (Figure 1.30I).[128] There is also design of star-shaped block copolymers with a cholic acid core and pendant amine groups

(Figure 1.30II).[129] The poly (allyl glycidyl ether) (PAGE) and polyethylene glycol (PEG) blocks contribute to the thermoresponsive properties of the material.

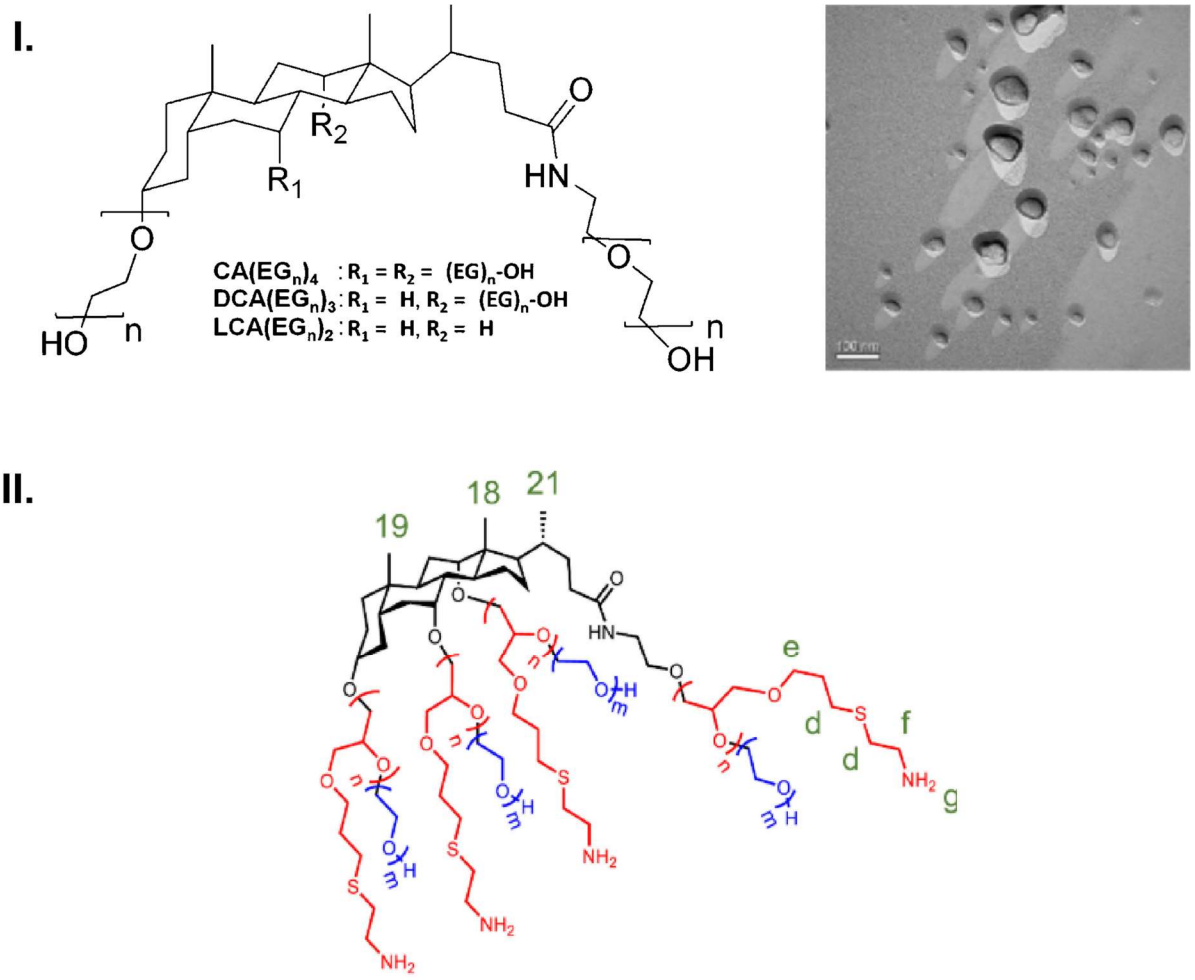

Figure 1.30. (I). Pegylated bile acid structures (left) and TEM micrographs of freeze-fractured $CA(EG_8)_4$ samples (right). (II) Structure of CA-(PAGE-NH_2-*b*-PEG) with a cholic acid core and poly (allyl glycidyl ether) (PAGE) and poly (ethylene glycol) (PEG) blocks. Figures reproduced with permission from ref. [128]. Copyright (2012) American Chemical Society and ref. [129]. Copyright (2021) Elsevier Ltd.

The dimer, trimer, and oligomer of bile acids also showed promising results in self-assembly studies (Figure 1.31). For example, Zhang et al. studied hydrogel formation by mixing cholic acid dimer with various acids.[31] Synthesized bile acid trimers have also proved to be effective hydrogelators in the presence of acetic acid.[130,131] The properties of oligomeric bile acids were

influenced by the repeating units and the spacer between them.[132,133] The bile acid oligomers can fold into nanocavities and defold under stimuli such as the polarity of the solvent[134] and metal ions.[135]

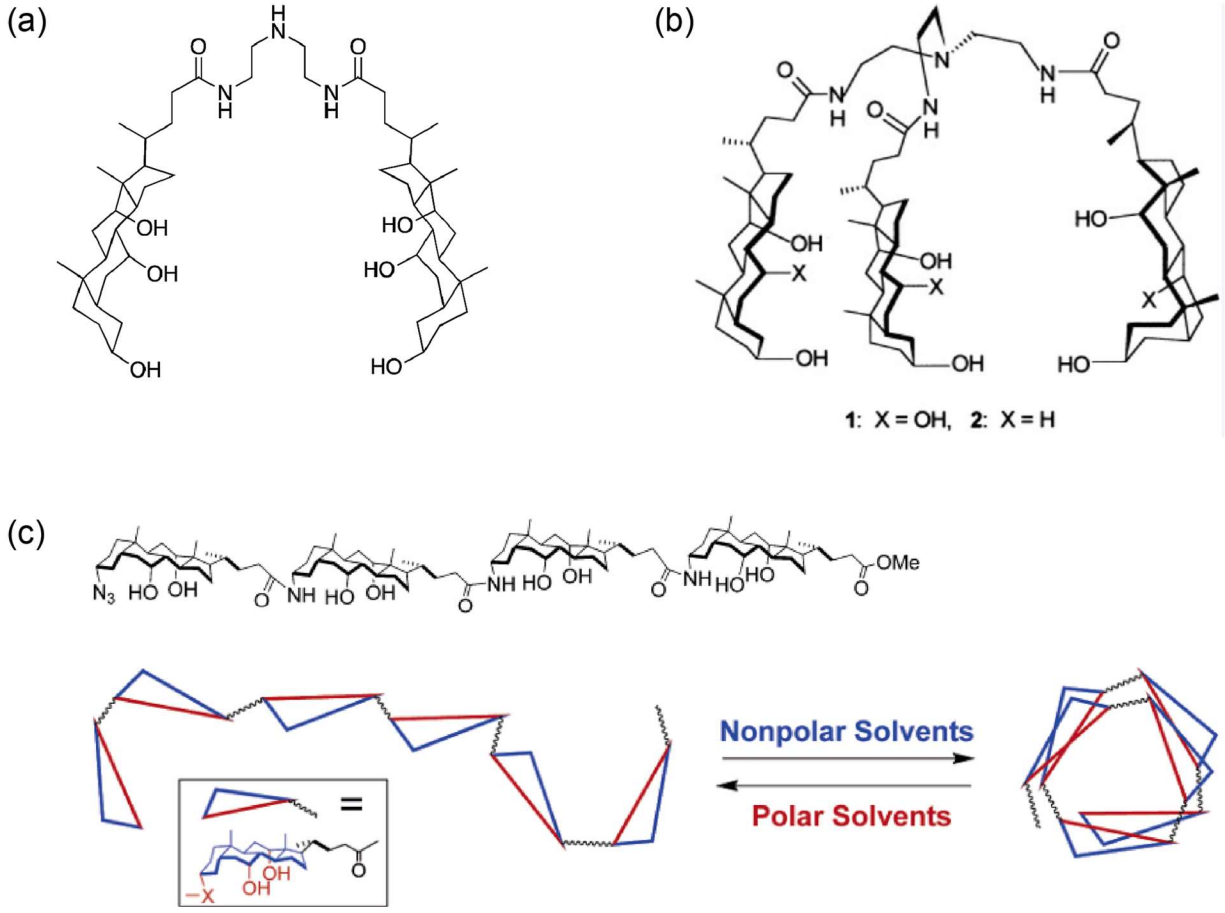

Figure 1.31. (a) Chemical structure of a dimeric derivative of cholic acid. Copyright (2016) Royal Society of Chemistry. (b) Related trimer derived from bile acids. Copyright (2001) Wiley-VCH Verlag GmbH, Weinheim, Fed. Rep. of Germany. (c) Cholate oligomers that fold/unfold with different solvents. Copyright (2005) American Chemical Society. Figures reproduced from ref. [85,130,134] with permission.

Owing to unique features of their structures, bile acids/salts and their derivatives provide many valuable tools for studies of self-assembly. The biocompatibility and abundance of bile acids make them promising candidates for biomedical applications like drug delivery and tissue engineering.

1.5 Research objectives and the content of the thesis

The objectives of this thesis include to understand gelation mechanism at the molecular level by spectroscopy and to explore conditions of gelation and crystallization by using various salts of bile acids.

This thesis contains five chapters, including this introductory chapter (Chapter 1) and the last chapter of conclusion and perspectives (Chapter 5). Chapters 2-4 are research manuscripts published or submitted to peer-reviewed journals. All the work presented has been mainly performed by the author of the thesis under the supervision of Prof. Julian Zhu and Prof. James D. Wuest. Our collaborators in the department of chemistry also contribute to the characterization and analysis of the results. Dr. Cédric Malveau helped with the NMR experiments and is the co-author for the research paper in Chapter 2. Dr. Thierry Maris contributed to the XRD measurements and the crystal structure analysis. Dr. Meng Zhang provided valuable suggestions on some designs of the experiments. Because of their contributions, Dr. Meng Zhang and Dr. Thierry Maris are co-authors for the research papers in Chapters 3 and 4. The thesis aims to understand better the relationship between gelation and crystallization at molecular level. The unique structure of bile acids makes them ideal candidates for a detailed, systematic study of molecular arrangements in gels and crystals. Hopefully, our research will shed light on the relationship between gelation and crystallization and inspire the design of new materials based on bile acids.

Chapter 2 shows the application of nuclear magnetic resonance (NMR) spectroscopy to understand the gelation process on the molecular level. We used different NMR techniques to probe hydrogel formation, and we analyzed molecular interactions in mixtures of sodium deoxycholate (NaDC) and formic acid.

Chapter 3 presents our systematic study of the aggregation of a series of ammonium salts of lithocholic acid in an aqueous environment. The nature of the aggregation changes from gelation to crystallization as the ammonium counterions are varied, and we analyzed the molecular arrangement by using X-ray diffraction (XRD) to reveals the intimate relationship between gelation and crystallization in this system.

Chapter 4 explores the relationship between crystallization and gelation in mixtures containing a broader range of bile acids and alkylamines. The effects of the hydrophobicity of bile

acids and the alkyl chain length of amines on self-assembled structures were examined in detail. The bile salts show a strong preference for edgewise association in the anisotropic growth of crystals and fibers.

Chapter 5 is an overall summary of the work in this thesis and the perspectives for further exploration of the gelation and crystallization relationship and the potential design of bile acids-based materials.

1.6 References

(1) Hanabusa, K.; Suzuki, M. FOCUS REVIEW Development of Low-Molecular-Weight Gelators and Polymer-Based Gelators. *Polym. J.* **2014**, *46*, 776–782. https://doi.org/10.1038/pj.2014.64.

(2) Fameau, A. L.; Rogers, M. A. The Curious Case of 12-Hydroxystearic Acid — the Dr. Jekyll & Mr. Hyde of Molecular Gelators. *Curr. Opin. Colloid Interface Sci.* **2020**, *45*, 68–82. https://doi.org/10.1016/J.COCIS.2019.12.006.

(3) TachibanaTaro; KambaraHideko. Studies of Helical Aggregates of Molecules. I. Enantiomorphism in the Helical Aggregates of Optically Active 12-Hydroxystearic Acid and Its Lithium Salt. *http://dx.doi.org/10.1246/bcsj.42.3422* **2006**, *42* (12), 3422–3424. https://doi.org/10.1246/BCSJ.42.3422.

(4) Thierry Brotin; Ralf Utermöhlen; Frédéric Fages; Henri Bouas-Laurent; Jean-Pierre Desvergne. A Novel Small Molecular Luminescent Gelling Agent for Alcohols. *J. Chem. Soc. Chem. Commun.* **1991**, *0* (6), 416–418. https://doi.org/10.1039/C39910000416.

(5) Terech, P.; Weiss, R. G. Low Molecular Mass Gelators of Organic Liquids and the Properties of Their Gels. *Chem. Rev.* **1997**, *97* (8), 3133–3159. https://doi.org/10.1021/cr9700282.

(6) Terech, P.; Everine Friol, S. Rheometry of an Androstanol Steroid Derivative Paramagnetic Organogel. Methodology for a Comparison with a Fatty Acid Organogel. **2007**. https://doi.org/10.1016/j.tet.2007.02.067.

(7) Terech, P.; Ramasseul, R.; Volino, F. Electron Spin Resonance Study of the Gel Formed by a Spin-Labeled Steroid in Cyclohexane and Determination of the Phase Diagram. *J. Colloid Interface Sci.* **1983**, *91* (1), 280–282. https://doi.org/10.1016/0021-9797(83)90334-X.

(8) Li, Y.; Holzwarth, J. F.; Bohne, C. Aggregation Dynamics of Sodium Taurodeoxycholate and Sodium Deoxycholate. *Langmuir* **1999**, *16* (4), 2038–2041. https://doi.org/10.1021/LA9903705.

(9) Meier, A. R.; Yehl, J. B.; Eckenroad, K. W.; Manley, G. A.; Strein, T. G.; Rovnyak, D. Stepwise Aggregation of Cholate and Deoxycholate Dictates the Formation and Loss of Surface-Available Chirally Selective Binding Sites. *Langmuir* **2018**, *34* (22), 6489–6501. https://doi.org/10.1021/ACS.LANGMUIR.8B00467.

(10) Zweep, N.; Van Esch, J. H. The Design of Molecular Gelators. https://doi.org/10.1039/9781849737371-00001.

(11) Singh, A.; Auzanneau, F. I.; Rogers, M. A. Advances in Edible Oleogel Technologies – A Decade in Review. *Food Res. Int.* **2017**, *97*, 307–317. https://doi.org/10.1016/J.FOODRES.2017.04.022.

(12) Singh, A.; Auzanneau, F.-I.; Corradini, M. G.; Grover, G.; Weiss, R. G.; Rogers, M. A. Molecular Nuances Governing the Self-Assembly of 1,3:2,4-Dibenzylidene-d-Sorbitol. *Langmuir* **2017**, *33* (41), 10907–10916. https://doi.org/10.1021/ACS.LANGMUIR.7B02191.

(13) Kumar, D. K.; Steed, J. W. Supramolecular Gel Phase Crystallization: Orthogonal Self-Assembly under Non-Equilibrium Conditions. *Chem. Soc. Rev.* **2014**, *43* (7), 2080–2088. https://doi.org/10.1039/c3cs60224a.

(14) Gallant, M.; Viet, M. T. P.; Viet, M. T. P.; Wuest, J. D. Use of Hydrogen Bonds To Control Molecular Aggregation. Association of Dipyridones Joined by Flexible Spacers. *J. Org. Chem.* **1991**, *56* (7), 2284–2286. https://doi.org/10.1021/jo00007a007.

(15) Ducharme, Y.; Wuest, J. D. Use of Hydrogen Bonds to Control Molecular Aggregation. Extensive, Self-Complementary Arrays of Donors and Acceptors. *J. Org. Chem.* **1988**, *53* (24), 5787–5789. https://doi.org/10.1021/jo00259a037.

(16) Fournier, J. H.; Maris, T.; Wuest, J. D.; Guo, W.; Galoppini E. Molecular Tectonics. Molecular Tectonics. Use of the Hydrogen Bonding of Boronic Acids To Direct Supramolecular Construction. *J. Am. Chem. Soc.* **2002**, *125* (4), 1002–1006. https://doi.org/10.1021/JA0276772.

(17) Chang, S. K.; Hamilton, A. D. Molecular Recognition of Biologically Interesting Substrates: Synthesis of an Artificial Receptor for Barbiturates Employing Six Hydrogen

Bonds. *J. Am. Chem. Soc.* **1988**, *110* (4), 1318–1319.

(18) Mahoney, M. W.; Jorgensen, W. L. A Five-Site Model for Liquid Water and the Reproduction of the Density Anomaly by Rigid, Nonpolarizable Potential Functions. *J. Chem. Phys.* **2000**, *112* (20), 8910. https://doi.org/10.1063/1.481505.

(19) Khalak, Y.; Baumeier, B.; Karttunen, M. Improved General-Purpose Five-Point Model for Water: TIP5P/2018. *J. Chem. Phys.* **2018**, *149* (22), 224507. https://doi.org/10.1063/1.5070137.

(20) Israelachvili, J. Intermolecular and Surface Forces. *Intermol. Surf. Forces* **2011**. https://doi.org/10.1016/C2009-0-21560-1.

(21) Thomas, G. Liquid Diffusion Applied to Analysis. *Proc. R. Soc. London* **1862**, *11*, 243–247. https://doi.org/10.1098/RSPL.1860.0048.

(22) D'Urso, E. M.; Fortier, G. New Hydrogel Based on Polyethylene Glycol Cross-Linked with Bovine Serum Albumin. *Biotechnol. Tech. 1994 82* **1994**, *8* (2), 71–76. https://doi.org/10.1007/BF00152843.

(23) Millon, L. E.; Mohammadi, H.; Wan, W. K. Anisotropic Polyvinyl Alcohol Hydrogel for Cardiovascular Applications. *J. Biomed. Mater. Res. Part B Appl. Biomater.* **2006**, *79B* (2), 305–311. https://doi.org/10.1002/JBM.B.30543.

(24) Jabbari, E.; Nozari, S. Swelling Behavior of Acrylic Acid Hydrogels Prepared by γ-Radiation Crosslinking of Polyacrylic Acid in Aqueous Solution. *Eur. Polym. J.* **2000**, *36* (12), 2685–2692. https://doi.org/10.1016/S0014-3057(00)00044-6.

(25) Yuan, Z.; Lu, W.; Liu, W.; Hao, J. Gel Phase Originating from Molecular Quasi-Crystallization and Nanofiber Growth of Sodium Laurate-Water System. *Soft Matter* **2008**, *4* (8), 1639–1644. https://doi.org/10.1039/b804157a.

(26) Zawko, S. A.; Schmidt, C. E. Assembly of Sodium Soap Fibers and Fibrillar Particles Triggered by Dissolution of Sodium Chloride Crystals. *Soft Matter* **2010**, *6* (14), 3289–3297. https://doi.org/10.1039/c002084b.

(27) Arakawa, H.; Takeda, K.; Higashi, S. L.; Shibata, A.; Kitamura, Y.; Ikeda, M. Self-Assembly and Hydrogel Formation Ability of Fmoc-Dipeptides Comprising α-Methyl-L-Phenylalanine. *Polym. J.* **2020**. https://doi.org/10.1038/s41428-019-0301-5.

(28) Madenci, D.; Egelhaaf, S. U. Self-Assembly in Aqueous Bile Salt Solutions. *Current Opinion in Colloid and Interface Science*. 2010.

https://doi.org/10.1016/j.cocis.2009.11.010.

(29) Goldshleger, N. F.; Lobach, A. S.; Baulin, V. E.; Tsivadze, A. Y. Supramolecular Gels Based on Bile Acid Salts. *Russ. Chem. Rev.* **2017**, *86* (4), 269–297. https://doi.org/10.1070/rcr4682.

(30) Di Gregorio, M. C.; Travaglini, L.; Del Giudice, A.; Cautela, J.; Pavel, N. V.; Galantini, L. Bile Salts: Natural Surfactants and Precursors of a Broad Family of Complex Amphiphiles. *Langmuir* **2019**, *35* (21), 6803–6821. https://doi.org/10.1021/acs.langmuir.8b02657.

(31) Zhang, M.; Waldron, K. C.; Zhu, X. X. Formation of Molecular Hydrogels from a Bile Acid Derivative and Selected Carboxylic Acids. *RSC Adv.* **2016**, *6* (42), 35436–35440. https://doi.org/10.1039/c6ra04536g.

(32) Zhang, M.; Ma, Z.; Wang, K.; Zhu, X. X. CO 2 Sequestration by Bile Salt Aqueous Solutions and Formation of Supramolecular Hydrogels. *ACS Sustain. Chem. Eng.* **2019**, *7* (4), 3949–3955. https://doi.org/10.1021/acssuschemeng.8b05112.

(33) Li, G.; Hu, Y.; Sui, J.; Song, A.; Hao, J. Hydrogelation and Crystallization of Sodium Deoxycholate a b c a b C. *88364750*.

(34) La Mesa, C.; Khan, A.; Fontell, K.; Lindman, B. Phase Diagrams and NMR Studies of Some Ternary Sodium Deoxycholate-Surfactant-Water Systems. *J. Colloid Interface Sci.* **1985**, *103* (2), 373–391. https://doi.org/10.1016/0021-9797(85)90116-X.

(35) Karthika, S.; Radhakrishnan, T. K.; Kalaichelvi, P. A Review of Classical and Nonclassical Nucleation Theories. *Cryst. Growth Des.* **2016**, *16* (11), 6663–6681. https://doi.org/10.1021/acs.cgd.6b00794.

(36) Yu, R.; Lin, N.; Yu, W; Liu, Y. X. Crystal Networks in Supramolecular Gels: Formation Kinetics and Mesoscopic Engineering Principles. *CrystEngComm* **2015**, *17* (42), 7986–8010. https://doi.org/10.1039/C5CE00854A.

(37) Sear, R. P. Heterogeneous and Homogeneous Nucleation Compared: Rapid Nucleation on Microscopic Impurities. *J. Phys. Chem. B* **2006**, *110* (10), 4985–4989. https://doi.org/10.1021/jp056377e.

(38) Steed, J. W.; Atwood, J. L. Supramolecular Chemistry: Second Edition. *Supramol. Chem. Second Ed.* **2009**, 1–970. https://doi.org/10.1002/9780470740880.

(39) Hirst, A. R.; Smith, D. K.; Liu, X. Y. Low Molecular Mass Gelators : Design, Self-

Assembly, Function. *Top. Curr. Chem.* **2005**, *256*, 237–273. https://doi.org/10.1007/b107178.

(40) Li, J. L.; Liu, X. Y. *Soft Fibrillar Materials: Fabrication and Applications*; John Wiley & Sons, 2013.

(41) Bennema, P. Spiral Growth and Surface Roughening: Developments since Burton, Cabrera and Frank. *J. Cryst. Growth* **1984**, *69* (1), 182–197. https://doi.org/10.1016/0022-0248(84)90027-7.

(42) Wang, R.; Liu, X.Y.; Xiong, J.; Li, J. Real-Time Observation of Fiber Network Formation in Molecular Organogel: Supersaturation-Dependent Microstructure and Its Related Rheological Property. *J. Phys. Chem. B* **2006**, *110* (14), 7275–7280. https://doi.org/10.1021/JP054531R.

(43) Wang, R.; Liu, X.Y.; Narayanan, J.; Xiong, J.; Li, J.-L. Architecture of Fiber Network: From Understanding to Engineering of Molecular Gels. *J. Phys. Chem. B* **2006**, *110* (51), 25797–25802. https://doi.org/10.1021/JP065101J.

(44) Kim, J.; Zhang, G.; Shi, M.; Suo, Z. Fracture, Fatigue, and Friction of Polymers in Which Entanglements Greatly Outnumber Cross-Links. *Science (80-.).* **2021**, *374* (6564), 212–216. https://doi.org/10.1126/SCIENCE.ABG6320.

(45) Lloyd, D. J. The Problem of Gel Structure. *Colloid Chem.* **1926**, *1*, 767–782.

(46) Takahashi, A.; Sakai, M.; Kato, T. Melting Temperature of Thermally Reversible Gel. VI. Effect of Branching on the Sol–Gel Transition of Polyethylene Gels. *Polym. J. 1980 125* **1980**, *12* (5), 335–341. https://doi.org/10.1295/polymj.12.335.

(47) Raghavan, S. R.; Cipriano, B. H. Gel Formation: Phase Diagrams Using Tabletop Rheology and Calorimetry. *Mol. Gels Mater. with Self-Assembled Fibrillar Networks* **2006**, 241–252. https://doi.org/10.1007/1-4020-3689-2_9.

(48) Slone, R. V. Encyclopedia of Polymer Science and Technology; Mark, HF, Ed. John Wiley & Sons: New York 2004.

(49) Miyoshi, E.; Takaya, T.; Nishinari, K. Effects of Salts on the Gel-Sol Transition of Gellan Gum by Differential Scanning Calorimetry and Thermal Scanning Rheology. *Thermochim. Acta* **1995**, *267* (C), 269–287. https://doi.org/10.1016/0040-6031(95)02485-9.

(50) Derkach, S. R.; Ilyin, S. O.; Maklakova, A. A.; Kulichikhin, V. G.; Malkin, A. Y. The Rheology of Gelatin Hydrogels Modified by κ-Carrageenan. *LWT - Food Sci. Technol.*

2015, *63* (1), 612–619. https://doi.org/10.1016/J.LWT.2015.03.024.

(51) Kiyotake, E. A.; Douglas, A. W.; Thomas, E. E.; Nimmo, S. L.; Detamore, M. S. Development and Quantitative Characterization of the Precursor Rheology of Hyaluronic Acid Hydrogels for Bioprinting. *Acta Biomater.* **2019**, *95*, 176–187. https://doi.org/10.1016/J.ACTBIO.2019.01.041.

(52) Sawatari, C.; Okumura, T.; Matsuo, M. Molecular Weight Dependence on the Morphological Properties of Polyethylene Gels. *Polym. J. 1986 1810* **1986**, *18* (10), 741–758. https://doi.org/10.1295/polymj.18.741.

(53) Venkatesan, R.; Nagarajan, N. R.; Paso, K.; Yi, Y. B.; Sastry, A. M.; Fogler, H. S. The Strength of Paraffin Gels Formed under Static and Flow Conditions. *Chem. Eng. Sci.* **2005**, *60* (13), 3587–3598. https://doi.org/10.1016/J.CES.2005.02.045.

(54) Günther, H. *NMR Spectroscopy: Basic Principles, Concepts and Applications in Chemistry*; John Wiley & Sons, 2013.

(55) Bloembergen, N.; Purcell, E. M.; Pound, R. V. Relaxation Effects in Nuclear Magnetic Resonance Absorption. *Phys. Rev.* **1948**, *73* (7), 679. https://doi.org/10.1103/PhysRev.73.679.

(56) Murata, Y.; Sugihara, G.; Fukuehlma, K.; Tanaka, M.; Matsushita, K. Study of the Micelle Formation of Sodium Deoxycholate. Concentration Dependence of Carbon-13 Nuclear Magnetic Resonance Chemical Shift. *J. Phys. Chem* **1982**, *86*, 4690–4694.

(57) Bertini, I.; Luchinat, C.; Parigi, G.; Ravera, E. Relaxation. *Solut. NMR Paramagn. Mol.* **2017**, 77–126. https://doi.org/10.1016/B978-0-444-63436-8.00004-1.

(58) Grant, D. M.; Harris, R. K. Encyclopedia of Nuclear Magnetic Resonance, Volume 9, Advances in NMR. *Spectroscopy* **1996**.

(59) Vögeli, B. The Nuclear Overhauser Effect from a Quantitative Perspective. *Prog. Nucl. Magn. Reson. Spectrosc.* **2014**, *78*, 1–46. https://doi.org/10.1016/J.PNMRS.2013.11.001.

(60) Tamesue, S.; Takashima, Y.; Yamaguchi, H.; Shinkai, S.; Harada, A. Photoswitchable Supramolecular Hydrogels Formed by Cyclodextrins and Azobenzene Polymers. *Angew. Chemie Int. Ed.* **2010**, *49* (41), 7461–7464. https://doi.org/10.1002/ANIE.201003567.

(61) Abian, O.; Vega, S.; Neira, J. L.; Velazquez-Campoy, A. High-Throughput Screening for Intrinsically Disordered Proteins by Using Biophysical Methods. *Protein Homeost. Dis.* **2020**, 359–387. https://doi.org/10.1016/B978-0-12-819132-3.00017-8.

(62) Atta-ur-Rahman; Choudhary, M. I.; Atia-tul-Wahab. Nuclear Overhauser Effect. *Solving Probl. with NMR Spectrosc.* **2016**, 227–264. https://doi.org/10.1016/B978-0-12-411589-7.00006-1.

(63) Krishnan, V. Ligand Screening by Saturation-Transfer Difference (STD) NMR Spectroscopy. *Curr. Anal. Chem.* **2005**, *1* (3), 307–320. https://doi.org/10.2174/157341105774573956.

(64) Yan, J.; Kline, A. D.; Mo, H.; Shapiro, M. J.; Zartler, E. R. The Effect of Relaxation on the Epitope Mapping by Saturation Transfer Difference NMR. *J. Magn. Reson.* **2003**, *163* (2), 270–276. https://doi.org/10.1016/S1090-7807(03)00106-X.

(65) Ramalhete, S. M.; Nartowski, K. P.; Sarathchandra, N.; Foster, J. S.; Round, A. N.; Angulo, J.; Lloyd, G. O.; Khimyak, Y. Z. Supramolecular Amino Acid Based Hydrogels: Probing the Contribution of Additive Molecules Using NMR Spectroscopy. *Chem. - A Eur. J.* **2017**, *23* (33). https://doi.org/10.1002/chem.201700793.

(66) Segarra-Maset, M. D.; Escuder, B.; Miravet, J. F. Selective Interaction of Dopamine with the Self-Assembled Fibrillar Network of a Molecular Hydrogel Revealed by STD-NMR. *Chem. - A Eur. J.* **2015**, *21* (40), 13925–13929. https://doi.org/10.1002/chem.201502018.

(67) Nonappa; Šaman, D.; Kolehmainen, E. Studies on Supramolecular Gel Formation Using DOSY NMR. *Magn. Reson. Chem.* **2015**, *53* (4), 256–260. https://doi.org/10.1002/MRC.4185.

(68) Šmejkalová, D.; Piccolo, A. Aggregation and Disaggregation of Humic Supramolecular Assemblies by NMR Diffusion Ordered Spectroscopy (DOSY-NMR). *Environ. Sci. Technol.* **2008**, *42* (3), 699–706. https://doi.org/10.1021/es071828p.

(69) Sajid Iqbal; Francisco Rodríguez-LLansola; Beatriu Escuder; F. Miravet, J.; Ingrid Verbruggen; Rudolph Willem. HRMAS 1H NMR as a Tool for the Study of Supramolecular Gels. *Soft Matter* **2010**, *6* (9), 1875–1878. https://doi.org/10.1039/B926785A.

(70) Liu, Y.; Guo, D.-S.; Zhang, H.-Y.; Ding, F.; Chen, K.; Song, H.-B. Supramolecular Assemblies of Sulfonatocalixarenes with Phenanthroline: Factors Governing Capsule Formation versus Bilayer Arrangements. https://doi.org/10.1002/chem.200600668.

(71) Bearden, J. A. X-Ray Wavelengths. *Rev. Mod. Phys.* **1967**, *39* (1), 78. https://doi.org/10.1103/RevModPhys.39.78.

(72) Whittig, L. D.; Allardice, W. R. X-Ray Diffraction Techniques. *Methods Soil Anal. Part 1 Phys. Mineral. Methods* **2018**, 331–362. https://doi.org/10.2136/SSSABOOKSER5.1.2ED.C12.

(73) Bunaciu, A. A.; Udriştioiu, E. gabriela; Aboul-Enein, H. Y. X-Ray Diffraction: Instrumentation and Applications. *http://dx.doi.org/10.1080/10408347.2014.949616* **2015**, *45* (4), 289–299. https://doi.org/10.1080/10408347.2014.949616.

(74) Hwang, I.; Jeon, W. S.; Kim, H.-J.; Kim, D.; Kim, H.; Selvapalam, N.; Fujita, N.; Shinkai, S.; Kim, K. Cucurbit[7]Uril: A Simple Macrocyclic, PH-Triggered Hydrogelator Exhibiting Guest-Induced Stimuli-Responsive Behavior. *Angew. Chemie* **2007**, *119* (1–2), 214–217. https://doi.org/10.1002/ANGE.200603149.

(75) Draper, E. R.; Dietrich, B.; McAulay, K.; Brasnett, C.; Abdizadeh, H.; Patmanidis, I.; Marrink, S. J.; Su, H.; Cui, H.; Schweins, R.; Seddon, A.; Adams, D. J. Using Small-Angle Scattering and Contrast Matching to Understand Molecular Packing in Low Molecular Weight Gels. *Matter* **2020**, *2* (3), 764–778. https://doi.org/10.1016/J.MATT.2019.12.028.

(76) Nair, P. *The Bile Acids Chemistry, Physiology, and Metabolism: Volume 1: Chemistry*; Springer Science & Business Media, 2013.

(77) Bachmann, V.; Kostiuk, B.; Unterweger, D.; Diaz-Satizabal, L.; Ogg, S.; Pukatzki, S. Bile Salts Modulate the Mucin-Activated Type VI Secretion System of Pandemic Vibrio Cholerae. *PLoS Negl. Trop. Dis.* **2015**, *9* (8), e0004031. https://doi.org/10.1371/JOURNAL.PNTD.0004031.

(78) Jia, Y. G.; Yu, Q.; Ma, Z.; Zhang, M.; Zhu, X. X. Tunable Upper Critical Solution Temperatures for Acrylamide Copolymers with Bile Acid Pendants. *Biomacromolecules* **2017**, *18* (8), 2663–2668. https://doi.org/10.1021/ACS.BIOMAC.7B00860/SUPPL_FILE/BM7B00860_SI_001.PDF.

(79) Ma, Z.; Zhu, X. X. Core Cross-Linked Micelles Made of Glycopolymers Bearing Dopamine and Cholic Acid Pendants. *Mol. Pharm.* **2018**, *15* (6), 2348–2354. https://doi.org/10.1021/ACS.MOLPHARMACEUT.8B00205/SUPPL_FILE/MP8B00205_SI_001.PDF.

(80) Gauthier, M. A.; Simard, P.; Zhang, Z.; Zhu, X. X. Bile Acids as Constituents for Dental Composites: In Vitro Cytotoxicity of (Meth)Acrylate and Other Ester Derivatives of Bile

Acids. *J. R. Soc. Interface* **2007**, *4* (17), 1145–1150. https://doi.org/10.1098/RSIF.2007.1018.

(81) Gauthier, M. A.; Zhang, Z.; Zhu, X. X. New Dental Composites Containing Multimethacrylate Derivatives of Bile Acids: A Comparative Study with Commercial Monomers. *ACS Appl. Mater. Interfaces* **2009**, *1* (4), 824–832. https://doi.org/10.1021/AM8002395/SUPPL_FILE/AM8002395_SI_001.PDF.

(82) Jia, Y. G.; Zhu, X. X. Nanocomposite Hydrogels of LAPONITE® Mixed with Polymers Bearing Dopamine and Cholic Acid Pendants. *RSC Adv.* **2016**, *6* (27), 23033–23037. https://doi.org/10.1039/c5ra26316f.

(83) Jia, Y. G.; Zhu, X. X. Self-Healing Supramolecular Hydrogel Made of Polymers Bearing Cholic Acid and β-Cyclodextrin Pendants. *Chem. Mater.* **2015**, *27* (1), 387–393. https://doi.org/10.1021/cm5041584.

(84) Jia, Y. G.; Jin, J.; Liu, S.; Ren, L.; Luo, J.; Zhu, X. X. Self-Healing Hydrogels of Low Molecular Weight Poly(Vinyl Alcohol) Assembled by Host-Guest Recognition. *Biomacromolecules* **2018**, *19* (2), 626–632. https://doi.org/10.1021/ACS.BIOMAC.7B01707/SUPPL_FILE/BM7B01707_SI_001.PDF .

(85) Zhang, M.; Strandman, S.; Waldron, K. C.; Zhu, X. X. Supramolecular Hydrogelation with Bile Acid Derivatives: Structures, Properties and Applications. *J. Mater. Chem. B* **2016**, *4* (47), 7506–7520. https://doi.org/10.1039/c6tb02270g.

(86) Jia, Y. G.; Zhang, M.; Zhu, X. X. CO2-Switchable Self-Healing Host-Guest Hydrogels. *Macromolecules* **2017**, *50* (24), 9696–9701. https://doi.org/10.1021/ACS.MACROMOL.7B02163/SUPPL_FILE/MA7B02163_SI_001.PDF.

(87) Russell, D. W. THE ENZYMES, REGULATION, AND GENETICS OF BILE ACID SYNTHESIS. **2003**. https://doi.org/10.1146/annurev.biochem.72.121801.161712.

(88) Chiang, J. Y. L. Regulation of Bile Acid Synthesis: Pathways, Nuclear Receptors, and Mechanisms. *J. Hepatol.* **2004**, *40* (3), 539–551. https://doi.org/10.1016/J.JHEP.2003.11.006.

(89) Federici, G. Bile Acids. *Lab. Guid. to Methods Biochem. Genet.* **2017**, 607–664. https://doi.org/10.1007/978-3-540-76698-8_27.

(90) Small, D. M. The Physical Chemistry of Cholanic Acids. *Bile Acids Chem. Physiol. Metab.* **1971**, 249–356. https://doi.org/10.1007/978-1-4757-0647-5_8.

(91) Madenci, D.; Egelhaaf, S. U. Self-Assembly in Aqueous Bile Salt Solutions. *Curr. Opin. Colloid Interface Sci.* **2010**, *15* (1–2), 109–115. https://doi.org/10.1016/j.cocis.2009.11.010.

(92) Paula, S.; Stis, W.; Tuchtenhagen, J.; Blume, A. Thermodynamics of Micelle Formation as a Function of Temperature: A High Sensitivity Titration Calorimetry Study. *J. Phys. Chem* **1995**, *99*, 11742–11751.

(93) Reis, S.; Moutinho, C. G.; Matos, C.; De Castro, B.; Gameiro, P.; Lima, J. L. F. C. Noninvasive Methods to Determine the Critical Micelle Concentration of Some Bile Acid Salts. *Anal. Biochem.* **2004**, *334* (1), 117–126. https://doi.org/10.1016/J.AB.2004.07.017.

(94) Matsuoka, K.; Moroi, Y. Micelle Formation of Sodium Deoxycholate and Sodium Ursodeoxycholate (Part 1). *Biochim. Biophys. Acta - Mol. Cell Biol. Lipids* **2002**, *1580* (2–3), 189–199. https://doi.org/10.1016/S1388-1981(01)00203-7.

(95) Hofmann, A. F.; Small, D. M. Detergent Properties of Bile Salts: Correlation with Physiological Function. *https://doi.org/10.1146/annurev.me.18.020167.002001* **2003**, *18*, 333–376. https://doi.org/10.1146/ANNUREV.ME.18.020167.002001.

(96) Garidel, P.; Hildebrand, A.; Neubert, R.; Blume, A. Thermodynamic Characterization of Bile Salt Aggregation as a Function of Temperature and Ionic Strength Using Isothermal Titration Calorimetry. *Langmuir* **2000**, *16* (12), 5267–5275. https://doi.org/10.1021/LA9912390.

(97) Carey, M. C.; Small, D. M. Micelle Formation by Bile Salts: Physical-Chemical and Thermodynamic Considerations. *Arch. Intern. Med.* **1972**, *130* (4), 506–527. https://doi.org/10.1001/ARCHINTE.1972.03650040040005.

(98) Norman, A.; Bergman, S.; Bak, T. A.; Varde, E.; Westin, G. The Conductance of Conjugated and Unconjugated Bile Acid Salts in Aqueous Solutions. Bile Acids and Steroids. 80. *Acta Chem. Scand.* **1960**, *14*, 1300–1309. https://doi.org/10.3891/acta.chem.scand.14-1300.

(99) Hofmann, A. F. The Function of Bile Salts in Fat Absorption. The Solvent Properties of Dilute Micellar Solutions of Conjugated Bile Salts.. *Biochem. J.* **1963**, *89* (1), 57–68. https://doi.org/10.1042/BJ0890057.

(100) Hofmann, A. F.; Roda, A. Physicochemical Properties of Bile Acids and Their Relationship to Biological Properties: An Overview of the Problem. *J. Lipid Res.* **1984**, *25* (13), 1477–1489. https://doi.org/10.1016/S0022-2275(20)34421-7.

(101) Small, D. M. Size and Structure of Bile Salt Micelles. **1968**, 31–52. https://doi.org/10.1021/ba-1968-0084.ch004.

(102) Waissbluth, O. L.; Morales, M. C.; Bohne, C. Influence of Planarity and Size on Guest Binding with Sodium Cholate Aggregates. *Photochem. Photobiol.* **2006**, *82* (4), 1030–1038. https://doi.org/10.1562/2006-02-14-RA-803.

(103) Ju, C.; Bohne, C. Dynamics of Probe Complexation to Bile Salt Aggregates. *J. Phys. Chem.* **1996**, *100* (9), 3847–3854. https://doi.org/10.1021/JP952657Q.

(104) Kawamura, H.; Murata, Y.; Yamaguchi, T.; Igimi, H.; Tanaka, M.; Sugihara, G.; Kratohvil, J. P. Spin-Label Studies of Bile Salt Micelles. *J. Phys. Chem.* **1989**, *93* (8), 3321–3326. https://doi.org/10.1021/j100345a087.

(105) Madenci, D.; Egelhaaf, S. U. Self-Assembly in Aqueous Bile Salt Solutions. *Curr. Opin. Colloid Interface Sci.* **2010**, *15* (1–2), 109–115. https://doi.org/10.1016/J.COCIS.2009.11.010.

(106) Campanelli, A. R.; Candeloro De Sanctis, S.; Chiessi, E.; Giglio, E.; Scaramuzza, L.; Sapienza, L.; le Moro, P. A. Sodium Glyco-and Taurodeoxycholate: Possible Helical Models for Conjugated Bile Salt Micelles.

(107) Campanelli, A. R.; Candeloro, S.; Sanctis, D. E.; Giglio, E.; Pavel, N. V.; Quagliata, C. From Crystal to Micelle: A New Approach to the Micellar Structure. *J. Incl. Phenom. Mol. Recognit. Chem.* **1989**, *7*, 391.

(108) Hofmann, A. F.; Mysels, K. J. Bile Acid Solubility and Precipitation in Vitro and in Vivo: The Role of Conjugation, PH, and Ca2+ Ions. *J. Lipid Res.* **1992**, *33* (5), 617–626. https://doi.org/10.1016/S0022-2275(20)41426-9.

(109) Rich, A.; Blow, D. M. Formation of a Helical Steroid Complex. *Nature* **1958**, *182* (4633), 423–426. https://doi.org/10.1038/182423a0.

(110) Blow, D. M.; Rich, A. Studies on the Formation of Helical Deoxycholate Complexes1, 2. *J. Am. Chem. Soc.* **1960**, *82* (14), 3566–3571.

(111) Sobotka, H.; Czeczowiczka, N. The Gelation of Bile Salt Solutions. *J. Colloid Sci.* **1958**, *13* (2), 188–191. https://doi.org/10.1016/0095-8522(58)90024-2.

(112) Kratohvil, J. P.; Hsu, W. P.; Kwok, D. I. How Large Are the Micelles of Di-α-Hydroxy Bile Salts at the Critical Micellization Concentrations in Aqueous Electrolyte Solutions? Results for Sodium Taurodeoxycholate and Sodium Deoxycholate. *Langmuir* **2002**, *2* (2), 256–258. https://doi.org/10.1021/LA00068A026.

(113) Sada, K.; Sugahara, M.; Kato, K.; Miyata, M. Controlled Expansion of a Molecular Cavity in a Steroid Host Compound. *J. Am. Chem. Soc.* **2001**, *123* (19), 4386–4392. https://doi.org/10.1021/JA0038528/SUPPL_FILE/JA0038528.CIF.

(114) Miki, K.; Masui, A.; Kasai, N.; Miyata, M.; Shibakami, M.; Takemoto, K. New Channel-Type Inclusion Compound of Steroidal Bile Acid. Structure of a 1:1 Complex between Cholic Acid and Acetophenone. *J. Am. Chem. Soc.* **1988**, *110* (19), 6594–6596. https://doi.org/10.1021/JA00227A067/SUPPL_FILE/JA00227A067_SI_001.PDF.

(115) Qiao, Y.; Lin, Y.; Wang, Y.; Yang, Z.; Liu, J.; Zhou, J.; Yan, Y.; Huang, J. Metal-Driven Hierarchical Self-Assembled One-Dimensional Nanohelices. *Nano Lett.* **2009**, *9* (12), 4500–4504. https://doi.org/10.1021/NL9028335.

(116) Qiao, Y.; Lin, Y.; Zhang, S.; Huang, J. Lanthanide-Containing Photoluminescent Materials: From Hybrid Hydrogel to Inorganic Nanotubes. https://doi.org/10.1002/chem.201003255.

(117) Chakrabarty, A.; Maitra, U.; Das, A. D. Metal Cholate Hydrogels: Versatile Supramolecular Systems for Nanoparticle Embedded Soft Hybrid Materials. *J. Mater. Chem.* **2012**, *22* (35), 18268–18274. https://doi.org/10.1039/C2JM34016J.

(118) Qiao, Y.; Wang, Y.; Yang, Z.; Lin, Y.; Huang, J. Self-Templating of Metal-Driven Supramolecular Self-Assembly: A General Approach toward 1D Inorganic Nanotubes. *Chem. Mater.* **2011**, *23* (5), 1182–1187. https://doi.org/10.1021/CM102649Y.

(119) Sada, K.; Sugahara, M.; Kato, K.; Miyata, M. Controlled Expansion of a Molecular Cavity in a Steroid Host Compound. *J. Am. Chem. Soc.* **2001**, *123* (19), 4386–4392. https://doi.org/10.1021/JA0038528/SUPPL_FILE/JA0038528.CIF.

(120) Noponen, V.; Toikkanen, K.; Kalenius, E.; Kuosmanen, R.; Salo, H.; Sievänen, E. Stimuli-Responsive Bile Acid-Based Metallogels Forming in Aqueous Media. *Steroids* **2015**, *97*, 54–61. https://doi.org/10.1016/j.steroids.2014.10.001.

(121) Dukh, M.; Šaman, D.; Kroulík, J.; Černý, I.; Pouzar, V.; Král, V.; Drašar, P. Metal Coordination as a Tool for Controlling the Self-Assembling and Gelation Properties of

Novel Type Cholic Amide–Phenanthroline Gelating Agent. *Tetrahedron* **2003**, *59* (23), 4069–4076. https://doi.org/10.1016/S0040-4020(03)00587-8.

(122) Di Gregorio, M. C.; Varenik, M.; Gubitosi, M.; Travaglini, L.; Pavel, N. V.; Jover, A.; Meijide, F.; Regev, O.; Galantini, L. Multi Stimuli Response of a Single Surfactant Presenting a Rich Self-Assembly Behavior. *RSC Adv.* **2015**, *5* (47), 37800–37806. https://doi.org/10.1039/c5ra01394a.

(123) Ryu, E. H.; Ellern, A.; Zhao, Y. High Guest Inclusion in 3β-Amino-7α,12α-Dihydroxycholan-24-Oic Acid Enabled by Charge-Assisted Hydrogen Bonds. *Tetrahedron* **2006**, *62* (29), 6808–6813. https://doi.org/10.1016/J.TET.2006.04.094.

(124) Vázquez Tato, J.; Meijide, F.; Antelo, A.; Alvarez Alcalde, M.; Jover, A.; Galantini, L.; Pavel, N. V. Supramolecular Structures Generated by a P- Tert-Butylphenylamide Derivative of Deoxycholic Acid. from Planar Sheets to Tubular Structures through Helical Ribbons. *Langmuir* **2010**, *26* (11), 7768–7773. https://doi.org/10.1021/LA904548K/SUPPL_FILE/LA904548K_SI_001.PDF.

(125) Travaglini, L.; D'annibale, A.; Schillén, K.; Olsson, U.; Sennato, S.; Pavel, N. V.; Galantini, L. Amino Acid – Bile Acid Based Molecules: Extremely Narrow Surfactant Nanotubes Formed by a Phenylalanine-Substituted Cholic Acid. *Chem. Commun.* **2012**, *48* (98), 12011–12013. https://doi.org/10.1039/C2CC36030F.

(126) Gubitosi, M.; Travaglini, L.; di Gregorio, M. C.; Pavel, N. V.; Vázquez Tato, J.; Sennato, S.; Olsson, U.; Schillén, K.; Galantini, L. Tailoring Supramolecular Nanotubes by Bile Salt Based Surfactant Mixtures. *Angew. Chemie* **2015**, *127* (24), 7124–7127. https://doi.org/10.1002/ANGE.201500445.

(127) Di Gregorio, M. C.; Severoni, E.; Travaglini, L.; Gubitosi, M.; Sennato, S.; Mura, F.; Redondo-Gómez, C.; Jover, A.; Pavel, N. V.; Galantini, L. Bile Acid Derivative-Based Catanionic Mixtures: Versatile Tools for Superficial Charge Modulation of Supramolecular Lamellae and Nanotubes. *Phys. Chem. Chem. Phys.* **2018**, *20* (28), 18957–18968. https://doi.org/10.1039/c8cp02745e.

(128) Dévédec, F. Le; Fuentealba, D.; Strandman, S.; Bohne, C.; Zhu, X. X. Aggregation Behavior of Pegylated Bile Acid Derivatives. *Langmuir* **2012**, *28* (37), 13431–13440. https://doi.org/10.1021/LA303218Q.

(129) Cunningham, A. J.; Feng, X.; Zhang, H.; Banquy, X.; Chain, J. L.; Zhu, X.-X.

Thermoresponsive Properties of Star-Shaped Amphiphilic Block Copolymers with a Cholic Acid Core and Functional Amine Groups. *Mater. Today Commun.* **2021**, *29*, 102816. https://doi.org/10.1016/J.MTCOMM.2021.102816.

(130) Maitra, U.; Mukhopadhyay, S.; Sarkar, A.; Rao, P.; Indi, S. S. Hydrophobic Pockets in a Nonpolymeric Aqueous Gel: Observation of Such a Gelation Process by Color Change. *Angew. Chemie* **2001**, *113* (12), 2341–2343.

(131) Mukhopadhyay, S.; Maitra, U.; Ira; Krishnamoorthy, G.; Schmidt, J.; Talmon, Y. Structure and Dynamics of a Molecular Hydrogel Derived from a Tripodal Cholamide. *J. Am. Chem. Soc.* **2004**, *126* (48), 15905–15914. https://doi.org/10.1021/JA046788T.

(132) Zhao, Y. Spacer-Dependent Folding and Aggregation of Oligocholates in SDS Micelles. *J. Org. Chem.* **2009**, *74* (19), 7470–7480. https://doi.org/10.1021/JO901651H/SUPPL_FILE/JO901651H_SI_001.PDF.

(133) Zhao, Y. Conformation of Oligocholate Foldamers with 4-Aminobutyroyl Spacers. *J. Org. Chem.* **2009**, *74* (2), 834–843. https://doi.org/10.1021/JO802201B/SUPPL_FILE/JO802201B_SI_001.PDF.

(134) Zhao, Y.; Zhong, Z. Oligomeric Cholates: Amphiphilic Foldamers with Nanometer-Sized Hydrophilic Cavities. *J. Am. Chem. Soc.* **2005**, *127* (50), 17894–17901. https://doi.org/10.1021/JA056151P/SUPPL_FILE/JA056151PSI20051026_045259.PDF.

(135) Zhao, Y.; Zhong, Z. Tuning the Sensitivity of a Foldamer-Based Mercury Sensor by Its Folding Energy. *J. Am. Chem. Soc.* **2006**, *128* (31), 9988–9989. https://doi.org/10.1021/JA062001I/SUPPL_FILE/JA062001ISI20060518_014623.PDF.

(136) Gyimesi, J.; Barcza, L. Dimerization: First Step for Micelle Preorganization of Bile Salts. *J. Incl. Phenom. Mol. Recognit. Chem. 1993 152* **1993**, *15* (2), 153–158. https://doi.org/10.1007/BF00710224.

(137) Gouin, S.; Zhu, X. X. Fluorescence and NMR Studies of the Effect of a Bile Acid Dimer on the Micellization of Bile Salts. *Langmuir* **1998**, *14* (15), 4025–4029. https://doi.org/10.1021/LA971155W.

(138) Egelhaaf, S. U.; Schurtenberger, P. Shape Transformations in the Lecithin-Bile Salt System: From Cylinders to Vesicles. *J. Phys. Chem.* **1994**, *98* (34), 8560–8573.

(139) Zhang, M.; Ma, Z.; Wang, K.; Zhu, X. X. CO 2 Sequestration by Bile Salt Aqueous Solutions and Formation of Supramolecular Hydrogels. *ACS Sustain. Chem. Eng.* **2019**, *7*

(4), 3949–3955. https://doi.org/10.1021/ACSSUSCHEMENG.8B05112/SUPPL_FILE/SC8B05112_SI_001.PDF.

(140) Zhang, M.; Fives, C.; Waldron, K. C.; Zhu, X. X. Self-Assembly of a Bile Acid Dimer in Aqueous Solutions: From Nanofibers to Nematic Hydrogels. *Langmuir* **2017**, *33* (4), 1084–1089. https://doi.org/10.1021/acs.langmuir.6b04033.

(141) Li, J.-L.; Liu, X.-Y. Architecture of Supramolecular Soft Functional Materials: From Understanding to Micro-/Nanoscale Engineering. *Adv. Funct. Mater.* **2010**, *20* (19), 3196–3216. https://doi.org/10.1002/ADFM.201000744.

(142) Lee, E. C. Y.; Steeno, G.; Wassermann, A. M.; Zhang, L.; Shah, F.; Price, D. A. Amine Promiscuity and Toxicology Analysis. *Bioorg. Med. Chem. Lett.* **2017**, *27* (3), 653–657. https://doi.org/10.1016/J.BMCL.2016.11.085.

(143) Du, X.; Zhou, J.; Xu, B. Supramolecular Hydrogels Made of Basic Biological Building Blocks. *Chem. – An Asian J.* **2014**, *9* (6), 1446–1472. https://doi.org/10.1002/ASIA.201301693.

(144) Ye, E.; Chee, P. L.; Prasad, A.; Fang, X.; Owh, C.; Yeo, V. J. J.; Loh, X. J. Supramolecular Soft Biomaterials for Biomedical Applications. **2015**, 107–125. https://doi.org/10.1007/978-981-287-152-7_5.

(145) Ryan, D. M.; Nilsson, B. L. Self-Assembled Amino Acids and Dipeptides as Noncovalent Hydrogels for Tissue Engineering. *Polym. Chem.* **2011**, *3* (1), 18–33. https://doi.org/10.1039/C1PY00335F.

(146) Wang, H.; Yang, Z. Short- Peptide -Based Molecular Hydrogels: Novel Gelation Strategies and Applications for Tissue Engineering and Drug Delivery. *Nanoscale* **2012**, *4* (17), 5259–5267. https://doi.org/10.1039/C2NR31149F.

(147) Friggeri, A.; Feringa, B. L.; Van Esch, J. Entrapment and Release of Quinoline Derivatives Using a Hydrogel of a Low Molecular Weight Gelator. *J. Control. Release* **2004**, *97* (2), 241–248. https://doi.org/10.1016/J.JCONREL.2004.03.012.

(148) Skilling, K. J.; Citossi, F.; Bradshaw, T. D.; Ashford, M.; Kellam, B.; Marlow, M. Insights into Low Molecular Mass Organic Gelators: A Focus on Drug Delivery and Tissue Engineering Applications. *Soft Matter* **2013**, *10* (2), 237–256. https://doi.org/10.1039/C3SM52244J.

(149) Zhao, X.; Huebsch, N.; Mooney, D. J.; Suo, Z. Stress-Relaxation Behavior in Gels with Ionic and Covalent Crosslinks. *J. Appl. Phys.* **2010**, *107* (6), 063509. https://doi.org/10.1063/1.3343265.

(150) Hashemnejad, S. M.; Kundu, S. Probing Gelation and Rheological Behavior of a Self-Assembled Molecular Gel. *Langmuir* **2017**, *33* (31), 7769–7779. https://doi.org/10.1021/acs.langmuir.7b01531.

(151) Li, J.; Suo, Z.; Vlassak, J. J. Stiff, Strong, and Tough Hydrogels with Good Chemical Stability. *J. Mater. Chem. B* **2014**, *2* (39), 6708–6713. https://doi.org/10.1039/C4TB01194E.

(152) Ito, K. Novel Cross-Linking Concept of Polymer Network: Synthesis, Structure, and Properties of Slide-Ring Gels with Freely Movable Junctions. *Polym. J. 2007 396* **2007**, *39* (6), 489–499. https://doi.org/10.1295/polymj.pj2006239.

(153) Rezaee, M.; Oskuee, R. K.; Nassirli, H.; Malaekeh-Nikouei, B. Progress in the Development of Lipopolyplexes as Efficient Non-Viral Gene Delivery Systems. *J. Control. Release* **2016**, *236*, 1–14. https://doi.org/10.1016/J.JCONREL.2016.06.023.

(154) Wytrwal, M.; Pichon, C. Polyallylamine Derivatives: Novel Nontoxic Transfection Agents. *Methods Mol. Biol.* **2016**, *1445*, 159–174. https://doi.org/10.1007/978-1-4939-3718-9_10.

(155) Kim, Y. H.; Baek, N. S.; Han, Y. H.; Chung, M. A.; Jung, S. D. Enhancement of Neuronal Cell Adhesion by Covalent Binding of Poly-d-Lysine. *J. Neurosci. Methods* **2011**, *202* (1), 38–44. https://doi.org/10.1016/J.JNEUMETH.2011.08.036.

(156) Laurent, N.; Wattiaux-De Coninck, S.; Mihaylova, E.; Leontieva, E.; Warnier-Pirotte, M. T.; Wattiaux, R.; Jadot, M. Uptake by Rat Liver and Intracellular Fate of Plasmid DNA Complexed with Poly-l-Lysine or Poly-d-Lysine. *FEBS Lett.* **1999**, *443* (1), 61–65. https://doi.org/10.1016/S0014-5793(98)01677-9.

(157) Kwoh, D. Y.; Coffin, C. C.; Lollo, C. P.; Jovenal, J.; Banaszczyk, M. G.; Mullen, P.; Phillips, A.; Amini, A.; Fabrycki, J.; Bartholomew, R. M.; Brostoff, S. W.; Carlo, D. J. Stabilization of Poly-l-Lysine/DNA Polyplexes for in Vivo Gene Delivery to the Liver. *Biochim. Biophys. Acta - Gene Struct. Expr.* **1999**, *1444* (2), 171–190. https://doi.org/10.1016/S0167-4781(98)00274-7.

(158) Vermeersch, H.; Remon, J. P. Immunogenicity of Poly-D-Lysine, a Potential Polymeric

Drug Carrier. *J. Control. Release* **1994**, *32* (3), 225–229. https://doi.org/10.1016/0168-3659(94)90232-1.

(159) 7.1: Structure of Water - Chemistry LibreTexts https://chem.libretexts.org/Courses/Chippewa_Valley_Technical_College/CVTC_Basic_Chemistry/07%3A_Solutions/7.01%3A_Structure_of_Water (accessed Oct 19, 2021).

(160) Xiong, J.; Liu, X.Y.; Li, J.; Vallon, M. W.. Architecture of Macromolecular Network of Soft Functional Materials: From Structure to Function. *J. Phys. Chem. B* **2007**, *111* (20), 5558–5563. https://doi.org/10.1021/JP070600L.

(161) Reeder, S. B. Emergence of 3D MR Elastography–Based Quantitative Markers for Diffuse Liver Disease. *https://doi.org/10.1148/radiol.2021211444* **2021**, *301* (1), 163–165. https://doi.org/10.1148/RADIOL.2021211444.

(162) Kulkarni, V. S.; Shaw, C. Rheological Studies. *Essent. Chem. Formul. Semisolid Liq. Dosages* **2016**, 145–182. https://doi.org/10.1016/B978-0-12-801024-2.00009-1.

(163) Wilson, D. I. What Is Rheology? *Eye 2018 322* **2017**, *32* (2), 179–183. https://doi.org/10.1038/eye.2017.267.

(164) Nebot, V. J.; Smith, D. K. *CHAPTER 2. Techniques for the Characterisation of Molecular Gels*; 2013. https://doi.org/10.1039/9781849737371-00030.

(165) Samateh, M.; Pottackal, N.; Manafirasi, S.; Vidyasagar, A.; Maldarelli, C.; John, G. Unravelling the Secret of Seed-Based Gels in Water: The Nanoscale 3D Network Formation. *Sci. Reports 2018 81* **2018**, *8* (1), 1–8. https://doi.org/10.1038/s41598-018-25691-3.

(166) Tachibana, T.; Kambara, H. Enantiomorphism in the Helical Aggregate of Lithium 12-Hydroxystearate. *J. Am. Chem. Soc.* **1965**, *87* (13), 3015–3016. https://doi.org/10.1021/ja01091a046.

(167) Hirst, A. R.; Miravet, J. F.; Escuder, B.; Noirez, L.; Castelletto, V.; Hamley, I. W.; Smith, D. K. Self-Assembly of Two-Component Gels: Stoichiometric Control and Component Selection. *Chem. - A Eur. J.* **2009**, *15* (2), 372–379. https://doi.org/10.1002/chem.200801475.

(168) Schnablegger, H.; Singh, Y. The SAXS Guide: Getting Acquainted with the Principles. *Anton Paar*. A-8054 Graz, Austria: Austria: Anton Paar GmbH 2013, p 124.

Chapter 2. Using Nuclear Magnetic Resonance Spectroscopy to Probe Hydrogels Formed by Sodium Deoxycholate

Abstract

Hydrogels of bile acids and their salts are promising materials for drug delivery, cellular immobilization, and other applications. However, these hydrogels are poorly understood at the molecular level, and further study is needed to allow improved materials to be created by design. We have used NMR spectroscopy to probe hydrogels formed from mixtures of formic acid and sodium deoxycholate (NaDC), a common bile acid salt. By assaying the ratio of deoxycholate molecules that are immobilized as part of the fibrillar network of the hydrogels and those that can diffuse, we have found that 65% remain free under typical conditions. The network appears to be composed of both the acid and salt forms of deoxycholate, possibly because a degree of charge inhibits excessive aggregation and precipitation of the fibrils. Spin-spin relaxation times provided a molecular-level estimate of the temperature of gel-sol transition (42 °C), which is virtually the same as the value determined by analyzing macroscopic parameters. Saturation transfer difference (STD) NMR spectroscopy established that formic acid, which is present mainly as formate, is not immobilized as part of the gelating network. In contrast, HDO interacts with the network, which presumably has a surface with exposed hydrophilic groups that form hydrogen bonds with water. Moreover, the STD NMR experiments revealed that the network is a dynamic entity, with molecules of deoxycholate associating and dissociating reversibly. This exchange appears to occur preferentially by contact of the hydrophobic edges or faces of free molecules of deoxycholate with those of molecules immobilized as components of the network. In addition, DOSY experiments revealed that gelation has little effect on the diffusion of free NaDC and HDO.

This chapter has been published as a research article: Puzhen Li, Cédric Malveau, X. X. Zhu, and James D. Wuest. "Using Nuclear Magnetic Resonance Spectroscopy to Probe Hydrogels Formed by Sodium Deoxycholate." *Langmuir* (**2021**).
(https://doi.org/10.1021/acs.langmuir.1c02175)

2.1 Introduction

Certain small molecules can associate reversibly in solution to form complex fibrillar structures that immobilize the solvent and yield gels.[1–6] In the case of water, small-molecule gelators are typically amphiphilic compounds with hydrophilic regions to ensure adequate solubility, along with hydrophobic regions to induce association in aqueous media. Important examples of hydrogelators include bile acids and salts,[7–13] which are steroids with multiple functions in mammals and other vertebrates,[14,15] such as facilitating the digestion of fats and the absorption of nutrients with poor solubility in water. Because bile acids and salts are biocompatible and abundant, their hydrogels are promising materials for use in drug delivery, cellular immobilization, and other applications.[16–21] Our group has worked extensively in these areas and has examined hydrogels formed by derivatives of bile acids in conjunction with carboxylic acids,[22] the sequestration of CO_2 by hydrogels of bile acid salts,[23] and other topics.[24]

A common bile acid salt, sodium deoxycholate (**1**), can form hydrogels under particular conditions of concentration, temperature, pressure, pH, and ionic strength.[25–37] Like other derivatives of bile acids, sodium deoxycholate (NaDC) is characterized by a degree of facial amphiphilicity, and its steroidal structure has an extended convex hydrophobic surface with axial methyl groups, as well as an opposing concave surface that exposes hydroxyl and carboxylate groups. The self-association of NaDC in water to form micelles has been studied in multiple ways, and the size and shape of aggregates depend on concentration. Various models have been advanced,[38] and primary association above an initial critical micellar concentration of about 10 mM appears to yield small aggregates consisting of a few molecules held together by interactions of their hydrophobic faces. Further association at higher concentrations may then produce larger secondary micelles and leads ultimately to hydrogelation.

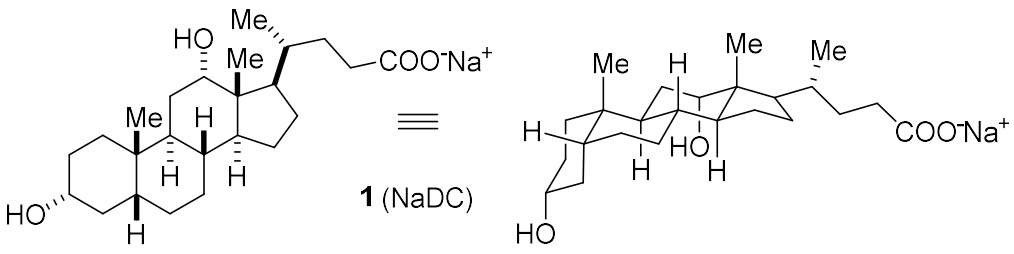

However, no current model of association accounts for all observations, and detailed information about aspects of the process of hydrogelation is not available, such as how the gelator and water interact at the molecular level. Learning how aqueous solutions of NaDC form gels will not necessarily explain how all hydrogelators work. However, the well-defined tetracyclic structures of NaDC and other bile acid salts limit the possible patterns of molecular association and ensure that aggregates in solution, in gels, and in the solid state will all have an important degree of structural similarity. As a result, studies of NaDC and related compounds promise to yield a highly detailed understanding of hydrogelation in a system of particular interest.

For further information about hydrogelation induced by NaDC, we turned to NMR spectroscopy, which can be used in diverse ways to probe the structure of gels and the interactions of their components.[39–43] The rotational correlation time, which is the time needed for a molecule to rotate by 1 radian, is longer when molecules are ordered within the fibrillar structures that give rise to gels than when they are free. As a result, certain signals in the NMR spectra of gels are broadened and can merge with the baseline to become invisible. In this way, integration of selected peaks can provide important information, such as the ratio of molecules that are incorporated in gelating networks relative to those that are free. Another valuable technique for studying gels is saturation transfer difference (STD) NMR.[44] In STD NMR, selected nuclei in a macromolecular structure are saturated, and magnetization is transferred by spin diffusion to other parts of the macromolecule, as well as to small molecules in close proximity ($\leq$ 5 Å). Signal intensities measured with selective saturation (I_{SAT}) will differ from those recorded without saturation (I_0), and the difference spectrum ($I_{STD} = I_0 - I_{SAT}$) will identify molecules that received saturation transfer by spin diffusion through the nuclear Overhauser effect. STD NMR was originally developed to study the binding of ligands by proteins, but it is also useful for probing gelation, as illustrated by analyses of fibrillar networks formed by hydrogelators derived from amino acids.[45,46] In addition, standard measurements of relaxation times and diffusion coefficients by NMR spectroscopy can provide complementary information about the assembly of gels. NMR spectroscopy has already been used to examine aggregates and hydrogels formed by NaDC and other bile acid salts,[47–49] but our work extends these earlier studies and provides valuable new information.

2.2 Materials and Methods

2.2.1 Preparation of Samples.

NaDC and formic acid were purchased from Sigma Aldrich and were used to prepare stock solutions in D_2O for NMR experiments and in H_2O for other studies. The solutions were mixed in various ratios and diluted to give the desired concentrations. To form hydrogels, the molar ratio of NaDC to formic acid needs to be approximately 5:1. The resulting mixtures were heated to produce solutions, which were then allowed to cool to 25 °C. Under typical conditions, the pH of the solutions was in the range 7.3–7.5. Samples for NMR experiments were prepared directly in standard 5-mm NMR tubes or in coaxial 5-mm NMR tubes containing an inner tube with outside and inside diameters of 3 mm and 2 mm, respectively. All ^{1}H NMR experiments were performed using a Bruker Avance II 400 NMR spectrometer, operating at 9.4 T (400 MHz frequency for ^{1}H), or a Bruker Avance 500 NMR spectrometer, operating at 11.74 T (500 MHz frequency for ^{1}H).

2.2.2 Measurements of Spin-Spin Relaxation Time (T_2).

The T_2 relaxation time of HDO was measured with the standard CPMG pulse sequence.[50,51] Temperatures were calibrated by using the temperature-dependent difference between the chemical shifts of the CH_2 and OH signals of ethylene glycol. Samples with three different nominal concentrations of NaDC and formic acid were prepared (Table 2.1). The samples were kept in NMR tubes for more than 12 h to ensure complete gelation. Values of T_2 for HDO in the samples were measured between 25 °C and 55 °C at intervals of 5 °C. For each data point, the sample was kept at the desired temperature for 20 min before measurements were made.

Table 2.1. Data Related to Measurements of Spin-Spin Relaxation Time (T_2)

Sample	NaDC (mM)[a]	Formic acid (mM)[a]	Sample state	$T_{gel-sol}$ (°C)
S1	20	4	Solution	-
S2	50	10	Transparent gel	42
S3	100	20	Opaque gel	42

[a]Nominal concentration, corresponding to the sum of acid and salt forms

2.2.3 Integration of Variable-Temperature (VT) 1D ^{1}H NMR Spectra.

VT 1D ^{1}H NMR spectra were recorded on a Bruker Avance II 400 NMR spectrometer at temperatures between 25 °C and 55 °C. Gels produced by mixing solutions of NaDC and formic acid in D_2O were prepared in the outer part of coaxial 5-mm NMR tubes, with solutions of maleic acid in D_2O in the inner part as an internal standard. Samples were first stabilized and analyzed at 25 °C, and then the temperature was increased to 55 °C at a rate of 5 °C/min and kept at 55 °C for 5, 15, or 30 min for the gels to melt completely. The temperature was then quickly decreased to 25 °C, and an NMR spectrum was recorded every 5 min to follow the gelation. The heating-cooling process was repeated three times for each sample to check the effect of thermal history. Values obtained by integrating peaks derived from NaDC, formic acid, and HDO in gelated states are reported as the averages from 20 spectra of NaDC/formic acid gel samples at 25 °C after the melting-gelation process. Changes in the integrations in the course of melting and gelation were measured and compared with integrations measured for the gels.

2.2.4 Saturation Transfer Difference (STD) NMR Spectroscopy.

Sample S2 (Table 2.1) was analyzed by STD NMR spectroscopy, using a Bruker Avance II 400 instrument. Selective saturation was achieved by using a train of 40 Gaussian pulses with a duration of 50 ms. The saturated NMR spectra were collected with on-resonance irradiation at 0 ppm (STD_{on}) and off-resonance irradiation at 40 ppm (STD_{off}). The longest saturation time was 20 s. Because saturation transfers magnetization from the gelating network to species bound to it,

differences in intensity between the STD_{on} and STD_{off} spectra identify species that interact with the network. The spin-lattice relaxation time (T_1) of different protons was also measured before the STD NMR experiments.

2.2.5 Diffusion Ordered NMR Spectroscopy (DOSY).

Samples for DOSY analysis were prepared by combining NaDC and formic acid in D_2O in a 5:1 molar ratio to give mixtures with nominal concentrations of NaDC in the range 10–100 mM. DOSY data were recorded at 25 °C using a Bruker Avance 500 NMR spectrometer with an STE-LED pulse sequence (stimulated echo with longitudinal eddy current delay). The gradient range was from 2.3 to 45 G/cm, and the number of gradients was 8. As controls, solutions of NaDC with the same concentration used in the corresponding NaDC/formic acid gels were also examined by DOSY.

2.2.6 Rheological Measurements.

An AR 2000 rheometer (TA Instruments) with a 40-mm steel cone and plate was used to measure the rheological properties of gels prepared in H_2O. Samples were melted to give homogeneous solutions and were transferred to the center of the rheometer plate. The samples were tested with 0.1% oscillatory strain at 20 °C until the values of the storage modulus (G') and the loss modulus (G") reached plateaus. To determine the gel-sol transition temperature of samples rheologically, once the G' and G" values reached the plateaus, the samples were heated to 65 °C with temperature increments of 1 °C. The samples were equilibrated at each temperature for 1 min, and the strain was kept at 0.1%.

2.2.7 Polarized-Light Optical Microscopy.

Gels were prepared in H_2O and were then melted. The resulting liquids were transferred to glass slides, placed under cover slips, and kept at 25 °C to allow the gels to reform. The samples were then observed using a Zeiss Axioskop polarized-light optical microscope.

2.3 Results and Discussion

Under specified conditions, adding formic acid to aqueous solutions of NaDC induces gelation. Suitable conditions were explored by using different concentrations of NaDC and various ratios of formic acid. When the concentrations of NaDC and formic acid were 50 and 10 mM,

respectively (corresponding to about 2% NaDC by weight), colorless transparent gels were formed overnight at 25 °C (Figure 2.1). NaDC/formic acid ratios above 5 yielded solutions that did not produce gels at 25 °C, and lower ratios led to precipitation. Because formic acid (pK_a 3.75) is substantially more acidic than deoxycholic acid (pK_a 5.89 above the critical micellar concentration),[52,53] each added equivalent of formic acid transforms an approximately equal amount of NaDC into the corresponding acid form. Under the conditions studied, hydrogelation requires an approximately 1:4 mixture of deoxycholic acid and the corresponding salt form, and formic acid is converted almost entirely into formate. To simplify discussion, we will refer to the nominal concentrations of NaDC and formic acid, which correspond to the sums of the acid and salt forms. When the NaDC/formic acid ratio was kept at 5, and the concentration of NaDC was increased to 100 mM, a colorless opaque gel was formed at 25 °C (Figure 2.1). An optical micrograph of this material under polarized light showed a fibrillar texture (Figure 2.1). We suggest that the higher concentration increases the density of fibrils, which can associate to form bundles large enough to scatter visible light, thereby creating an opaque gel instead of the transparent form produced at 50 mM.

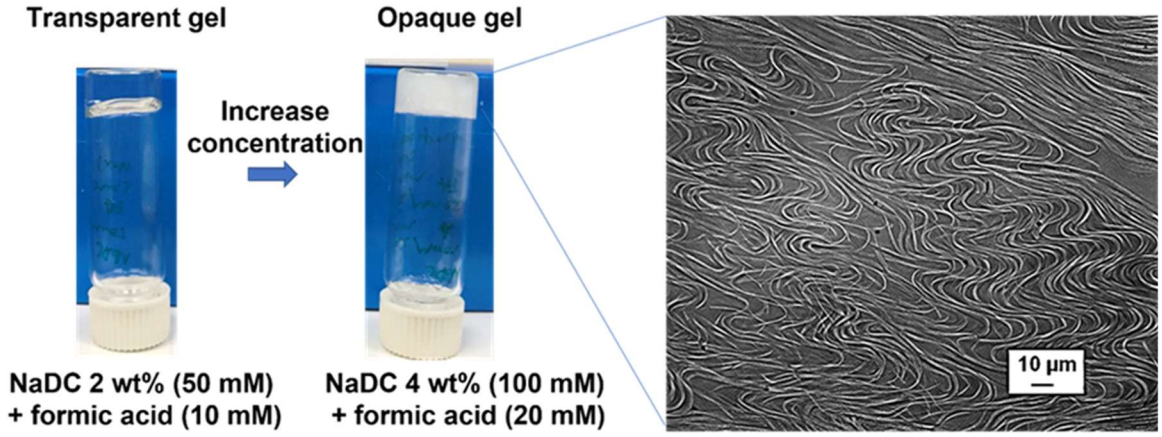

Figure 2.1. Hydrogels formed when solutions of NaDC and formic acid in H_2O are mixed in a 5:1 ratio. The images show the transparent gel formed when the nominal concentration of NaDC is 50 mM, the opaque gel produced at 100 mM, and the fibrillar texture of the opaque gel, as revealed by polarized-light optical microscopy.

NaDC and formic acid were mixed in a 5:1 ratio in D_2O at three different nominal concentrations of NaDC (20, 50, and 100 mM) to give samples S1, S2, and S3, respectively. Spin-spin relaxation times (T_2) of HDO in the samples were measured at various temperatures, and the resulting data are summarized in Table 2.1 and Figure 2.2. Both samples S2 (50 mM) and S3 (100 mM) gave gels at 25 °C and showed non-linear increases in T_2 in the range 35–45 °C; in contrast, sample S1 (20 mM) was fluid, and T_2 increased linearly with temperature. In samples S2 and S3, the marked increase in T_2 denotes transition from a gel to a solution. The resulting data were fitted to a sigmoidal curve, and a plot of the first derivative showed that $T_{gel\text{-}sol}$ is 42 °C for both samples S2 and S3 (Table 2.1). The storage modulus (G') and loss modulus (G'') of the gels were also determined at different temperatures (Figure 2.S1). From these measurements of macroscopic behavior, $T_{gel\text{-}sol}$ (the point at which G' and G'' become equal) is about 42 °C, which is the same as $T_{gel\text{-}sol}$ determined at the molecular level by NMR spectroscopy (Table 2.1). These values are also consistent with estimates of $T_{gel\text{-}sol}$ for a related NaDC/HCl gel system (~40 °C), based on changes in specific conductivity.[54]

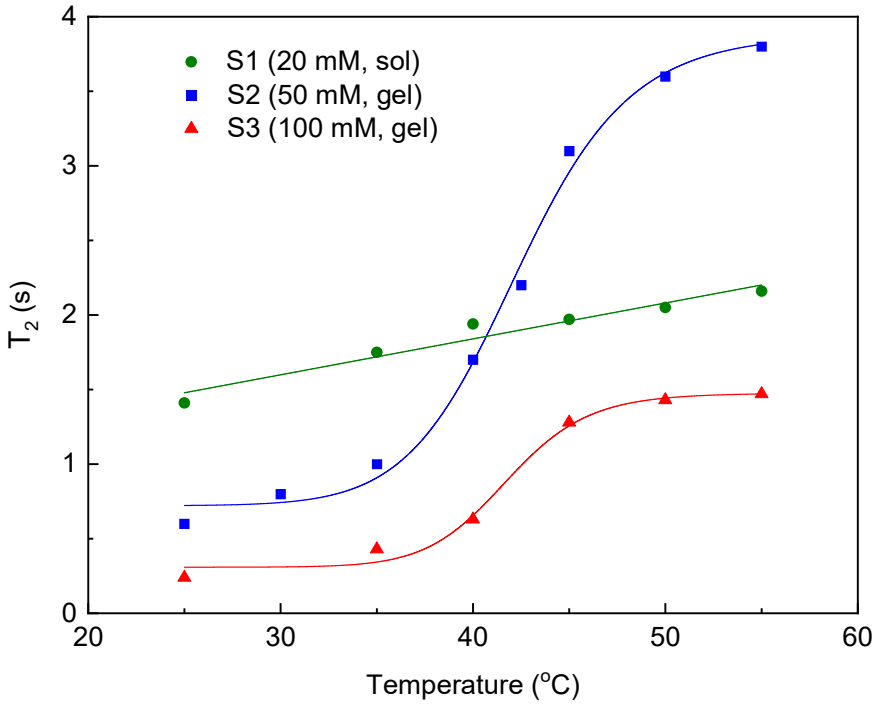

Figure 2.2. Spin-spin relaxation times (T_2) of HDO as a function of temperature, as measured by NMR spectroscopy in samples prepared by mixing solutions of NaDC and formic acid in D_2O in a 5:1 ratio, using three different nominal concentrations of NaDC.

To determine the proportion of molecules that are bound as part of the fibrillar network in NaDC hydrogels and those that remain free in solution, we used VT ^{1}H NMR spectroscopy to track signals assigned to NaDC, formate, and HDO, and we analyzed how their integration varies during the course of melting and gelation (Figure 2.3). Initial experiments were carried out with sample S2 (nominally 50 mM NaDC) in coaxial NMR tubes with a solution of maleic acid in D_2O as internal standard. Integrations and chemical shifts for all peaks were monitored. The chemical shifts of all species except HDO were essentially unchanged by variations in temperature; however, the integrations of all measurable protons in NaDC increased as a result of melting. This can be attributed to disassembly of the network present in the gelated state and formation of a solution. Subsequent cooling induced reformation of the gel within 5 h at 25 °C, and integration of NaDC signals decreased and returned to the value observed before heating. The results were reproducible in several heating-cooling cycles and were not affected by the length of the incubation time at

55 °C. The consistency of our observations confirms that under the conditions chosen, regeneration of the gel is not seeded and accelerated by deoxycholate aggregates that survive melting.[55] In contrast, integrations corresponding to formate and HDO remained nearly constant during the process of melting and reformation of a gel, as shown in Figure 2.S2. This suggests that the fibrillar network formed by associated molecules of NaDC and deoxycholic acid has a mainly hydrophobic interior that cannot immobilize significant quantities of small polar species such as formate and water.

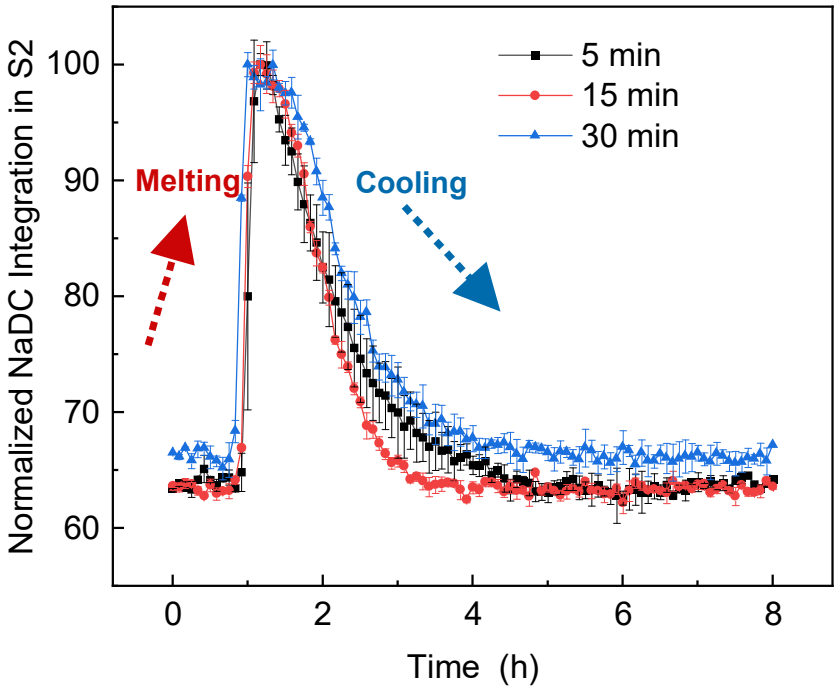

Figure 2.3. Changes in the integration of NaDC signals (nominal concentration 50 mM) as hydrogels were heated, melted, and reformed by cooling, as measured by VT ^{1}H NMR spectroscopy as a function of time. Integrations were normalized with respect to maleic acid as an internal standard. Melts were held at 55 °C for 5 min (black squares), 15 min (red circles), and 30 min (blue triangles). For each incubation time and for each sample, the melting-cooling procedure was repeated three times.

Opaque gels, which were formed at a higher nominal concentration of NaDC (100 mM), were also examined by VT ^{1}H NMR spectroscopy (Figure 2.S3), and quantitative analyses of integrations using both 50 mM samples (S2) and 100 mM samples (S3) are summarized in Table 2.2. In both S2 (transparent gel) and S3 (opaque gel), the integration of signals attributed to NaDC decreased by approximately 35% in the gelated state relative to the melt. This value can be considered to measure the fraction of molecules immobilized in the fibrillar network. Because the bulk samples contain NaDC and the corresponding bile acid in a ratio of 4:1, the observed changes in integration establish that the fibrillar network does not consist of the acid form alone, but must incorporate both the free acid and its salt. This is an important conclusion, because it suggests that effective gelation requires that the fibrils have a degree of charge, possibly to prevent excessive aggregation and precipitation.

Table 2.2. Decreases in the Integration of Proton Signals in VT ^{1}H NMR Spectra as Hydrogels Derived from NaDC are Reformed After Melting and Incubation

Sample	Species	Decreased integration (%) at different incubation times			Average (%)
		5 min	15 min	30 min	
S2 (50 mM)	NaDC	35.9	36.6	33.6	35.4 ± 1.6
	formate	6.5	4.1	5.4	5.4 ± 1.2
	HDO	1.7	2.6	3.3	2.5 ± 0.8
S3 (100 mM)	NaDC	35.1	34.8	34.5	34.8 ± 0.3
	formate	2.9	7.5	4.5	5.0 ± 2.3
	HDO	2.4	4.1	2.8	3.1 ± 0.9

To further explore the structure and dynamics of hydrogels formed by NaDC, we used STD NMR experiments to examine the transfer of magnetization from the fibrillar network to species free to interact with it (Figure 2.4). Differences in the intensity of signals of free species observed in on-resonance spectra (I_{SAT}) and in off-resonance experiments (I_0) reflect interaction of the

species with the network (Figure 2.4A). The ratio $(I_0\text{-}I_{SAT})/I_0$ gives the fractional STD response, which is represented by η_{STD}. The value of T_1 for formic acid (~22 s at 25 °C) is much larger than those of HDO (~4 s at 25 °C) and NaDC (~1 s at 25 °C), so formate should reach higher plateau. However, the corresponding value of η_{STD} proved to be almost zero (Figure 2.4B), confirming that formic acid induces gelation by converting an approximately equivalent amount of NaDC into the corresponding acid but does not interact in a significant way with the resulting network. This conclusion is consistent with the absence of marked changes in the integration of formate in VT ^{1}H NMR experiments in which NaDC hydrogels are melted and reformed (Table 2.2).

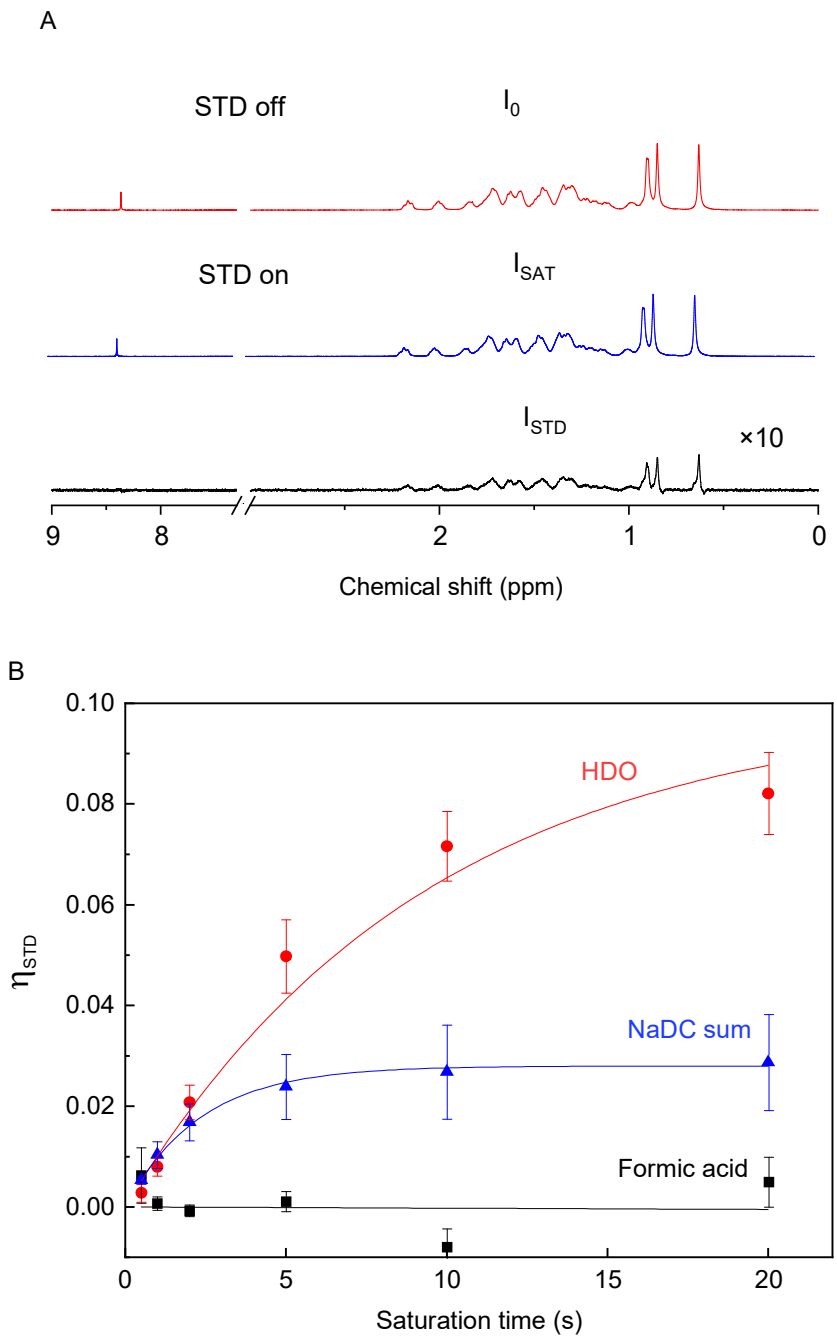

Figure 2.4. (A) STD NMR spectra of a hydrogel formed by NaDC under standard conditions (nominal concentration 50 mM), showing the off-resonance spectrum (red), the on-resonance experiment (blue), and the difference (black). The difference spectrum is increased in scale by a factor of 10. (B) Values of η_{STD} for different species as a function of saturation time. The curve

labeled “NaDC sum” represents the summed integrations of all detectable protons in the NMR spectrum of NaDC (in salt and acid forms).

In contrast, Figure 2.4B shows that free HDO and NaDC interact with the fibrillar network of the gel. This finding establishes that the network has a hydrated surface, on which exposed hydrophilic OH, COOH, and COO^- groups form hydrogen bonds with water. In addition, the network is a dynamic entity, with molecules of deoxycholate associating and dissociating reversibly. The behavior of HDO and NaDC can be assessed in more detail by using eq 1 to examine how η_{STD} depends on the saturation time t, on the saturation rate constant δ that measures how rapidly exchange reaches a steady state, and on η_{STD}^{MAX}, which is the value of η_{STD} when the saturation time is infinite. Higher values of T_1 make η_{STD} reach its plateau value more slowly. To remove the influence of different values of T_1 on δ, values of $\eta_{STD}^{MAX} \cdot \delta$ (which represents the initial slope at zero saturation time) were calculated and compared.[56] Similar values of $\eta_{STD}^{MAX} \cdot \delta$ are observed for HDO (1.1×10^{-2} s^{-1}) and NaDC (1.2×10^{-2} s^{-1}, as measured for all detectable protons). The rate constant observed for NaDC is much slower than the one measured for exchange involving aggregates in solution, which occurs in the microsecond domain.[57] This difference supports the conclusion that the STD NMR experiments probe the exchange of NaDC between the structure of the gel and the aqueous phase.

$$\eta_{STD} = \eta_{STD}^{MAX}\left(1 - e^{-\delta t}\right) \qquad (1)$$

Close analysis of the values of δ for specific protons of deoxycholate provides additional insight. Figure 2.5 provides individual plots of η_{STD} as a function of saturation time t for four individual protons, and Table 2.3 compiles the corresponding values of $\eta_{STD}^{MAX} \cdot \delta$, which vary from 0.7×10^{-2} s^{-1} to 2.2×10^{-2} s^{-1}. The smallest value corresponds to CH_2 α to the carboxyl group and the largest value to one of the axial methyl groups. This is consistent with the hypothesis that exchange occurs preferentially by contact of the hydrophobic edges or faces of free molecules of deoxycholate with those of molecules immobilized as components of the fibrillar network. The apparent mode of preferred exchange provides an intriguing suggestion that the growth of fibrils

or crystals composed of deoxycholate may occur in an analogous way, by adding individual molecules or micellar clusters to existing assemblies in ways that maximize the contact of hydrophobic surfaces.

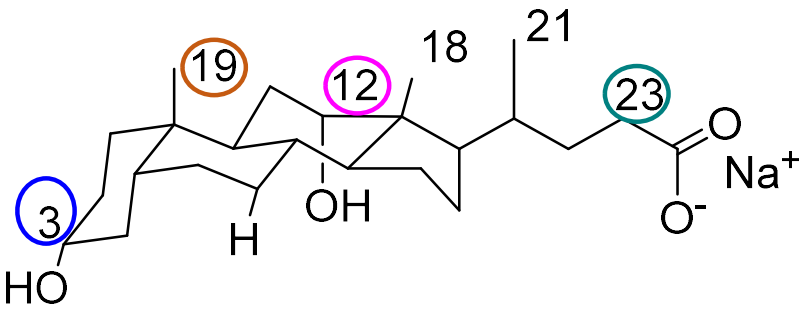

A

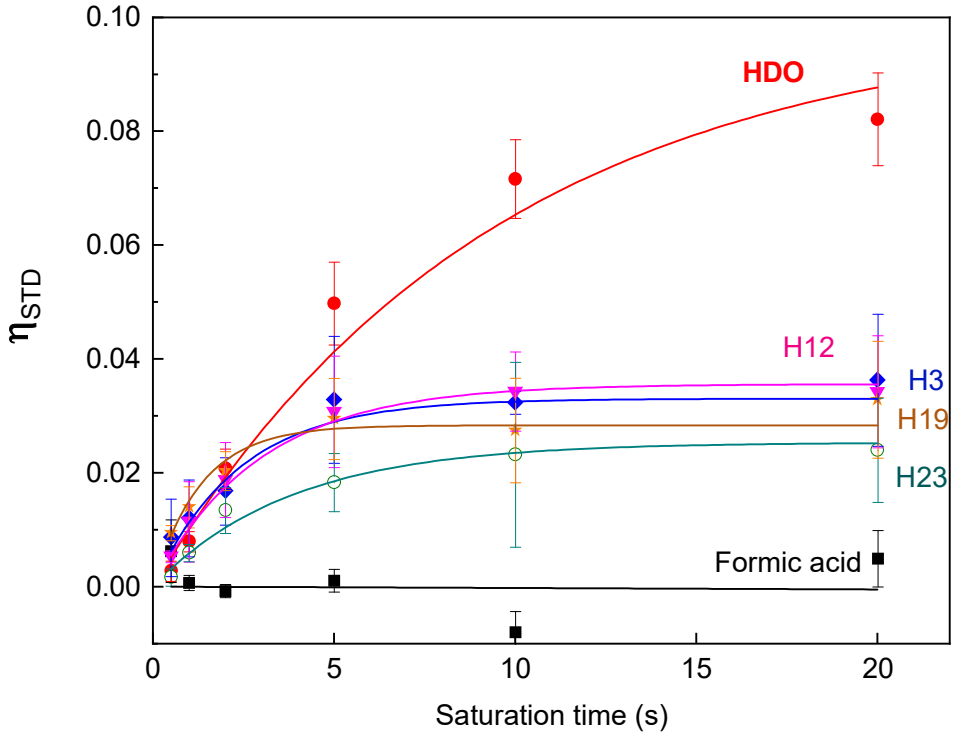

B

Figure 2.5. (A) Assignment of certain specific protons in NaDC. (B) Plots of η_{STD} as a function of saturation time for HDO, formate, and selected protons in NaDC in sample S2 (50 mM).

Table 2.3. Adjusted Rate Constants for Exchange ($\boldsymbol{\eta_{STD}^{MAX} \cdot \delta}$) for Different Assigned Protons in NaDC in Sample S2 (50 mM)

Proton signals	HDO	NaDC			
		23	12	3	19
Rate constant $\eta_{STD}^{MAX} \cdot \delta$ (k × 10^{-2} s^{-1})	1.1 ± 0.4	0.7 ± 0.3	1.2 ± 0.1	1.4 ± 0.2	2.2 ± 0.4

DOSY NMR experiments were carried out to study the diffusion of HDO and NaDC in hydrogels. Figure 2.6 shows that the diffusion coefficients of both components of the gels are similar to those measured in aqueous solutions of NaDC at the same concentrations. However, it is important to note that DOSY experiments only assess the behavior of molecules that remain free to diffuse in solution. As shown by VT ^{1}H NMR spectra, about 35% of the molecules of NaDC are immobilized as components of the fibrillar network, thereby preventing their diffusion but making them invisible in DOSY experiments. The measured diffusion coefficient of NaDC reflects only the part that remains dissolved in aqueous solution. Although STD NMR experiments show binding of HDO to the fibrillar network, the concentration of pure water (55.5 M) is much higher than the nominal concentration of NaDC (50 mM), so DOSY experiments cannot distinguish the small fraction of molecules of water bound to the gel network from those that remain free to diffuse.

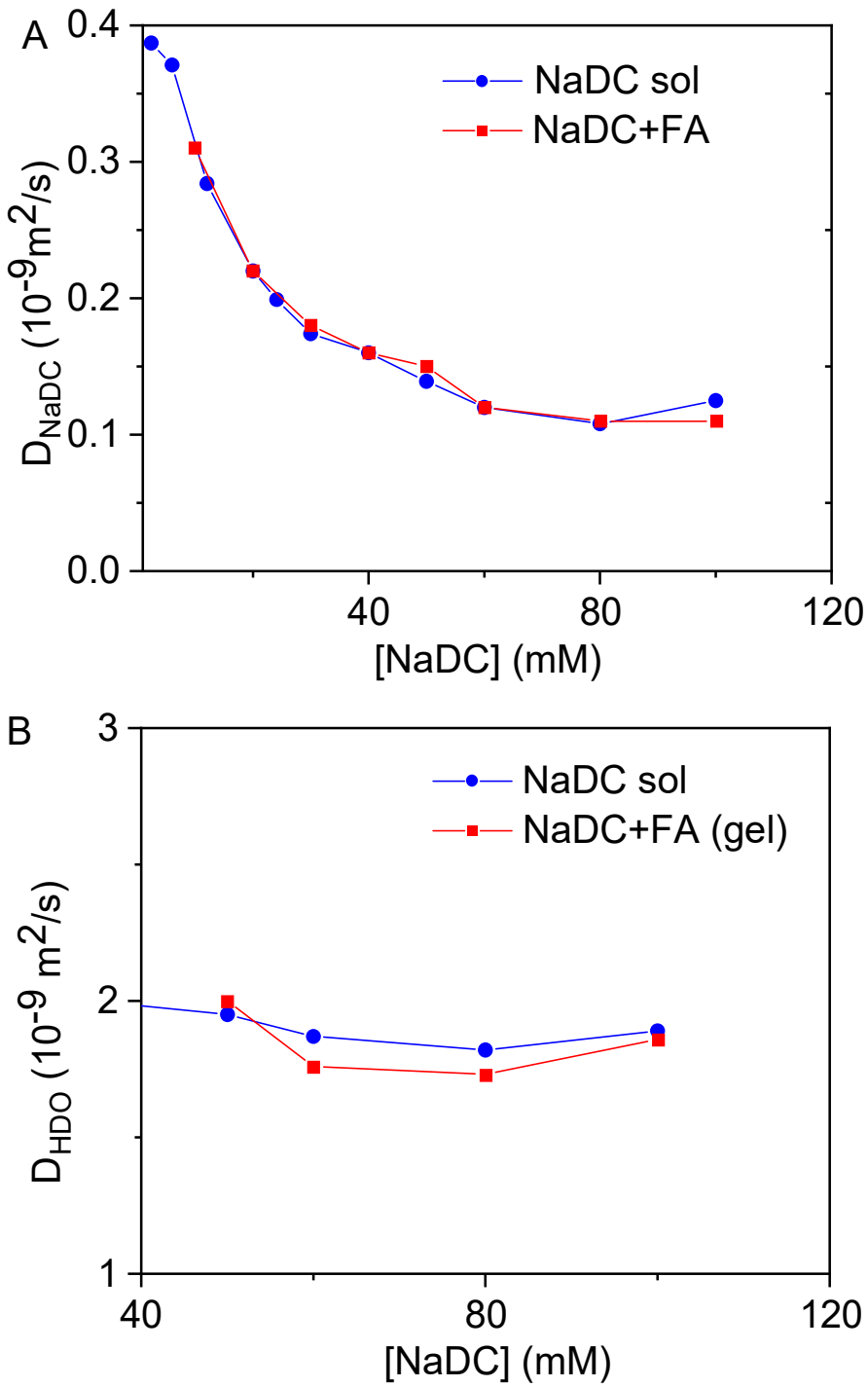

Figure 2.6. Plots of diffusion coefficients (D) as a function of the nominal concentration of NaDC, as measured by DOSY experiments for NaDC (Figure 2.6A) and HDO (Figure 2.6B). Values shown in blue correspond to diffusion measured in solutions of NaDC in D_2O, and those in red correspond to diffusion in mixtures produced by adding formic acid in the standard 1:5 ratio. Gelation occurred at nominal concentrations of NaDC ≥ 40 mM.

2.4 Conclusions

Bile acids and their salts occupy a special position in the realm of hydrogelation because their well-defined structures restrict how associated molecules can be positioned with respect to neighbors, thereby ensuring that their organization in gels, solid forms, and other states will be closely analogous. We have used various tools of NMR spectroscopy to probe hydrogelation induced by these compounds, with NaDC chosen as a representative example. Integration of signals in the spectra of hydrogels produced by mixtures of NaDC and formic acid has revealed that most molecules of NaDC and the corresponding bile acid remain free under typical conditions (65%). The fibrillar network of the gel is composed of both the protonated and unprotonated forms of deoxycholate, and the presence of charge may help prevent excessive aggregation and precipitation. Spin-spin relaxation times showed that a molecular-level estimate of $T_{\text{gel-sol}}$ (42 °C) matches values obtained by macroscopic methods. Formic acid is needed in the system to ensure partial protonation of NaDC and subsequent gelation; however, STD NMR spectroscopy has established that formate is not incorporated to a significant degree as a component of the fibrillar network of the gels. In contrast, interaction with HDO indicates that the network has a surface with exposed hydrophilic groups. In addition, STD NMR experiments showed that free molecules of deoxycholate associate reversibly with the network by interactions of complementary hydrophobic regions. This observation suggests that fibrils or crystals composed of deoxycholate may grow in an analogous way. In these ways, NMR experiments have provided a deeper understanding of hydrogelation and the associative behavior of NaDC and related derivatives of bile acids.

Notes. The authors have no competing interests to declare.

2.5 Supporting Information

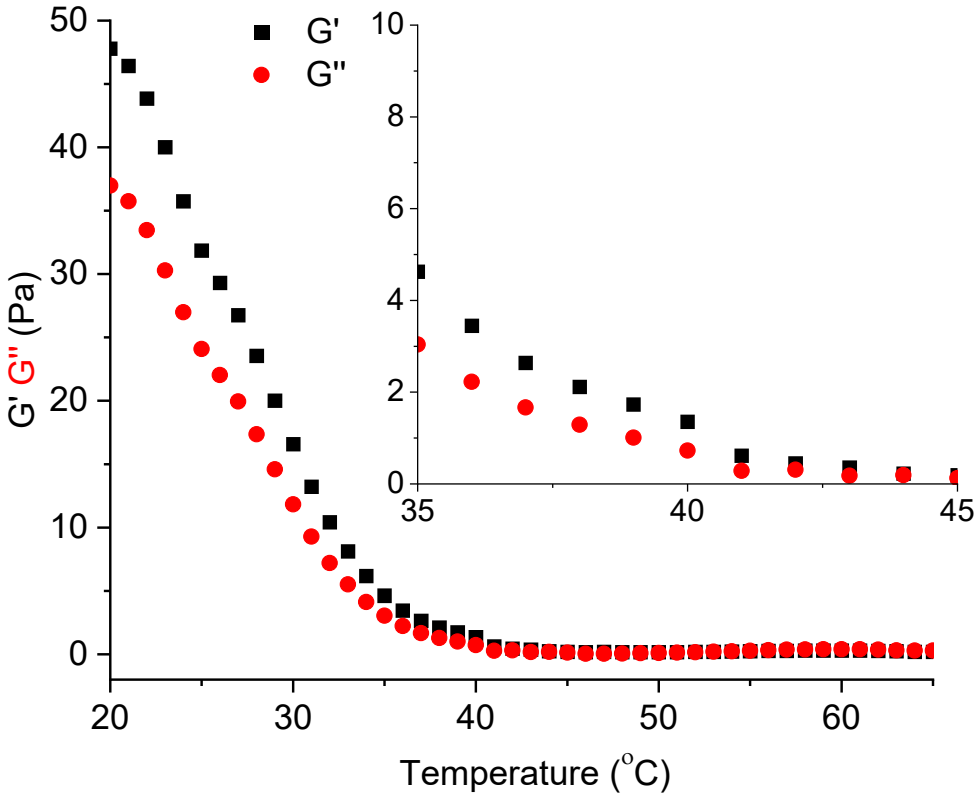

Figure 2.S1. Graph showing how the storage modulus G' (black squares) and loss modulus G" (red circles) of a hydrogel prepared from NaDC (100 mM) vary as a function of temperature.

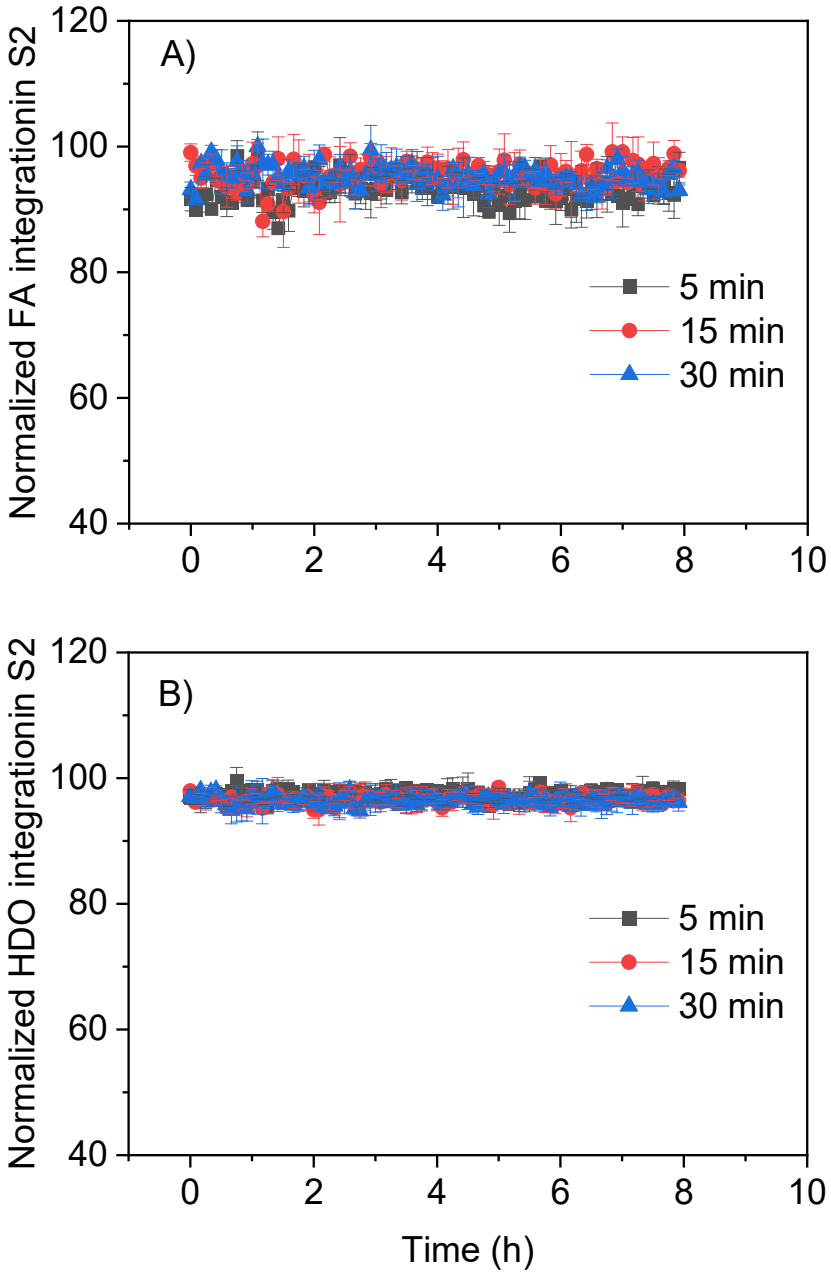

Figure 2.S2. Changes in the integration of signals of formate and HDO as a hydrogel formed from NaDC is heated, melted, and reformed by cooling, as measured by VT ^{1}H NMR spectroscopy as a function of time. (A) Plot showing the integration of signals derived from formate. (B) Plot showing the integration of signals derived from HDO. In both plots, integrations were normalized with respect to a solution of maleic acid in D_2O as an internal standard, and the nominal concentration of NaDC used in the experiment was 50 mM. Melts were held at 55 °C for 5 min

(black squares), 15 min (red circles), and 30 min (blue triangles). For each incubation time and for each sample, the melting-cooling procedure was repeated three times.

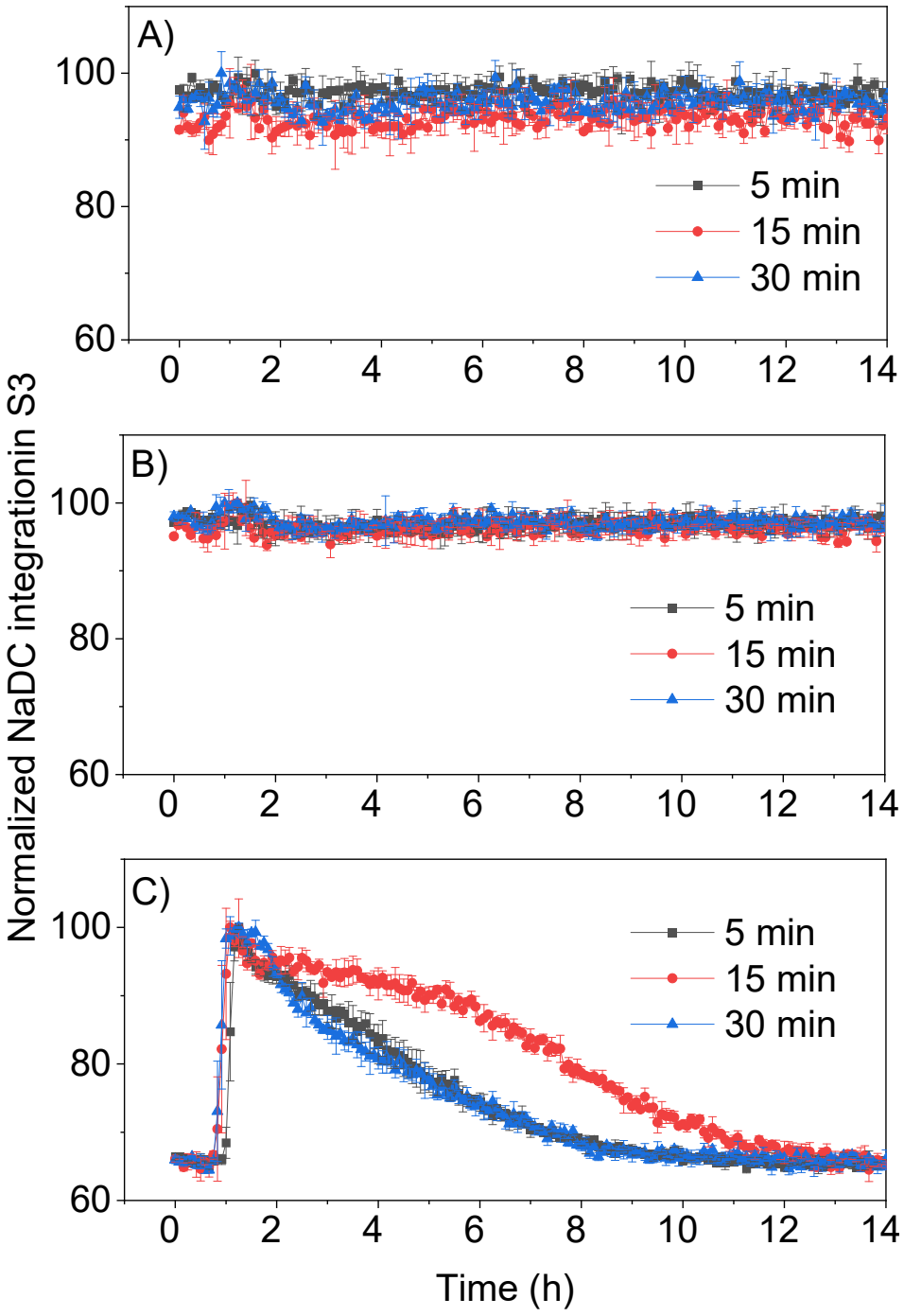

Figure 2.S3. Changes in the integration of signals as a hydrogel formed from NaDC is heated, melted, and reformed by cooling, as measured by VT ^{1}H NMR spectroscopy as a function of time. (A) Plot showing the integration of signals derived from formate. (B) Plot showing the integration of signals derived from HDO. (C) Plot showing the integration of signals derived from NaDC. In all plots, integrations were normalized with respect to a solution of maleic acid in D_2O as an internal standard, and the nominal concentration of NaDC used in the experiments was 100 mM. Melts were held at 55 °C for 5 min (black squares), 15 min (red circles), and 30 min (blue triangles). For each incubation time and for each sample, the melting-cooling procedure was repeated three times.

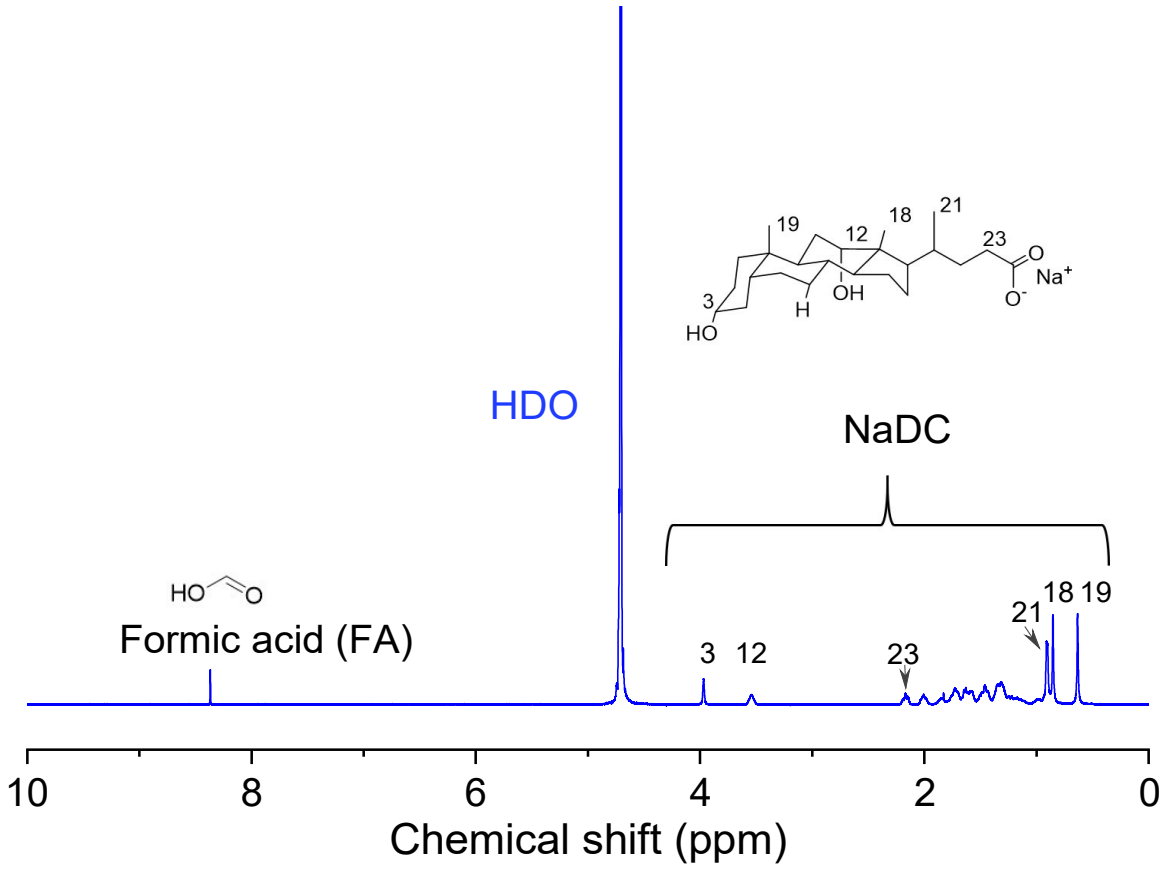

Figure 2.S4. ^{1}H NMR spectrum of a hydrogel formed from a 5:1 mixture of NaDC and formic acid in D_2O. Signals assigned to certain specific protons are labeled.

2.6 Acknowledgments.

Financial support from the Natural Sciences and Engineering Research Council (NSERC) of Canada (RGPIN-2019-05469 and RGPIN-2020-06517) is gratefully acknowledged. In addition, JDW thanks the Canada Research Chairs Program for its generous support. The authors are grateful to reviewers of the manuscript for their constructive comments.

Dedication. Dedicated to the memory of the late Françoise Winnik, whose deep understanding of molecular materials and devotion to science made her a valued friend, colleague, and model.

2.7 References

1. Draper, E. R.; Adams, D. J. Low-Molecular-Weight Gels: The State of the Art. *Chem* **2017**, *3*, 390–410.
2. Hanabusa, K.; Suzuki, M. Physical Gelation by Low-Molecular-Weight Compounds and Development of Gelators. *Bull. Chem. Soc. Jpn.* **2016**, *89*, 174–182.
3. Du, X.; Zhou, J.; Shi, J.; Xu, B. Supramolecular Hydrogelators and Hydrogels: From Soft Matter to Molecular Biomaterials. *Chem. Rev.* **2015**, *115*, 13165–13307.
4. Sangeetha, N. M.; Maitra, U. Supramolecular Gels: Functions and Uses. *Chem. Soc. Rev.* **2005**, *34*, 821–836.
5. Estroff, L. A.; Hamilton, A. D. Water Gelation by Small Organic Molecules. *Chem. Rev.* **2004**, *104*, 1201–1217.
6. Terech, P.; Weiss, R. G. Low Molecular Mass Gelators of Organic Liquids and the Properties of Their Gels. *Chem. Rev.* **1997**, *97*, 3133–3159.
7. Bariya, D.; Anand, V.; Mishra, S. Recent Advances in the Bile Acid Based Conjugates/Derivatives Towards Their Gelation Applications. *Steroids* **2021**, *165*, 108769.
8. di Gregorio, M. C.; Travaglini, L.; Del Giudice, A.; Cautela, J.; Pavel, N. V.; Galantini, L. Bile Salts: Natural Surfactants and Precursors of a Broad Family of Complex Amphiphiles. *Langmuir* **2019**, *35*, 6803–6821.
9. Goldshleger, N. F.; Lobach, A. S.; Baulin, V. E.; Tsivadze, A. Y. Supramolecular Gels Based on Bile Acid Salts. *Russ. Chem. Rev.* **2017**, *86*, 269–297.
10. Zhang, M.; Strandman, S.; Waldron, K. C.; Zhu, X. X. Supramolecular Hydrogelation with Bile Acid Derivatives: Structure, Properties and Applications. *J. Mater. Chem. B* **2016**, *4*, 7506–7520.
11. Svobodová, H.; Noponen, V.; Kolehmainen, E.; Sievänen, E. Recent Advances in Steroidal Supramolecular Gels. *RSC Adv.* **2012**, *2*, 4985–5007.
12. Madenci, D.; Egelhaaf, S. U. Self-Assembly in Aqueous Bile Salt Solutions. *Curr. Opin. Colloid Interface Sci.* **2010**, *15*, 109–115.
13. Calabresi, M.; Andreozzi, P.; La Mesa, C. Supra-Molecular Association and Polymorphic Behaviour In Systems Containing Bile Acid Salts. *Molecules* **2007**, *12*, 1731–1754.

14. Hofmann, A. F.; Hagey, L. R. Bile Acids: Chemistry, Pathochemistry, Biology, Pathobiology, and Therapeutics. *Cell. Mol. Life Sci.* **2008**, *65*, 2461–2483.
15. Mukhopadhyay, S.; Maitra, U. Chemistry and Biology of Bile Acids. *Curr. Sci.* **2004**, *87*, 1666–1683.
16. Shokry, D. S.; Waters, L. J.; Parkes, G. M. B.; Mitchell, J. C.; Snowden, M. J. Formation of a Bile Salt–Drug Hydrogel to Predict Human Intestinal Absorption. *J. Pharm. Sci.* **2019**, *108*, 279–287.
17. Pavlović, N.; Goločorbin-Kon, S.; Danić, M.; Stanimirov, B.; Al-Salami, H.; Stankov, K.; Mikov, M. Bile Acids and Their Derivatives as Potential Modifiers of Drug Release and Pharmacokinetic Profiles. *Front. Pharmacol.* **2018**, *9*, 1283.
18. Faustino, C.; Serafim, C.; Rijo, P.; Pinto Reis, C. Bile Acids and Bile Acid Derivatives: Use in Drug Delivery Systems and as Therapeutic Agents. *Expert Opin. Drug Deliv.* **2016**, *13*, 1133–1148.
19. Sharma, R.; Long, A.; Gilmer, J. F. Advances in Bile Acid Medicinal Chemistry. *Curr. Med. Chem.* **2011**, *18*, 4029–4052.
20. Virtanen, E.; Kolehmainen, E. Use of Bile Acids in Pharmacological and Supramolecular Applications. *Eur. J. Org. Chem.* **2004**, 3385–3399.
21. Enhsen, A.; Kramer, W.; Wess, G. Bile Acids in Drug Discovery. *Drug Discov. Today* **1998**, *3*, 409–418.
22. Zhang, M.; Waldron, K. C.; Zhu, X. X. Formation of Molecular Hydrogels from a Bile Acid Derivative and Selected Carboxylic Acids. *RSC Adv.* **2016**, *6*, 35436–35440.
23. Zhang, M.; Ma, Z.; Wang, K.; Zhu, X. X. CO_2 Sequestration by Bile Salt Aqueous Solutions and Formation of Supramolecular Hydrogels. *ACS Sustainable. Chem. Eng.* **2019**, *7*, 3949–3955.
24. Zhang, M. Supramolecular Hydrogels Based on Bile Acids and Their Derivatives. Ph. D. Thesis, Université de Montréal: Montréal, October 2016.
25. Mukherjee, K.; Barman, A.; Biswas, R. Impact of the Aggregation Behaviour of Sodium Cholate and Sodium Deoxycholate on Aqueous Solution Structure and Dynamics: A Combined Time Resolved Fluorescence and Dielectric Relaxation Spectroscopic Study. *J. Mol. Liq.* **2016**, *222*, 495–502.

26. McNeel, K. E.; Das, S.; Siraj, N.; Negulescu, I. I.; Warner, I. M. Sodium Deoxycholate Hydrogels: Effects of Modifications on Gelation, Drug Release, and Nanotemplating. *J. Phys. Chem. B* **2015**, *119*, 8651–8659.
27. Bogdanova, L. R.; Gnezdilov, O. I.; Idiyatullin, B. Z.; Kurbanov, R. K.; Zuev, Y. F.; Us'yarov, O. G. Micellization in Sodium Deoxycholate Solutions. *Colloid J.* **2012**, *74*, 1–6.
28. Li, R.; Carpentier, E.; Newell, E. D.; Olague, L. M.; Heafey, E.; Yihwa, C.; Bohne, C. Effect of the Structure of Bile Salt Aggregates on the Binding of Aromatic Guests and the Accessibility of Anions. *Langmuir* **2009**, *25*, 13800–13808.
29. Adhikari, A.; Dey, S.; Mandal, U.; Das, D. K.; Ghosh, S.; Bhattacharyya, K. Femtosecond Solvation Dynamics in Different Regions of a Bile Salt Aggregate: Excitation Wavelength Dependence. *J. Phys. Chem. B* **2008**, *112*, 3575–3580.
30. Pártay, L. B.; Sega, M.; Jedlovszky, P. Morphology of Bile Salt Micelles as Studied by Computer Simulation Methods. *Langmuir* **2007**, *23*, 12322–12328.
31. Sen, S.; Dutta, P.; Mukherjee, S.; Bhattacharyya, K. Solvation Dynamics in Bile Salt Aggregates. *J. Phys. Chem. B* **2002**, *106*, 7745–7750.
32. Jover, A.; Meijide, F.; Rodríguez Núñez, E.; Vázquez Tato, J. Aggregation Kinetics of Sodium Deoxycholate in Aqueous Solution. *Langmuir* **1998**, *14*, 4359–4363.
33. D'Alagni, M.; D'Archivio, A. A.; Galantini, L.; Giglio, E. Structural Study of the Micellar Aggregates of Sodium Chenodeoxycholate and Sodium Deoxycholate. *Langmuir* **1997**, *13*, 5811–5815.
34. Lopez, F.; Samseth, J.; Mortensen, K.; Rosenqvist, E.; Rouch, J. Micro- and Macrostructural Studies of Sodium Deoxycholate Micellar Complexes in Aqueous Solutions. *Langmuir* **1996**, *12*, 6188–6196.
35. Kano, K.; Tatemoto, S.; Hashimoto, S. Specific Interactions between Sodium Deoxycholate and Its Water-Insoluble Analogues. Mechanisms for Premicelle and Micelle Formation of Sodium Deoxycholate. *J. Phys. Chem.* **1991**, *95*, 966–970.
36. Zakrzewska, J.; Marković, V.; Vučelić, D.; Feigin, L.; Dembo, A.; Mogilevsky, L. Investigation of Aggregation Behavior of Bile Salts by Small-Angle X-ray Scattering. *J. Phys. Chem.* **1990**, *94*, 5078–5081.

37. Mazer, N. A.; Carey, M. C.; Kwasnick, R. F.; Benedek, G. B. Quasielastic Light Scattering Studies of Aqueous Biliary Lipid Systems. Size, Shape, and Thermodynamics of Bile Salt Micelles. *Biochemistry* **1979**, *18*, 3064–3075.
38. Kratohvil, J. P.; Hsu, W. P.; Kwok, D. I. How Large Are the Micelles of Di-α-hydroxy Bile Salts at the Critical Micellization Concentrations in Aqueous Electrolyte Solutions? Results for Sodium Taurodeoxycholate and Sodium Deoxycholate. *Langmuir* **1986**, *2*, 256–258.
39. Nonappa; Kolehmainen, E. Solid State NMR Studies of Gels Derived from Low Molecular Mass Gelators. *Soft Matter* **2016**, *12*, 6015–6026.
40. Wallace, M.; Iggo, J. A.; Adams, D. J. Using Solution State NMR Spectroscopy to Probe NMR Invisible Gelators. *Soft Matter* **2015**, *11*, 7739–7747.
41. Nonappa; Šaman, D.; Kolehmainen, E. Studies on Supramolecular Gel Formation Using DOSY NMR. *Magn. Reson. Chem.* **2015**, *53*, 256–260.
42. Yu, G.; Yan, X.; Han, C.; Huang, F. Characterization of Supramolecular Gels. *Chem. Soc. Rev.* **2013**, *42*, 6697–6722.
43. Shapiro, Y. E. Structure and Dynamics of Hydrogels and Organogels: An NMR Spectroscopy Approach. *Prog. Polym. Sci.* **2011**, *36*, 1184–1253.
44. Angulo, J.; Nieto, P. M. STD-NMR: Application to Transient Interactions between Biomolecules–a Quantitative Approach. *Eur. Biophys. J.* **2011**, *40*, 1357–1369.
45. Ramalhete, S. M.; Nartowski, K. P.; Sarathchandra, N.; Foster, J. S.; Round, A. N.; Angulo, J.; Lloyd, G. O.; Khimyak, Y. Z. Supramolecular Amino Acid Based Hydrogels: Probing the Contribution of Additive Molecules Using NMR Spectroscopy. *Chem. Eur. J.* **2017**, *23*, 8014–8024.
46. Segarra-Maset, M. D.; Escuder, B.; Miravet, J. F. Selective Interaction of Dopamine with the Self-Assembled Fibrillar Network of a Molecular Hydrogel Revealed by STD-NMR. *Chem. Eur. J.* **2015**, *21*, 13925–13929.
47. Liu, A.-h.; Mao, S.-z.; Liu, M.-l.; Du, Y.-r. Aggregation Behavior of Sodium Deoxycholate and Its Interaction with Cetyltrimethylammonium Bromide in Aqueous Solution Studied by NMR Spectroscopy. *Colloid Polym. Sci.* **2008**, *286*, 1629–1636.
48. Campredon, M.; Quiroa, V.; Thevand, A.; Allouche, A.; Pouzard, G. NMR Studies of Bile Acid Salts: 2D NMR Studies of Aqueous and Methanolic Solutions of Sodium Cholate and Deoxycholate. *Magn. Reson. Chem.* **1986**, *24*, 624–629.

49. Conte, G.; Di Blasi, R.; Giglio, E.; Parretta, A.; Pavel, N. V. Nuclear Magnetic Resonance and X-ray Studies on Micellar Aggregates of Sodium Deoxycholate. *J. Phys. Chem.* **1984**, *88*, 5720–5724.
50. Meiboom, S.; Gill, D. Modified Spin-Echo Method for Measuring Nuclear Relaxation Times. *Rev. Sci. Instrum.* **1958**, *29*, 688–691.
51. Carr, H. Y.; Purcell, E. M. Effects of Diffusion on Free Precession in Nuclear Magnetic Resonance Experiments. *Phys. Rev.* **1954**, *94*, 630–638.
52. Farkaš, Z.; Poša, M.; Tepavčević, V. Determination of pK_a Values of Oxocholanoic Acids by Potentiometric Titration. *J. Surfact. Deterg.* **2014**, *17*, 609–614.
53. Ekwall, P.; Rosendahl, T.; Löfman, N. Studies on Bile Acid Salt Solutions. I. The Dissociation Constants of the Cholic and Desoxycholic Acids. *Acta Chem. Scand.* **1957**, *11*, 590–598.
54. Botré, C.; Cicconetti, P. A.; Lionetti, G.; Marchetti, M. Cation Radius and Deoxycholic Acid Polymer-Like Structure Stability. *J. Pharm. Sci.* **1967**, *56*, 1035–1037.
55. Blow, D. M.; Rich, A. Studies on the Formation of Helical Deoxycholate Complexes. *J. Am. Chem. Soc.* **1960**, *82*, 3566–3571.
56. Mayer, M.; James, T. L. NMR-Based Characterization of Phenothiazines as a RNA Binding Scaffold. *J. Am. Chem. Soc.* **2004**, *126*, 4453–4460.
57. Li, Y.; Holzwarth, J. F.; Bohne, C. Aggregation Dynamics of Sodium Taurodeoxycholate and Sodium Deoxycholate. *Langmuir* **2000**, *16*, 2038–2041.

Chapter 3. Probing the Relationship Between Gelation and Crystallization by Using Salts of Lithocholic Acid

Abstract

Hydrogels derived from lithocholic acid (LCA), other bile acids, and their salts are promising materials for drug delivery, cellular immobilization, and other applications. We have found that ammonium salts of LCA are particularly useful for probing the mechanism of hydrogelation and for understanding the relationship between molecular organization in gels and crystals. The well-defined amphiphilic steroidal structure of the lithocholate anion favors a consistent pattern of association under different conditions. However, the nature of the resulting aggregates can be controlled by systematically varying the ammonium counterions, giving rise to hydrogels, mixtures of fibrils and crystals, or only crystals under essentially identical conditions of assembly. By using tools for studying gels in tandem with methods of crystal engineering, we have developed a detailed understanding of the association of ammonium lithocholates. In particular, our work suggests how molecules of lithocholate are arranged in networked fibrils that give rise to hydrogelation, provides evidence that gelation and crystallization are intimately related in this system, and helps explain in molecular detail why certain salts give rise to gels and others favor crystallization.

This chapter has been published as a research article: Puzhen Li, Meng Zhang, Thierry Maris, X. X. Zhu, and James D. Wuest. "Probing the Relationship Between Gelation and Crystallization by Using Salts of Lithocholic Acid." *Crystal Growth & Design* (**2021**). (https://pubs.acs.org/doi/10.1021/acs.cgd.1c01182)

3.1 Introduction

Gels are semisolid materials in which large amounts of liquid are immobilized within nonfluid networks.[1,2] The materials are uniquely useful because they combine a degree of solid-like resistance to deformation (elasticity) with a liquid-like ability to change shape (viscosity). Of special importance are hydrogels, which result when the incorporated liquid is water.[3–8] Hydrogels are widespread in nature and occur in the human body in diverse forms, such as cartilage, tendons, and the vitreous humor of the eye. In addition, synthetic hydrogels have a vast range of industrial applications. The broad utility and diverse behavior of hydrogels provide ample motivation to learn how the materials are formed, how the associative properties of hydrogelators depend on their molecular structures, and how improved gels can be made by design. Many families of hydrogelators have been studied extensively; nevertheless, the structures they adopt remain unclear, and the relationship between gelation and other manifestations of molecular association such as crystallization continues to be investigated.

Typically, gelation occurs when dissolved substances interact to generate complex interconnected fibrillar structures that immobilize the surrounding solvent. Potential gelating agents include polymers, as well as small well-defined molecules that can associate reversibly to form extended networks.[9–16] In particular, water can be gelled by various classes of small amphiphilic molecules that have polar regions to ensure adequate aqueous solubility, along with hydrophobic features to induce aggregation. In general, families of small-molecule hydrogelators have been discovered serendipitously, and factors distinguishing effective gelators from substances that prefer to remain in solution, crystallize, or precipitate in other forms remain obscure. Occasionally, compounds that form gels can also be induced to crystallize, although rarely under the conditions used for gelation.[17–30] In addition, gels have sometimes been observed to yield crystalline precipitates on standing, showing that in certain cases gelation is favored kinetically but not thermodynamically.[31–44] In general, however, the kinetic and thermodynamic relationship between gelation and crystallization remains unclear.[45–47]

Most known small-molecule hydrogelators have structures that are flexible, can adopt multiple conformations, and have functional groups that can allow molecular association to occur in many ways. Moreover, compounds can usually crystallize in various polymorphic and solvated forms.[48] As a consequence, there is no compelling reason in most cases to expect studies of single

crystals by X-ray diffraction to reveal the structure of the fibrillar networks of gels in molecular detail, even when crystals of the gelator are formed within the gel itself or under similar conditions. So far, these circumstances have made it impossible to reach fully compelling conclusions about how molecules are ordered in complex assemblies of the type that cause hydrogelation.

To acquire a deeper understanding of the structure of hydrogels and to probe the relationship between gelation and crystallization, we elected to study families of small-molecule amphiphiles with structural features that force molecular association to occur according to a consistent pattern. If such compounds can be induced to form both hydrogels and crystals, structural studies carried out by X-ray diffraction will simultaneously reveal how the molecules are organized in the fibrillar structures of gels. Such studies may not reveal how all hydrogelators work; however, a finely detailed portrait of the behavior of a particular series of compounds will emerge, allowing molecular structure and properties to be correlated in a way that is likely to yield valuable new insights about gelation and crystallization.

In seeking suitable systems for study, we were drawn to bile acids and their salts,[49–55] which are natural steroids present in mammals and other vertebrates to serve various purposes, such as facilitating the digestion of fats and the absorption of nutrients with poor solubility in water.[56–58] Examples include lithocholic acid (**1**) and deoxycholic acid (**2**), which will be abbreviated as LCA and DCA, respectively. As illustrated by LCA and DCA, bile acids have amphiphilic structures in which an extended convex hydrophobic surface is combined with hydrophilic hydroxyl and carboxyl groups. This amphiphilicity allows bile acids, their salts, and other derivatives to form biocompatible hydrogels that are promising materials for use in drug delivery, cellular immobilization, and other applications.[59–64] Our group has worked extensively with these materials, and we have examined hydrogels formed by derivatives of bile acids in conjunction with carboxylic acids,[65] the sequestration of CO_2 by hydrogels containing bile acid salts,[66] and related topics.[51,67,68]

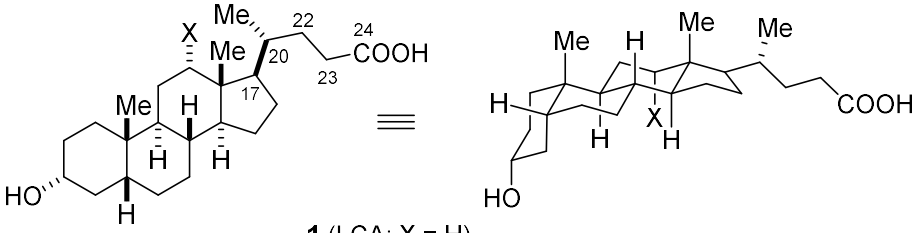

1 (LCA; X = H)
2 (DCA; X = OH)

3.2 Results and Discussion

LCA has low solubility in water at pH 7, but solutions of the corresponding NH_4^+ salt with concentrations of about 50 mM (2 wt%) can be obtained by warming aqueous mixtures made by combining LCA and NH_3 in a 1:16 molar ratio. Cooling the solutions to 25 °C led reproducibly to the formation of hydrogels, which were characterized by standard methods, including optical microscopy, electron microscopy, and rheological measurements. Analogous results were observed when NH_3 was replaced by $MeNH_2$ and $EtNH_2$, again in 16-fold molar excess relative to LCA. Optical micrographs of the three hydrogels are shown in Figure 3.1, electron micrographs appear in Figure 3.2a–c, and rheological data are included in the Supporting Information. In all cases, the micrographs confirm that ordered fibrillar structures are formed by association of the ammonium lithocholates, at least in a dried state,[69] suggesting that crosslinking or entanglement of the aggregates underlies the observed hydrogelation.

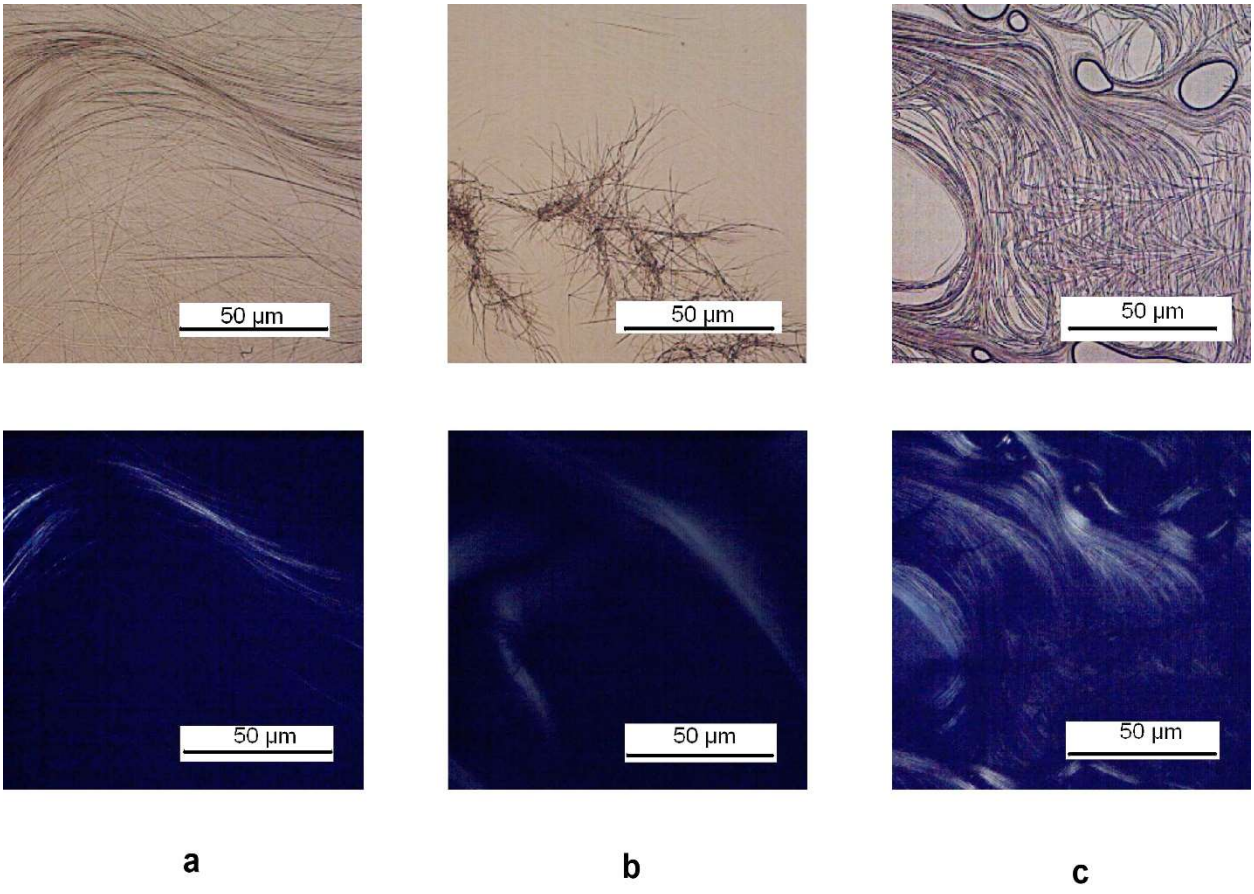

Figure 3.1. Fibrillar textures in hydrogels formed by three ammonium lithocholates under standard conditions, as imaged by optical microscopy under normal light (upper row) and polarized light (lower row). (a) NH_4^+ salt. (b) $MeNH_3^+$ salt. (c) $EtNH_3^+$ salt.

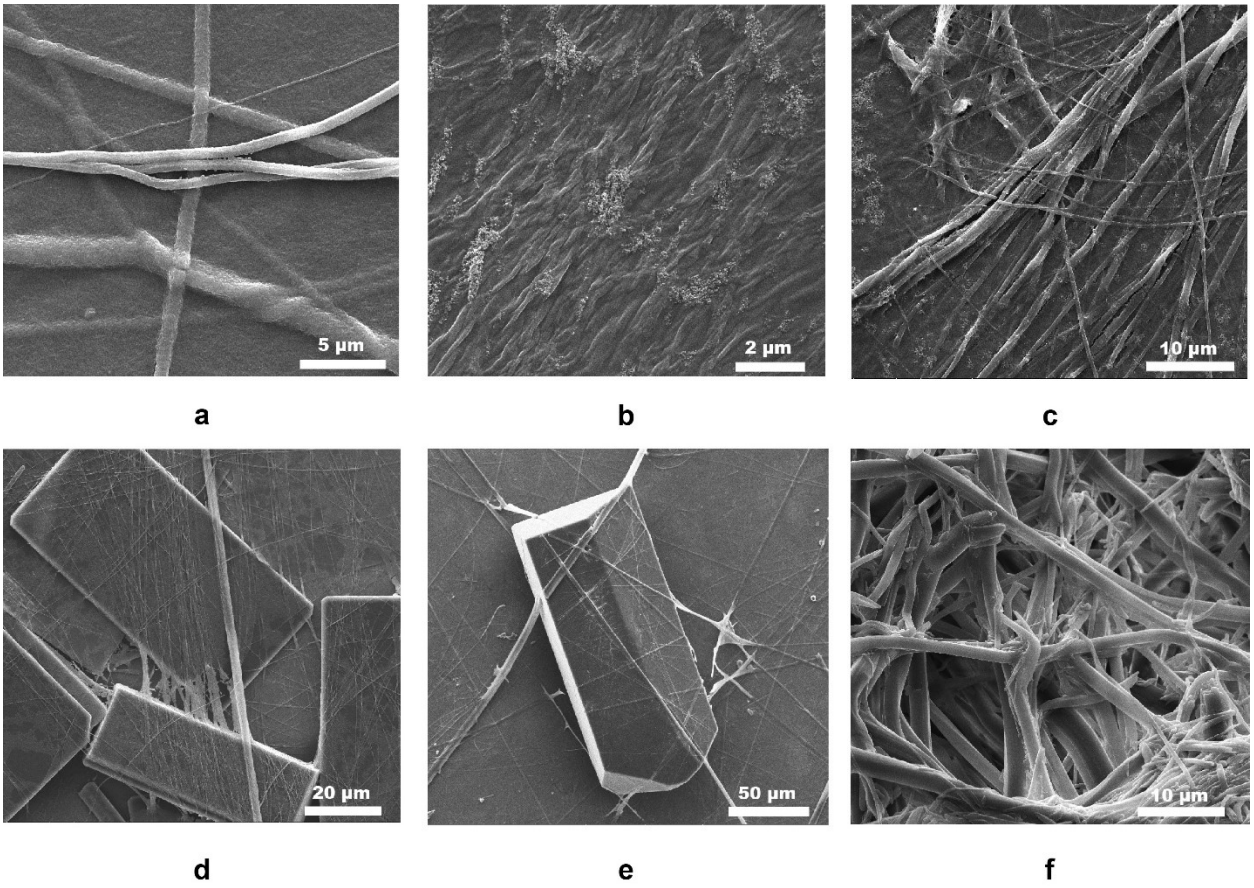

Figure 3.2. Morphologies formed by ammonium lithocholates, as imaged by scanning electron microscopy. (a) NH_4^+ salt. (b) $MeNH_3^+$ salt. (c) $EtNH_3^+$ salt. (d) $PrNH_3^+$ salt. (e) *i*-$PrNH_3^+$ salt. (f) Cyclopropylammonium salt.

Further experiments revealed that cooling aqueous solutions of the $PrNH_3^+$ salt under the same conditions yielded an ungelled mixture of fibrillar structures and acicular crystals, and solutions of the $BuNH_3^+$ salt produced only crystals (Figure 3.3). Faster cooling did not promote the formation of gels. The dependence of the outcome on the length of linear alkyl chains led us to examine the behavior of ammonium salts with branched chains. The *i*-$PrNH_3^+$ salt gave an ungelled mixture of fibrils and acicular crystals similar to the one formed by the $PrNH_3^+$ salt, whereas the cyclopropylammonium salt yielded a hydrogel (Figure 3.3). Scanning electron micrographs of dried samples (Figures 3.2d–f) confirm that the cyclopropylammonium salt behaves unlike the *i*-$PrNH_3^+$ and $PrNH_3^+$ salts.

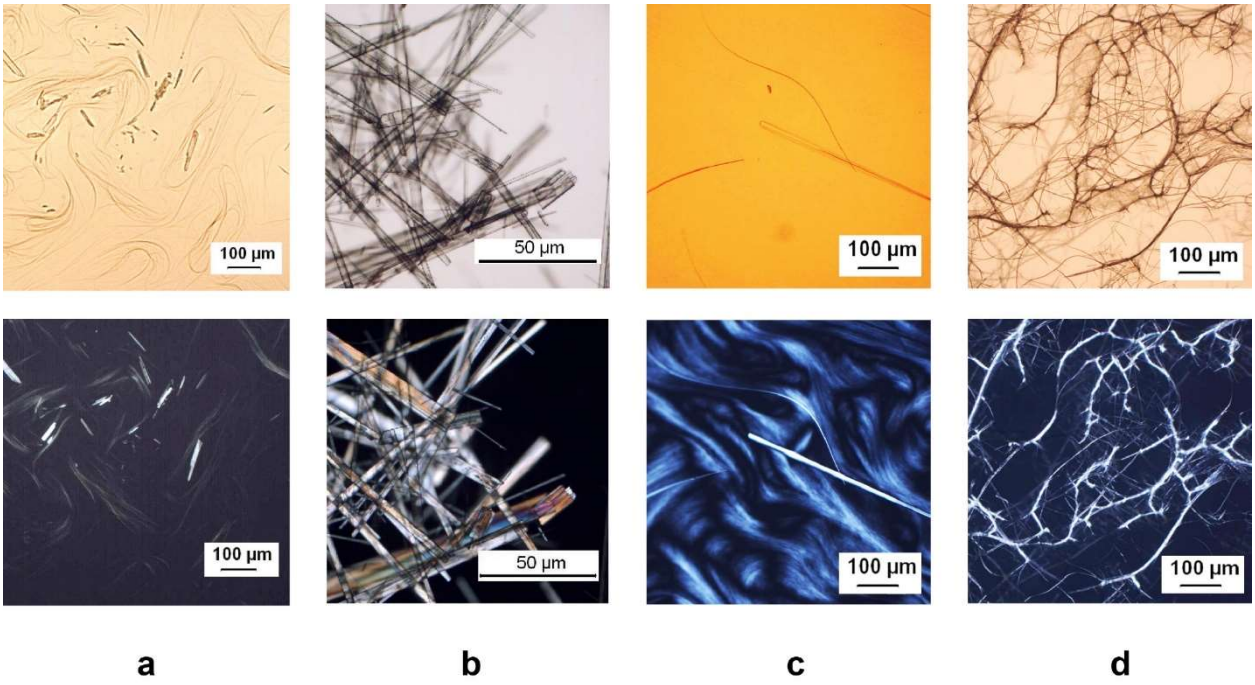

Figure 3.3. Products obtained when solutions of four ammonium lithocholates were prepared and cooled under standard conditions, as imaged by optical microscopy under normal light (upper row) and polarized light (lower row). (a) $PrNH_3^+$ salt. (b) $BuNH_3^+$ salt. (c) *i*-$PrNH_3^+$ salt. (d) Cyclopropylammonium salt.

When viscous mixtures produced initially by cooling aqueous solutions of the *i*-$PrNH_3^+$ salt were kept at 25 °C for extended periods, no significant changes occurred, and both crystals and fibrils were still present after several months. This suggests that converting the fibrillar components of gels into crystals is not favored thermodynamically in the lithocholate system or is simply very slow at 25 °C, despite the presence of solvent and the potential ability of existing crystals to act as seeds. In addition, gentle warming of aqueous mixtures containing crystals and fibrils of the *i*-$PrNH_3^+$ salt led to selective redissolution of the fibrils, but subsequent cooling again produced a mixture of crystals and fibrils, and the presence of residual crystals did not seed crystallization of the entire sample. This observation is consistent with the hypothesis that crystals and fibrils are formed by closely related processes and have similar thermodynamic stabilities, at least in the case of the *i*-$PrNH_3^+$ salt of LCA.

These initial observations demonstrated that the behavior of ammonium lithocholates is sensitive to small structural changes. RNH_3^+ salts cause hydrogelation when R is compact (H, Me,

Et, and cyclopropyl), induce the formation of both fibrils and crystals when R = Pr or *i*-Pr, and yield only crystals when larger alkyl groups are present (R = Bu). Crystallization is also favored by salts of all other butylammonium isomers (Figure 3.4), as well as by primary ammonium salts with larger alkyl groups such as pentyl and cyclohexyl. Replacing primary C_3 alkylammonium cations ($PrNH_3^+$ and *i*-$PrNH_3^+$) with secondary or tertiary C_3 analogues ($EtMeNH_2^+$ or Me_3NH^+) prevented crystallization, and optical micrographs of cooled solutions exhibited fibrillar textures like those shown in Figure 3.1. Solutions of the $EtMeNH_2^+$ salt gradually yielded hydrogels during storage at 25 °C for one month, whereas solutions of the Me_3NH^+ salt were viscous but remained fluid under similar conditions. In these ways, ammonium lithocholates show unique behavior. In no other case has a family of homologues been reported to form gels, fibrils, crystals, or mixtures of these forms under essentially identical conditions. This provides a special opportunity to explore how preferences for gelation and crystallization depend on small changes in structure, and it allows the boundary between the two alternative modes of molecular organization to be mapped in fine detail.

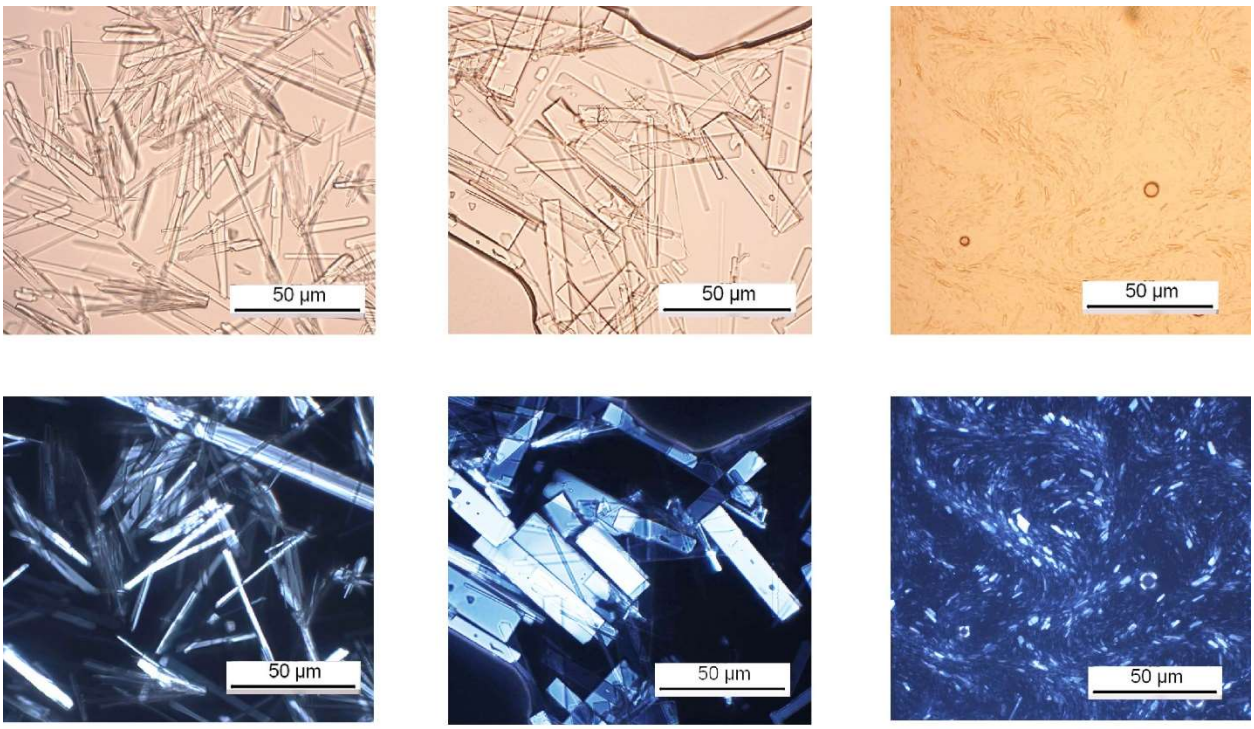

Figure 3.4. Structures obtained when solutions of butylammonium lithocholates with branched alkyl chains were prepared and cooled under standard conditions, as imaged by optical microscopy

under normal light (upper row) and polarized light (lower row). (a) *sec*-$BuNH_3^+$ salt. (b) *iso*-$BuNH_3^+$ salt. (c) *tert*-$BuNH_3^+$ salt.

Among the ammonium lithocholates, the $PrNH_3^+$ and *i*-$PrNH_3^+$ salts are particularly noteworthy for three reasons: (1) Under identical conditions, the compounds yield both crystals and fibrillar structures characteristic of gels; (2) the compounds differ by a single atom of carbon from salts that normally give only gels or crystals; and (3) as shown in Figures 3.3a and 3.3c, the compounds tend to crystallize as thin needles with extended morphologies related to those of the fibrils involved in gelation. As a result, the propylammonium salts appear to mark the boundary between gelation and crystallization in the lithocholate system, and both types of organization are observed simultaneously. The well-defined tetracyclic structure of lithocholate is expected to enforce a consistent pattern of molecular packing. As a result, we reasoned that the structures of the $PrNH_3^+$ and *i*-$PrNH_3^+$ salts, as determined by X-ray diffraction using crystals grown under conditions that also produce fibrils, would help reveal how molecules are organized in the fibrils. In addition, such structural studies promised to help reveal why lower homologues (with fewer CH_2 groups) and higher homologues (with more CH_2 groups) show divergent tendencies to form gels or crystals.

Crystals of the *i*-$PrNH_3^+$ salt of LCA proved to have the composition LCA^- *i*-$PrNH_3^+ \bullet H_2O$ and to belong to the monoclinic space group $P2_1$. Additional crystallographic data are provided in Table 3.1, and views of the structure appear in Figure 3.5. The structure can be described as consisting of layers in which adjacent lithocholate anions are aligned head-to-tail with the *c*-axis (Figure 3.5a). The layers are terminated by OH and COO^- groups, and within the layers each anion is surrounded by six neighbors (Figure 3.5b). In this way, the hydrophobic steroidal core of lithocholate anions is segregated from hydrophilic regions. The six- and five-membered rings of lithocholate adopt normal conformations, and the side chain is partially extended, as indicated by the torsion angles C17–C20–C22–C23 and C20–C22–C23–C24, which are 153° and 71°, respectively (see the structure of LCA for numbering). The OH and COO^- groups of lithocholate form multiple O–H···O and N–H···O hydrogen bonds with *i*-$PrNH_3^+$ cations and ordered molecules of water. Specifically, each *i*-$PrNH_3^+$ cation interacts with the COO^- groups of three lithocholate anions to form three N–H···O hydrogen bonds with N···O distances in the range 2.79–2.86 Å. In addition, each COO^- group engages in three N–H···O hydrogen bonds with *i*-$PrNH_3^+$

cations, and an O–H···O hydrogen bond is formed with water ($d_{O\cdots O}$ = 2.801(2) Å). Packing of lithocholate anions in the layers creates small cavities that accommodate the methyl groups of *i*-$PrNH_3^+$ cations (Figure 3.5c).

Table 3.1. Structural Data for Ammonium Lithocholates, as Determined by Single-Crystal X-Ray Diffraction

compound	**LCA⁻ *i*-$PrNH_3^+$ • H_2O**	**LCA⁻ $PrNH_3^+$**	**LCA⁻ $BuNH_3^+$**	**LCA⁻ $PentylNH_3^+$**	**LCA⁻ *c*-$HexylNH_3^+$**
crystal syst	monoclinic	orthorhombic	monoclinic	monoclinic	monoclinic
space group	$P2_1$	$P2_12_12_1$	$P2_1$	$P2_1$	$P2_1$
a (Å)	12.2848(2)	7.4151(4)	9.6884(3)	11.0046(3)	11.1747(4)
b (Å)	7.0415(1)	10.4713(5)	7.6904(2)	7.5468(2)	7.5361(3)
c (Å)	15.9198(3)	32.5598(16)	18.3154(6)	17.3286(5)	17.8459(7)
α (deg)	90	90	90	90	90
β (deg)	109.277(1)	90	100.544(2)	107.764(1)	106.761(2)
γ (deg)	90	90	90	90	90
V (Å^3)	1299.91(4)	2528.1(2)	1341.60(7)	1370.52(7)	1439.02(10)
Z	2	4	2	2	2
Z′	1	1	1	1	1
ρ_{calc} (g · cm^{-3})	1.159	1.145	1.113	1.124	1.098
T (K)	150	150	150	100	100
R_1, $I > 2\sigma(I)$	0.0277	0.0449	0.0410	0.0437	0.0445
wR_2, $I > 2\sigma(I)$	0.0760	0.1192	0.1109	0.1190	0.1228
$\Delta\rho_{max}/\Delta\rho_{min}$ (e · Å^{-3})	0.238/-0.140	0.284/-0.175	0.353/-0.333	0.577/-0.339	0.300/-0.479
GoF	1.016	1.083	1.086	1.051	1.028

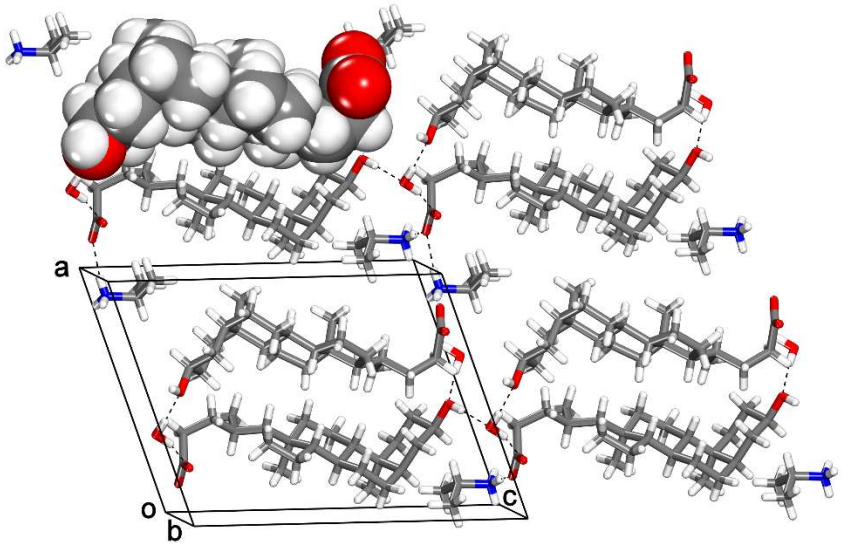

a

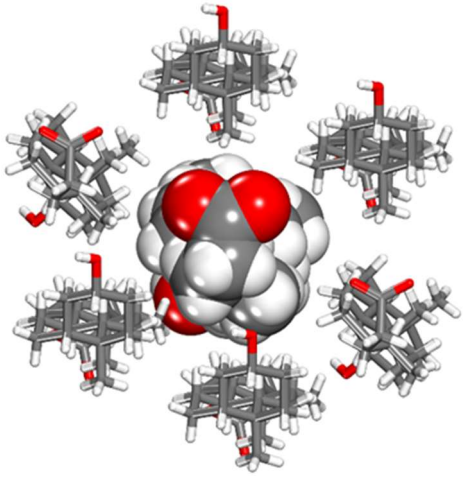

b

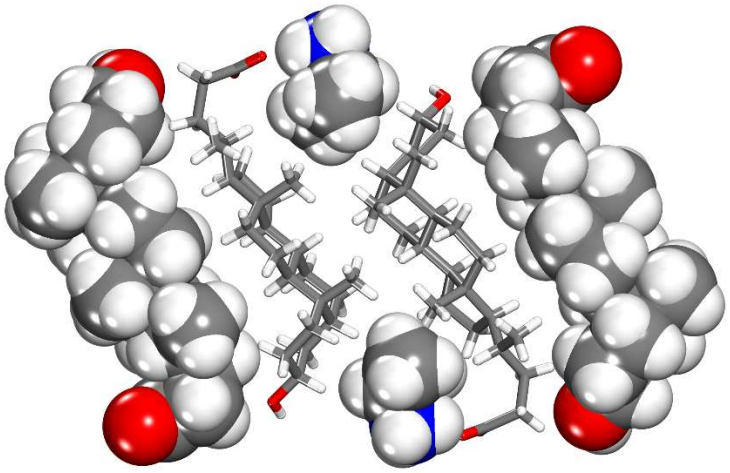

c

Figure 3.5. Representations of the structure of crystals of LCA^- *i*-$PrNH_3^+ \bullet H_2O$ grown from H_2O. (a) View along the *b*-axis showing the cross sections of part of two layers of lithocholate anions, separated by regions in which OH and COO^- groups form multiple hydrogen bonds with *i*-$PrNH_3^+$ cations and H_2O. (b) View along the *c*-axis showing a central lithocholate anion surrounded by six neighbors. (c) View along the *b*-axis showing how cavities in layers of lithocholate anions accommodate the aliphatic part of *i*-$PrNH_3^+$ cations. In all views, selected ions are shown in space-filling representations. Hydrogen bonds in Figure 3.5a are indicated by broken lines. Atoms of carbon appear in gray, hydrogen in white, nitrogen in blue, and oxygen in red.

For comparison, the structure of crystals of the $PrNH_3^+$ salt of LCA was also determined by X-ray diffraction. The crystals were found to have the composition LCA^- $PrNH_3^+$ and to belong to the orthorhombic space group $P2_12_12_1$. Table 3.1 includes additional crystallographic data, and Figure 3.6 provides a view of the structure. Even though crystals of the *i*-$PrNH_3^+$ and $PrNH_3^+$ salts differ in space group and unit-cell parameters, the molecular organization is closely similar. Again, lithocholate anions are hexagonally packed in antiparallel orientations to produce layers terminated by OH and COO^- groups (Figure 3.6). Normal conformations are adopted by the six- and five-membered rings, and the torsion angles C17–C20–C22–C23 and C20–C22–C23–C24 (169° and 69°, respectively) show that the side chain is partially extended. Each COO^- group takes part in two

N–H···O hydrogen bonds with $PrNH_3^+$ cations ($d_{N\cdots O}$ = 2.717(4) and 2.783(3) Å), as well as one O–H···O hydrogen bond with the OH group of an adjacent lithocholate anion ($d_{O\cdots O}$ = 2.694(3) Å). Each $PrNH_3^+$ cation forms three N–H···O hydrogen bonds, two with COO^- groups and one with an OH group ($d_{N\cdots O}$ = 2.809(3) Å). Packing of the lithocholate anions leaves insufficient volume within the layers to accommodate the alkyl groups of the $PrNH_3^+$ cations, which are located entirely in the interlamellar region.

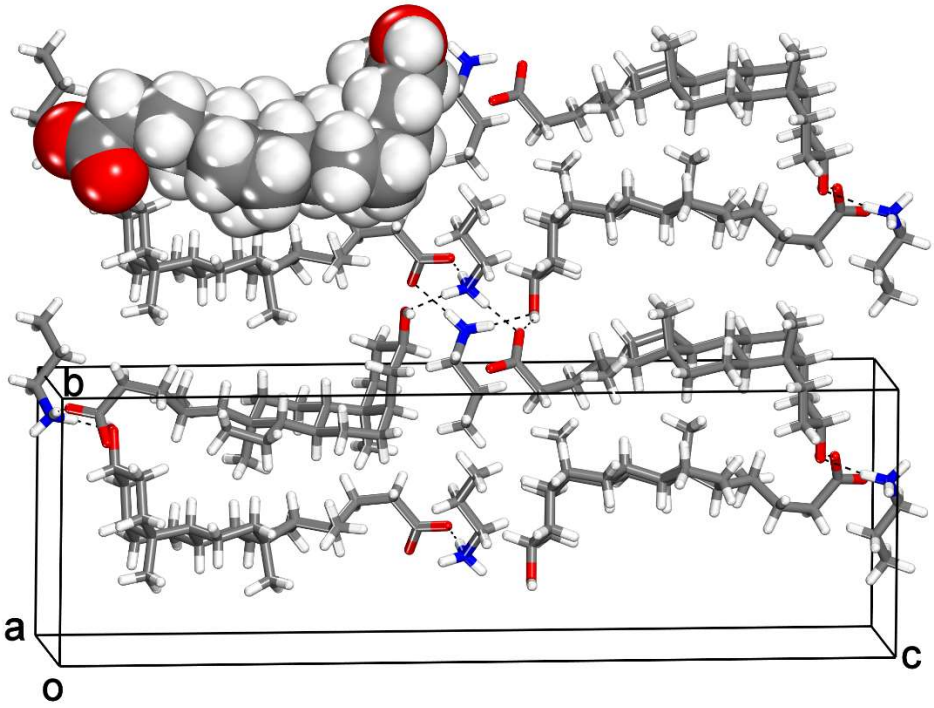

Figure 3.6. Representation of the structure of crystals of LCA^- $PrNH_3^+$ grown from H_2O, as viewed along the *a*-axis. The view shows that lithocholate anions are aligned in an antiparallel manner to define layers bounded by regions in which OH and COO^- groups form multiple hydrogen bonds with $PrNH_3^+$ cations. A space-filling representation is used to highlight a single lithocholate anion, hydrogen bonds are indicated by broken lines, and atoms are shown in their standard colors.

Further evidence that crystalline ammonium lithocholates adopt a consistent pattern of molecular organization was obtained by determining the structures of crystals of the butyl-, pentyl-,

and cyclohexylammonium salts. Crystals of the butylammonium salt proved to have the composition LCA^- $BuNH_3^+$ and to belong to the monoclinic space group $P2_1$. Additional crystallographic data are presented in Table 3.1, and a view of the structure appears in Figure 3.7. As observed in the *i*-$PrNH_3^+$ and $PrNH_3^+$ salts, the structure of the $BuNH_3^+$ salt consists of layers in which lithocholate anions are hexagonally packed in antiparallel orientations. The steroidal core of lithocholate adopts its standard conformation, and the side chain is fully extended (the torsion angles C17–C20–C22–C23 and C20–C22–C23–C24 are 173° and 172°, respectively), The layers are separated by hydrophilic regions in which OH and COO^- groups form hydrogen bonds with $BuNH_3^+$ cations. Each COO^- group engages in two N–H···O hydrogen bonds with $BuNH_3^+$ cations ($d_{N\cdots O}$ = 2.735(2) and 2.804(2) Å), as well as one O–H···O hydrogen bond with the OH group of an adjacent lithocholate anion ($d_{O\cdots O}$ = 2.611(2) Å). Each $BuNH_3^+$ cation forms three N–H···O hydrogen bonds, two with COO^- groups and one with an OH group ($d_{N\cdots O}$ = 2.804(2) Å). The structures of the pentylammonium and cyclohexylammonium salts are closely analogous and are presented in the Supporting Information.

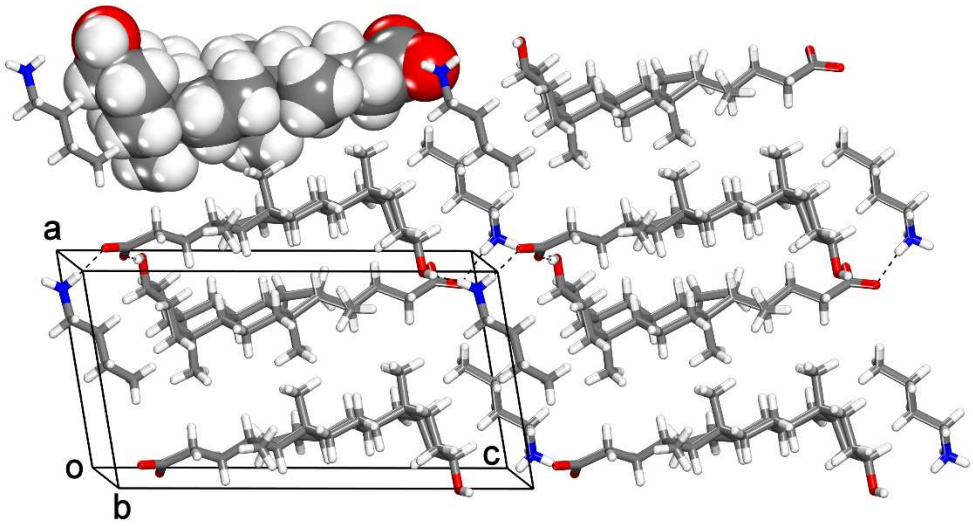

Figure 3.7. Representation of the structure of crystals of LCA^- $BuNH_3^+$ grown from H_2O, as viewed along the *b*-axis. The view shows that lithocholate anions are aligned in an antiparallel manner to produce layers bounded by regions in which OH and COO^- groups form multiple hydrogen bonds with $BuNH_3^+$ cations. A space-filling representation is used to highlight a single

lithocholate anion, hydrogen bonds are indicated by broken lines, and atoms are shown in their standard colors.

Without exception, crystals of the *i*-$PrNH_3^+$, $PrNH_3^+$, $BuNH_3^+$, pentylammonium, and cyclohexylammonium salts of LCA have similar layered structures, demonstrating that homologous ammonium lithocholates have a pronounced tendency to conserve a single pattern of molecular association. This conclusion is reinforced by the observation that the same pattern is also found in crystals of LCA itself and in other salts grown under various conditions.[70–73] The preference is strong enough to be maintained despite differences in counterions, even when water is replaced by other media of crystallization. Clearly, the characteristic shape and amphiphilicity of lithocholate anions strongly favor the formation of layered structures composed of hexagonally-packed antiparallel molecules. Related structures are also adopted by other bile acids and salts.[74,75] Moreover, crystals of the alkylammonium lithocholates all have similar morphological preferences for forming needles or elongated thin plates. These consistent structural similarities suggest that aggregates formed under other conditions, such as fibrils present in hydrogels formed by the NH_4^+, $MeNH_3^+$, $EtNH_3^+$, and cyclopropylammonium salts, have the same molecular organization. Similarly, fibrils co-deposited along with crystals from solutions of the *i*-$PrNH_3^+$ and $PrNH_3^+$ salts may also be structurally analogous. In addition, it is possible that related structural preferences help determine how molecules are ordered in micellar aggregates formed by the salts in water.

To test the hypothesis that crystals and fibrils produced by ammonium lithocholates have closely related structures, we compared the simulated powder X-ray diffraction pattern of crystals of the $PrNH_3^+$ salt of LCA grown from water with the pattern recorded for mixtures of fibrils and crystals obtained by freeze-drying bulk samples. The patterns proved to be closely similar (Figure 3.8), and related patterns were also observed for crystals and fibrils derived from aqueous solutions of the *i*-$PrNH_3^+$ salt (Supporting Information). These findings are consistent with the hypothesis that fibrils and crystals composed of the $PrNH_3^+$ and *i*-$PrNH_3^+$ salts of LCA have similar molecular arrangements; however, other minor phases also appear to be present, and the relative contributions of fibrils and crystals to the overall diffraction patterns cannot be fully established. Solids obtained by freeze-drying gels derived from the NH_4^+, $MeNH_3^+$, $EtNH_3^+$, and cyclopropylammonium salts were found to have only low degrees of crystallinity (Supporting Information).

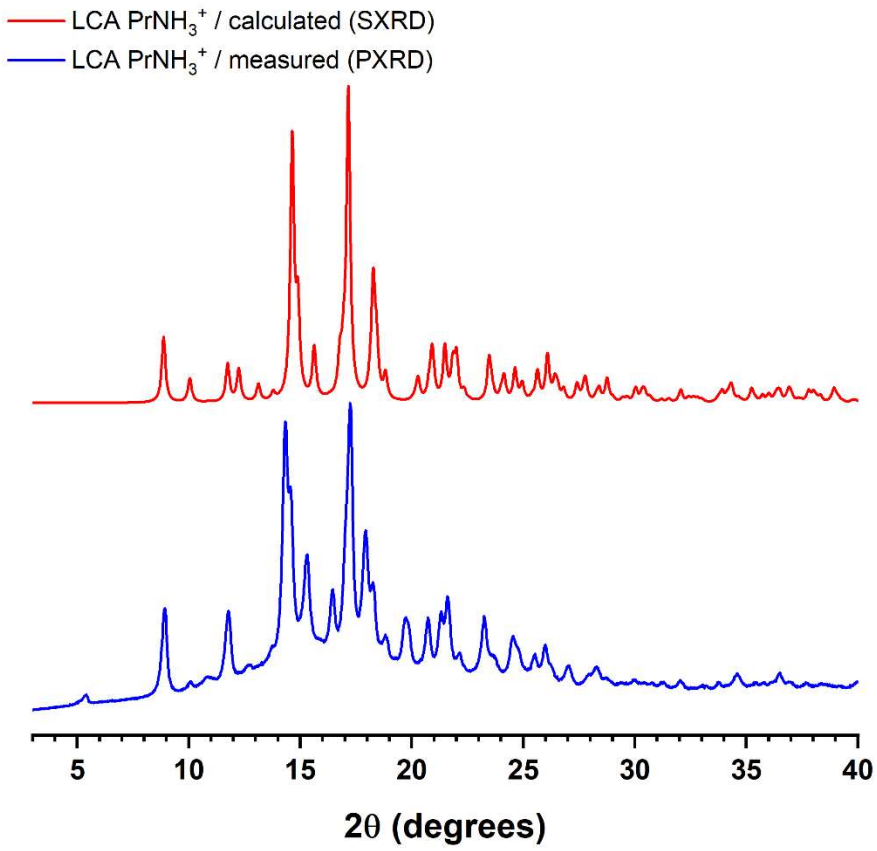

Figure 3.8. Simulated powder X-ray diffraction pattern (red) for crystals of the $PrNH_3^+$ salt of LCA grown from water and experimental pattern (blue) recorded for a mixture of crystals and fibrils, as obtained by freeze-drying the product resulting from cooling an aqueous solution of the salt.

As the alkyl group R in RNH_3^+ salts of LCA becomes larger, solubility in water generally decreases, thereby creating conditions that favor bulk precipitation rather than the formation of fibrillar structures with large exposed surfaces of high energy. By comparing the structure of the *i*-$PrNH_3^+$ salt with those of the $PrNH_3^+$, $BuNH_3^+$, pentylammonium, and cyclohexylammonium analogues, we identified a feature that may explain in molecular detail why the preference for gelation changes to a preference for crystallization as the group R increases in size. When R is compact (H, Me, Et, *i*-Pr, and cyclopropyl), it can be nestled within the hydrophobic layers of lithocholate anions, but larger groups can only be accommodated in the interlamellar region. In all observed structures, the *c*-axis is approximately orthogonal to lamella composed of lithocholate anions, and hydrophilic OH and COO^- groups are primarily exposed on surfaces parallel to the *ab*-

plane. As a result, the most stable ordered aggregates in aqueous media are expected to be those with the largest exposed (001) surfaces, and preferential growth of micelles, fibrils, or crystals should therefore occur along the *a*- or *b*-axes. In principle, growth can occur by adding molecules to the surface individually or as preformed micellar clusters. In either case, the well-defined amphiphilic structure of lithocholate mandates a single mode of organization that favors markedly anisotropic growth of aggregates. As the alkyl groups of RNH_3^+ become larger, however, the *ab*-surfaces of lamella become less hydrophilic, growth becomes less conspicuously anisotropic, and crystallization competes sucessfully with the formation of fibrils and gels.

Additional information about the association of ammonium lithocholates was obtained by indexing the faces of individual acicular crystals of the *i*-$PrNH_3^+$ and $BuNH_3^+$ salts (Figures 3.5 and 3.7). In both cases, direct measurement of the dimensions of crystals showed that growth along the *b*-axis is at least 10 times faster than that along the *a*- or *c*-axes. The observation of slow growth along the *c*-axis is consistent with the hypothesis that (001) faces of ordered aggregates are hydrophilic and correspond to the surfaces of lowest energy in aqueous media. In contrast, the (010) faces expose the primarily hydrophobic edges of lithocholate anions and are therefore expected to be surfaces of high energy. Because fibrils composed of ammonium lithocholates appear to have similar internal molecular organization, they are expected to show a strong preference for anisotropic growth in which individual molecules or micellar aggregates are added fastest to surfaces that expose the hydrophobic edges of lithocholate anions.

Studies of the evolution of fibrils and crystals by optical microscopy and scanning electron microscopy confirmed that their formation is closely related. Although cooling aqueous solutions of various primary C_4 alkylammonium lithocholates yielded only crystals (Figures 3.3b and 3.4), the secondary C_4 diethylammonium salt appears to form both fibrils and crystals (Figure 3.9a). Many have aspect ratios that exceed 50:1, sub-micron diameters, and an ability to accommodate significant curvature without fracturing. In addition, the fibrillar structures display a tendency to form sheafs and bundles, and larger crystals often incorporate regions suggesting that growth has occurred by oriented attachment, in which neighboring crystallites unite by growing together at suitable angles and distances.

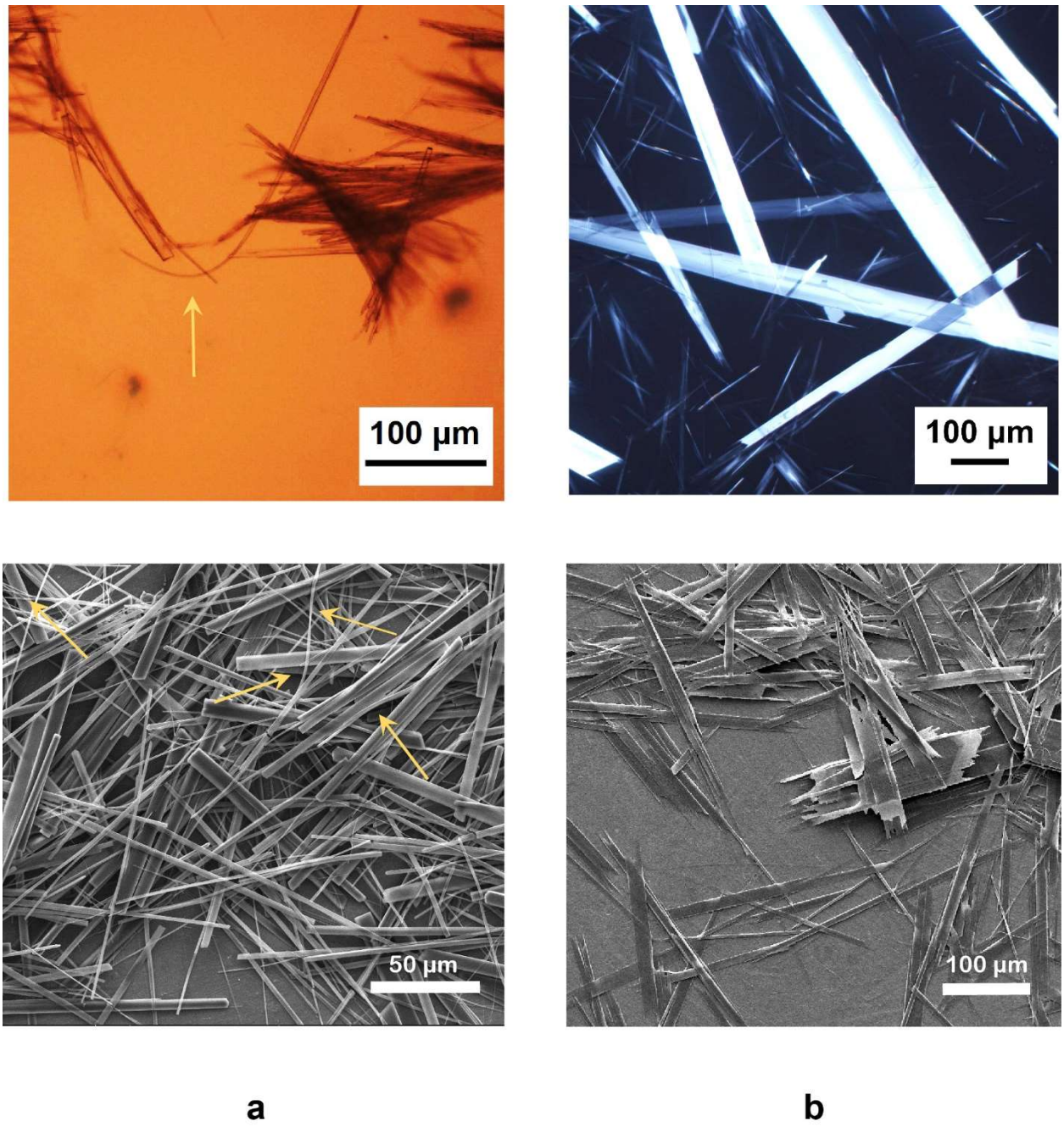

Figure 3.9. (a) Optical micrograph (upper image) and scanning electron micrograph (lower image) showing fibrils and crystals formed by cooling an aqueous solution of the $Et_2NH_2^+$ salt of LCA. Yellow arrows identify selected areas of significant curvature. (b) Analogous images of crystals formed by cooling an aqueous solution of the pentylammonium salt.

Further evidence suggesting that fibrils and crystals result from similar processes of molecular association has been obtained by examining crystals of the pentylammonium salt of LCA. Optical and electron micrographs in Figure 3.9b show crystals at various stages of highly anisotropic growth. Every large crystal can be seen to be terminated by one or more characteristic spicules located primarily at the corners of the crystals, where growth is presumably favored by diffusion. The spicules may arise from preferred growth of crystals along the direction of the hydrophobic edges of lithocholate molecules (*b*-axis), as established rigorously in the cases of the structurally analogous *i*-$PrNH_3^+$ and $BuNH_3^+$ salts. As the spicules grow, starting primarily from opposite corners, space between them is filled in. Crystals in the image are viewed along the direction of slowest growth and are dominated by exposed (001) faces, which have the highest density of polar OH and COO^- groups in contact with the surrounding aqueous medium. The images in Figure 3.9b thereby establish a plausible link between crystallization and the formation of fibrillar structures characteristic of gels.

3.3 Conclusions

Ammonium salts of LCA provide a special opportunity to explore hydrogelation and to probe the relationship between gelation and crystallization in molecular detail. The well-defined amphiphilic steroidal structure of the lithocholate anion ensures that a consistent pattern of molecular organization is likely to be maintained under diverse circumstances. However, the result of aggregation can be controlled by systematically varying the ammonium counterions, giving rise to hydrogels, mixtures of fibrils and crystals, or only crystals under essentially identical conditions of assembly. By using optical microscopy, single-crystal X-ray diffraction, scanning electron microscopy, and other methods, we have drawn a detailed portrait of molecular association taking place near the boundary between gelation and crystallization. In particular, our work helps reveal the internal structure of networked fibrils that give rise to hydrogelation in the ammonium lithocholate system, suggests that gelation and crystallization are closely related in this system, and shows in detail why certain alkylammonium salts give rise to gels, why others favor crystallization, and why the tendency to crystallize increases as the alkyl group becomes larger.

Our findings do not necessarily explain how other gelators work. However, the approach that we have taken, in which tools used to study gels are employed in tandem with the methods of crystal engineering, is likely to continue to provide valuable insights. In using this approach, we

have identified families of compounds able to form gels or crystals under similar conditions, and we have established their preferred patterns of molecular association by structural analyses using single-crystal X-ray diffraction. The boundary between gelation and crystallization can then be mapped by altering the components in logical ways. Using salts in studies of this type is advantageous because the primary gelating ion can be kept constant. In this way, new structural analogues do not need to be made by complex syntheses, and variation can be introduced simply by changing the counterion.

3.4 Experimental Section

3.4.1 Materials.

Lithocholic acid (LCA, 95%), ethylamine (70 wt % solution in water), N-ethylmethylamine (97%), propylamine (98%), isopropylamine (99%), cyclopropylamine (98%), trimethylamine (40 wt % solution in water), butylamine (99%), sec-butylamine (99%), isobutylamine (99%), pentylamine (99%), cyclohexylamine (99%), and tert-butylamine (99%) were purchased from Sigma-Aldrich (Oakville, ON, Canada). Ammonium hydroxide (30 wt % solution in water) was purchased from EMD Chemicals Inc. Methylamine (40 wt % solution in water) was purchased from Fisher Scientific Company. All reagents were used as received. Hydrogels and stock solutions of amines were prepared with water purified by a Milli-Q system.

3.4.2 Sample preparation.

A weighed amount of LCA was mixed with water purified by a Milli-Q system, and a stock solution of amine was added. The mixture was warmed and sonicated until a solution was produced. The resulting nominal concentrations of LCA and amine were typically 50 mM and 800 mM, respectively. Samples were allowed to cool to 25 °C and kept at that temperature for at least 24 h before gelation or crystallization phenomena were examined. Essentially complete deprotonation of LCA requires only one equivalent of amine. Excesses were added to increase the solubility of ammonium lithocholates or the rate of dissolution.

3.4.3 Illustrative preparation of bulk samples of crystalline ammonium lithocholates (LCA^- $BuNH_3^+$).

LCA (0.0094 g, 0.025 mmol) was mixed with water (0.60 mL) purified by a Milli-Q system. An aqueous solution of butylamine (1.0 M, 0.40 mL, 0.40 mmol) was added, and the resulting mixture was warmed at 60 °C and sonicated until a solution was produced. The solution was allowed to cool to 25 °C and was kept at that temperature for 24 h to permit crystallization to take place. The mother liquors were removed by pipette, and the solid was washed with cold water (3 × 0.5 mL) and dried in vacuo. This yielded LCA^- $BuNH_3^+$ (0.0086 g, 0.019 mmol, 76%) as a colorless solid.

3.4.4 Rheological studies.

Rheological properties of the hydrogels were measured using a TA Instruments AR 2000 rheometer, with an acrylic cone geometry 60 mm in diameter. All measurements were conducted with a fixed gap of 68 μm between the cone and the plate. Hydrogels were warmed to produce homogeneous solutions before the rheological tests. Aliquots of the solutions were transferred to the center of the rheometer plate, and a very small oscillatory strain of 0.1% was applied at 20 °C to record the storage moduli (G') and loss moduli (G'') until a plateau was reached. Oscillatory frequency sweep studies of the hydrogels were conducted in the linear viscoelastic region at 20 °C with a constant strain of 0.1%, for a scale from 0.1 to 100 Hz. Oscillatory strain sweep experiments were performed at 20 °C from 0.01% to 100% with a constant frequency of 1 Hz. Oscillatory stress sweep experiments were performed at 20 °C from 0.1 to 100 Pa with a constant frequency of 1 Hz.

3.4.5 Polarized optical microscopy.

Samples were transferred to a glass slide, placed under a cover slide, and then observed at 25 °C using a Zeiss Axioskop polarized-light optical microscope.

3.4.6 Scanning electron microscope.

Samples for analysis were transferred to Al mounts, placed under vacuum at 25 °C, and coated with Pt. The coated samples were then imaged using an FEI Quanta 450 field-emission scanning electron microscope at the Facility for Electron Microscopy Research at McGill University.

Notes. The authors have no competing financial interests to declare.

3.5 Supporting Information

3.5.1 Additional Crystallographic Information

Data were collected at 150 K using a Bruker Venture Metaljet diffractometer with GaKα radiation (λ = 1.34139 Å) or at 100 K using a Bruker Smart APEX II diffractometer with an Incoatec Microfocus CuKα source (λ = 1.54179 Å). The second instrument was used for compounds LCA^- pentylNH_3^+ and LCA^- *c*-hexylNH_3^+. The cell lattice parameters were determined using reflections taken from three sets of 104 or 180 frames measured and harvested within the *APEX3* suite of programs.[1] Integration of frames was performed using *SAINT*,[1] and a semiempirical absorption correction was applied with *SADABS*.[2] The structures were solved using a dual space and intrinsic phasing approach with *SHELXT*,[3] and the refinement was carried out using *SHELXL*-2018/3.[4] In crystals of LCA^- *c*-hexylNH_3^+, the *c*-hexylNH_3^+ cation was found to be disordered and was refined using a model with three different orientations.

X-ray powder diffraction patterns were recorded using a Malvern Panalytical Empyrean-3 diffractometer with CuK_α radiation. The measured patterns were compared with calculated patterns using Mercury software.[5] The patterns were modeled using a profile with a unique value of FWHM adjusted to match the profiles of the experimental patterns.

3.5.2 Thermal Atomic Displacement Parameter Plots

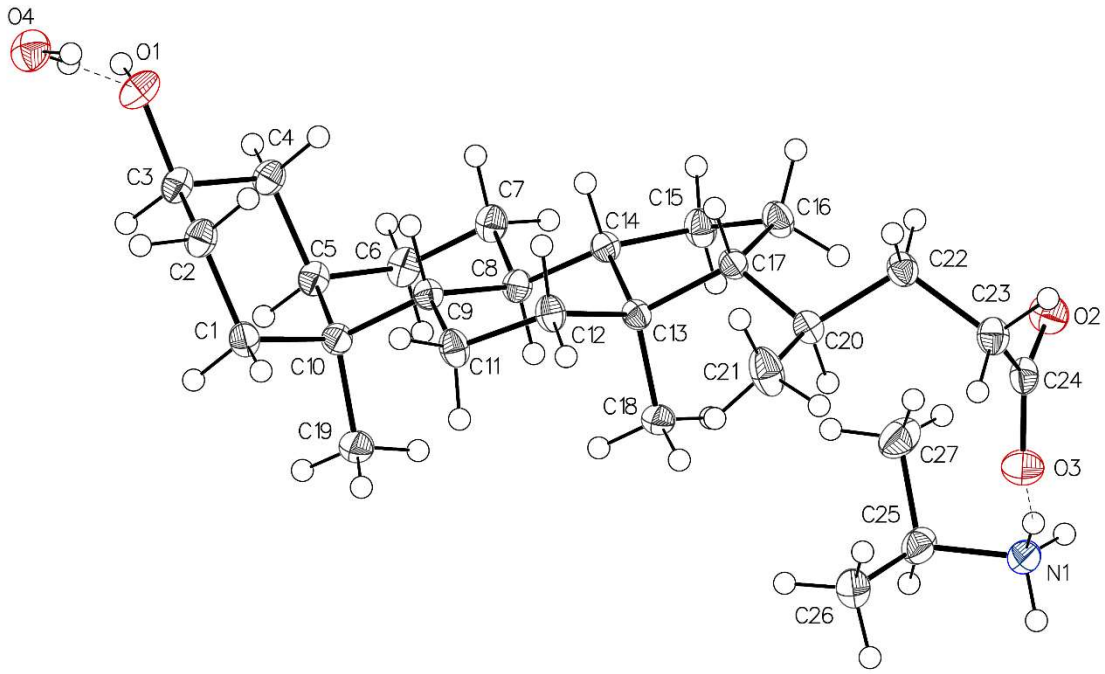

Figure 3.S1. Thermal atomic displacement ellipsoid plot with the atomic numbering scheme for the structure of crystals of LCA^- i-$PrNH_3^+$ • H_2O. The ellipsoids of non-hydrogen atoms are drawn at the 50% probability level, and hydrogen atoms are represented by a sphere of arbitrary size. Intermolecular hydrogen bonds are shown as dashed lines.

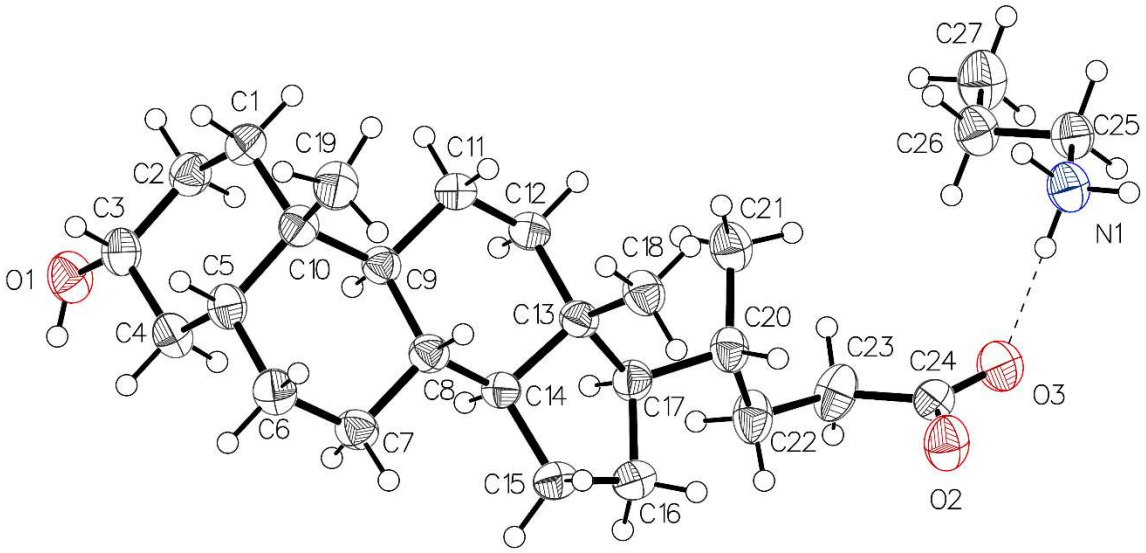

Figure 3.S2. Thermal atomic displacement ellipsoid plot with the atomic numbering scheme for the structure of crystals of LCA^- $PrNH_3^+$. The ellipsoids of non-hydrogen atoms are drawn at the 50% probability level, and hydrogen atoms are represented by a sphere of arbitrary size. An intermolecular hydrogen bond is represented by a dashed line.

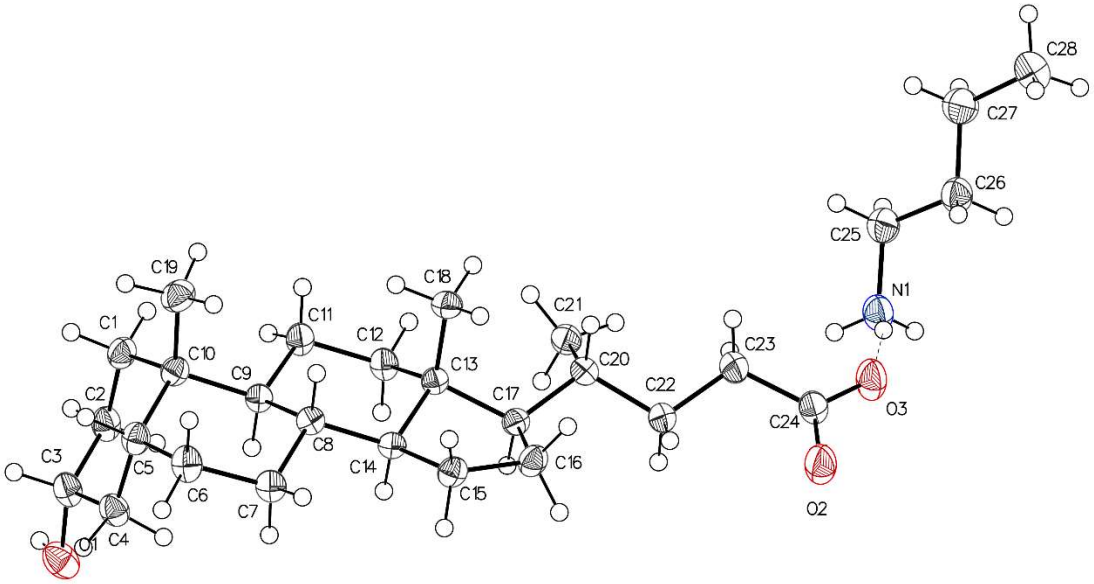

Figure 3.S3. Thermal atomic displacement ellipsoid plot with the atomic numbering scheme for the structure of crystals of LCA^- $BuNH_3^+$. The ellipsoids of non-hydrogen atoms are drawn at the 50% probability level, and hydrogen atoms are represented by a sphere of arbitrary size. An intermolecular hydrogen bond is represented by a dashed line.

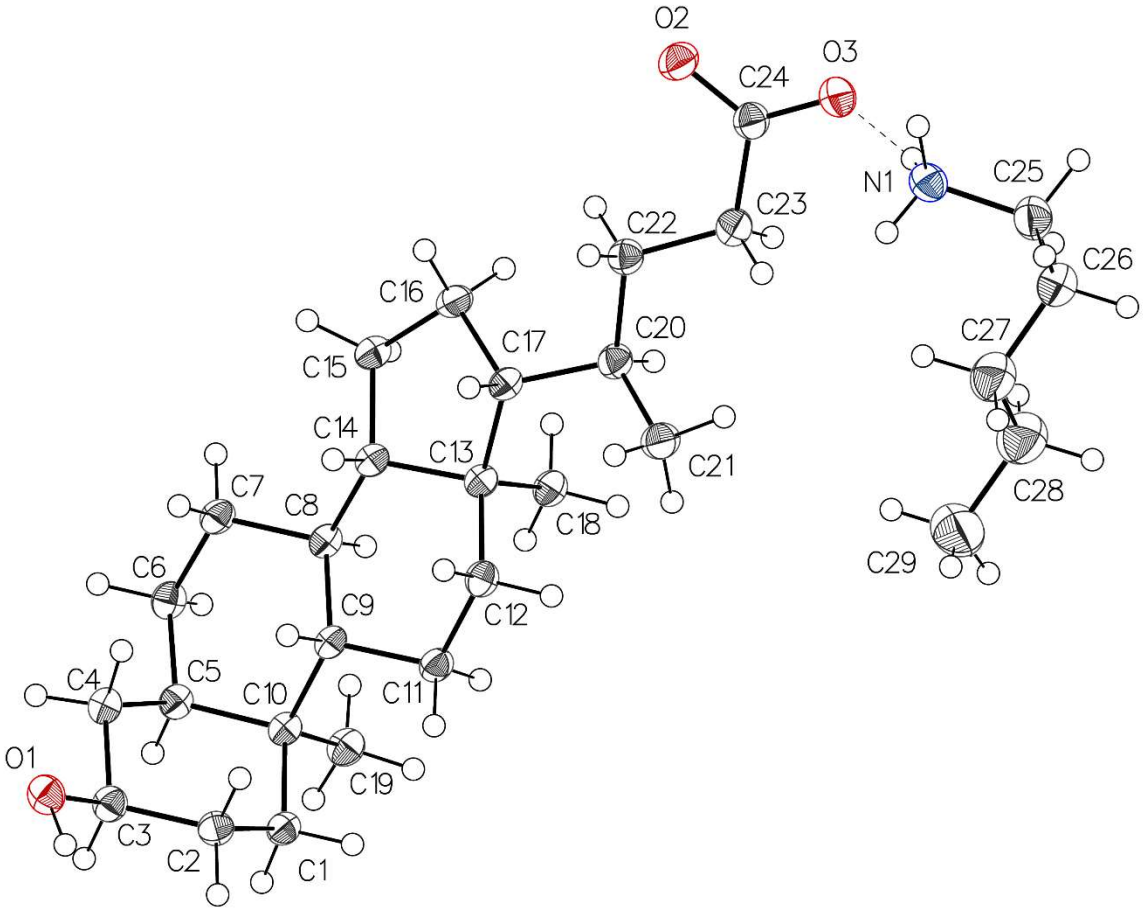

Figure 3.S4. Thermal atomic displacement ellipsoid plot with the atomic numbering scheme for the structure of crystals of LCA^- pentylNH_3^+. The ellipsoids of non-hydrogen atoms are drawn at the 50% probability level, and hydrogen atoms are represented by a sphere of arbitrary size. An intermolecular hydrogen bond is represented by a dashed line.

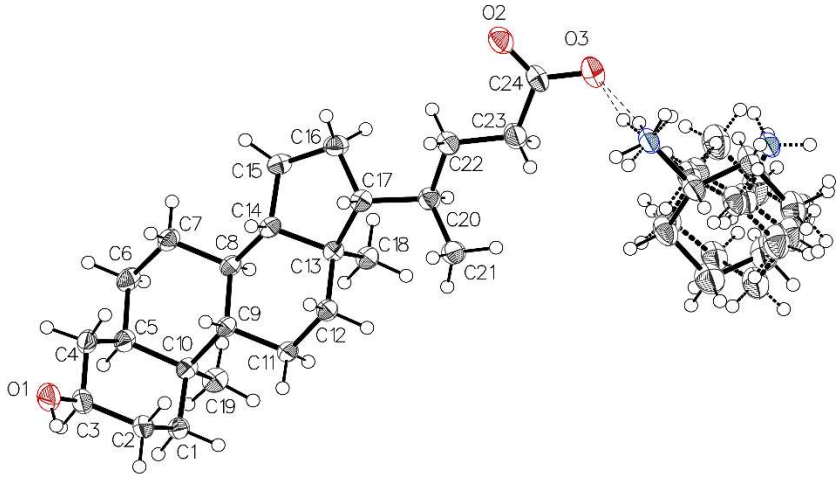
O2
O3
C24
C23
C16
C15
C17
C22
C14
C7
C20
C8
C6
C18
C13
C21
C9
C5
C12
C4
C10
C11
O1
C19
C3
C2
C1

a

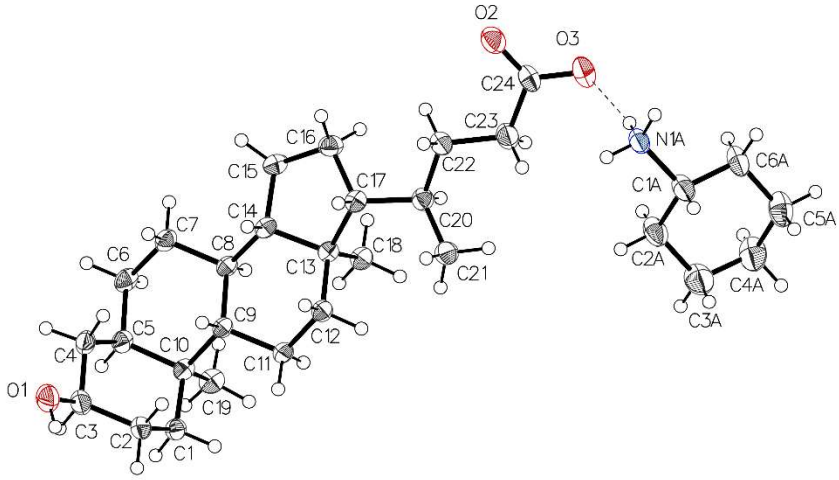
O2
O3
C24
C23
N1A
C16
C6A
C15
C22
C1A
C17
C5A
C14
C7
C20
C2A
C8
C6
C18
C13
C21
C4A
C9
C5
C12
C3A
C4
C10
C11
O1
C19
C3
C2
C1

b

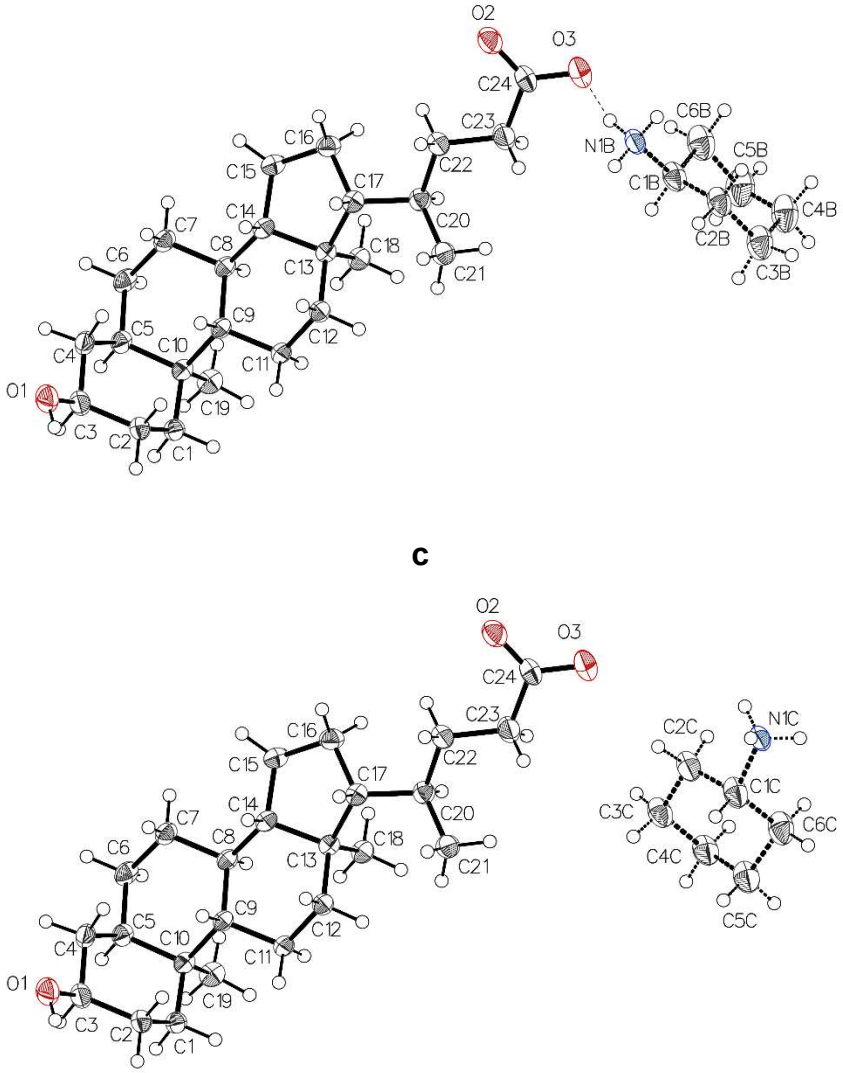

Figure 3.S5. Thermal atomic displacement ellipsoid plot with the atomic numbering scheme for the structure of crystals of LCA^- *c*-hexylNH_3^+. The ellipsoids of non-hydrogen atoms are drawn at the 50% probability level, and hydrogen atoms are represented by a sphere of arbitrary size. Intermolecular hydrogen bonds are shown as dashed lines. (a) View with all disordered parts included for the cyclohexylNH_3^+. (b)–(d) Separate views for each disordered part.

3.5.3 Indexing Crystal Faces

***i*-PrNH$_3^+$ Salt of LCA**

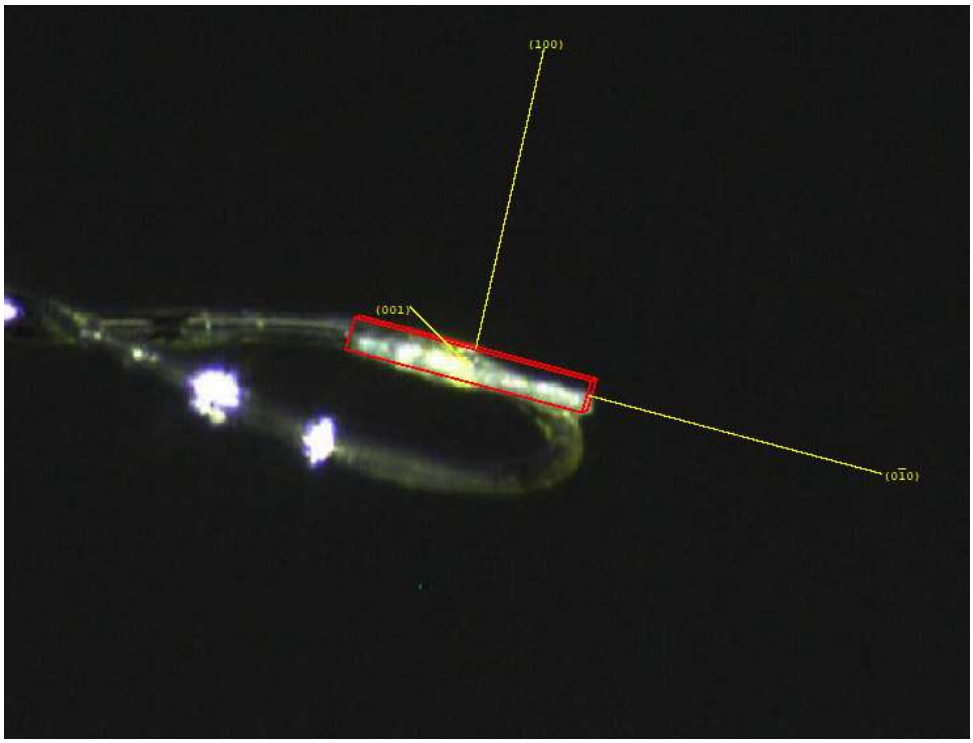

HKL Faces & Distances:

FACE	0	-1	0	0.095
FACE	0	1	0	0.148
FACE	0	0	1	0.013
FACE	0	0	-1	0.006
FACE	1	0	0	0.014
FACE	-1	0	0	0.017

$BuNH_3^+$ Salt of LCA

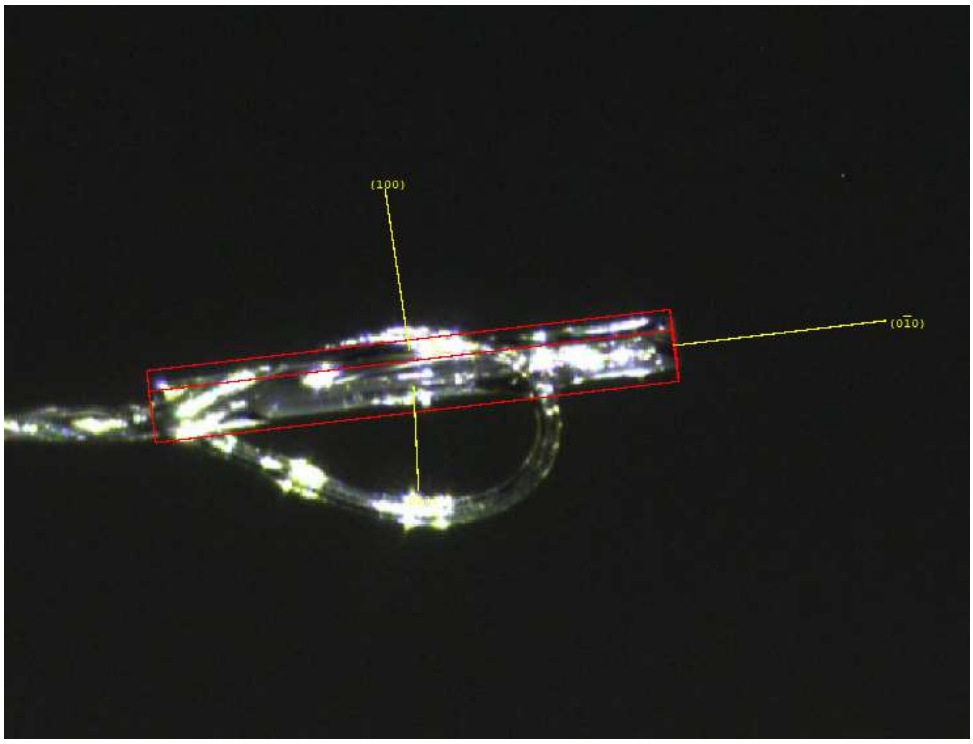

HKL Faces & Distances:

FACE	0	-1	0	0.251
FACE	0	1	0	0.493
FACE	1	0	0	0.044
FACE	-1	0	0	0.038
FACE	0	0	-1	0.026
FACE	0	0	1	0.019

3.5.4 X-Ray Powder Diffraction

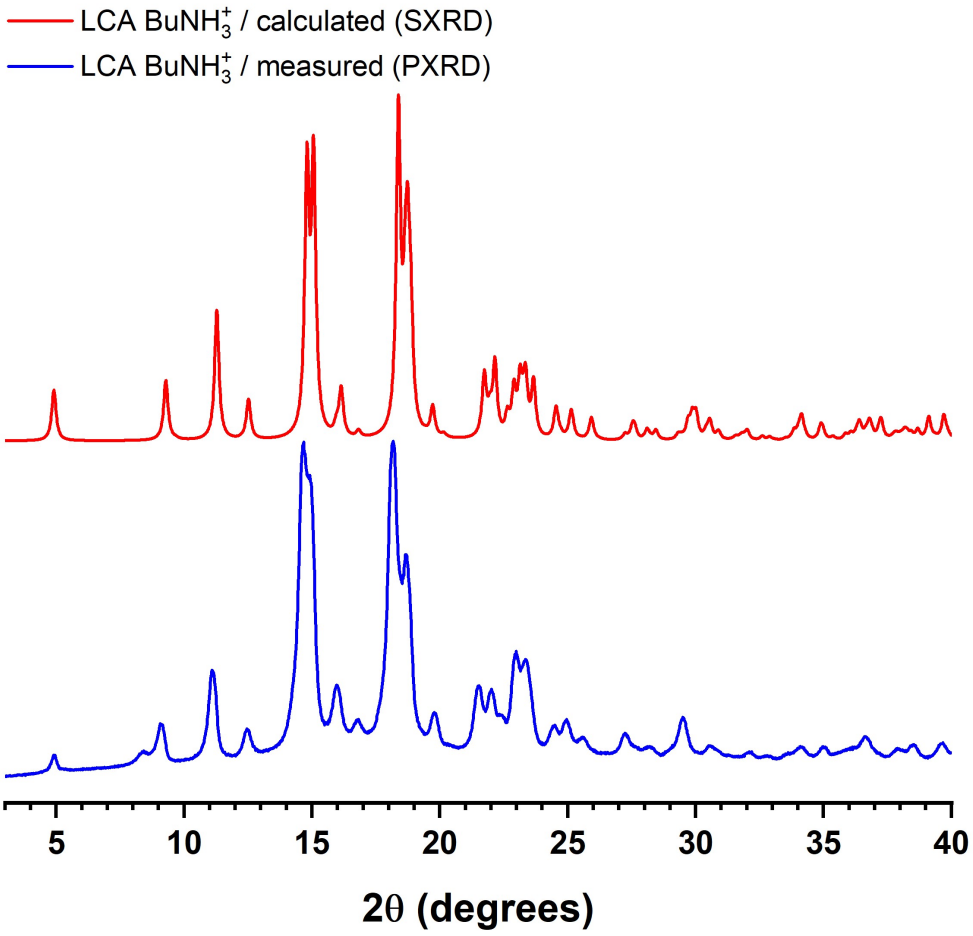

Figure 3.S6. Simulated X-ray powder diffraction pattern (red) for crystals of the $BuNH_3^+$ salt of LCA grown from water and experimental pattern (blue) recorded for crystals obtained by cooling an aqueous solution of the salt.

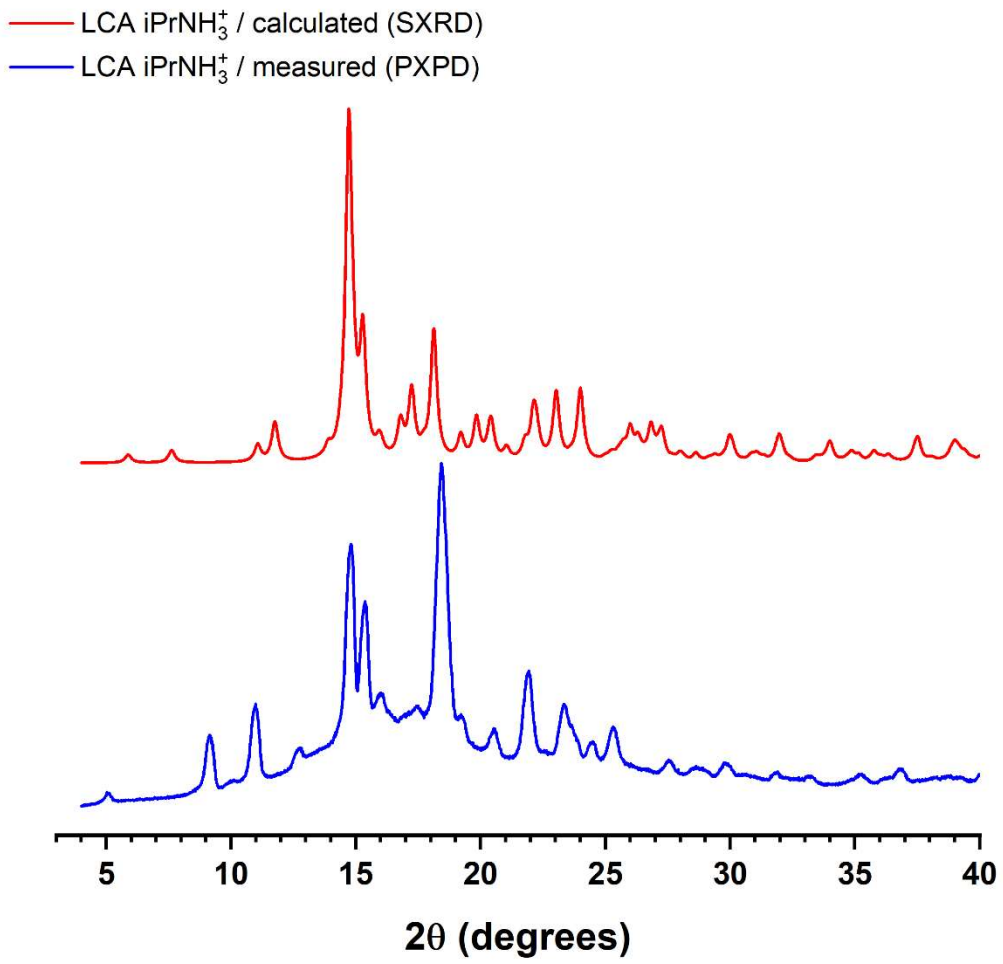

Figure 3.S7. Simulated X-ray powder diffraction pattern (red) for crystals of the *i*-$PrNH_3^+$ salt of LCA grown from water and experimental pattern (blue) recorded for a mixture of crystals and fibrils, as obtained by freeze-drying the product resulting from cooling an aqueous solution of the salt.

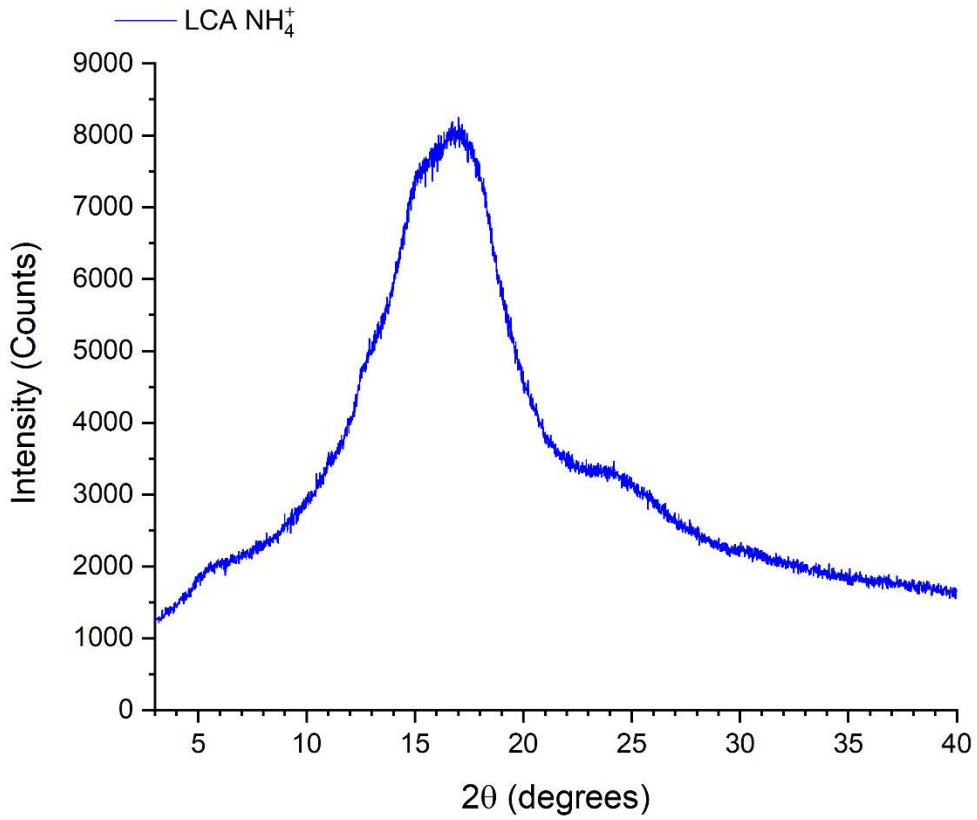

Figure 3.S8. Measured X-ray powder diffraction pattern for a sample of the NH_4^+ salt of LCA, as obtained by freeze-drying the gel resulting from cooling an aqueous solution of the salt.

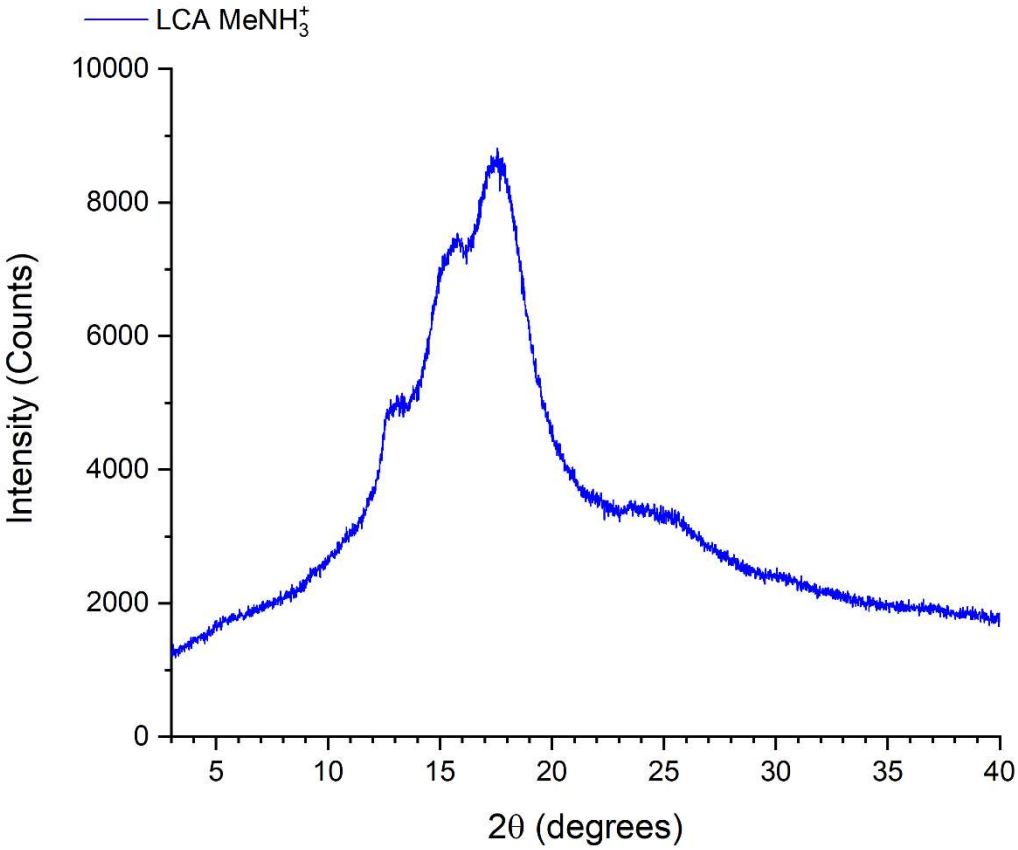

Figure 3.S9. Measured X-ray powder diffraction pattern for a sample of the $MeNH_3^+$ salt of LCA, as obtained by freeze-drying the gel resulting from cooling an aqueous solution of the salt.

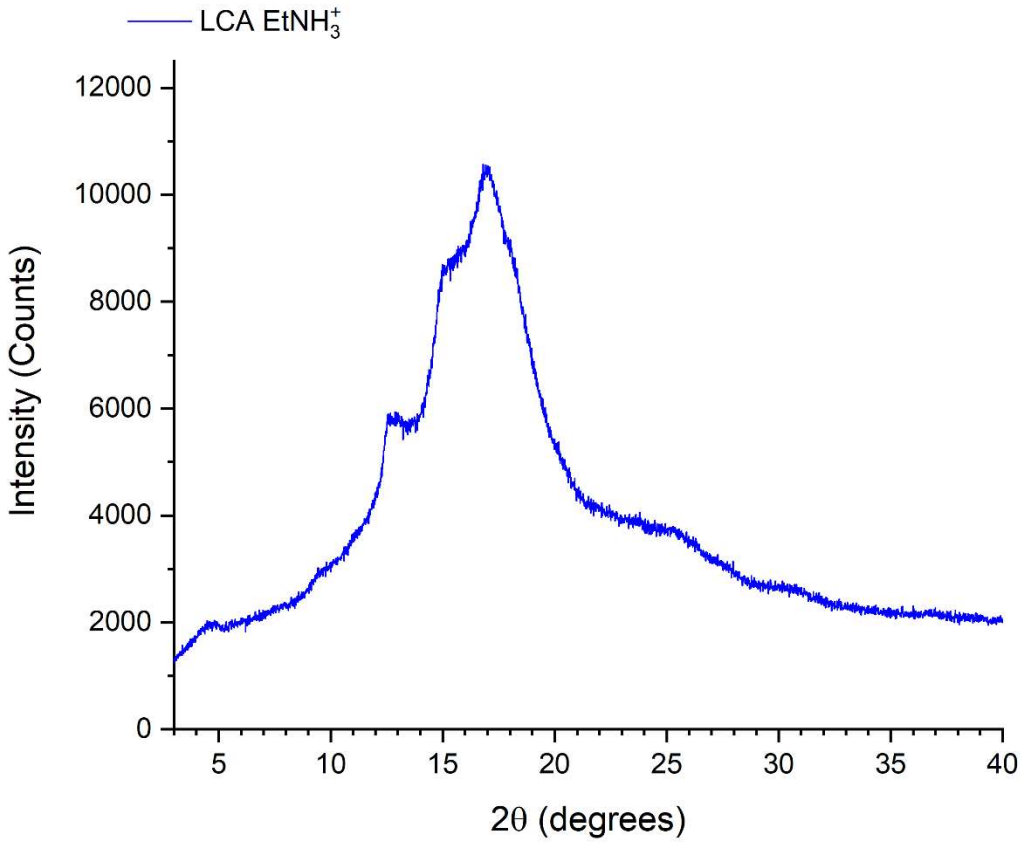

Figure 3.S10. Measured X-ray powder diffraction pattern for a sample of the $EtNH_3^+$ salt of LCA, as obtained by freeze-drying the gel resulting from cooling an aqueous solution of the salt.

3.5.5 Rheological Properties of Gels

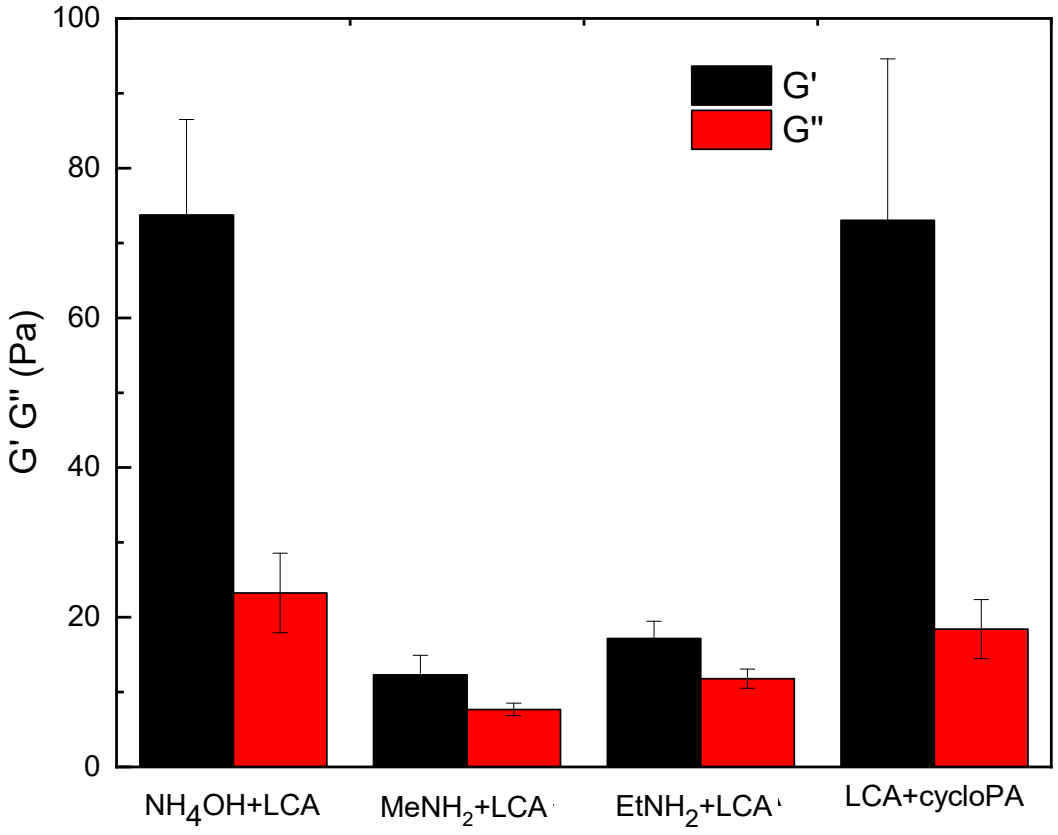

Figure 3.S11. Storage moduli (G') and loss moduli (G") of hydrogels prepared from LCA (50 mM) and different amines (800 mM).

.

References

(1) Bruker (2017). *APEX3* and *SAINT*, Bruker AXS Inc., Madison, Wisconsin, USA.

(2) Krause, L.; Herbst-Irmer, R.; Sheldrick, G. M.; Stalke, D. Comparison of Silver and Molybdenum Microfocus X-Ray Sources for Single-Crystal Structure Determination. *J. Appl. Cryst*. **2015**, *48*, 3–10.

(3) Sheldrick, G. M. *SHELXT* – Integrated Space-Group and Crystal-Structure Determination. *Acta Crystallogr*. **2015**, *A71*, 3–8.

(4) Sheldrick, G. M. Crystal Structure Refinement with *SHELXL*. *Acta Crystallogr*. **2015**, *C71*, 3–8.

(5) Macrae, C. F.; Sovago, I.; Cottrell, S. J.; Galek, P. T. A.; McCabe, P.; Pidcock, E.; Platings, M.; Shields, G. P.; Stevens, J. S.; Towler, M.; Wood, P. A. *Mercury 4.0*: From Visualization to Analysis, Design and Prediction. *J. Appl. Cryst.* **2020**, *53*, 226–235.

3.6 Accession Codes

CCDC 2113200−2113204 contain the supplementary crystallographic data for this paper. These data can be obtained free of charge via www.ccdc.cam.ac.uk/data_request/cif, by emailing data_request@ccdc.cam.ac.uk, or by contacting The Cambridge Crystallographic Data Centre, 12 Union Road, Cambridge CB2 1EZ, UK; fax: +44 1223 336033.

3.7 Acknowledgments

Financial support from the Natural Sciences and Engineering Research Council (NSERC) of Canada (RGPIN-2019-05469 and RGPIN-2020-06517) is gratefully acknowledged. We also thank the Canada Foundation for Innovation (Project 30910), the Canada Research Chairs Program, and the Université de Montréal for their generous support. We are also grateful to Xue-Dong Liu at the Facility for Electron Microscopy Research at McGill University for helping us obtain scanning electron micrographs.

3.8 References

1. Richtering, W.; Saunders, B. R. Gel Architectures and Their Complexity. *Soft Matter* **2014**, *10*, 3695–3702.
2. Almdal, K.; Dyre, J.; Hvidt, S.; Kramer, O. Towards a Phenomenological Definition of the Term 'Gel'. *Polym. Gels Networks* **1993**, *1*, 5–17.
3. Mondal, S.; Das, S.; Nandi, A. K. A Review on Recent Advances in Polymer and Peptide Hydrogels. *Soft Matter* **2020**, *16*, 1404–1454.
4. Du, X.; Zhou, J.; Shi, J.; Xu, B. Supramolecular Hydrogelators and Hydrogels: From Soft Matter to Molecular Biomaterials. *Chem. Rev.* **2015**, *115*, 13165–13307.
5. Ahmed, E. M. Hydrogel: Preparation, Characterization, and Applications: A Review. *J. Adv. Res.* **2015**, *6*, 105–121.
6. de Loos, M.; Feringa, B. L.; van Esch, J. H. Design and Application of Self-Assembled Low Molecular Weight Hydrogels. *Eur. J. Org. Chem.* **2005**, 3615–3631.
7. Estroff, L. A.; Hamilton, A. D. Water Gelation by Small Organic Molecules. *Chem. Rev.* **2004**, *104*, 1201–1217.
8. Menger, F. M.; Caran, K. L. Anatomy of a Gel. Amino Acid Derivatives That Rigidify Water at Submillimolar Concentrations. *J. Am. Chem. Soc.* **2000**, *122*, 11679–11691.
9. Chu, C.-W.; Schalley, C. A. Recent Advances on Supramolecular Gels: From Stimuli-Responsive Gels to Co-Assembled and Self-Sorted Systems. *Org. Mater.* **2021**, *3*, 25–40.
10. Draper, E. R.; Adams, D. J. Low-Molecular-Weight Gels: The State of the Art. *Chem* **2017**, *3*, 390–410.
11. Hanabusa, K.; Suzuki, M. Physical Gelation by Low-Molecular-Weight Compounds and Development of Gelators. *Bull. Chem. Soc. Jpn.* **2016**, *89*, 174–182.
12. James, S. L.; Lloyd, G. O.; Zhang, J. Supramolecular Gels in Crystal Engineering. *CrystEngComm* **2015**, *17*, 7976–7977.
13. Yu, G.; Yan, X.; Han, C.; Huang, F. Characterization of Supramolecular Gels. *Chem. Soc. Rev.* **2013**, *42*, 6697–6722.
14. Dastidar, P. Supramolecular Gelling Agents: Can They be Designed? *Chem. Soc. Rev.* **2008**, *37*, 2699–2715.
15. Sangeetha, N. M.; Maitra, U. Supramolecular Gels: Functions and Uses. *Chem. Soc. Rev.* **2005**, *34*, 821–836.

16. Terech, P.; Weiss, R. G. Low Molecular Mass Gelators of Organic Liquids and the Properties of Their Gels. *Chem. Rev.* **1997**, *97*, 3133–3159.
17. Khavasi, H. R.; Esmaeili, M. Is Gelation Behavior Predictable through a Crystal Engineering Approach? A Case Study in Four Similar Coordination Compounds. *Langmuir* **2019**, *35*, 4660–4671.
18. Farahani, A. D.; Martin, A. D.; Iranmanesh, H.; Bhadbhade, M. M.; Beves, J. E.; Thordarson, P. A Gel- and Solid-State-Structure of Dialanine and Diphenylalanine Amphiphiles: Importance of C···H interactions in Gelation. *ChemPhysChem* **2019**, *20*, 972–983.
19. Löfman, M.; Lahtinen, M.; Rissanen, K.; Sievänen, E. Two-Component Self-Assembly with Solvent Leading to "Wet" and Microcrystalline Organogel Fibers. *J. Colloid Interface Sci.* **2015**, *438*, 77–86.
20. Vidyasagar, A.; Sureshan, K. M. Stoichiometric Sensing to Opt between Gelation and Crystallization. *Angew. Chem. Int. Ed.* **2015**, *54*, 12078–12082.
21. Raeburn, J.; Mendoza-Cuenca, C.; Cattoz, B. N.; Little, M. A.; Terry, A. E.; Cardoso, A. Z.; Griffiths, P. C.; Adams, D. J. The Effect of Solvent Choice on the Gelation and Final Hydrogel Properties of Fmoc–Diphenylalanine. *Soft Matter* **2015**, *11*, 927–935.
22. Houton, K. A.; Morris, K. L.; Chen, L.; Schmidtmann, M.; Jones, J. T. A.; Serpell, L. C.; Lloyd, G. O.; Adams, D. J. On Crystal versus Fiber Formation in Dipeptide Hydrogelator Systems. *Langmuir* **2012**, *28*, 9797–9806.
23. Kapoor, I.; Schön, E.-M.; Bachl, J.; Kühbeck, D.; Cativiela, C.; Saha, S.; Banerjee, R.; Roelens, S.; Marrero-Tellado, J. J.; Díaz Díaz, D. Competition Between Gelation and Crystallisation of a Peculiar Multicomponent Liquid System Based on Ammonium Salts. *Soft Matter* **2012**, *8*, 3446–3456.
24. Muro-Small, M. L.; Chen, J.; McNeil, A. J. Dissolution Parameters Reveal Role of Structure and Solvent in Molecular Gelation. *Langmuir* **2011**, *27*, 13248–13253.
25. Hwang, I.; Jeon, W. S.; Kim, H.-J.; Kim, D.; Kim, H.; Selvapalam, N.; Fujita, N.; Shinkai, S.; Kim, K. Cucurbit[7]uril: A Simple Macrocyclic, pH-Triggered Hydrogelator Exhibiting Guest-Induced Stimuli-Responsive Behavior. *Angew. Chem. In. Ed.* **2007**, *46*, 210–213.

26. Lebel, O.; Perron, M.-È.; Maris, T.; Zalzal, S. F.; Nanci, A.; Wuest, J. D. A New Class of Selective Low-Molecular-Weight Gelators Based on Salts of Diaminotriazinecarboxylic Acids. *Chem. Mater.* **2006**, *18*, 3616–3626.
27. Stanley, C. E.; Clarke, N.; Anderson, K. M.; Elder, J. A.; Lenthall, J. T.; Steed, J. W. Anion Binding Inhibition of the Formation of a Helical Organogel. *Chem. Commun.* **2006**, 3199–3201.
28. Kumar, D. K.; Jose, D. A.; Das, A.; Dastidar, P. First Snapshot of a Nonpolymeric Hydrogelator Interacting with its Gelling Solvents. *Chem. Commun.* **2005**, 4059–4061.
29. Hsu, W.-P.; Koo, K.-K.; Myerson, A. S. The Gel-Crystallization of l-Phenylalanine and Aspartame from Aqueous Solutions. *Chem. Eng. Commun.* **2002**, *189*, 1079–1090.
30. Ostuni, E.; Kamaras, P.; Weiss, R. G. Novel X-Ray Method for In Situ Determination of Gelator Strand Structure: Polymorphism of Cholesteryl Anthraquinone-2-carboxylate. *Angew. Chem. Int. Ed.* **1996**, *35*, 1324–1326.
31. Guterman, T.; Levin, M.; Kolusheva, S.; Levy, D.; Noor, N.; Roichman, Y.; Gazit, E. Real-Time In-Situ Monitoring of a Tunable Pentapeptide Gel–Crystal Transition. *Angew. Chem. Int. Ed.* **2019**, *58*, 15869–15875.
32. Andrews, J. L.; Pearson, E.; Yufit, D. S.; Steed, J. W.; Edkins, K. Supramolecular Gelation as the First Stage in Ostwald's Rule. *Cryst. Growth Des.* **2018**, *18*, 7690–7700.
33. Feng, H.; Du, Y.; Tang, F.; Ji, N.; Zhao, X.; Zhao, H.; Chen, Q. Silver Ions Blocking Crystallization of Guanosine-Based Hydrogel for Potential Antimicrobial Applications. *RSC Adv.* **2018**, *8*, 15842–15852.
34. Liu, X.; Fei, J.; Wang, A.; Cui, W.; Zhu, P.; Li, J. Transformation of Dipeptide-Based Organogels into Chiral Crystals by Cryogenic Treatment. *Angew. Chem. Int. Ed.* **2017**, *56*, 2660–2663.
35. Barker, E. C.; Martin, A. D.; Garvey, C. J.; Goh, C. Y.; Jones, F.; Mocerino, M.; Skelton, B. W.; Ogden, M. I.; Becker, T. Thermal Annealing Behaviour and Gel to Crystal Transition of a Low Molecular Weight Hydrogelator. *Soft Matter* **2017**, *13*, 1006–1011.
36. Guo, M.; Yin, Q.; Li, Y.; Huang, Y.; Zhang, Z.; Zhou, L. Gel-Crystal Transition During Crystallization of Cefpiramide. *Chem. Lett.* **2017**, *46*, 1292–1295.

37. Liu, J.; Xu, F.; Sun, Z.; Pan, Y.; Tian, J.; Lin, H.-C.; Li, X. A Supramolecular Gel Based on a Glycosylated Amino Acid Derivative with the Properties of Gel to Crystal Transition. *Soft Matter* **2016**, *12*, 141–148.
38. Liyanage, W.; Brennessel, W. W.; Nilsson, B. L. Spontaneous Transition of Self-Assembled Hydrogel Fibrils into Crystalline Microtubes Enables a Rational Strategy to Stabilize the Hydrogel State. *Langmuir* **2015**, *31*, 9933–9942.
39. Kumar, D. K.; Steed, J. W. Supramolecular Gel Phase Crystallization: Orthogonal Self-Assembly Under Non-Equilibrium Conditions. *Chem. Soc. Rev.* **2014**, *43*, 2080–2088.
40. Aiyappa, H. B.; Saha, S.; Garai, B.; Thote, J.; Kurungot, S.; Banerjee, R. A Distinctive $PdCl_2$-Mediated Transformation of Fe-Based Metallogels into Metal–Organic Frameworks. *Cryst. Growth Des.* **2014**, *14*, 3434–3437.
41. Xu, Y.; Kang, C.; Chen, Y.; Bian, Z.; Qiu, X.; Gao, L.; Meng, Q. In Situ Gel-to-Crystal Transition and Synthesis of Metal Nanoparticles Obtained by Fluorination of a Cyclic β-Aminoalcohol Gelator. *Chem. Eur. J.* **2012**, *18*, 16955–16961.
42. Roy, B.; Bairi, P.; Nandi, A. K. Metastability in a Bi-Component Hydrogel of Thymine and 6-Methyl-1,3,5-triazine-2,4-diamine: Ultrasound *vs.* Thermo Gelation. *Soft Matter* **2012**, *8*, 2366–2369.
43. Wang, Y.; Tang, L.; Yu, J. Investigation of Spontaneous Transition from Low-Molecular-Weight Hydrogel into Macroscopic Crystals. *Cryst. Growth Des.* **2008**, *8*, 884–889.
44. Moffat, J. R.; Smith, D. K. Metastable Two-Component Gel—Exploring the Gel–Crystal Interface. *Chem. Commun.* **2008**, 2248–2250.
45. Sasselli, I. R.; Halling, P. J.; Ulijn, R. V.; Tuttle, T. Supramolecular Fibers in Gels Can Be at Thermodynamic Equilibrium: A Simple Packing Model Reveals Preferential Fibril Formation *versus* Crystallization. *ACS Nano* **2016**, *10*, 2661–2668.
46. Adams, D. J.; Morris, K.; Chen, L.; Serpell, L. C.; Bacsa, J.; Day, G. M. The Delicate Balance Between Gelation and Crystallisation: Structural and Computational Investigations. *Soft Matter* **2010**, *6*, 4144–4156.
47. Terech, P. Metastability and Sol Phases: Two Keys for the Future of Molecular Gels? *Langmuir* **2009**, *25*, 8370–8372.
48. Bernstein, J. *Polymorphism in Molecular Crystals*; Oxford University Press: New York, 2002.

49. Bariya, D.; Anand, V.; Mishra, S. Recent Advances in the Bile Acid Based Conjugates/Derivatives Towards Their Gelation Applications. *Steroids* **2021**, *165*, 108769.
50. Goldshleger, N. F.; Lobach, A. S.; Baulin, V. E.; Tsivadze, A. Y. Supramolecular Gels Based on Bile Acid Salts. *Russ. Chem. Rev.* **2017**, *86*, 269–297.
51. Zhang, M.; Strandman, S.; Waldron, K. C.; Zhu, X. X. Supramolecular Hydrogelation with Bile Acid Derivatives: Structure, Properties and Applications. *J. Mater. Chem. B* **2016**, *4*, 7506–7520.
52. Svobodová, H.; Noponen, V.; Kolehmainen, E.; Sievänen, E. Recent Advances in Steroidal Supramolecular Gels. *RSC Adv.* **2012**, *2*, 4985–5007.
53. Madenci, D.; Egelhaaf, S. U. Self-Assembly in Aqueous Bile Salt Solutions. *Curr. Opin. Colloid Interface Sci.* **2010**, *15*, 109–115.
54. Calabresi, M.; Andreozzi, P.; La Mesa, C. Supra-Molecular Association and Polymorphic Behaviour in Systems Containing Bile Acid Salts. *Molecules* **2007**, *12*, 1731–1754.
55. Terech, P.; Sangeetha, N. M.; Maitra, U. Molecular Hydrogels from Bile Acid Analogues with Neutral Side Chains: Network Architectures and Viscoelastic Properties. Junction Zones, Spherulites, and Crystallites: Phenomenological Aspects of the Gel Metastability. *J. Phys. Chem. B* **2006**, *110*, 15224–15233.
56. di Gregorio, M. C.; Cautela, J.; Galantini, L. Physiology and Physical Chemistry of Bile Acids. *Int. J. Mol. Sci.* **2021**, *22*, 1780.
57. Hofmann, A. F.; Hagey, L. R. Bile Acids: Chemistry, Pathochemistry, Biology, Pathobiology, and Therapeutics. *Cell. Mol. Life Sci.* **2008**, *65*, 2461–2483.
58. Mukhopadhyay, S.; Maitra, U. Chemistry and Biology of Bile Acids. *Curr. Sci.* **2004**, *87*, 1666–1683.
59. Shokry, D. S.; Waters, L. J.; Parkes, G. M. B.; Mitchell, J. C.; Snowden, M. J. Formation of a Bile Salt–Drug Hydrogel to Predict Human Intestinal Absorption. *J. Pharm. Sci.* **2019**, *108*, 279–287.
60. Pavlović, N.; Goločorbin-Kon, S.; Danić, M.; Stanimirov, B.; Al-Salami, H.; Stankov, K.; Mikov, M. Bile Acids and Their Derivatives as Potential Modifiers of Drug Release and Pharmacokinetic Profiles. *Front. Pharmacol.* **2018**, *9*, 1283.

61. Faustino, C.; Serafim, C.; Rijo, P.; Pinto Reis, C. Bile Acids and Bile Acid Derivatives: Use in Drug Delivery Systems and as Therapeutic Agents. *Expert Opin. Drug Deliv.* **2016**, *13*, 1133–1148.
62. Sharma, R.; Long, A.; Gilmer, J. F. Advances in Bile Acid Medicinal Chemistry. *Curr. Med. Chem.* **2011**, *18*, 4029–4052.
63. Virtanen, E.; Kolehmainen, E. Use of Bile Acids in Pharmacological and Supramolecular Applications. *Eur. J. Org. Chem.* **2004**, 3385–3399.
64. Enhsen, A.; Kramer, W.; Wess, G. Bile Acids in Drug Discovery. *Drug Discov. Today* **1998**, *3*, 409–418.
65. Zhang, M.; Waldron, K. C.; Zhu, X. X. Formation of Molecular Hydrogels from a Bile Acid Derivative and Selected Carboxylic Acids. *RSC Adv.* **2016**, *6*, 35436–35440.
66. Zhang, M.; Ma, Z.; Wang, K.; Zhu, X. X. CO_2 Sequestration by Bile Salt Aqueous Solutions and Formation of Supramolecular Hydrogels. *ACS Sustainable. Chem. Eng.* **2019**, *7*, 3949–3955.
67. Zhang, M. Supramolecular Hydrogels Based on Bile Acids and Their Derivatives. Ph. D. Thesis, Université de Montréal: Montréal, October 2016.
68. Li, P.; Malveau, C.; Zhu, X. X.; Wuest, J. D. Using NMR Spectroscopy to Probe Hydrogels Formed by Sodium Deoxycholate. *Langmuir* **2021**, submitted for publication.
69. Adams, D. J. Does Drying Affect Gel Networks? *Gels* **2018**, *4*, 32.
70. Nassimbeni, L. R.; Báthori, N. B.; Curtin, T.-L. Ammonium Salts of Lithocholic Acid: Structures and Kinetics. *Cryst. Growth Des.* **2012**, *12*, 4144–4148.
71. Ikonen, S.; Nonappa; Kolehmainen, E. Supramolecular Architectures Formed by Co-Crystallization of Bile Acids and Melamine. *CrystEngComm* **2010**, *12*, 4304–4311.
72. Pal, A.; Basit, H.; Sen, S.; Aswal, V. K.; Bhattacharya, S. Structure and Properties of Two Component Hydrogels Comprising Lithocholic Acid and Organic Amines. *J. Mater. Chem.* **2009**, *19*, 4325–4334.
73. Arora, S. K.; Germain, G.; Declercq, J. P. The Crystal and Molecular Structure of Lithocholic Acid. *Acta Crystallogr.* **1976**, *B32*, 415–419.
74. Meijide, F.; de Frutos, S.; Soto, V. H.; Jover, A.; Seijas, J. A.; Vázquez-Tato, M. P.; Fraga, F.; Vázquez Tato, J. A Standard Structure for Bile Acids and Derivatives. *Crystals* **2018**, *8*, 86.

75. Miyata, M.; Tohnai, N.; Hisaki, I. Supramolecular Chirality in Crystalline Assemblies of Bile Acids and Their Derivatives; Three-Axial, Tilt, Helical, and Bundle Chirality. *Molecules* **2007**, *12*, 1973–2000.

Chapter 4. Probing the Relationship Between Crystallization and Gelation by Using Ammonium Salts of Various Bile Acids

Abstract

Hydrogels formed from aqueous solutions of bile acids and their salts are biocompatible materials that promise to be useful in drug delivery, cellular immobilization, and other applications. These materials are considered to result from self-association of the components to give networks of fibrils; however, the molecular structure of the fibrils has not yet been established with certainty. Previous work has shown that ammonium salts of lithocholic acid can form both crystals and hydrogels under the same conditions. Structural analyses of these salts by single-crystal X-ray diffraction revealed that lithocholate anions are invariably arranged in similar ways, leading to the suggestion that the fibrils causing hydrogelation have closely related structures. This hypothesis has now been strengthened by additional studies of the behavior of ammonium salts of lithocholic acid and other bile acids. In this new work, both crystallization and fibril-induced gelation are again observed, and the crystals tend to have fibril-like acicular morphologies that reflect rapid growth by edge-to-edge association of bile anions. When the ammonium cations are small, the crystals have closely related structures. The observation that simple ammonium salts of many bile acids consistently favor the same pattern of molecular organization in crystalline solids reinforces the hypothesis that the fibrils responsible for hydrogelation have analogous internal structures.

This chapter has been summarized as a research article and submitted for publication: Puzhen Li, Meng Zhang, Thierry Maris, X. X. Zhu, and James D. Wuest. "Probing the Relationship Between Crystallization and Gelation by Using Ammonium Salts of Bile Acids." Accepted by *Crystal Growth & Design*.

4.1 Introduction

In typical hydrogels, large quantities of water are immobilized by relatively small amounts of added substances that associate to give rise to entangled or crosslinked fibrillar networks.[1–6] The resulting gels are uniquely useful because they combine the properties of solids (such as resistance to deformation) with those of liquids (such as the ability to change shape). Hydrogels are common in nature, are found in the human body in various forms, including cartilage, tendons, and the vitreous humor of the eye, and have many industrial applications. The wide-ranging properties and broad utility of hydrogels provide a strong incentive to understand in detail how the materials are formed and behave, as a basis for making improved gels by design. Despite extensive research, however, the internal structures of the fibrillar networks that underlie typical gelation are generally unclear, and further study is needed to reveal how gelation, crystallization, and other associative phenomena are related.

Potential hydrogelating agents include both polymers and small molecules that can form extended networks by association in water.[7–14] As a source of detailed understanding of hydrogelation, small-molecule agents are advantageous because they have uniform, well-defined structures, allowing the properties of gels to be correlated with specific molecular features of the gelators. Small-molecule hydrogelators are usually amphiphilic compounds with polar regions to ensure adequate aqueous solubility and with hydrophobic features to induce aggregation. Families of small-molecule hydrogelators have typically been discovered by accident, and structural differences between effective gelators and analogues that prefer to crystallize or to precipitate in other forms are often subtle. In certain cases, gelators can also be induced to crystallize, although rarely under the same conditions that yield gels.[15–28] Occasionally, gels yield crystalline precipitates on standing, establishing that gelation is favored kinetically in these systems but not thermodynamically.[29–42] This behavior is not universal, however, and the kinetic and thermodynamic relationship between crystallization and gelation is not always clear.[43–45]

Most reported small-molecule hydrogelators have flexible structures and can adopt diverse conformations. In addition, the compounds often have multiple functional groups that can engage in intermolecular interactions and cause association to occur in various ways. As a result, gelators have the potential to crystallize as markedly different polymorphs and solvates.[46] For this reason, structural analyses of crystals by X-ray diffraction cannot always be expected to reveal the internal

structure of the fibrillar networks of gels in molecular detail, even when the gelator crystallizes from the gel itself or under similar conditions. However, uncertainty about the relationship between crystallization and gelation can be reduced or even eliminated by examining the behavior of families of compounds in which molecular aggregation follows a consistent pattern. Whenever such families can be induced to crystallize and also to produce hydrogels or related fibrillar aggregates, structural analyses of the crystals by X-ray diffraction will simultaneously show how the molecules are likely to be arranged in the fibrillar structures of gels.

Attractive candidates for studies of this type are bile acids and their salts,[47–53] which are present in mammals and other vertebrates to facilitate the digestion of fats and the absorption of nutrients with poor solubility in water.[54–56] The family of bile acids includes lithocholic acid (**1**; LCA), deoxycholic acid (**2**; DCA), chenodeoxycholic acid (**3**; CDCA), and cholic acid (**4**; CA), which increase in hydrophilicity as the number of hydroxyl groups increases. These compounds have a tetracyclic steroidal structure that includes an extended convex hydrophobic face and an opposing concave hydrophilic face with hydroxyl and carboxyl groups. The resulting amphiphilicity gives rise to the formation of biocompatible hydrogels that are promising for use in drug delivery, cellular immobilization, and other applications.[57–62] Our group has worked actively in these areas,[15,49,63–66] and we have studied hydrogels formed by mixing carboxylic acids with derivatives of bile acids,[63] ways to sequester CO_2 in hydrogels containing bile acid salts,[64] and other topics.[65,66] Experience with bile acids and their derivatives has shown that a properly adjusted level of solubility in water is a prerequisite for hydrogelation.

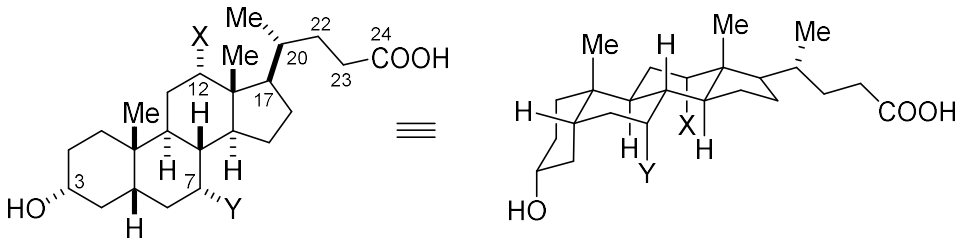

1 (LCA; X = Y = H)
2 (DCA; X = OH, Y = H)
3 (CDCA; X = H, Y = OH)
4 (CA; X = Y = OH)

In earlier work,[15] we reported that crystals, hydrogels, or mixtures of crystals and fibrillar structures characteristic of gels are formed by aqueous solutions of salts $LCA^- RNH_3^+$ under similar conditions, in a way that depends on the size of the group R. Analysis by single-crystal and powder X-ray diffraction suggested that crystals and fibrils have closely related structures in this system. Moreover, typical crystals have acicular morphologies similar to those of the fibrils. The markedly anisotropic growth of both crystals and fibrils appears to result from preferential edge-to-edge association of lithocholate anions, which yields assemblies with the largest possible hydrophilic surfaces in contact with the surrounding aqueous medium.

To test the generality of these conclusions and to further explore the relationship between crystallization and gelation, we have now examined the structures of additional ammonium salts of LCA, as well as the behavior of ammonium salts of other bile acids. This extensive new work, which includes the analysis of eight additional structures by single-crystal X-ray diffraction, has (1) strengthened evidence of a close structural and morphological relationship between crystals and fibrils in the previously studied case of LCA, and (2) shown that a close relationship also exists in the case of other bile acids. This new work has strengthened evidence of a close structural and morphological relationship between crystals and fibrils in the case of LCA, and our additional observations show that the relationship also extends to other bile acids. By establishing that a large set of simple ammonium salts of bile acids all crystallize from water to form structures with closely related patterns of molecular organization, our results reinforce the hypothesis that hydrogelation caused by these compounds results from the formation of fibrils with analogous molecular structures.

4.2 Results and Discussion

The solubility of LCA in water is poor at pH 7. However, previous work showed that solutions of various RNH_3^+ salts (including R = H and R = C_1–C_6 alkyl or cycloalkyl groups) with concentrations of about 50 mM (2 wt%) can be obtained by warming aqueous mixtures of LCA and RNH_2 in a 1:16 molar ratio. One equivalent of RNH_2 is sufficient to deprotonate LCA quantitatively, and an excess is used to increase solubility or facilitate dissolution. As summarized in Table 4.1-4.2, cooling the solutions to 25 °C led either to the formation of hydrogels (when R = H, methyl, ethyl, and cyclopropyl), to mixtures containing both acicular crystals and fibrils of the

type associated with gelation (when R = *i*-propyl and propyl), or only to crystals (when R = butyl, *s*-butyl, *i*-butyl, *t*-butyl, pentyl, and cyclohexyl). DCA is more soluble in water than LCA, and new work has shown that gelation or crystallization occurs only when RNH_3^+ salts of DCA incorporate R groups with at least three atoms of carbon (Tables 4.1–4.2). Related RNH_3^+ salts of CDCA and CA proved to give solutions under these conditions with all R groups containing fewer than six

Table 4.1 Ability of RNH_3^+ Salts of Selected Bile Acids to Form Aqueous Solutions (S), Hydrogels (G), Fibrils (F), or Crystals (C) Under Standard Conditions (25 °C, Nominal Concentration of Bile Acid = 50 mM)

	NH_4^+	methylNH_3^+	ethylNH_3^+	propylNH_3^+	butylNH_3^+	pentylNH_3^+	hexylNH_3^+
LCA^-	G	G	G	C + F	C	C	*
DCA^-	S	S	S	G	G	G	C
$CDCA^-$	S	S	S	S	S	S	*
CA^-	S	S	S	S	S	S	C

*Salt insoluble in warm water under standard conditions.

atoms of carbon (Tables 4.1–4.2). Hydrogels derived from salts of DCA were characterized by standard methods, including optical microscopy and scanning electron microscopy. Electron micrographs of representative lyophilized gels revealed that fibrillar structures are formed, at least in the dried state (Figure 4.1).[67] Data summarized in Tables 1–2 were gathered under the same conditions to allow comparisons to be made and trends to be discerned. However, the ability of any particular salt to form solutions, gels, fibrils, or crystals can be expected to depend on the conditions selected.

Table 4.2. Effect of Branched Alkyl Chains and Rings on the Ability of RNH_3^+ Salts of Selected Bile Acids to Form Aqueous Solutions (S), Hydrogels (G), Fibrils (F), or Crystals (C) Under Standard Conditions (25 °C, Nominal Concentration of Bile Acid = 50 mM)

	R = C_3			R = C_4				R = C_6	
	cyclopropyl	*i*-propyl	propyl	butyl	*s*-butyl	*i*-butyl	*t*-butyl	cyclohexyl	hexyl
LCA^-	G	C + F	C + F	C	C	C	C	C	*
DCA^-	S	S	G	G	S	S	S	C	C
CA^-	S	S	S	S	S	S	S	S	C

*Salt insoluble in warm water under standard conditions.

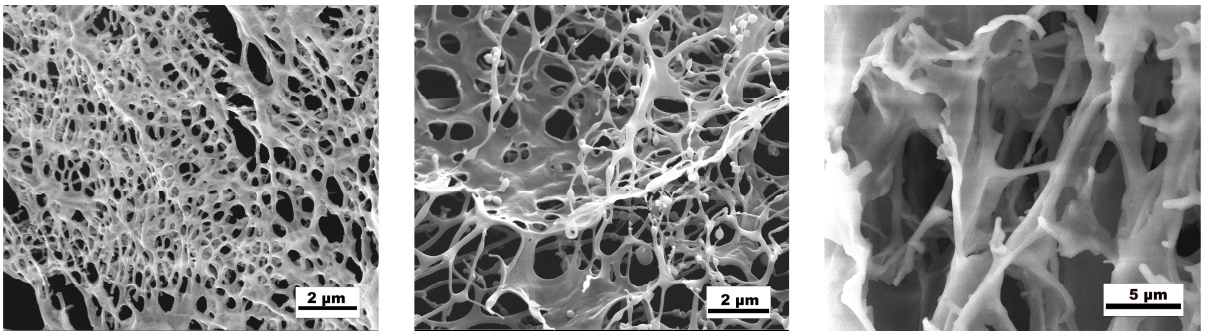

Figure 4.1. Morphologies produced by lyophilizing hydrogels derived from selected alkylammonium salts of DCA, as imaged by scanning electron microscopy. (a) PropylNH_3^+ salt. (b) ButylNH_3^+ salt. (c) PentylNH_3^+ salt.

Table 4.1-4.2 confirm that self-association of ammonium salts of bile acids in aqueous media generally increases as the salts become less hydrophilic, starting from the most ($CA^- NH_4^+$) to the

least (LCA^- hexylNH_3^+). In this series, a preference for forming solutions is gradually replaced by a tendency to give gels and finally crystals. Under the conditions used, the most hydrophilic salts form solutions, salts with marginal solubility induce gelation, and the least hydrophilic salts tend to crystallize. In addition, Table 4.1 indicates that ammonium salts of DCA are somewhat more associated than analogues derived from CDCA, although the two bile acids have the same number of hydroxyl groups and similar solubilities in water at pH 3.[68] Moreover, the behavior of ammonium salts of bile acids is sensitive to small structural changes, as exemplified in the case of LCA by the transition from gels (cyclopropylNH_3^+), to mixtures of fibrils and crystals (*i*-propylNH_3^+ and propylNH_3^+), and then to crystals (butylNH_3^+) as the alkyl group is altered slightly (Table 4.2).

Related behavior is shown by salts of bile acids derived from secondary alkylamines, tertiary alkylamines, and pyridine, as summarized in Table 4.3. The formation of solutions, gels, fibrils, and crystals was again observed, depending on the degree of hydrophilicity of the salts and their tendency to self-associate in aqueous media. Together, the data shown in Tables 4.1–4.3 establish

Table 4.3. Ability of $R_2NH_2^+$ Salts, R_3NH^+ Salts, and Pyridinium Salts of Selected Bile Acids to Form Aqueous Solutions (S), Hydrogels (G), Fibrils (F), or Crystals (C) Under Standard Conditions (25 °C, Nominal Concentration of Bile Acid = 50 mM)

	Secondary ammonium ($R_2NH_2^+$)				Tertiary ammonium (R_3NH^+)		Pyridinium
	dimethyl	diethyl	ethylmethyl	dipropyl	trimethyl	triethyl	
LCA^-	F	C + F	G	*	F	F	F
DCA^-	S	S	S	C	S	S	G
CA^-	S	S	S	S	S	S	C

*Salt insoluble in warm water under standard conditions.

that the associative behavior of simple ammonium salts of bile acids straddles the border between gelation and crystallization. As a result, systematic variation of the bile anion and ammonium cation can help define the position of the border and reveal why a particular salt lies on one side or the other.

Structural Analysis of LCA$^-$ *i*-PrNH$_3^+$. Cooling warm aqueous solutions of LCA$^-$ *i*-PrNH$_3^+$ yielded fibrils and monoclinic $P2_1$ crystals of the monohydrate LCA$^-$ *i*-PrNH$_3^+$ • H_2O, as reported previously.[15] Under these conditions, monoclinic $P2_1$ crystals of the anhydrous salt LCA$^-$ *i*-PrNH$_3^+$ were observed to appear concomitantly, and the structure was solved by single-crystal X-ray diffraction. Table 4.4 summarizes additional crystallographic data, and Figure 4.2 shows that the structures of the monohydrate and anhydrous forms are closely similar. In both cases, neighboring lithocholate anions are aligned head-to-tail to form layers terminated by OH and COO$^-$ groups. In this way, the hydrophobic steroidal core of lithocholate anions is segregated from hydrophilic regions. In both solid forms, the six- and five-membered rings of lithocholate adopt normal conformations, and the side chain is partially extended. In the anhydrous form, the torsional angles C17–C20–C22–C23 and C20–C22–C23–C24 are 172° and 59°, respectively (see the structure of LCA for numbering). In the previously reported monohydrate,[15] the corresponding angles are 153° and 71°, showing that small conformational changes accompany the gain or loss of water. In both solid forms, each *i*-PrNH$_3^+$ cation interacts with the COO$^-$ groups of three lithocholate anions to form three N–H···O hydrogen bonds with similar N···O distances (2.74–2.85 Å in the anhydrous form).[69] In addition, each COO$^-$ group in both forms engages in three N–H···O hydrogen bonds with *i*-PrNH$_3^+$ cations and also forms an O–H···O hydrogen bond. In the anhydrous form, this hydrogen bond results from the direct interaction of COO- with the OH group at C3 in a neighboring bile anion, but in the monohydrate the two groups interact indirectly via an intervening molecule of water.

Understanding of the associative behavior of ammonium salts of LCA, as summarized in previous work,[15] is significantly extended by discovery of the anhydrous form of LCA- i-PrNH3+ and the similarity of its structure to that of the monohydrate. This salt is noteworthy because it gives rise to fibrils characteristic of gels, as well as to both hydrated and anhydrous crystalline forms with closely related structures. These observations tighten the connection between crystallization and gelation involving ammonium salts of bile acids and strengthen the hypothesis

that molecular organization in both states of matter is analogous. Moreover, the structural similarity of the hydrated and anhydrous forms suggests that incorporating water in micellar aggregates of bile salts does not necessarily disrupt standard patterns of molecular association determined by their unique amphiphilic characteristics.

Table 4.4. Structural Data for Ammonium Salts of LCA, DCA, and CA, as Determined by Single-Crystal X-Ray Diffraction

compound	**LCA$^-$ *i*-PrNH$_3^+$**	**LCA$^-$ PrNH$_3^+$**	**DCA$^-$ Pr$_2$NH$_2^+$ • 2 H$_2$O**	**DCA$^-$ cyclohexylNH$_3^+$**	**DCA$^-$ octylNH$_3^+$**	**CA$^-$ hexylNH$_3^+$ • H$_2$O**	**CA$^-$ octylNH$_3^+$ • 2 H$_2$O**	**CA$^-$ 1-adamantylNH$_3^+$ • 3.5 H$_2$O**
crystal syst	monoclinic	monoclinic	orthorhombic	monoclinic	monoclinic	monoclinic	monoclinic	monoclinic
space group	$P2_1$	$P2_1$	$P2_12_12_1$	$P2_1$	$P2_1$	$P2_1$	$P2_1$	$C2$
a (Å)	12.9687(14)	9.8247(8)	7.5730(3)	10.2444(2)	11.8383(2)	13.9188(2)	13.6675(3)	28.0367(16)
b (Å)	6.8993(7)	7.5533(7)	11.0104(4)	7.6716(2)	7.7270(1)	7.9078(1)	7.5914(2)	7.5296(4)
c (Å)	14.8695(15)	17.2646(12)	36.2681(14)	18.0614(4)	17.0565(3)	14.5323(2)	16.1130(3)	17.7558(10)
α (deg)	90	90	90	90	90	90	90	90
β (deg)	106.707(6)	96.125(5)	90	90.471(1)	104.126(1)	110.581(1)	97.613(1)	113.990(3)
γ (deg)	90	90	90	90	90	90	90	90
V (Å^3)	1274.3(2)	1273.87(18)	3024.1(2)	1419.41(6)	1513.06(4)	1497.44(4)	1657.08(6)	3424.5(3)
Z	2	2	4	2	2	2	2	4
Z'	1	1	1	1	1	1	1	1
ρ_{calc} (g · cm^{-3})	1.135	1.136	1.164	1.151	1.145	1.170	1.150	1.208
T (K)	150	100	100	100	100	100	100	100
R_1, $I > 2\sigma(I)$	0.0748	0.0586	0.0360	0.0344	0.0291	0.0288	0.0802	0.0563
wR_2, $I > 2\sigma(I)$	0.1912	0.1314	0.0953	0.0872	0.0758	0.0776	0.2230	0.1396
$\Delta\rho_{max}/\Delta\rho_{min}$ (e ·Å^{-3})	0.246/-0.213	0.241/-0.261	0.29/-0.23	0.23/-0.21	-0.17/0.24	0.24/-0.16	0.55/-0.47	-0.39/0.45
GoF	1.004	1.055	1.069	1.052	1.045	1.027	1.061	1.034

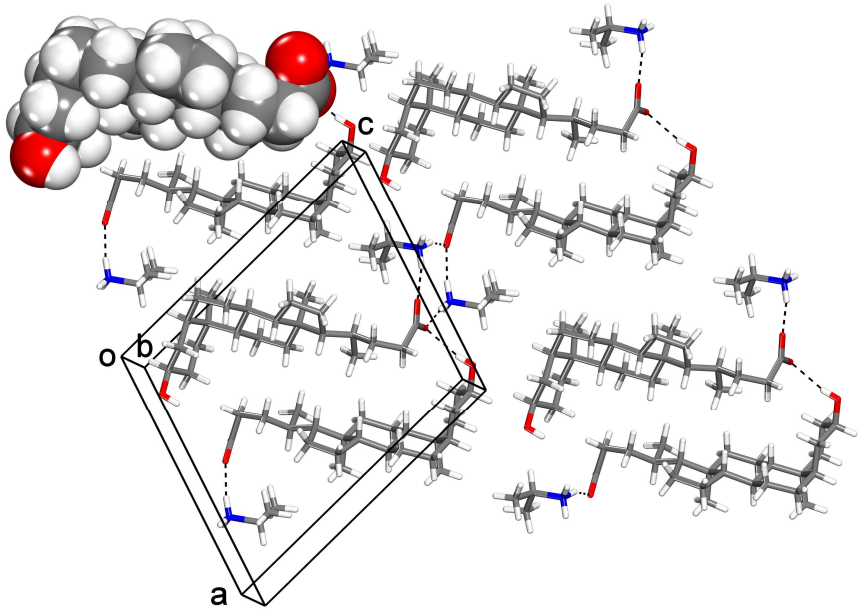

Figure 4.2. Representation of the structure of crystals of anhydrous LCA^- *i*-$PrNH_3^+$ grown from H_2O, showing the cross sections of part of two layers of lithocholate anions, separated by regions in which OH, COO^-, and *i*-$PrNH_3^+$ engage in multiple hydrogen bonds. A selected anion is shown in a space-filling representation, and hydrogen bonds are indicated by broken lines. Atoms of carbon appear in gray, hydrogen in white, nitrogen in blue, and oxygen in red.

Structural Analysis of LCA^- $PrNH_3^+$. When warm aqueous solutions of LCA^- $PrNH_3^+$ are cooled, crystals of the known anhydrous orthorhombic $P2_12_12_1$ form are produced along with fibrils, as previously reported.[15] In addition, we observed crystals of a new anhydrous monoclinic $P2_1$ polymorph. Structural data obtained by single-crystal X-ray diffraction are presented in Table 4.4, and a view of the structure appears in Figure 4.3. In the new form, the six- and five-membered rings of lithocholate have normal conformations, and the side chain is almost fully extended. The torsional angles C17–C20–C22–C23 and C20–C22–C23–C24 are 170° and 179°, respectively (see the structure of LCA for numbering), whereas in the known $P2_12_12_1$ form,[15] the corresponding angles are 169° and 69°.

Despite differences in the conformation of lithocholate, both polymorphs have similar layered structures in which adjacent anions are aligned head-to-tail. In both forms, each COO^- group takes part in two N–H···O hydrogen bonds with $PrNH_3^+$ cations ($d_{N\cdots O}$ = 2.723(4) and 2.724(5) Å in the new $P2_1$ polymorph, and $d_{N\cdots O}$ = 2.717(4) and 2.783(3) Å in the known $P2_12_12_1$ form), as well as one O–H···O hydrogen bond with the OH group of an adjacent lithocholate anion ($d_{O\cdots O}$ = 2.674(X) and 2.694(3) Å in the $P2_1$ and $P2_12_12_1$ forms, respectively). Each $PrNH_3^+$ cation forms three N–H···O hydrogen bonds, two with COO^- groups and one with an OH group ($d_{N\cdots O}$ = 2.787(4) and 2.809(3) Å in the $P2_1$ and $P2_12_12_1$ forms, respectively). In both polymorphs, the structure of the interlamellar ionic region is maintained by the cyclic hydrogen-bonded array represented by structure **5**. Crystals of LCA- $PrNH_3^+$ • EtOH grown from ethanol have been reported to belong to the monoclinic P21 space group and to have a lamellar structure closely related to those of the unsolvated forms.[70] In all cases, packing of the bile anions leaves too little volume within the layers to accommodate the alkyl groups of the $PrNH_3^+$ cations, which are located entirely in the interlamellar region. The structure of the new monoclinic $P2_1$ form of LCA^- $PrNH_3^+$ shows that even when polymorphism arises, the characteristic lamellar arrangement of bile anions is retained. The conservation of these features reinforces the conclusion that fibrils produced concomitantly by LCA^- $PrNH_3^+$ have a similar lamellar structure.

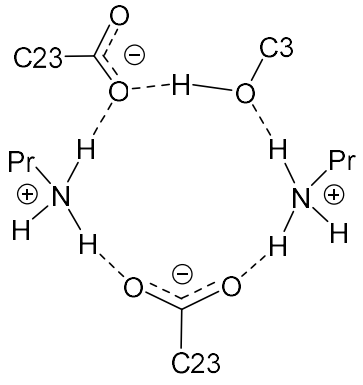

5

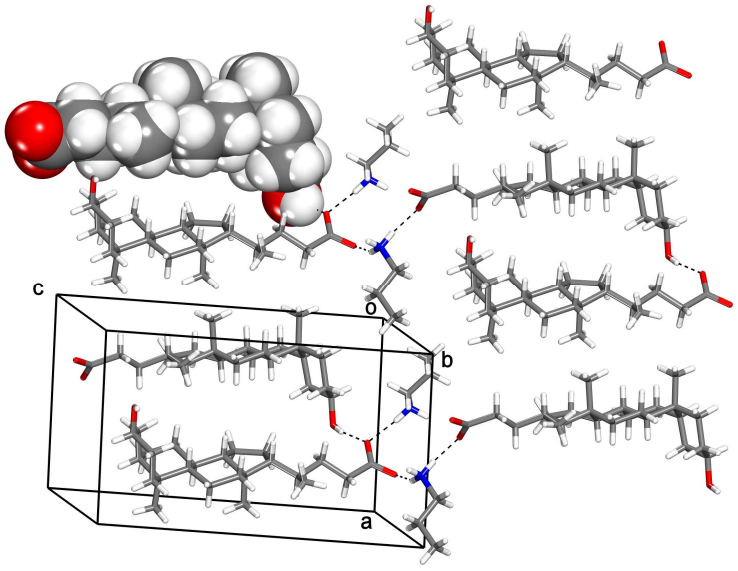

Figure 4.3. Representation of the structure of crystals of the monoclinic $P2_1$ polymorph of LCA^- $PrNH_3^+$ grown from H_2O, showing the cross sections of part of two layers of lithocholate anions, separated by regions in which OH, COO^-, and $PrNH_3^+$ engage in multiple hydrogen bonds. A selected anion is shown in a space-filling representation, hydrogen bonds are indicated by broken lines, and atoms appear in standard colors.

Structural Analysis of DCA^- $Pr_2NH_2^+$ • 2 H_2O. Structural analyses of simple ammonium salts of LCA by single-crystal X-ray diffraction, reported both in previous work,[15] and significant understanding has been added by the new studies of solvates and polymorphs summarized above. Together, this work shows that lithocholate anions are consistently arranged in similar ways. Moreover, the observed extends to salts of bile acids other than LCA. A 1:4 mixture of DCA and dipropylamine in water was warmed to give a solution of the corresponding ammonium salt (~50 mM). Cooling the solution to 25 °C induced the formation of long thin prisms (Figure 4.4a), and their structure was determined by X-ray diffraction. The crystals were found to have the composition DCA^- $Pr_2NH_2^+$ • 2 H_2O and to belong to the orthorhombic space group $P2_12_12_1$. Various crystallographic data are provided in Table 4, and views of the structure appear in Figure 4.5.

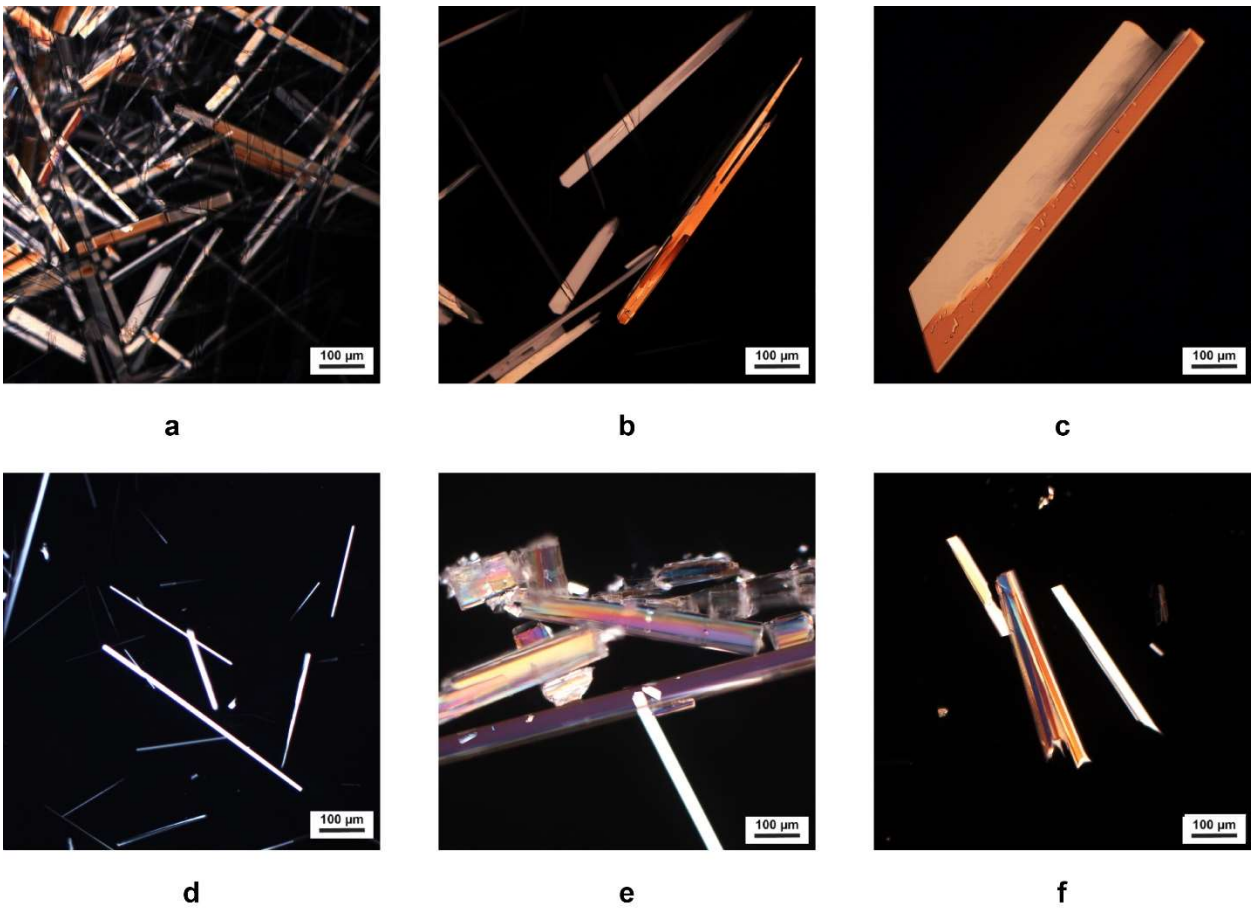

Figure 4.4. Representative crystals of ammonium salts of bile acids grown from water, as imaged by optical microscopy under polarized light. (a) DCA^- $Pr_2NH_2^+$ • 2 H_2O. (b) DCA^- cyclohexylNH_3^+. (c) DCA^- octylNH_3^+. (d) CA^- 1-adamantylNH_3^+ • 3.5 H_2O. (e) CA^- hexylNH_3^+ • H_2O. (f) CA^- octylNH_3^+ • 2 H_2O.

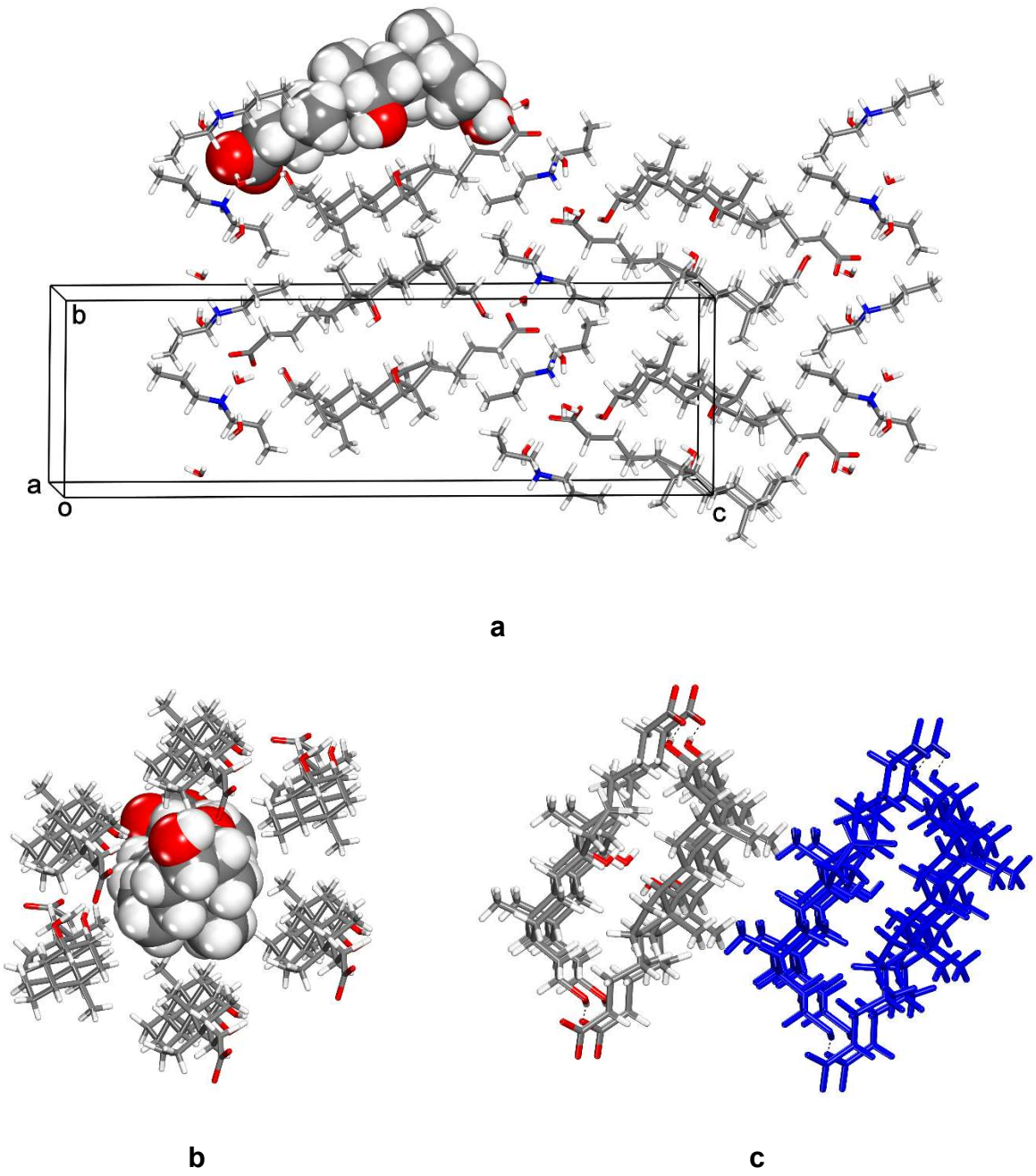

Figure 4.5. Representations of the structure of crystals of DCA^{-} $Pr_2NH_2^{+}$ • 2 H_2O grown from water. (a) View along the *a*-axis showing the cross sections of part of two layers of deoxycholate anions, separated by ionic regions. (b) View showing how each deoxycholate anion in the layers has six neighbors aligned approximately along the *c*-axis. (c) View along the *a*-axis showing how the layers are composed of side-by-side helices (one highlighted in blue), in which each

deoxycholate anion is linked to the next by O–H···O hydrogen bonds formed by OH and COO^- groups. Selected anions are shown in space-filling representations, and hydrogen bonds are indicated by broken lines. Unless indicated otherwise, atoms appear in standard colors.

As in the case of related ammonium lithocholates,[15] the structure of $DCA^- Pr_2NH_2^+$ is lamellar (Figure 4.5a). Layers of bile anions are terminated by surfaces parallel to the *ab*-plane with a high density of OH and COO^- groups, and the layers are separated by intervening $Pr_2NH_2^+$ cations and molecules of water. The five- and six-membered rings of the steroidal core of DCA^- adopt normal conformations. In addition, the side chain is almost fully extended, as indicated by the torsional angles C17–C20–C22–C23 and C20–C22–C23–C24, which are 180° and 171°, respectively (see the structure of DCA for the numbering of atoms in the side chain). Within the layers, each bile anion is surrounded by six neighbors (Figure 4.5b), as observed in related LCA salts.[15] Packing of deoxycholate anions in the layers creates small cavities that accommodate the propyl groups of $Pr_2NH_2^+$ cations (Figure 4.5a).

Deoxycholate anions in the layered structure of the $Pr_2NH_2^+$ salt form hydrogen-bonded helices that are aligned with the *a*-axis and packed side-by-side (Figure 4.5c). In the helices, each anion is linked to the next by O–H···O hydrogen bonds ($d_{O\cdots O}$ = 2.700(2) Å), with OH groups at C3 acting as donors and COO^- groups as acceptors. The other OH groups of deoxycholate at C12 do not engage in hydrogen bonding and point toward the interiors of the helices, where they are isolated from polar parts of the structure. In the ionic interlamellar region, each COO^- group also forms an ionic N–H···O hydrogen bond with a nearby $Pr_2NH_2^+$ cation ($d_{N\cdots O}$ = 2.767(2) Å), as well as two O–H···O hydrogen bonds with two ordered molecules of water ($d_{O\cdots O}$ = 2.733(2) and 2.765(2) Å). Each $Pr_2NH_2^+$ cation also forms an N–H···O hydrogen bond with a molecule of water ($d_{N\cdots O}$ = 2.796(2) Å), two molecules of water interact directly to form an additional O–H···O hydrogen bond ($d_{O\cdots O}$ = 2.729(2) Å), and one of the molecules of water also serves as donor in an O–H···O hydrogen bond involving the OH group of deoxycholate at C3 ($d_{O\cdots O}$ = 2.780(2) Å). In these ways, the structure of the interlamellar region is maintained by the formation of a total of six N–H···O and O–H···O hydrogen bonds per formula unit $DCA^- Pr_2NH_2^+ \cdot 2\ H_2O$. Five of these hydrogen bonds hold the OH group at C3, the COO^- group, $Pr_2NH_2^+$, and two molecules of water in cyclic array **6**. Each deoxycholate anion engages in a total of five hydrogen bonds (1 N–H···O and 4 O–H···O).

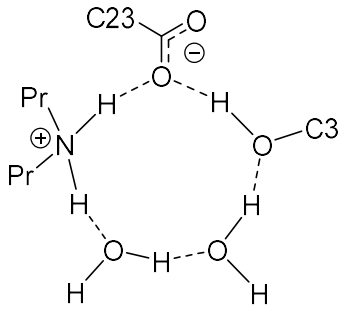

6

Crystals of DCA$^-$ CyclohexylNH$_3^+$. Warming and sonicating a 1:2 mixture of DCA and cyclohexylamine in water gave a solution of the corresponding ammonium salt with a nominal concentration of 50 mM. Cooling the solution to 25 °C caused the formation of long thin prisms (Figure 4.4b). The crystals proved to have the composition DCA$^-$ cyclohexylNH$_3^+$ and to belong to the monoclinic space group $P2_1$. Table 4.4 summarizes additional crystallographic data, and Figure 4.3 provides views of the structure. As in the case of related ammonium lithocholates,[15] the structure of DCA$^-$ cyclohexylNH$_3^+$ incorporates layers of bile anions (Figure 4.6a). The steroidal core of DCA$^-$ has a normal conformation, and the side chain is almost fully extended, with torsional angles C17–C20–C22–C23 and C20–C22–C23–C24 of 171° and 172°, respectively. Bile anions within the layers are aligned with the *c*-axis, surrounded by six neighbors, and linked along the *b*-axis by O–H···O hydrogen bonds ($d_{O\cdots O}$ = 2.642(3) Å), with OH groups at C3 acting as donors and COO$^-$ groups as acceptors (Figure 4.6b). As observed in the structure of the Pr$_2$NH$_2^+$ salt, intralamellar hydrogen bonding produces helical chains that pack side-by-side to create each layer. Again, the OH groups of deoxycholate at C12 do not contribute to association by forming hydrogen bonds. Each cyclohexylNH$_3^+$ cation interacts with three nearby bile anions by forming N–H···O hydrogen bonds with COO$^-$ groups and OH groups at C3. Although the Pr$_2$NH$_2^+$ and cyclohexylNH$_3^+$ salts of DCA incorporate significantly different cations and crystallize from water in different space groups, their structures are closely similar. In both cases, the bile anion forms layers composed of hydrogen-bonded helices.

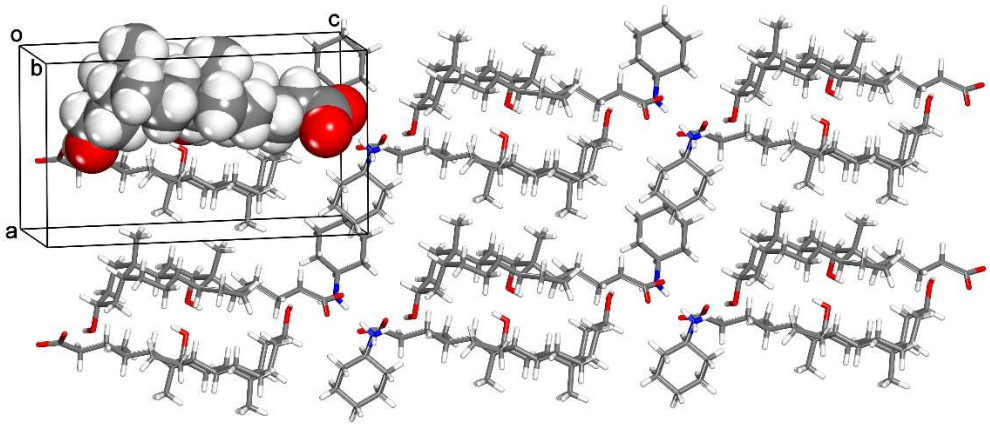

a

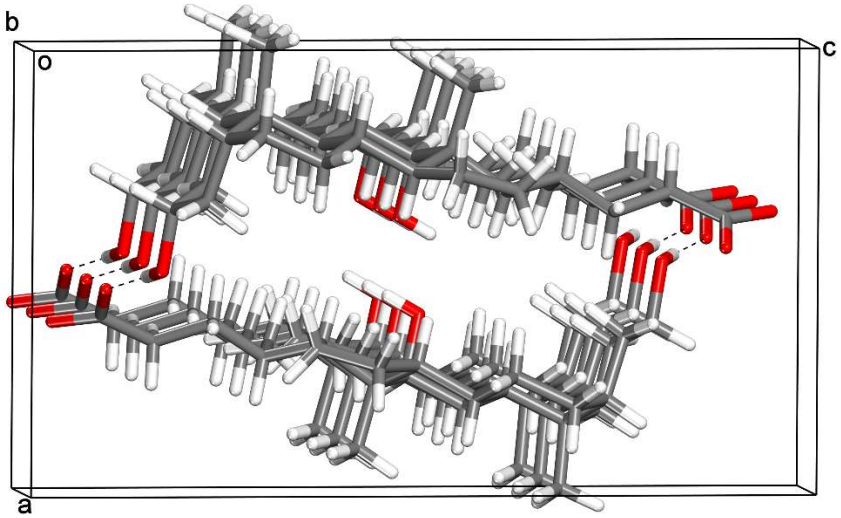

b

Figure 4.6. Representations of the structure of crystals of DCA^- cyclohexylNH_3^+ grown from water. (a) View along the *b*-axis showing the cross sections of part of three layers of deoxycholate anions, with one anion highlighted in a space-filling representation. (b) View along the *b*-axis showing deoxycholate anions linked by intralamellar O–H···O hydrogen bonds to form a helical chain. Hydrogen bonds are indicated by broken lines, and atoms are shown in standard colors.

Crystals of DCA^- OctylNH_3^+. A 1:1 mixture of DCA and octylamine in water was warmed to give a solution of the corresponding ammonium salt with a nominal concentration of 50 mM. Cooling the solution to 25 °C induced the formation of long thin prisms (Figure 4.4c). The crystals were found to have the composition DCA^- octylNH_3^+ and to belong to the monoclinic space group

$P2_1$. Additional crystallographic data are presented in Table 4.4, and a view of the structure is shown in the Supporting Information. The structure is similar to those of other ammonium salts of bile acids grown from water and is very closely related to the structure of DCA^- cyclohexylNH_3^+, as suggested by the identity of the space groups and the similarity of unit cell parameters. The steroidal core of DCA^- in the octylNH_3^+ salt has a normal conformation with almost fully extended side chains, which have torsional angles C17–C20–C22–C23 and C20–C22–C23–C24 of 176° and 171°, respectively. Again, the bile anions are arranged in layers composed of helical chains aligned with the *b*-axis and held together by O–H···O hydrogen bonds involving OH groups at C3 and COO^- groups ($d_{O\cdots O}$ = 2.626(2) Å). The OH groups of deoxycholate at C12 do not take part in hydrogen bonding, and each octylNH_3^+ cation interacts with three nearby bile anions by forming N–H···O hydrogen bonds with COO^- groups and OH groups at C3.

Bile acids and their derivatives are noted for their ability to form crystals that accommodate other molecules as guests, and various inclusion compounds have been studied in detail.[70–72] In previous work of this type, $CH_3(CH_2)_nNH_3^+$ salts of DCA with n = 0–4 were crystallized from aliphatic alcohols, and their structures were determined by X-ray diffraction.[73] Crystals of all five salts proved to belong to the monoclinic space group $P2_1$ and to form an isostructural series. In addition, a related study has shown that other simple alkylammonium deoxycholates crystallize from organic solvents in the monoclinic space group $P2_1$ as layered structures.[74] Together, these earlier reports and our studies of the crystallization of the $Pr_2NH_2^+$, cyclohexylNH_3^+, and octylNH_3^+ salts of DCA reveal a consistent pattern of molecular organization in which the bile anion forms closely related anionic hydrogen-bonded sheets, even though the ammonium cations vary widely and the crystallizations were carried out under different conditions.

The tendency of simple alkylammonium salts of DCA to crystallize as lamellar structures, regardless of the identity of the alkyl group or the solvent, suggests that the fibrils in hydrogels formed by the propylNH_3^+, butylNH_3^+, and pentylNH_3^+ salts (Table 4.1) have a similar internal molecular organization. If so, the most hydrophilic faces of fibrillar aggregates are expected to be parallel to (110), and anisotropic growth along the *a*- or *b*-axes should give rise to structures that are favored by stabilizing interactions with the surrounding aqueous medium. In the case of simple ammonium salts of LCA,[15] crystals are known to grow fastest along the direction corresponding to the purely hydrophobic edges of lithocholate anions. DCA is identical to LCA except for the

addition of a single OH group at C12, which plays no significant role in controlling the association of DCA^- cyclohexylNH_3^+ and DCA^- octylNH_3^+. As a result, crystals of alkylammonium salts of DCA should also grow fastest in the direction favored by related salts of LCA. This hypothesis was tested by indexing and measuring crystals of DCA^- $Pr_2NH_2^+$ (Figure 4.4a), which confirmed that growth along the *a*-axis is typically about 15–20 times faster than along the *b*-axis, and that growth in the *ab*-plane is much faster than that along the *c*-axis. This observation supports the conclusion that (001) faces of ordered aggregates are hydrophilic and correspond to the surfaces of lowest energy in aqueous media.

Crystals of CA^- HexylNH_3^+ • H_2O. The apparent tendency of simple ammonium salts of both LCA and DCA to adopt similar patterns of molecular organization in crystals and in gels suggested that salts of CDCA, CA, or other bile acids might also behave in the same way. In exploring this possibility, we warmed a 1:2 mixture of CA and hexylamine in water to give a solution of the corresponding ammonium salt with a nominal concentration of 50 mM. Long prisms appeared when the solution was cooled to 25 °C (Figure 4.4e) and were found by X-ray diffraction to have the composition CA^- hexylNH_3^+ • H_2O and to belong to the monoclinic space group $P2_1$. Table 4.4 compiles additional crystallographic data, and Figure 4.7 provides views of the structure. As generally observed for simple ammonium salts of LCA and DCA, CA^- hexylNH_3^+ forms a structure that can be described as lamellar, although the bile anions are offset in a way that allows greater interaction of the OH groups with water and the ammonium cations (Figure 4.7a). The steroidal core of the bile anion adopts a normal conformation, and the side chain is partially extended, with torsional angles C17–C20–C22–C23 and C20–C22–C23–C24 of 63° and 151°, respectively. Within the layers, bile anions are joined by O–H···O hydrogen bonds involving COO^- groups and OH groups at C12 ($d_{O\cdots O}$ = 2.676(2) Å) and C7 ($d_{O\cdots O}$ = 2.778(2) Å) to form helical chains aligned with the *b*-axis. Each hexylNH_3^+ cation forms three N–H···O hydrogen bonds, one with a molecule of water, another with the COO^- group of an adjacent bile anion, and the third with the OH group at C12 of another bile anion. Each cholate anion in the structure takes part in a total of 10 intermolecular hydrogen bonds (2 N–H···O and 8 O–H···O), whereas each deoxycholate anion in the related structure of DCA^- octylNH_3^+ forms only 5 (3 N–H···O and 2 O–H···O). This difference underscores the role of the added OH group in CA in increasing the density of hydrogen bonds.

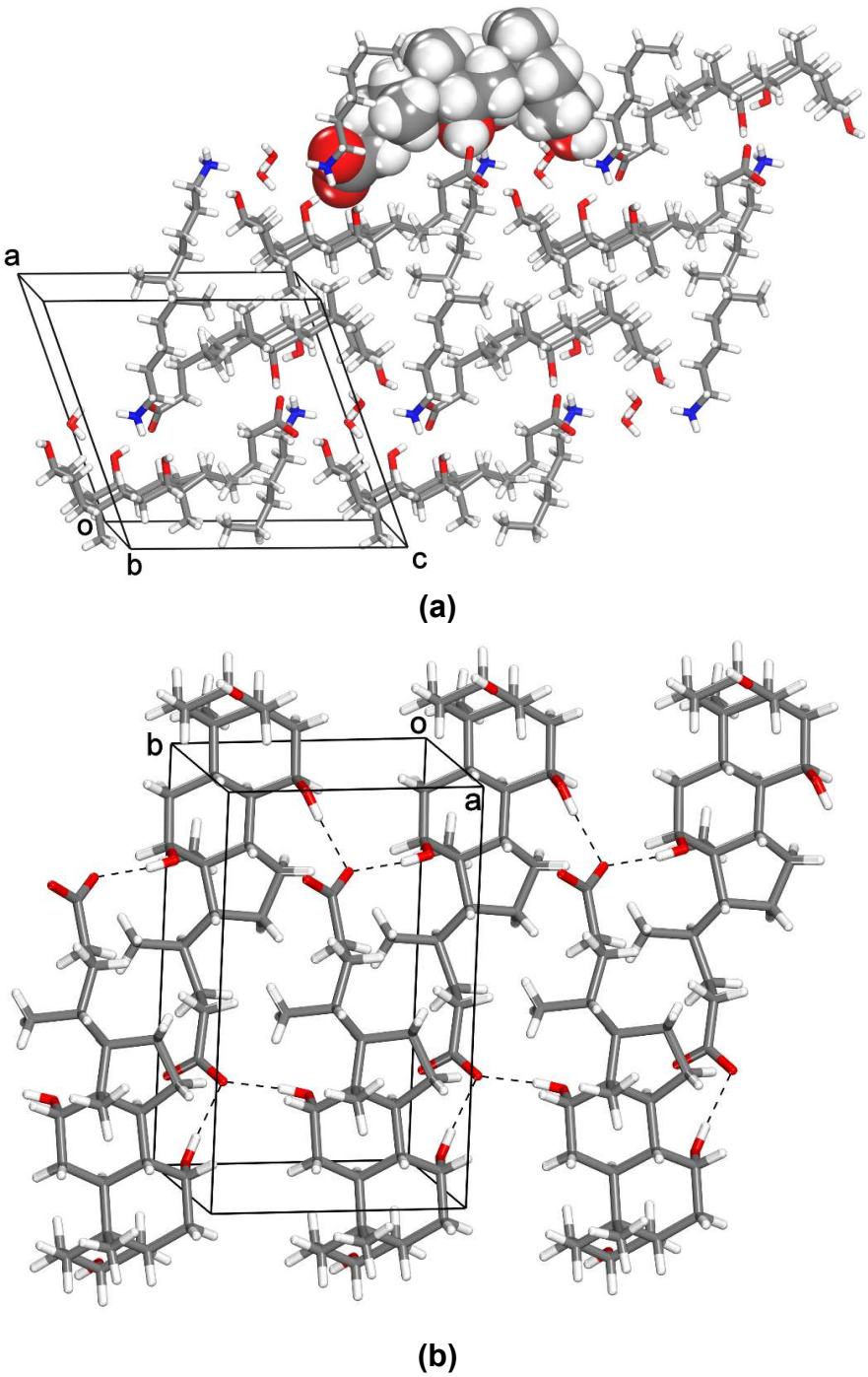

Figure 4.7. Representations of the structure of crystals of CA^- hexylNH_3^+ • H_2O grown from water. (a) View along the *b*-axis showing the cross sections of part of two layers of cholate anions, with one anion highlighted in a space-filling representation. (b) View showing how cholate anions are linked by O–H···O hydrogen bonds to form helical chains aligned with the *b*-axis. Hydrogen bonds are indicated by broken lines, and atoms appear in standard colors.

Crystals of CA^- hexylNH_3^+ have a structure similar to those of simple alkylammonium salts of LCA and DCA, and crystallization again occurs with high anisotropy to produce needles or elongated thin prisms, as shown in Figure 4.4e. If ammonium salts of CA aggregate fastest along the hydrophobic edges of anions, as observed in the cases of LCA and DCA, then crystals of the type shown in Figure 4.4e should be elongated along the *b*-axis. This prediction was confirmed by indexing and measuring crystals of CA^- hexylNH_3^+, which confirmed that growth along the *b*-axis is about 50 times faster than along the *a*-axis.

Crystals of CA^- OctylNH_3^+ • 2 H_2O. Previous researchers have reported other structures incorporating CA or its salts, including alkylammonium salts CA^- $CH_3(CH_2)_nNH_3^+$ with n = 9, 11, 13, and 15.[75] These compounds form structures that deviate even more significantly than CA^- hexylNH_3^+ (Figure 4.7) from the characteristic lamellar architectures favored by related alkylammonium salts of LCA and DCA. To probe the origin of these structural alterations and to provide a complete series of salts CA^- $CH_3(CH_2)_nNH_3^+$ (n = 5, 7, 9, 11, 13, and 15) for which structural data are available, we grew crystals of the octylammonium salt by mixing CA and octylamine in a 1:1 ratio in water, warming to give a solution of the corresponding ammonium salt with a nominal concentration of 50 mM, and cooling the solution to 25 °C. This yielded long thin prisms (Figure 4.4f), which proved to have the composition CA^- octylNH_3^+ • 2 H_2O and to belong to the monoclinic space group $P2_1$. Additional crystallographic data are presented in Table 4.4, and views of the structure are shown in Figure 4.8. The conformation of the steroidal core of the bile anion is normal, and the side chain is extended, with torsional angles C17–C20–C22–C23 and C20–C22–C23–C24 of 168° and 161°, respectively. A conspicuous feature of the structure is the formation of chains in which each bile anion is linked head-to-tail in a slightly offset manner to two others by a total of four O–H···O hydrogen bonds involving COO^- groups as acceptors and OH groups at C12 and C7 as donors ($d_{O\cdots O}$ = 2.732(5) and 2.768(6) Å, respectively), as shown in Figure 4.8a. The chains are aligned with the *b*-axis and are packed side-by-side to form sheets separated by molecules of water and partially disordered octylNH_3^+ cations. The resulting structure may be favored because it places extended octyl groups in close proximity to one another and to the hydrophobic surface of cholate anions, and it simultaneously creates areas in which the polar COO^- and OH groups of the bile anions can form stabilizing interactions with molecules of water and the NH_3^+ groups of the cations (Figure 4.8b).

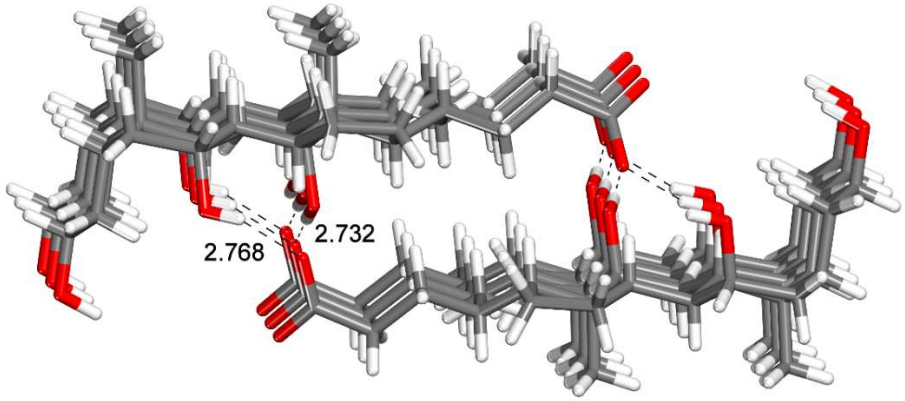

(a)

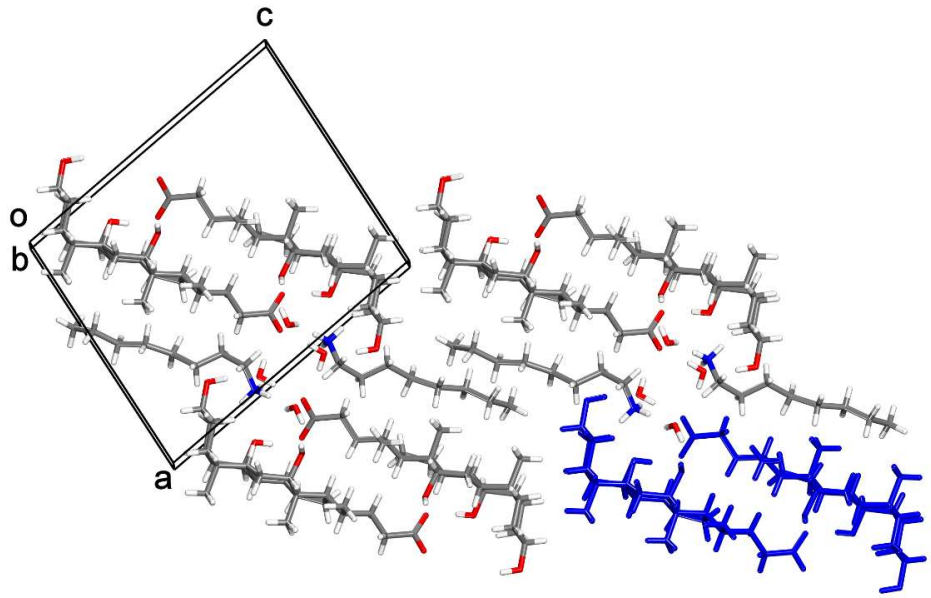

(b)

Figure 4.8. Representations of the structure of crystals of CA^- octylNH_3^+ • 2 H_2O grown from water. (a) View showing part of a chain in which cholate anions are linked head-to-tail in a slightly offset manner by O–H···O hydrogen bonds involving COO^- groups as acceptors and OH groups at C12 and C7 as donors, with O···O distances given in Å and hydrogen bonds indicated by broken lines. (b) View along the *b*-axis showing the cross sections of part of two layers of cholate anions separated by intervening molecules of water and octylNH_3^+ cations. A single hydrogen-bonded

chain of cholate anions is highlighted in blue, and the cations are shown as fully ordered. Unless indicated otherwise, atoms appear in standard colors.

Crystals of CA^- 1-AdamantylNH_3^+ • 3.5 H_2O. To assess the potential structure-disrupting effects of even larger ammonium cations, we mixed CA and 1-adamantylamine in a 1:1 ratio in water under conditions used to make other ammonium salts of CA. Warming the mixture gave a colorless opaque slurry, and slowly cooling the slurry to 25 °C induced the formation of long thin prisms (Figure 4.4d), which were found to have the composition CA^- 1-adamantylNH_3^+ • 3.5 H_2O and to belong to the monoclinic space group *C*2. Table 4.4 includes additional crystallographic data, and Figure 4.9 provides views of the structure, which is dramatically different from those of previously characterized ammonium salts of bile acids. The steroidal core of the bile anion is slightly disordered but has a normal conformation, and the side chain is partially extended, with torsional angles C17–C20–C22–C23 and C20–C22–C23–C24 of 59° and 172°, respectively. Cholate anions are linked head-to-tail to create chains aligned with the *c*-axis (Figure 4.9a), which pack to form corrugated sheets parallel to the *bc*-plane. The sheets stack in a way that pairs the hydrophobic faces of cholate anions and simultaneously creates large channels that include disordered 1-adamantylNH_3^+ cations (Figure 4.9b).

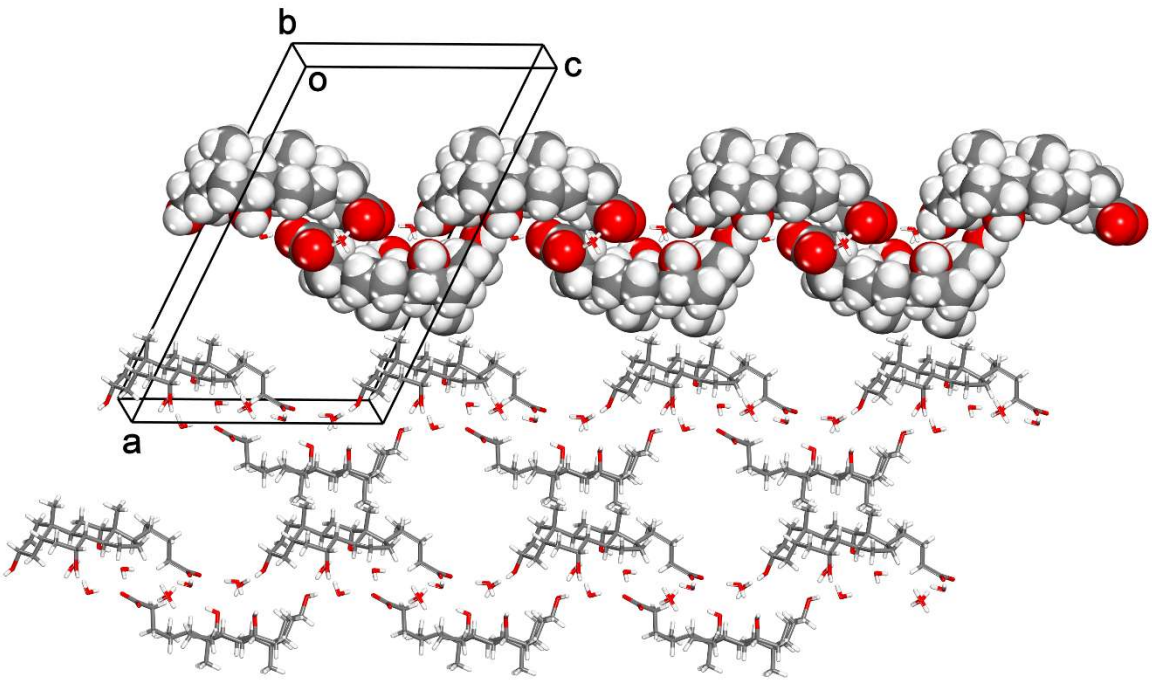

(a)

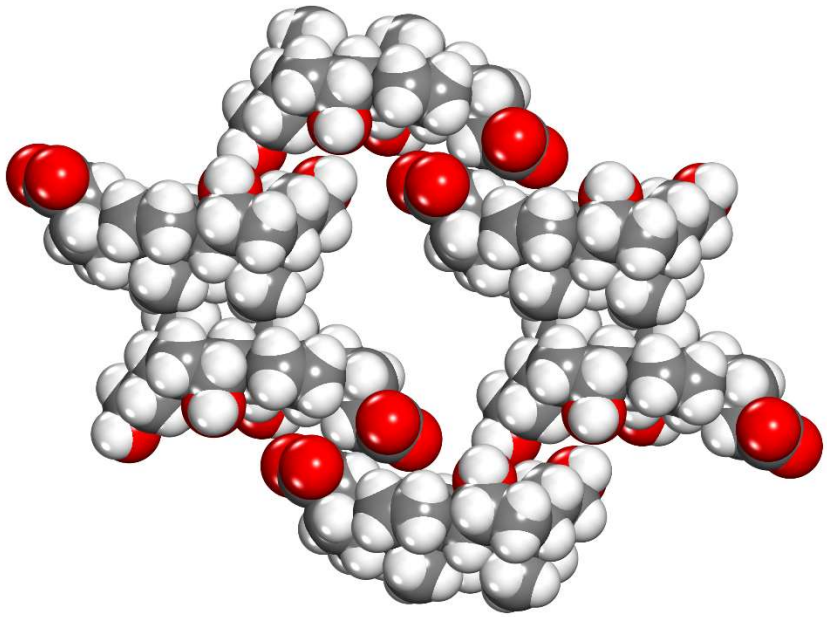

(b)

Figure 4.9. Representations of the structure of crystals of CA^- 1-adamantylNH_3^+ • 3.5 H_2O grown from water. (a) View along the *b*-axis showing the cross sections of three corrugated sheets composed of chains of cholate anions linked head-to-tail along the *c*-axis by hydrogen bonds

involving intervening molecules of water. One corrugated sheet is highlighted by showing it in a space-filling representation. (b) View along the *b*-axis showing six CA^- anions in space-filling representations that define the cross section of a channel that accommodates disordered 1-adamantylNH_3^+ cations. CA^- anions are shown as fully ordered, disordered cations are omitted, and atoms appear in standard colors.

A noteworthy feature of the structure is that cholate anions are not linked directly by hydrogen bonds to form chains, but rather are connected only by intervening molecules of water (Figure 4.9a). No cholate–cholate hydrogen bonds are present, even though each bile anion incorporates a COO^- group and three OH groups. Although the crystallization of simple ammonium salts of bile acids favors the formation of lamellar structures, other salts can behave differently. In particular, the unusual structure of CA^- 1-adamantylNH_3^+ underscores the ability of bile acids and their derivatives to produce crystalline solids in which the components are arranged in many different ways.

Nevertheless, simple ammonium salts consistently form crystals with a lamellar pattern of molecular organization and fiber-like acicular morphologies resulting from a preference for side-to-side association of bile anions (Figure 4.4). This uniform behavior, which results from the characteristic structural features of bile acids and is observed regardless of the state of hydration or polymorphism, provides strong circumstantial evidence that ammonium salts of bile acids induce gelation by forming fibrils with an analogous internal structure. If so, the ability of a particular salt to form a hydrogel or crystals depends not on how molecules are ordered in the associated state, but rather on kinetic and thermodynamic factors that control growth. In this model, fibrils and hydrogels result from exaggerated side-by-side growth, whereas needles and extended plates are formed when significant growth can also occur in other directions.

Solids produced by lyophilizing hydrogels derived from ammonium salts of DCA (Figure 4.1) proved to be amorphous,[76] but additional evidence that gelation and crystallization are structurally analogous phenomena was obtained by IR spectroscopy. The NH stretching vibration band in the IR spectrum of the solid from the lyophilized hydrogel of DCA^- butylNH_3^+ (Figure 4.10a) shows the presence of more free NH groups in the range of 3300-3500 cm^{-1} than in the spectrum of crystalline LCA^- butylNH_3^+, while the hydrogen-bonded NH groups (3070-3350 cm^{-1}) have similar relative intensities. This difference is less pronounced between the spectrum of

crystalline DCA^- octylNH_3^+ and that of the solid of the lyophilized hydrogel of DCA^- pentylNH_3^+ (Figure 4.10b). In both cases, the extra C=O band close to 1700 cm^{-1} confirms the more complex presence of free and hydrogen-bonded carboxylic groups in the samples made from the hydrogels.

4.3 Conclusions

Simple ammonium salts of the bile acids LCA, DCA, CDCA, and CA offer a family of related compounds that can be used to probe the phenomenon of hydrogelation and to determine how molecules are organized in crystals and in the fibrillar structures that give rise to gels. The well-defined amphiphilic structure of bile anions ensures that consistent patterns of molecular organization are maintained, and the ammonium cations can be varied to yield hydrogels, mixtures of fibrils and crystals, or only crystals under closely similar conditions. Single-crystal X-ray diffraction has confirmed that bile anions consistently favor lamellar arrangements in salts incorporating small ammonium ions, and preferred edge-to-edge association of the anions tends to produce acicular crystals that resemble the fibrils underlying gelation. The observation that simple ammonium salts of various bile acids consistently favor the same pattern of molecular organization in crystals grown from water reinforces the hypothesis that the fibrils responsible for hydrogelation have closely related internal structures.

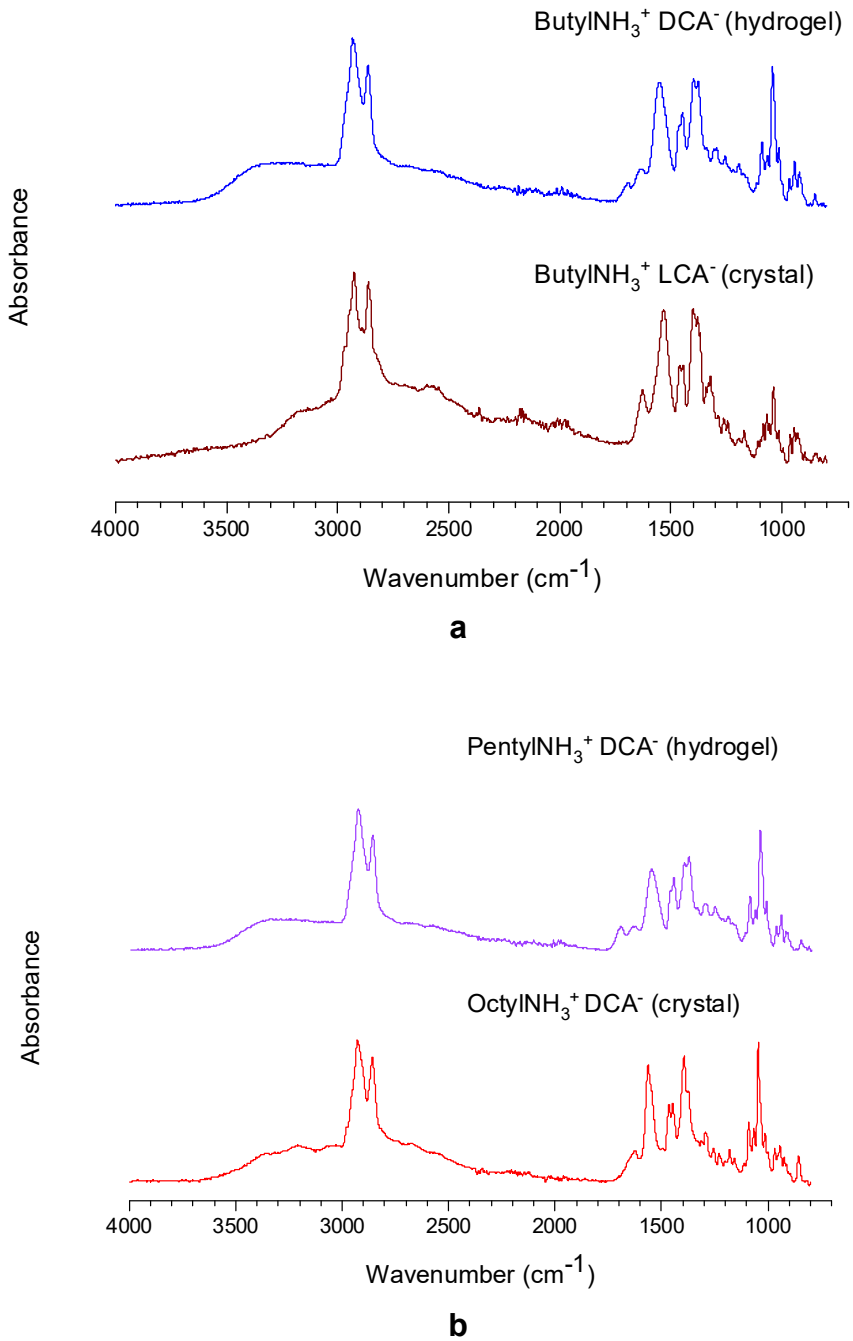

Figure 4.10. Comparisons of IR spectra of crystalline ammonium salts of bile acids and solids obtained by lyophilizing related hydrogels. (a) LCA^- butylNH_3^+ (crystalline) and DCA^- butylNH_3^+ (produced from hydrogel). (b) DCA^- octylNH_3^+ (crystalline) and DCA^- pentylNH_3^+ (produced from hydrogel).

4.4 Experimental Section

4.4.1 Materials

Lithocholic acid (LCA, 95%), deoxycholic acid (DCA, 99%), chenodeoxycholic acid (CDCA, 98%), cholic acid (CA, 98%), ethylamine (70 wt % solution in water), propylamine (98%), butylamine (99%), dipropylamine (99%), pentyamine (99%), hexylamine (99%), cyclohexylamine (99%), octylamine (99%), and 1-adamantylamine (97%), dimethylamine (40 wt % solution in water), diethylamine (99%), ethylmethylamine (97%), trimethylamine (99%), and triethylamine (99%) were purchased from Sigma-Aldrich (Oakville, ON, Canada). Ammonium hydroxide (30 wt % solution in water) was purchased from EMD Chemicals Inc. Methylamine (40 wt % solution in water) was purchased from Fisher Scientific Company. All reagents were used as received. Solutions were prepared with water purified by a Milli-Q system.

4.4.2 Sample preparation.

In typical experiments, a weighed amount of the bile acid was mixed with water, a stock solution of the selected amine in water was added, and the resulting mixture was warmed and sonicated to give a solution. The resulting nominal concentrations of bile acids were 50 mM, and the nominal concentrations of amines ranged from 50 mM to 200 mM. The samples were allowed to cool to 25 °C and kept at that temperature for at least 24 h before gelation or crystallization phenomena were examined. In the cases of octylamine and 1-adamantylamine, which are poorly soluble in water, the two compounds were added directly to mixtures of bile acids in water, but the experiments were otherwise similar.

4.4.3 Illustrative preparation of bulk samples of crystalline ammonium salts of bile acids (CA^- hexyl$NH_3^+ \bullet H_2O$)

CA (0.020 g, 0.050 mmol) was treated with an aqueous solution of hexylamine (1.0 mL, 0.10 M, 0.10 mmol). The mixture was warmed and sonicated at 60 °C to produce a solution, which was allowed to cool to 25 °C and was kept at that temperature for 1 day to allow crystallization to occur. The mother liquors were removed, and the crystals were washed with cold water (3 × 0.5 mL) and dried in vacuo. This yielded CA^- hexyl$NH_3^+ \bullet H_2O$ as a colorless solid (0.016 g, 0.030 mmol, 60%).

4.4.4 Attenuated Total Reflection (ATR) Fourier-Transform Infrared (FTIR) Spectroscopy.

Hydrogels were lyophilized for 48 h and then analyzed using a Bruker Alpha-P ATR FTIR instrument. All measurements were made at 25 °C.

4.4.5 Polarized optical microscopy

Samples were transferred to a glass slide, placed under a cover slide, and then observed at 25 °C using a Zeiss Axioskop polarized-light optical microscope.

4.4.6 Scanning electron microscope.

Samples for analysis were transferred to Al mounts, placed under vacuum at 25 °C, and coated with Pt. The coated samples were then imaged using an FEI Quanta 450 field-emission scanning electron microscope at the Facility for Electron Microscopy Research at McGill University.

Notes. The authors have no competing financial interests to declare.

4.5 Supporting Information

4.5.1 Additional Crystallographic Information

Reflection data were collected at 100 K using a Bruker Smart diffractometer (three-circle fixed chi platform) equipped with an Incoatec Microfocus CuKα source (λ = 1.54179 Å) and an APEX II CCD detector. The cell lattice parameters were determined using reflections taken from three sets of 180 frames measured and harvested within the *APEX3* suite of programs.[1] Integration of frames was performed using *SAINT*,[1] and a semiempirical absorption correction was applied with *SADABS*.[2] The structures were solved using a dual space and intrinsic phasing approach with *SHELXT*,[3] and the refinement was carried out using *SHELXL*-2018/3.[4] The Flack parameters were determined by refining an inversion twin for all structures except for those of CA^- hexylNH_3^+ • H_2O and CA^- octylNH_3^+ • 2 H_2O.[5] In these two cases, the Flack parameters were obtained from quotients of intensity differences in Friedel pairs (Parsons' z factor).[6]

In crystals of CA^- octylNH_3^+ • 2 H_2O, the octylNH_3^+ cation was found to be disordered and was refined using a model with two different conformations (Figure 4.S5). Disorder was also observed in crystals of CA^- 1-adamantylNH_3^+ • 3.5 H_2O, affecting both the 1-adamantylNH_3^+ cation and part of the CA^- anion (Figure 4.S6).

4.5.2 Thermal Atomic Displacement Parameter Plots

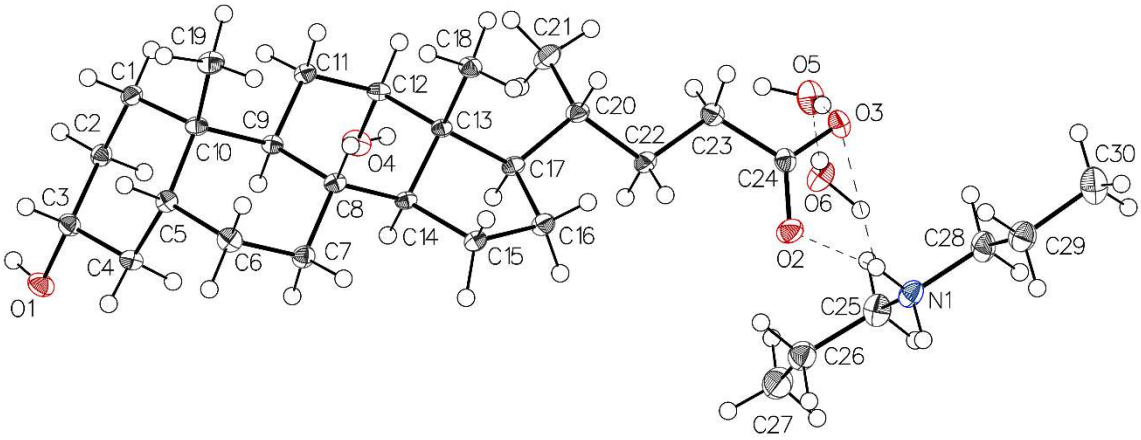

Figure 4.S1. Thermal atomic displacement ellipsoid plot with the atomic numbering scheme for the structure of crystals of DCA^- $Pr_2NH_2^+$ • 2 H_2O. The ellipsoids of non-hydrogen atoms are drawn at the 50% probability level, and hydrogen atoms are represented by a sphere of arbitrary size. Intermolecular hydrogen bonds are shown as dashed lines.

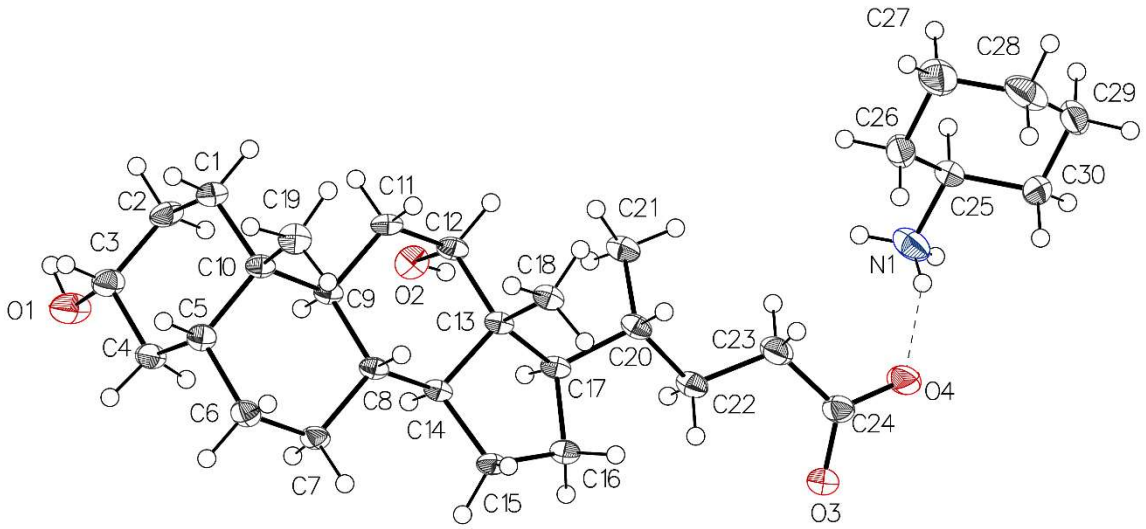

Figure 4.S2. Thermal atomic displacement ellipsoid plot with the atomic numbering scheme for the structure of crystals of DCA^- cyclohexylNH_3^+. The ellipsoids of non-hydrogen atoms are drawn at the 50% probability level, and hydrogen atoms are represented by a sphere of arbitrary size. An intermolecular hydrogen bond is represented by a dashed line.

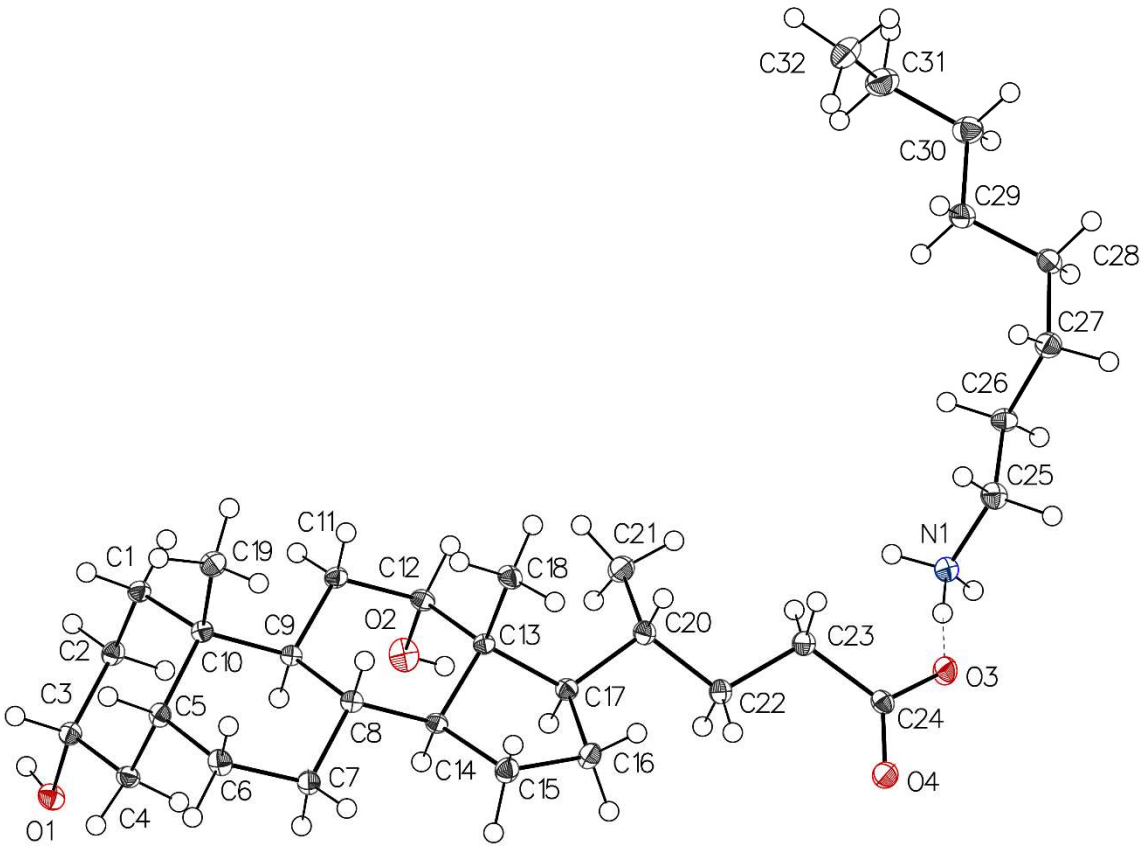

Figure 4.S3. Thermal atomic displacement ellipsoid plot with the atomic numbering scheme for the structure of crystals of DCA^- octylNH_3^+. The ellipsoids of non-hydrogen atoms are drawn at the 50% probability level, and hydrogen atoms are represented by a sphere of arbitrary size. An intermolecular hydrogen bond is represented by a dashed line.

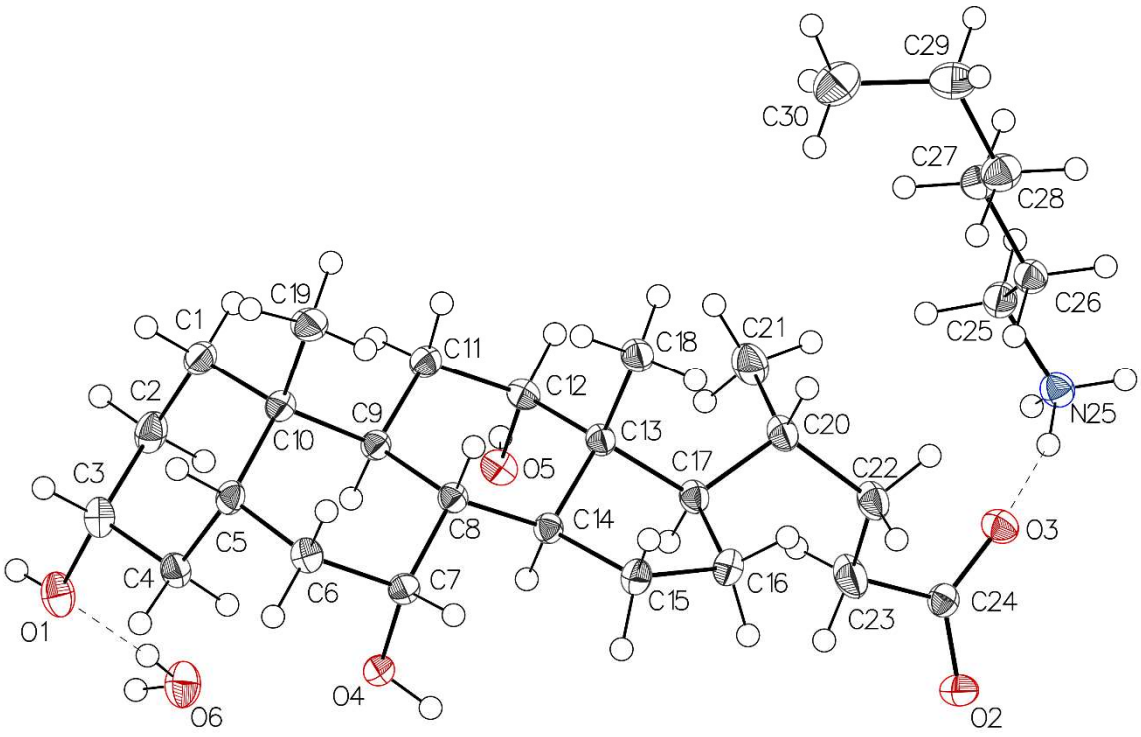

Figure 4.S4. Thermal atomic displacement ellipsoid plot with the atomic numbering scheme for the structure of crystals of CA^- hexylNH_3^+ • H_2O. The ellipsoids of non-hydrogen atoms are drawn at the 50% probability level, and hydrogen atoms are represented by a sphere of arbitrary size. Intermolecular hydrogen bonds shown as dashed lines.

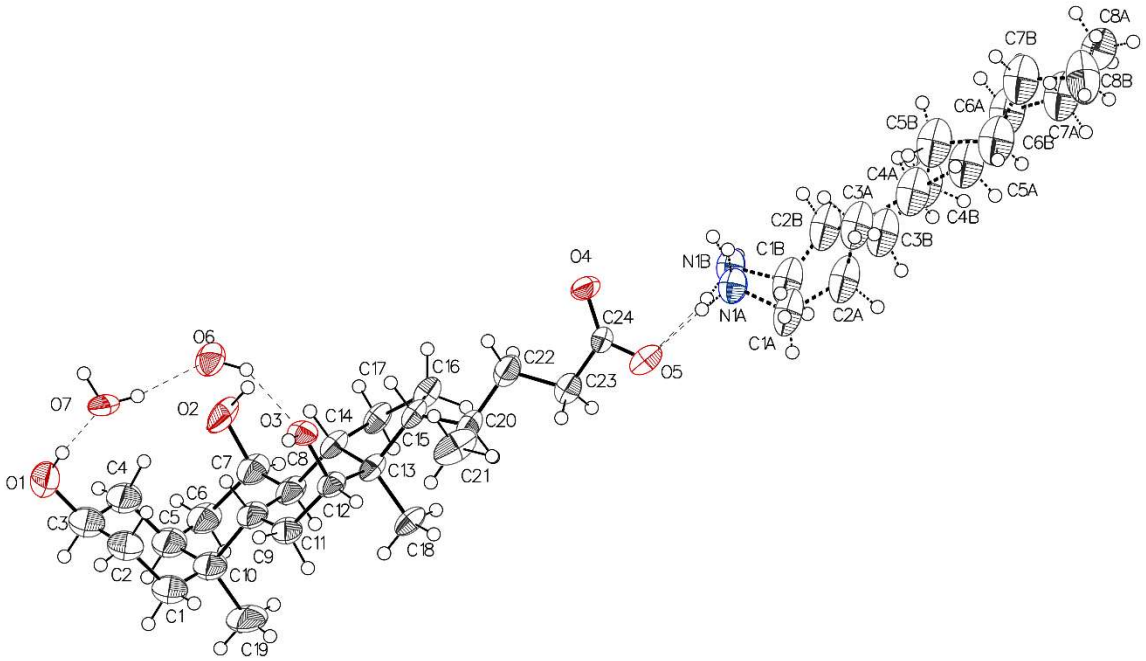
C8A
C7B
C8B
C6A
C5B
C7A
C6B
C4A
C5A
C3A
C4B
C2B
C3B
C1B
N1B
O4
C24
N1A
C2A
C1A
O6
C22
C17
C16
C23
O5
O7
O2
O3
C14
C20
C15
C7
C8
C13
C21
C4
C6
C12
C5
C3
C11
C9
C18
C2
C10
C1
C19

a

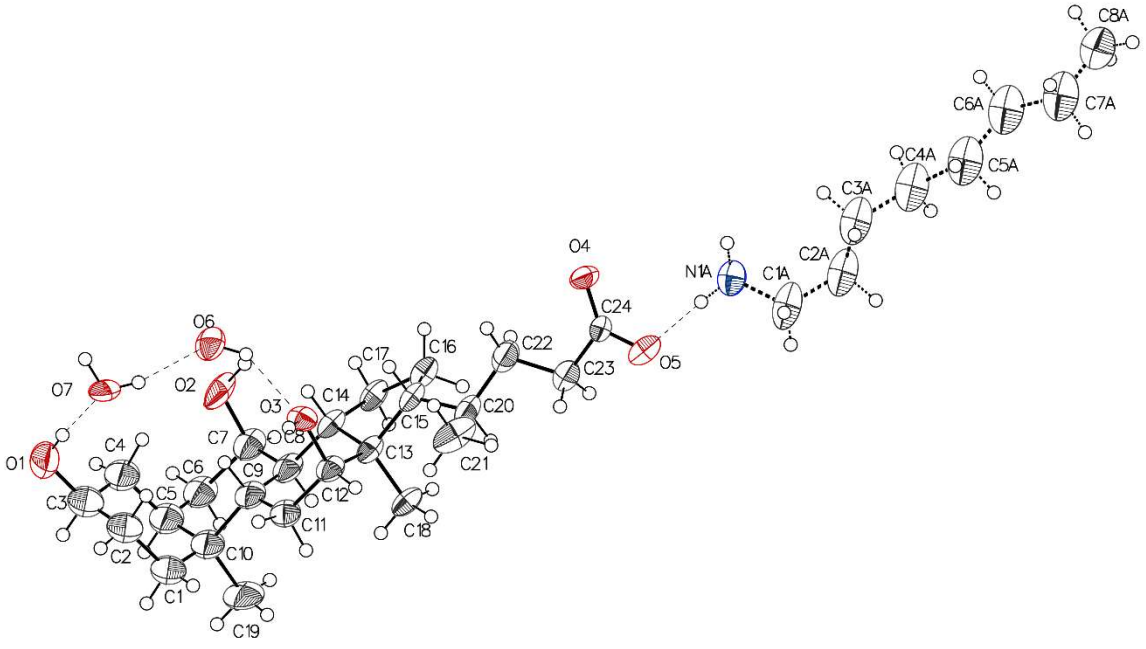
C8A
C6A
C7A
C4A
C5A
C3A
O4
N1A
C1A
C2A
C24
O6
C22
C17
C16
C23
O5
O7
O2
O3
C14
C20
C15
C7
C8
C13
C21
C4
C6
C9
C12
C5
C3
C11
C18
C2
C10
C1
C19

b

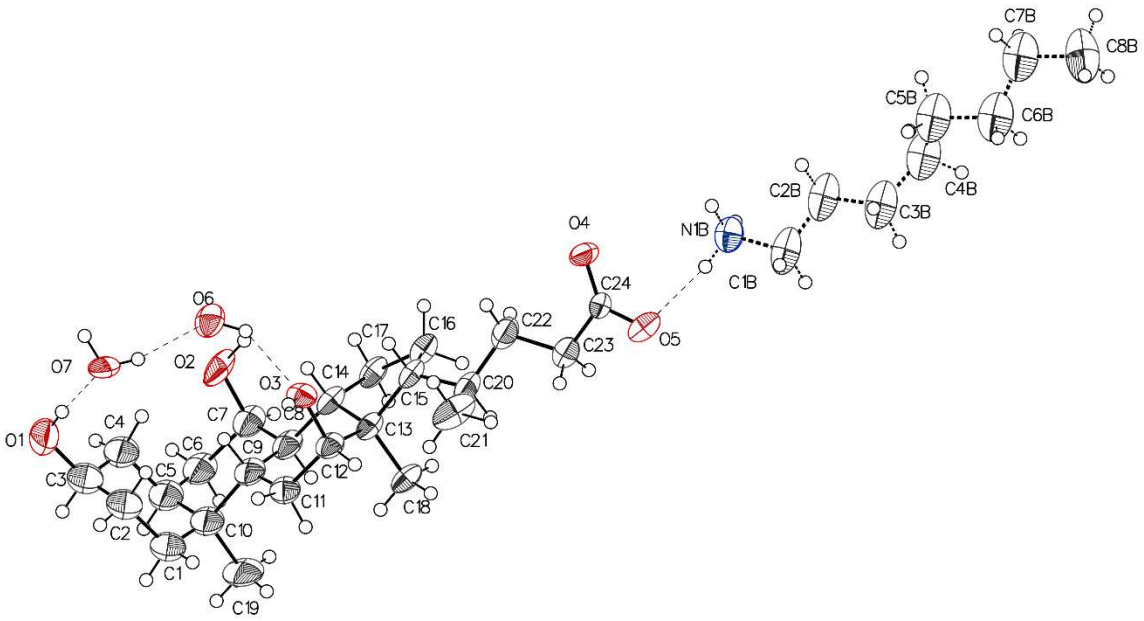

c

Figure 4.S5. Thermal atomic displacement ellipsoid plots with the atomic numbering scheme for the structure of crystals of CA^- octylNH_3^+ • 2 H_2O. The ellipsoids of non-hydrogen atoms are drawn at the 50% probability level, and hydrogen atoms are represented by a sphere of arbitrary size. Intermolecular hydrogen bonds are shown as dashed lines. (a) View with all disordered parts included for the octylNH_3^+ cation. (b)–(c) Separate views for each disordered part.

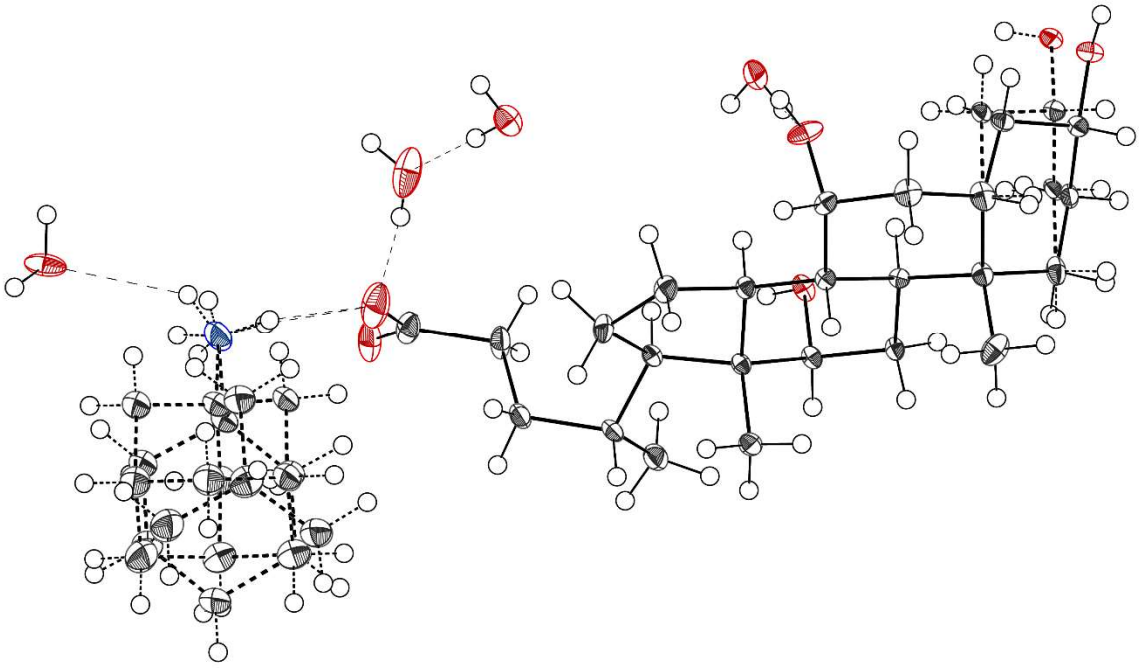

a

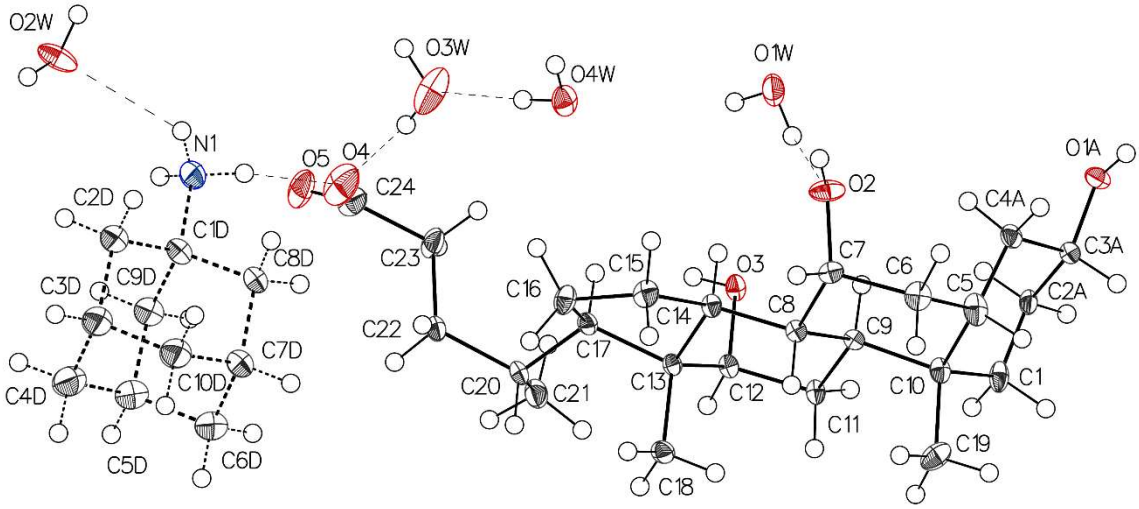
O2W
O3W
O4W
O1W
N1
O5
O4
C24
O2
O1A
C4A
C2D
C1D
C23
C15
O3
C7
C6
C3A
C8D
C16
C5
C2A
C3D
C9D
C14
C8
C22
C17
C9
C7D
C10D
C20
C21
C13
C12
C10
C1
C4D
C11
C19
C5D
C6D
C18

b

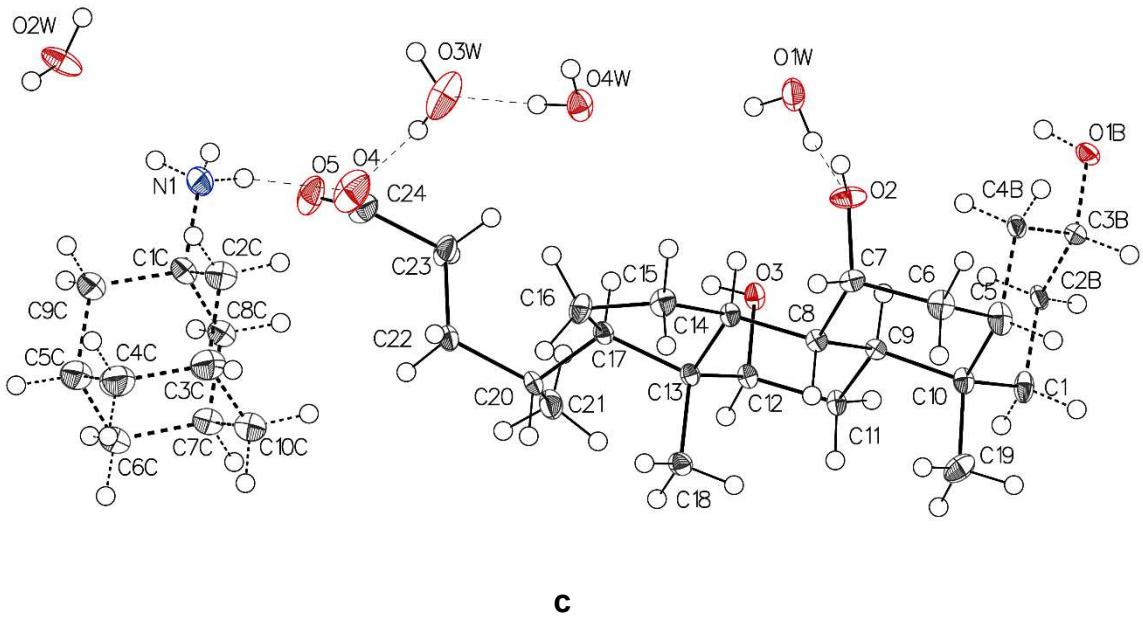

c

Figure 4.S6. Thermal atomic displacement ellipsoid plots with the atomic numbering scheme for the structure of crystals of CA^- 1-adamantylNH_3^+ • 3.5 H_2O. The ellipsoids of non-hydrogen atoms are drawn at the 50% probability level, and hydrogen atoms are represented by a sphere of arbitrary size. Intermolecular hydrogen bonds are shown as dashed lines. (a) View with all disordered parts included for the 1-adamantylNH_3^+ cation. (b)–(c) Separate views for each disordered part.

4.5.3 Indexing Crystal Faces

DCA^{-} $Pr_2NH_2^{+}$ • 2 H_2O

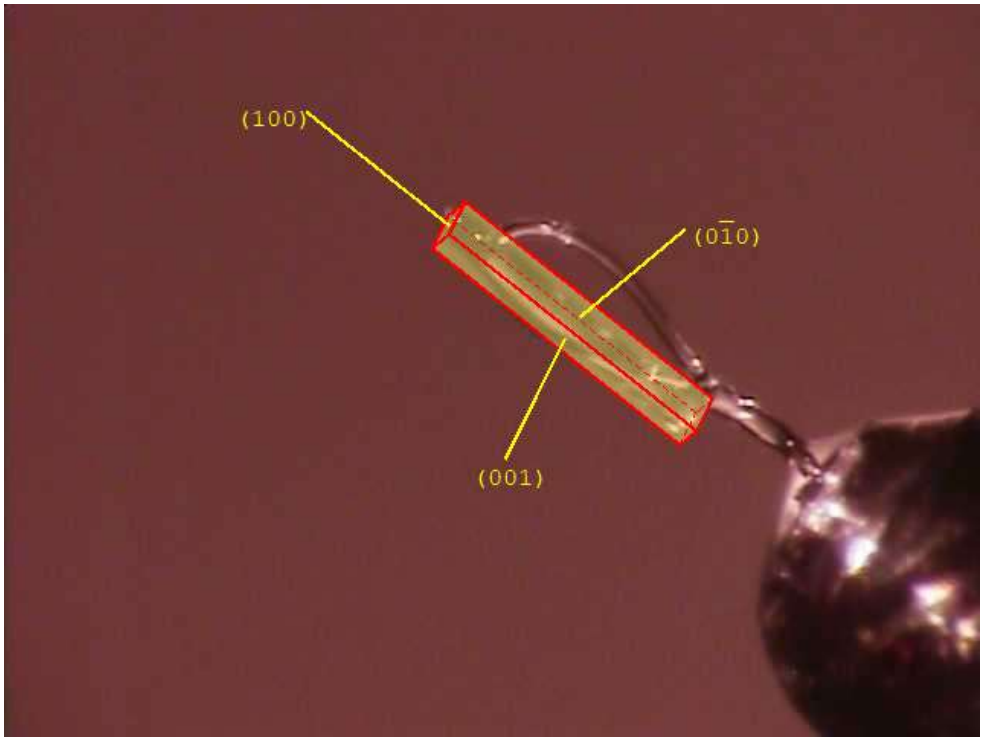

HKL Faces & Relative Distances to Center of Crystal:

FACE	1 0 0	0.227
FACE	-1 0 0	0.599
FACE	0 1 0	0.012
FACE	0 -1 0	0.037
FACE	0 0 -1	0.013
FACE	0 0 1	0.069

4.5.4 Powder X-Ray Diffraction

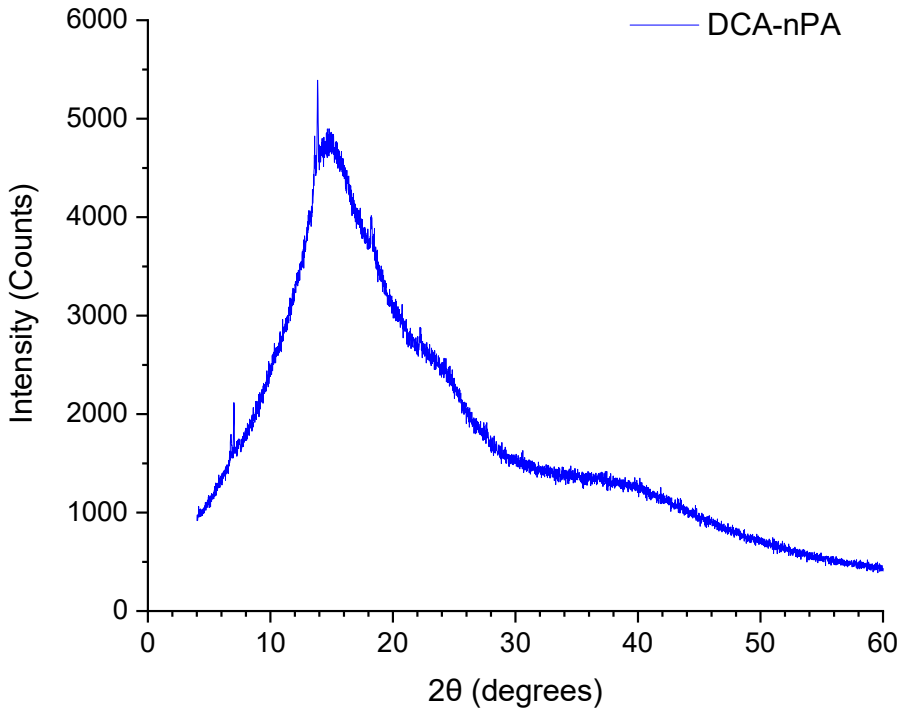

Figure 4.S7. Powder X-ray diffraction pattern of the solid obtained by lyophilizing the hydrogel produced by cooling an aqueous solution of the propylammonium salt of DCA.

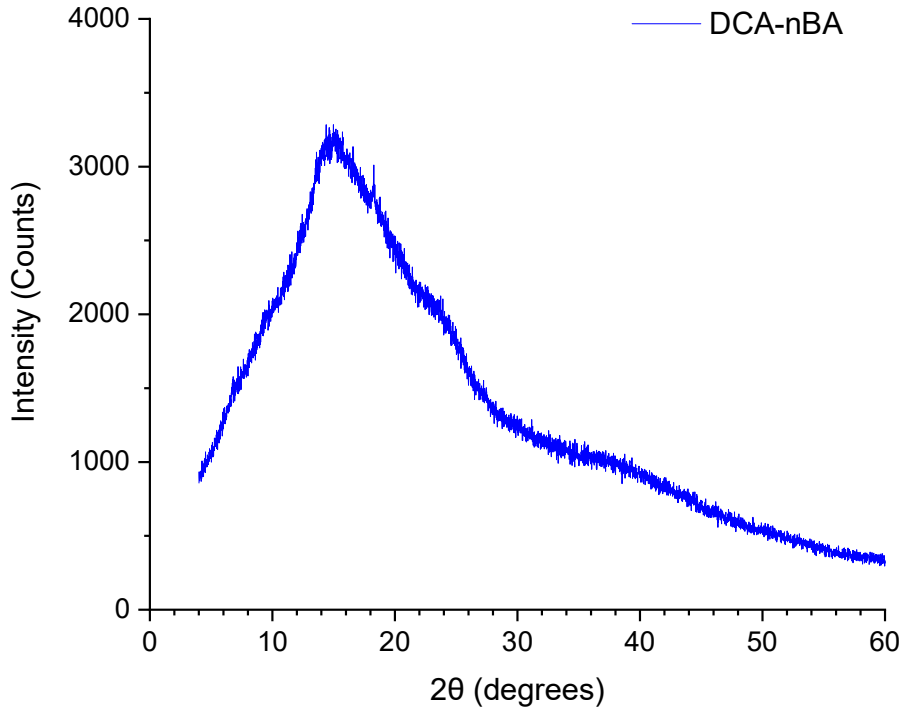

Figure 4.S8. Powder X-ray diffraction pattern of the solid obtained by lyophilizing the hydrogel produced by cooling an aqueous solution of the butylammonium salt of DCA.

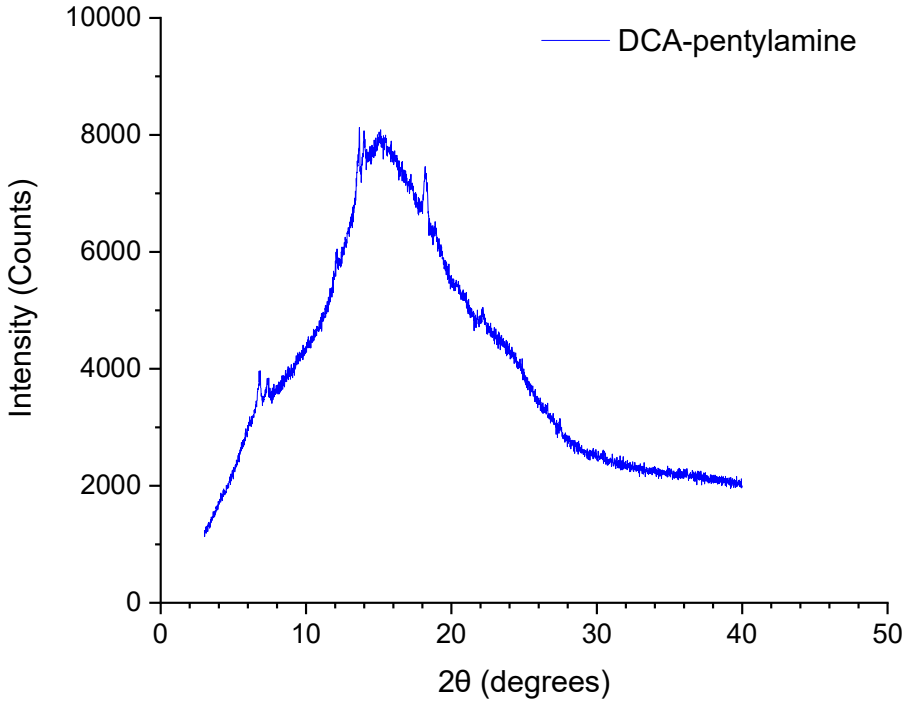

Figure 4.S9. Powder X-ray diffraction pattern of the solid obtained by lyophilizing the hydrogel produced by cooling an aqueous solution of the pentylammonium salt of DCA.

4.5.5 FT-IR Spectroscopy

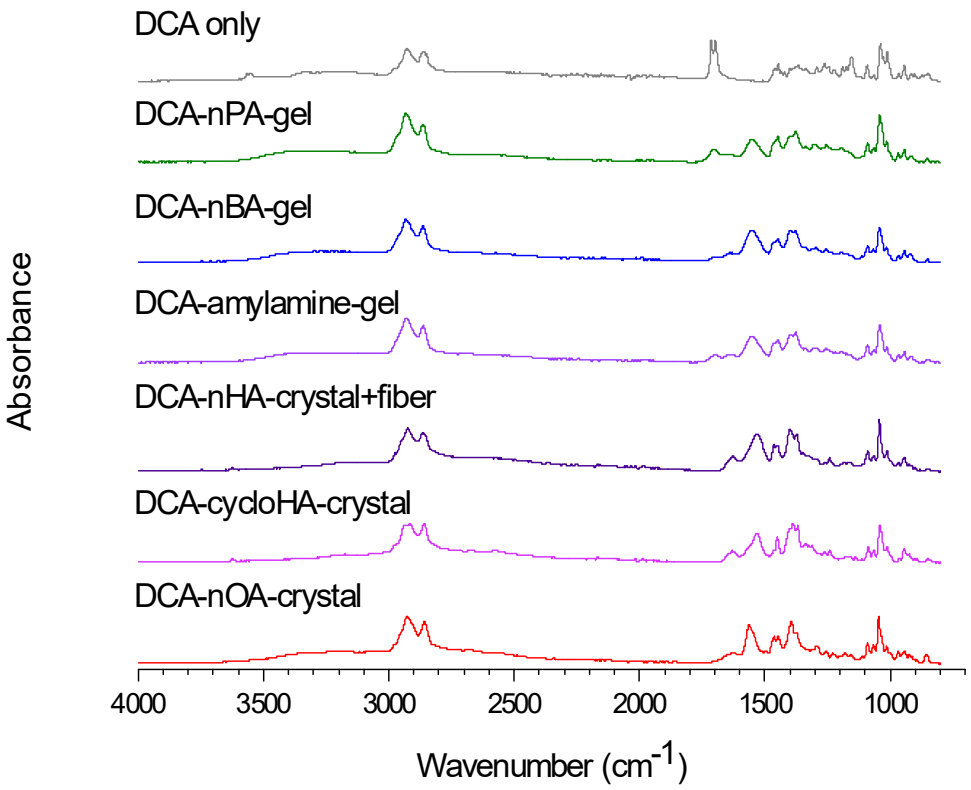

Figure 4.S10. Comparison of FT-IR spectra of DCA, crystals of alkylammonium salts of DCA, and solids obtained by lyophilizing hydrogels produced by cooling aqueous solutions of alkylammonium salts of DCA. Small peaks corresponding to DCA in certain lyophilized samples arise from partial evaporation of volatile alkylamines.

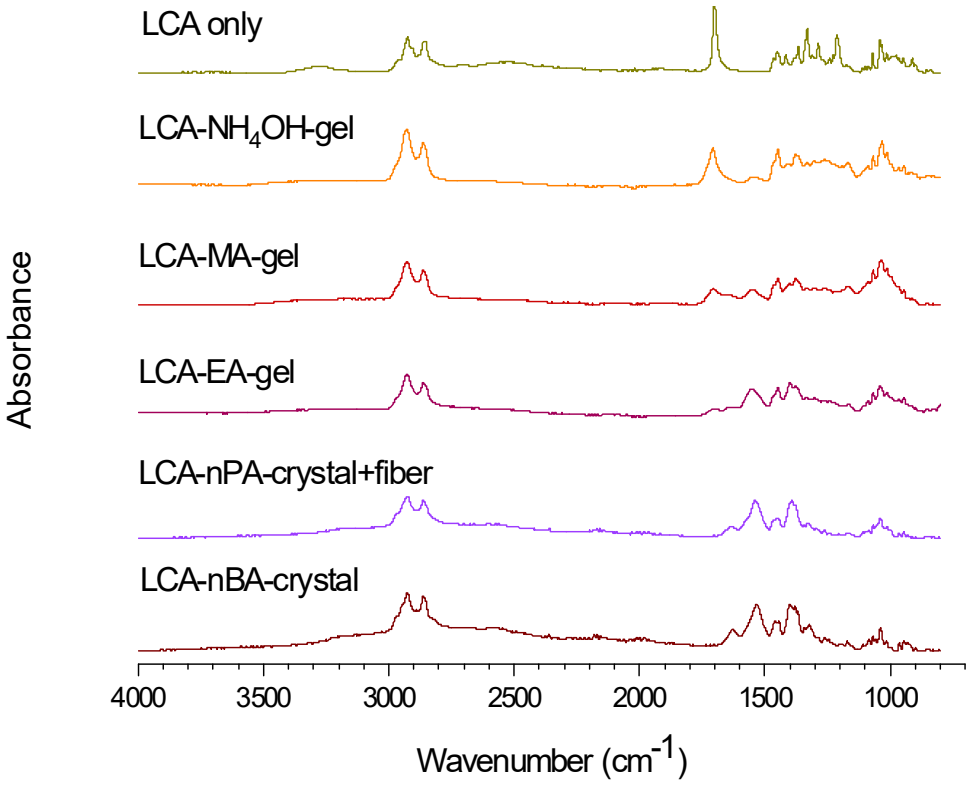

Figure 4.S11. Comparison of FT-IR spectra of LCA, crystals of alkylammonium salts of LCA, and solids obtained by lyophilizing hydrogels produced by cooling aqueous solutions of ammonium salts of LCA. Small peaks corresponding to LCA in certain lyophilized samples arise from partial evaporation of volatile amines.

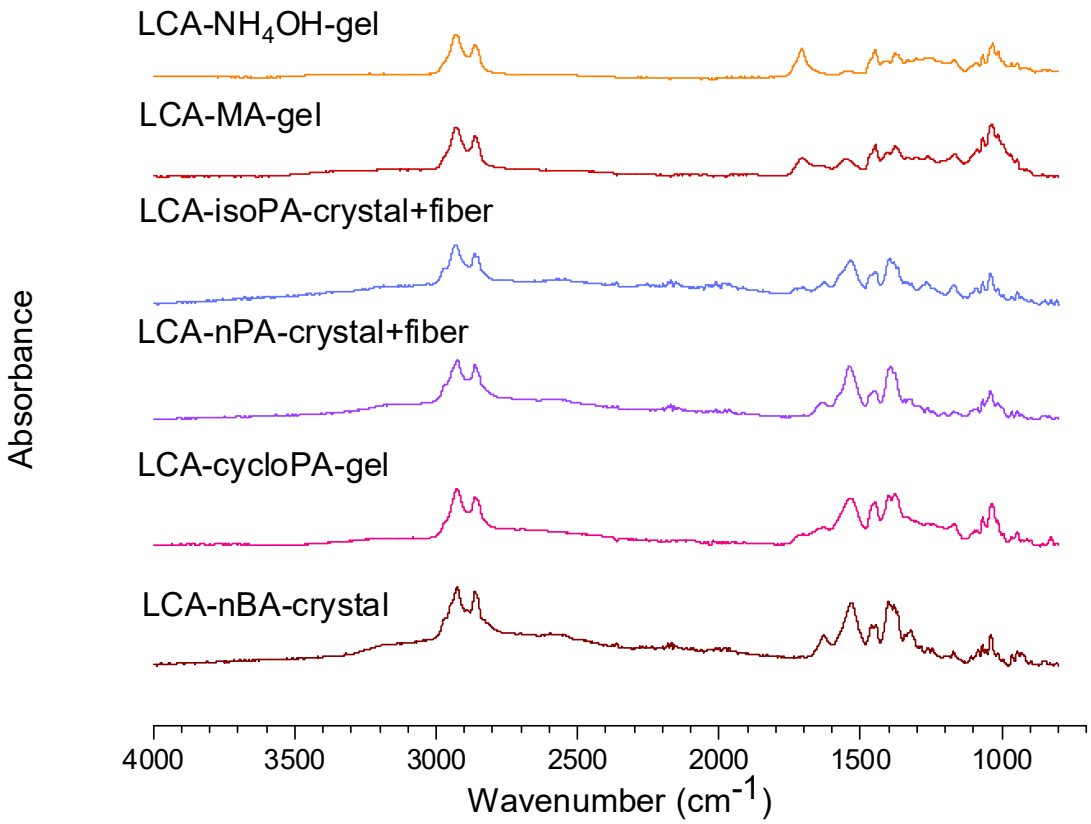

Figure 4.S12. Comparison of FT-IR spectra of crystals of alkylammonium salts of LCA and solids obtained by lyophilizing hydrogels and mixtures produced by cooling aqueous solutions of ammonium salts of LCA. Small peaks corresponding to LCA in certain lyophilized samples arise from partial evaporation of volatile amines.

4.5.6 References

(1) Bruker (2017). *APEX3* and *SAINT*, Bruker AXS Inc., Madison, Wisconsin, USA.

(2) Krause, L.; Herbst-Irmer, R.; Sheldrick, G. M.; Stalke, D. Comparison of Silver and Molybdenum Microfocus X-Ray Sources for Single-Crystal Structure Determination. *J. Appl. Cryst*. **2015**, *48*, 3–10.

(3) Sheldrick, G. M. *SHELXT* – Integrated Space-Group and Crystal-Structure Determination. *Acta Crystallogr*. **2015**, *A71*, 3–8.

(4) Sheldrick, G. M. Crystal Structure Refinement with *SHELXL*. *Acta Crystallogr*. **2015**, *C71*, 3–8.

(5) Flack, H. D.; Bernardinelli, G. Reporting and Evaluating Absolute-Structure and Absolute-Configuration Determinations. *J. Appl. Crystallogr*. **2000**, *33*, 1143–1148.

(6) Parsons, S.; Flack, H. D.; Wagner, T. Use of Intensity Quotients and Differences in Absolute Structure Refinement. *Acta Crystallogr*. **2013**, *B69*, 249–259.

4.6 Accession Codes

CCDC 2124387−2124392 and 2158010-2158011 contain the supplementary crystallographic data for this paper. These data can be obtained free of charge via www.ccdc.cam.ac.uk/data_request/cif, by emailing data_request@ccdc.cam.ac.uk, or by contacting The Cambridge Crystallographic Data Centre, 12 Union Road, Cambridge CB2 1EZ, UK; fax: +44 1223 336033.

4.7 Acknowledgments

The authors include members of the Centre québécois sur les matériaux fonctionnels (CQMF), which is funded by Fonds de recherche du Québec – Nature et Technologies (FRQNT). In addition, financial support from the Natural Sciences and Engineering Research Council (NSERC) of Canada (RGPIN-2019-05469 and RGPIN-2020-06517) is gratefully acknowledged. We also thank the Canada Foundation for Innovation (Project 30910), the Canada Research Chairs Program, and the Université de Montréal for their generous support. We are also grateful to Alicia

Nonbo for her help and suggestions, and we thank Xue-Dong Liu at the Facility for Electron Microscopy Research at McGill University for helping us obtain scanning electron micrographs. In addition, we are grateful to reviewers of the manuscript for their constructive criticism.

4.8 References

1. Mondal, S.; Das, S.; Nandi, A. K. A Review on Recent Advances in Polymer and Peptide Hydrogels. *Soft Matter* **2020**, *16*, 1404–1454.
2. Du, X.; Zhou, J.; Shi, J.; Xu, B. Supramolecular Hydrogelators and Hydrogels: From Soft Matter to Molecular Biomaterials. *Chem. Rev.* **2015**, *115*, 13165–13307.
3. Ahmed, E. M. Hydrogel: Preparation, Characterization, and Applications: A Review. *J. Adv. Res.* **2015**, *6*, 105–121.
4. de Loos, M.; Feringa, B. L.; van Esch, J. H. Design and Application of Self-Assembled Low Molecular Weight Hydrogels. *Eur. J. Org. Chem.* **2005**, 3615–3631.
5. Estroff, L. A.; Hamilton, A. D. Water Gelation by Small Organic Molecules. *Chem. Rev.* **2004**, *104*, 1201–1217.
6. Menger, F. M.; Caran, K. L. Anatomy of a Gel. Amino Acid Derivatives That Rigidify Water at Submillimolar Concentrations. *J. Am. Chem. Soc.* **2000**, *122*, 11679–11691.
7. Chu, C.-W.; Schalley, C. A. Recent Advances on Supramolecular Gels: From Stimuli-Resonsive Gels to Co-Assembled and Self-Sorted Systems. *Org. Mater.* **2021**, *3*, 25–40.
8. Draper, E. R.; Adams, D. J. Low-Molecular-Weight Gels: The State of the Art. *Chem* **2017**, *3*, 390–410.
9. Hanabusa, K.; Suzuki, M. Physical Gelation by Low-Molecular-Weight Compounds and Development of Gelators. *Bull. Chem. Soc. Jpn.* **2016**, *89*, 174–182.
10. James, S. L.; Lloyd, G. O.; Zhang, J. Supramolecular Gels in Crystal Engineering. *CrystEngComm* **2015**, *17*, 7976–7977.
11. Yu, G.; Yan, X.; Han, C.; Huang, F. Characterization of Supramolecular Gels. *Chem. Soc. Rev.* **2013**, *42*, 6697–6722.
12. Dastidar, P. Supramolecular Gelling Agents: Can They be Designed? *Chem. Soc. Rev.* **2008**, *37*, 2699–2715.

13. Sangeetha, N. M.; Maitra, U. Supramolecular Gels: Functions and Uses. *Chem. Soc. Rev.* **2005**, *34*, 821–836.
14. Terech, P.; Weiss, R. G. Low Molecular Mass Gelators of Organic Liquids and the Properties of Their Gels. *Chem. Rev.* **1997**, *97*, 3133–3159.
15. Li, P.; Zhang, M.; Maris, T.; Zhu, X. X.; Wuest, J. D. Probing the Relationship between Gelation and Crystallization by Using Salts of Lithocholic Acid. *Cryst. Growth Des.* **2022**, *22*, 643–652.
16. Khavasi, H. R.; Esmaeili, M. Is Gelation Behavior Predictable through a Crystal Engineering Approach? A Case Study in Four Similar Coordination Compounds. *Langmuir* **2019**, *35*, 4660–4671.
17. Farahani, A. D.; Martin, A. D.; Iranmanesh, H.; Bhadbhade, M. M.; Beves, J. E.; Thordarson, P. A Gel- and Solid-State-Structure of Dialanine and Diphenylalanine Amphiphiles: Importance of C···H interactions in Gelation. *ChemPhysChem* **2019**, *20*, 972–983.
18. Löfman, M.; Lahtinen, M.; Rissanen, K.; Sievänen, E. Two-Component Self-Assembly with Solvent Leading to "Wet" and Microcrystalline Organogel Fibers. *J. Colloid Interface Sci.* **2015**, *438*, 77–86.
19. Vidyasagar, A.; Sureshan, K. M. Stoichiometric Sensing to Opt between Gelation and Crystallization. *Angew. Chem. Int. Ed.* **2015**, *54*, 12078–12082.
20. Raeburn, J.; Mendoza-Cuenca, C.; Cattoz, B. N.; Little, M. A.; Terry, A. E.; Cardoso, A. Z.; Griffiths, P. C.; Adams, D. J. The Effect of Solvent Choice on the Gelation and Final Hydrogel Properties of Fmoc–Diphenylalanine. *Soft Matter* **2015**, *11*, 927–935.
21. Houton, K. A.; Morris, K. L.; Chen, L.; Schmidtmann, M.; Jones, J. T. A.; Serpell, L. C.; Lloyd, G. O.; Adams, D. J. On Crystal versus Fiber Formation in Dipeptide Hydrogelator Systems. *Langmuir* **2012**, *28*, 9797–9806.
22. Kapoor, I.; Schön, E.-M.; Bachl, J.; Kühbeck, D.; Cativiela, C.; Saha, S.; Banerjee, R.; Roelens, S.; Marrero-Tellado, J. J.; Díaz Díaz, D. Competition Between Gelation and Crystallisation of a Peculiar Multicomponent Liquid System Based on Ammonium Salts. *Soft Matter* **2012**, *8*, 3446–3456.
23. Muro-Small, M. L.; Chen, J.; McNeil, A. J. Dissolution Parameters Reveal Role of Structure and Solvent in Molecular Gelation. *Langmuir* **2011**, *27*, 13248–13253.

24. Hwang, I.; Jeon, W. S.; Kim, H.-J.; Kim, D.; Kim, H.; Selvapalam, N.; Fujita, N.; Shinkai, S.; Kim, K. Cucurbit[7]uril: A Simple Macrocyclic, pH-Triggered Hydrogelator Exhibiting Guest-Induced Stimuli-Responsive Behavior. *Angew. Chem. In. Ed.* **2007**, *46*, 210–213.
25. Lebel, O.; Perron, M.-È.; Maris, T.; Zalzal, S. F.; Nanci, A.; Wuest, J. D. A New Class of Selective Low-Molecular-Weight Gelators Based on Salts of Diaminotriazinecarboxylic Acids. *Chem. Mater.* **2006**, *18*, 3616–3626.
26. Stanley, C. E.; Clarke, N.; Anderson, K. M.; Elder, J. A.; Lenthall, J. T.; Steed, J. W. Anion Binding Inhibition of the Formation of a Helical Organogel. *Chem. Commun.* **2006**, 3199–3201.
27. Kumar, D. K.; Jose, D. A.; Das, A.; Dastidar, P. First Snapshot of a Nonpolymeric Hydrogelator Interacting with its Gelling Solvents. *Chem. Commun.* **2005**, 4059–4061.
28. Hsu, W.-P.; Koo, K.-K.; Myerson, A. S. The Gel-Crystallization of 1-Phenylalanine and Aspartame from Aqueous Solutions. *Chem. Eng. Commun.* **2002**, *189*, 1079–1090.
29. Guterman, T.; Levin, M.; Kolusheva, S.; Levy, D.; Noor, N.; Roichman, Y.; Gazit, E. Real-Time In-Situ Monitoring of a Tunable Pentapeptide Gel–Crystal Transition. *Angew. Chem. Int. Ed.* **2019**, *58*, 15869–15875.
30. Andrews, J. L.; Pearson, E.; Yufit, D. S.; Steed, J. W.; Edkins, K. Supramolecular Gelation as the First Stage in Ostwald's Rule. *Cryst. Growth Des.* **2018**, *18*, 7690–7700.
31. Feng, H.; Du, Y.; Tang, F.; Ji, N.; Zhao, X.; Zhao, H.; Chen, Q. Silver Ions Blocking Crystallization of Guanosine-Based Hydrogel for Potential Antimicrobial Applications. *RSC Adv.* **2018**, *8*, 15842–15852.
32. Liu, X.; Fei, J.; Wang, A.; Cui, W.; Zhu, P.; Li, J. Transformation of Dipeptide-Based Organogels into Chiral Crystals by Cryogenic Treatment. *Angew. Chem. Int. Ed.* **2017**, *56*, 2660–2663.
33. Barker, E. C.; Martin, A. D.; Garvey, C. J.; Goh, C. Y.; Jones, F.; Mocerino, M.; Skelton, B. W.; Ogden, M. I.; Becker, T. Thermal Annealing Behaviour and Gel to Crystal Transition of a Low Molecular Weight Hydrogelator. *Soft Matter* **2017**, *13*, 1006–1011.
34. Guo, M.; Yin, Q.; Li, Y.; Huang, Y.; Zhang, Z.; Zhou, L. Gel-Crystal Transition During Crystallization of Cefpiramide. *Chem. Lett.* **2017**, *46*, 1292–1295.

35. Liu, J.; Xu, F.; Sun, Z.; Pan, Y.; Tian, J.; Lin, H.-C.; Li, X. A Supramolecular Gel Based on a Glycosylated Amino Acid Derivative with the Properties of Gel to Crystal Transition. *Soft Matter* **2016**, *12*, 141–148.
36. Liyanage, W.; Brennessel, W. W.; Nilsson, B. L. Spontaneous Transition of Self-Assembled Hydrogel Fibrils into Crystalline Microtubes Enables a Rational Strategy to Stabilize the Hydrogel State. *Langmuir* **2015**, *31*, 9933–9942.
37. Kumar, D. K.; Steed, J. W. Supramolecular Gel Phase Crystallization: Orthogonal Self-Assembly Under Non-Equilibrium Conditions. *Chem. Soc. Rev.* **2014**, *43*, 2080–2088.
38. Aiyappa, H. B.; Saha, S.; Garai, B.; Thote, J.; Kurungot, S.; Banerjee, R. A Distinctive $PdCl_2$-Mediated Transformation of Fe-Based Metallogels into Metal–Organic Frameworks. *Cryst. Growth Des.* **2014**, *14*, 3434–3437.
39. Xu, Y.; Kang, C.; Chen, Y.; Bian, Z.; Qiu, X.; Gao, L.; Meng, Q. In Situ Gel-to-Crystal Transition and Synthesis of Metal Nanoparticles Obtained by Fluorination of a Cyclic β-Aminoalcohol Gelator. *Chem. Eur. J.* **2012**, *18*, 16955–16961.
40. Roy, B.; Bairi, P.; Nandi, A. K. Metastability in a Bi-Component Hydrogel of Thymine and 6-Methyl-1,3,5-triazine-2,4-diamine: Ultrasound *vs.* Thermo Gelation. *Soft Matter* **2012**, *8*, 2366–2369.
41. Wang, Y.; Tang, L.; Yu, J. Investigation of Spontaneous Transition from Low-Molecular-Weight Hydrogel into Macroscopic Crystals. *Cryst. Growth Des.* **2008**, *8*, 884–889.
42. Moffat, J. R.; Smith, D. K. Metastable Two-Component Gel—Exploring the Gel–Crystal Interface. *Chem. Commun.* **2008**, 2248–2250.
43. Sasselli, I. R.; Halling, P. J.; Ulijn, R. V.; Tuttle, T. Supramolecular Fibers in Gels Can Be at Thermodynamic Equilibrium: A Simple Packing Model Reveals Preferential Fibril Formation *versus* Crystallization. *ACS Nano* **2016**, *10*, 2661–2668.
44. Adams, D. J.; Morris, K.; Chen, L.; Serpell, L. C.; Bacsa, J.; Day, G. M. The Delicate Balance Between Gelation and Crystallisation: Structural and Computational Investigations. *Soft Matter* **2010**, *6*, 4144–4156.
45. Terech, P. Metastability and Sol Phases: Two Keys for the Future of Molecular Gels? *Langmuir* **2009**, *25*, 8370–8372.
46. Bernstein, J. *Polymorphism in Molecular Crystals*; Oxford University Press: New York, 2002.

47. Bariya, D.; Anand, V.; Mishra, S. Recent Advances in the Bile Acid Based Conjugates/Derivatives Towards Their Gelation Applications. *Steroids* **2021**, *165*, 108769.
48. Goldshleger, N. F.; Lobach, A. S.; Baulin, V. E.; Tsivadze, A. Y. Supramolecular Gels Based on Bile Acid Salts. *Russ. Chem. Rev.* **2017**, *86*, 269–297.
49. Zhang, M.; Strandman, S.; Waldron, K. C.; Zhu, X. X. Supramolecular Hydrogelation with Bile Acid Derivatives: Structure, Properties and Applications. *J. Mater. Chem. B* **2016**, *4*, 7506–7520.
50. Svobodová, H.; Noponen, V.; Kolehmainen, E.; Sievänen, E. Recent Advances in Steroidal Supramolecular Gels. *RSC Adv.* **2012**, *2*, 4985–5007.
51. Madenci, D.; Egelhaaf, S. U. Self-Assembly in Aqueous Bile Salt Solutions. *Curr. Opin. Colloid Interface Sci.* **2010**, *15*, 109–115.
52. Calabresi, M.; Andreozzi, P.; La Mesa, C. Supra-Molecular Association and Polymorphic Behaviour in Systems Containing Bile Acid Salts. *Molecules* **2007**, *12*, 1731–1754.
53. Terech, P.; Sangeetha, N. M.; Maitra, U. Molecular Hydrogels from Bile Acid Analogues with Neutral Side Chains: Network Architectures and Viscoelastic Properties. Junction Zones, Spherulites, and Crystallites: Phenomenological Aspects of the Gel Metastability. *J. Phys. Chem. B* **2006**, *110*, 15224–15233.
54. di Gregorio, M. C.; Cautela, J.; Galantini, L. Physiology and Physical Chemistry of Bile Acids. *Int. J. Mol. Sci.* **2021**, *22*, 1780.
55. Hofmann, A. F.; Hagey, L. R. Bile Acids: Chemistry, Pathochemistry, Biology, Pathobiology, and Therapeutics. *Cell. Mol. Life Sci.* **2008**, *65*, 2461–2483.
56. Mukhopadhyay, S.; Maitra, U. Chemistry and Biology of Bile Acids. *Curr. Sci.* **2004**, *87*, 1666–1683.
57. Shokry, D. S.; Waters, L. J.; Parkes, G. M. B.; Mitchell, J. C.; Snowden, M. J. Formation of a Bile Salt–Drug Hydrogel to Predict Human Intestinal Absorption. *J. Pharm. Sci.* **2019**, *108*, 279–287.
58. Pavlović, N.; Goločorbin-Kon, S.; Danić, M.; Stanimirov, B.; Al-Salami, H.; Stankov, K.; Mikov, M. Bile Acids and Their Derivatives as Potential Modifiers of Drug Release and Pharmacokinetic Profiles. *Front. Pharmacol.* **2018**, *9*, 1283.

59. Faustino, C.; Serafim, C.; Rijo, P.; Pinto Reis, C. Bile Acids and Bile Acid Derivatives: Use in Drug Delivery Systems and as Therapeutic Agents. *Expert Opin. Drug Deliv.* **2016**, *13*, 1133–1148.
60. Sharma, R.; Long, A.; Gilmer, J. F. Advances in Bile Acid Medicinal Chemistry. *Curr. Med. Chem.* **2011**, *18*, 4029–4052.
61. Virtanen, E.; Kolehmainen, E. Use of Bile Acids in Pharmacological and Supramolecular Applications. *Eur. J. Org. Chem.* **2004**, 3385–3399.
62. Enhsen, A.; Kramer, W.; Wess, G. Bile Acids in Drug Discovery. *Drug Discov. Today* **1998**, *3*, 409–418.
63. Zhang, M.; Waldron, K. C.; Zhu, X. X. Formation of Molecular Hydrogels from a Bile Acid Derivative and Selected Carboxylic Acids. *RSC Adv.* **2016**, *6*, 35436–35440.
64. Zhang, M.; Ma, Z.; Wang, K.; Zhu, X. X. CO_2 Sequestration by Bile Salt Aqueous Solutions and Formation of Supramolecular Hydrogels. *ACS Sustainable. Chem. Eng.* **2019**, *7*, 3949–3955.
65. Zhang, M. Supramolecular Hydrogels Based on Bile Acids and Their Derivatives. Ph. D. Thesis, Université de Montréal: Montréal, October 2016.
66. Li, P.; Malveau, C.; Zhu, X. X.; Wuest, J. D. Using NMR Spectroscopy to Probe Hydrogels Formed by Sodium Deoxycholate. *Langmuir* **2021**, DOI: 10.1021/acs.langmuir.1c02175.
67. Adams, D. J. Does Drying Affect Gel Networks? *Gels* **2018**, *4*, 32.
68. Fini, A.; Roda, A.; Fugazza, R; Grigolo, B. Chemical Properties of Bile Acids: III. Bile Acid Structure and Solubility in Water. *J. Solution Chem.* **1985**, *14*, 595–603.
69. Sada, K.; Tani, T.; Shinkai, S. Organic Ammonium Carboxylates as Supramolecular Building Blocks: The Role of Ionic Hydrogen Bonding. *Synlett* **2006**, 2364–2374.
70. Meijide, F.; de Frutos, S.; Soto, V. H.; Jover, A.; Seijas, J. A.; Vázquez-Tato, M. P.; Fraga, F.; Vázquez Tato, J. A Standard Structure for Bile Acids and Derivatives. *Crystals* **2018**, *8*, 86.
71. Miyata, M.; Tohnai, N.; Hisaki, I. Supramolecular Chirality in Crystalline Assemblies of Bile Acids and Their Derivatives; Three-Axial, Tilt, Helical, and Bundle Chirality. *Molecules* **2007**, *12*, 1973–2000.
72. Nakano, K.; Aburaya, K.; Hisaki, I.; Tohnai, N.; Miyata, M. Flexible Host Frameworks with Diverse Cavities in Inclusion Crystals of Bile Acids and Their Derivatives. *Chem. Rec.* **2009**, *9*, 124–135.

73. Sada, K.; Shiomi, N.; Miyata, M. Nanocavities with Fine Adjustment in Channel-Type Inclusion Crystals of Alkylammonium Deoxycholates. Control of Molecular Cavities by Partial Filling of Molecular Channels. *J. Am. Chem. Soc.* **1998**, *120*, 10543–10544.
74. Jacobs, A.; Báthori, N. B.; Nassimbeni, L. R.; Sebogisi, B. K. Salts of (+)-Deoxycholic Acid with Amines: Structure, Thermal Stability, Kinetics of Salt Formation, Decomposition and Chiral Resolution. *CrystEngComm* **2013**, *15*, 931–939.
75. Tomašić, V.; Štefanić, Z. Cholic Acid as Host for Long Linear Molecules: A Series of Co-Crystals with *N*-Alkylammonia. *CrystEngComm* **2007**, *9*, 1124–1128.
76. For additional details, see the Supporting Information.

Chapter 5. Conclusions and perspectives

5.1 General conclusions

Gelation is a broadly existing phenomenon in the laboratory and nature. Researchers worldwide have focused on understanding the packing patterns of molecules in crystals/gels and how molecular structure variations can affect the organization of self-assembly. With all the gel research in the past hundred years, scientists explored the applications and properties of the gels. However, some fundamental aspects of gels remain unclear, such as the mechanism and condition of gelation, molecular interactions, and arrangement in gels. The study of gelation on the molecular level is quite challenging. It is usually difficult to directly obtain spatial information about the gelators in the gel network by using XRD or other methods commonly used in crystal analysis. My Ph.D. research has aimed to provide more information and better understanding about these essential questions related to the self-assembly of gelators, thereby benefiting the design and manufacture of gels.

5.1.1 Bile acids: a gelation model system

Bile acids/salts are natural amphiphiles with rigid skeletons and variable hydrophilicity. They can form different self-assembled structures in the aqueous environment. Therefore, we have used the bile acids/salts system to understand the gelation process and the relationship between crystals and gels. It is known the minimum number of aggregation for bile acids is 2, meaning two bile acid molecules can form the simplest micelle in water by sticking back to back. [136,137] The primary aggregates form secondary aggregates as higher concentrations.[8] Bile salts form cylindrical micelles in the gastrointestinal track for the dissolution of fats in food.[138] It was shown previously that the formation of molecular gels takes place when the molecules reached a certain condition of "marginal solubility".[31] The insoluble molecular species can precipitate or crystalize, while the more soluble species yield a clear solution. It was also found that the molecular gels in the microscopic level have nanofibers and bundles of fibers as shown by TEM.[32] The self-assembly of bile acids and their complexes is a pre-requisite for the gelation process. Then several questions may be posed on the relationship of gelation and crystallization (precipitation): Is gelation an intermediate step of crystallization or a final step of thermodynamic process separate from crystallization? In other words, is gelation a kinetic intermediate, at least in some cases, toward

final crystallization? What are the internal and external conditions that will lead to gelation, crystallization, and formation of amorphous precipitates? What the similarity and difference in the molecular arrangements in hydrogel fibers and crystals? What kind of interactions are involved in the gelation and crystallization process?

Clearly, bile acids and their derivatives provide a useful and unique model for the study of molecular gelation and crystallization. In this study, we focussed on the use of different bile acids with amines with varying substitution groups and different numbers of substitution groups (primary, secondary, tertiary, and quaternary amines) by changing the hydrophilicity of the pairs systematically in water in an attempt to find the general trend of the states of the mixtures (solutions, gels, crystals or precipitates). The observation and analysis should provide insights and understanding of such processes.

5.1.2 Understanding of gelation at a molecular level

We would like to understand what happed to the molecules involved in the gelation process. We have previously used FT-IR spectroscopy and observed the importance of the hydrogen-bonding in the formation of fibers (clear gels) and fiber bundles (opaque gels).[139] Higher concentrations of the system led to the alignments of the fibers with the formation of morphology similar to nematic liquid crystals.[140]

In this work, we chose to use NMR techniques to study the gelation process of a mixture of NaDC and formic acid. As a non-destructive method of testing, NMR provided some information on the gelation process in molecular gels. For example, at low concentrations of the gelator ($\leq$ 4 wt%) in the NaDC gel system, the percentage of molecules of the gelator immobilized in the gel is only about 35%.

DOSY-NMR revealed that the diffusion coefficients of the species in gels are quite similar to those in gelator solutions of the same concentration. Different NMR techniques also disclosed intermolecular interactions and dynamics involving gelators, solvent molecules, and additives in the gel-sol transition. In addition, NMR experiments also provided valuable spatial information about the gel. Quantitative analysis of STD-NMR results revealed that the hydrophobic convex regions of the bile acid were buried inside the fiber, while the hydrophilic parts faced the aqueous environment. All these NMR-based explorations of gel-sol interactions and other relationships

have contributed to a better understanding of hydrogels on the molecular level. These results also enlightened our further investigations on the molecular arrangement of the gelator in the fibers of the gel.

The information obtained from NMR spectroscopy is rather limited, but it is a step toward the understanding of the molecular interactions involved in the gelation process. It is worthwhile to study further the formation of molecular gels by other spectroscopic and microscopic techniques.

5.1.3. Study of crystallization by X-ray diffraction

Studying molecular arrangement in fibrils or gel networks has always been challenging. Owing to the random orientation of the fibrils in gels, it is of great difficulty to use characterization methods for crystalline materials, such as XRD, to gain spatial information about molecules in the fibrils. For some flexible gelators, such as fatty acids, the self-assembled structures may vary a lot with the conditions, hindering the attempt to deduce spatial information about the gel by extrapolating from the structure of crystals of gelators. In our experiments with bile salts, however, the rigid steroid structure of bile acids favors a consistent association pattern. Based on our observations, ammonium salts of lithocholic acid exhibit interesting aggregation changes as the ammonium counterions are varied, and hydrogels, fibril/crystal mixtures, or only crystals are all generated under approximately the same assembly conditions. This shows that the self-assembly of ammonium lithocholates is closely related to the identity of RNH_3^+. Gels with fibrous structures were obtained for hydrophilic and compact R (H, Me, Et, and cyclopropyl). Crystals and fibers were found to coexist when R = Pr or *i*-Pr. Larger and more hydrophobic R (butyl and its isomer, pentyl, and cyclohexyl) were found to favor crystallization. Structural analysis of these different crystals with XRD revealed a persistent packing pattern in which the lithocholate anions are packed in an antiparallel manner to form lamellar structures. In this pattern, the hydrophilic surface of these lamellas consists of a high density of OH and COO^- groups, which are exposed to the aqueous environment or form multiple hydrogen bonds with amines in the interlamellar region. The direction of fastest crystal growth proved to be along the hydrophobic edges of bile anions. The gel fibers also showed evidently anisotropic growth as needle-shaped crystals. Through detailed and systematic study, and through comparison of the patterns of molecular organization adopted by various ammonium lithocholates, our research has revealed the close relationship between crystallization and gelation in this system.

The growth pattern of edge-to-edge association of bile anions was also observed in our study of ammonium salts of bile acids other than lithocholic acid. Both gelation and crystallization again occurred under similar conditions, and the family of ammonium salts of different bile acids enabled us to further explore the boundary between gelation and crystallization. Our results have suggested that bile anions associate edgewise along the direction of anisotropic growth of fibers and crystals, generating assemblies with the largest possible hydrophilic surfaces. Our research has also yielded insights into the influence of specific molecular features on the association patterns of bile salts. It is observed that the increased hydrophobicity of the salts can facilitate their self-association, resulting in a tendency to shift from solutions to gels and to crystals.

The goal of my Ph.D. research has been to contribute to the knowledge of the mechanism and relationship of gelation and crystallization by systematically analyzing the self-assembly process of bile salts. We strategically took advantage of the rigid steroid structure and the variable hydrophilicity of bile salts to reveal the close structural relationship between fibrils and crystals. Our research enhanced the fundamental understanding of gelation on the molecular level using NMR, XRD, and other characterization methods. In the study of gelation conditions, we found that the solubility of both bile anions and ammonium cations will affect the morphology. The gelation usually happened for the salts with marginal solubility.

5.1.4. Kinetics and thermodynamics of gelation

The outcome of mixing of the bile acids with different amines depends on the hydrophilic or hydrophobic character of the ion pairs and their concentrations. The kinetics and thermodynamics of the processes of gelation and crystallization is an interesting physical chemistry subject that needs to be further explored for the better design of molecular materials and to reveal the conditions needed for the formation of gels and crystals and the possibility of conversion between fibers and crystals. Even though the crystal structures may provide some clue to the molecular structures of the fibers in the gels, the preliminary results seem to indicate that the formations of fibers and crystals may be on different thermodynamic paths, each corresponding to a separate energy minimum, and the transfer between fibers and crystals may not be achievable over time or through simple thermal treatment. Moreover, the influence of solubility or hydrophilicity of the amphiphilic molecules on the gelation and crystallization process is an essential topic to be further explored. In addition to these theoretical and mechanistic studies of gelation, hydrogels based on bile salts are

also promising candidates for biomedical applications owing to their biocompatibility and abundance. Therefore, our research can also contribute to the design and manufacture of gels in many different practical applications in the future.

5.2 Perspectives

5.2.1 Crystallographic mismatch nucleation and growth study

Our research studied the molecular arrangement of fibers by analyzing the boundary of the gels and crystals. The trend of moving from the formation of gels to the production of crystals with increasing hydrophobicity of bile salts was also observed in our systematic study. There are still many interesting issues to be further explored. For example, what are the factors that predetermine whether fibers or crystals are formed, and can fibers and crystals interconvert? A study of nucleation and growth may provide us with more information.

According to the branching theory introduced in Chapter 1, crystallographic mismatch nucleation and growth will determine the relationship of the daughter fibers/crystals with the parent fiber/crystal.[39] The corresponding tip/side branching creates junctions in the gel network in different ways, shown as the spherulitic or less branched fibrillar network in the gel (Figure 1.9).

One of the crucial factors controlling crystallographic mismatch nucleation is the interfacial structural match between nuclei and the underlying surface, which acts as a heterogeneous nucleation seed (Figure 1.7).[39,141] In preliminary experiments, we have explored the use of crystals of ammonium salts of bile acids as seeds to test the possibility of heterogeneous nucleation in different systems containing supersaturated bile salts.

These seeding experiments will be continued to allow us to evaluate to what extent the crystallographic mismatch branching (CMB) theory applies to our bile salt systems. We can also explore the influences of different bile salt anions and ammonium counterions on the interfacial structural match, which can be expected to affect the morphology of new crystals/fibers emerging from the seeds.

In addition to using existing crystals of ammonium salts of bile acids as seeds to get new crystals or fibers, we can also examine other factors such as the degree of supersaturation and temperature on the morphology of the self-assembled structures.[39,42,43] Most of the crystals and fibrillar networks obtained in our research are needle-like with relatively few branches. Spherulitic structures are also observed, as in the gel formed from deoxycholic acid and propylamine, but they are typically uncommon in our systems. Monitoring crystallization or formation of fibrillar networks under various assembly conditions will contribute to crystal/gel engineering knowledge and inspire new designs of bile acid-related gelators or crystals.

5.2.2 Macromolecular gel systems composed of polymers and small molecules

The gels described in Chapters 2–4 are made of small molecules, and their study provides valuable information on the molecular association and on the relationship between gelation and crystallization. Molecular gels have certain advantages over polymeric gels, such as simple gel-sol transition and easy degradation, contributing the ease in selected applications. However, molecular hydrogels produced from bile acids and alkylamines are mechanically weak. Additionally, the cytotoxicity of low molecular weight amines, especially secondary and tertiary amines,[142] may limit the use of these materials in bio-related applications such as cell culture,[143,144] tissue engineering,[145,146] or drug delivery.[147,148]The mechanical properties of gels greatly depend on the density and type of interactions in the interconnected network.[44,149–152] Noncovalent junctions in molecular gels (such as chain entanglements, hydrophobic interactions, hydrogen bonds, and even ionic bonds) are generally weaker than covalent bonds and crosslinks in polymeric gels. Therefore, it is interesting and useful to apply the same gelation conditions by mixing a polymer with a small molecule or by mixing two different polymers aiming at the condition of marginal solubility in water. Our plan is to replace the low molecular weight amines with polymeric amines, such as polyallylamine (PAA), polyethylenimine (PEI), and polylysine (PL) (Figure 5.1). The polymer chain will affect the movement and spatial relationship of amines. Promising results were obtained in preliminary experiments, and we obtained gels from some of the mixtures of polymeric amines and bile acids (Figure 5.2). We will continue working on the hybrid system to systematically study and compare the influence of chirality, hydrophobicity, repeating units, and polymer structures on the morphologies and properties of the materials.

PAA and PEI are widely studied polymers for gene delivery and nanocarriers for drugs or proteins.[153,154] These systems may achieve multifunction in drug delivery and transfection. Hydrophobic drugs can be encapsulated in the bile acid aggregates, while PAA and PEI can function as the gene carrier. This approach may help us obtain drug/gene carriers without complicated functionalization and synthesis. The biomedical applications of the hydrogels formed by polymeric amines and bile acids will be also studied.

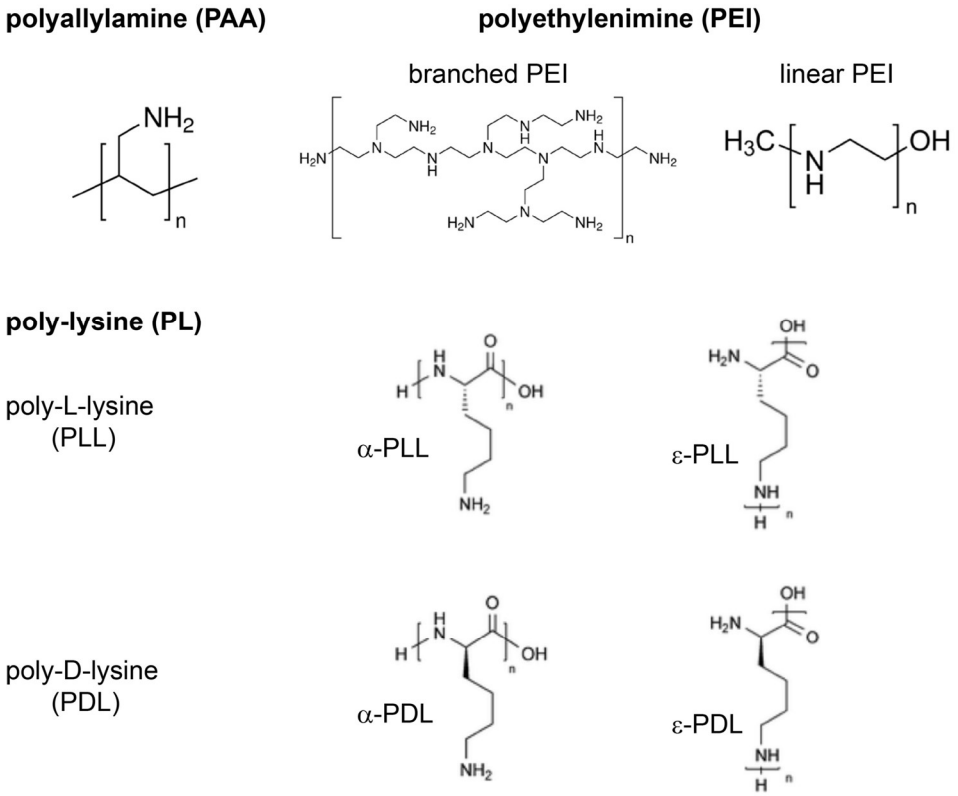

Figure 5.1 Chemical structures of PAA, PEI, and PL. α and ε correspond to the peptide bonds formed through α or ε amino groups in lysine.

PL is a biocompatible polypeptide composed of the chiral amino acid lysine (D or L) linked by α or ε amino groups. Study of the self-assembled structures and interactions of different types of PL with bile acids can provide us with valuable information about the self-assembly of polymers and small molecules. Macromolecular hydrogels may be useful biomaterials. Poly-L-lysine and poly-D-lysine behave differently in cell interaction and cellular process, such as cell adhesion,[155] intracellular degradation,[156,157] and immunogenicity.[158] By varying the identity of both bile acids

and polymers, adjusting their ratio, and changing the pH, we can tune the properties of the such gels for various applications such as cell culture, tissue engineering, and drug/gene delivery.

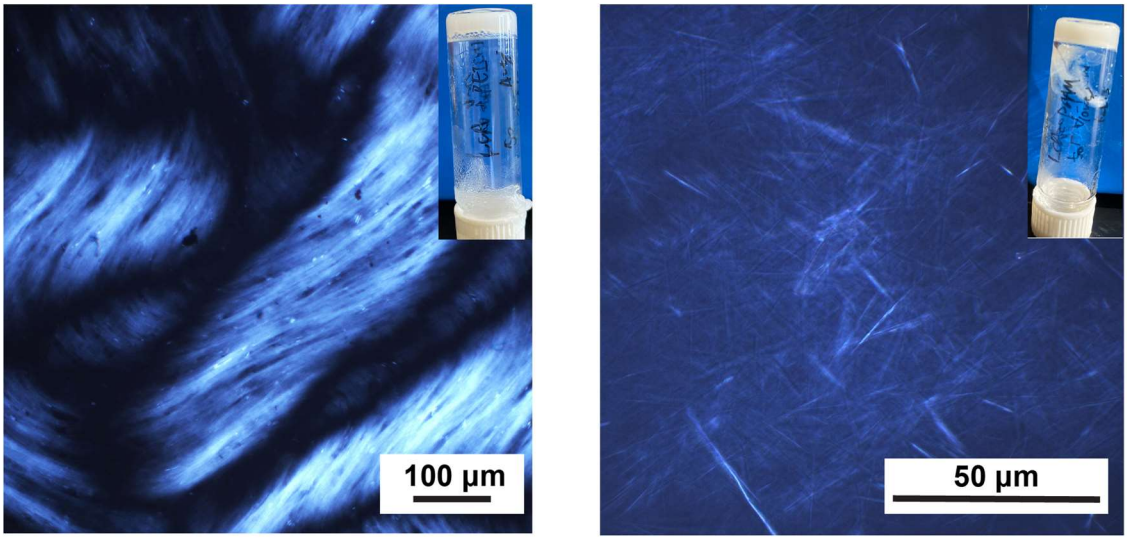

Figure 5.2 Fibrillar textures in hydrogels formed by lithocholic acid (LCA) with polymeric amines at room temperature observed by optical microscopy under polarized light. The pictures of hydrogels are inserted on the top right conner of each microscope image. (a) Hydrogel of LCA (50 mM, 2 wt%) + PEI (4 wt%, branched, $M_w \approx 800$ g/mol). (b) Hydrogel of LCA (50 mM, 2 wt%) + PAA (10 wt%, $M_w \approx 15000$ g/mol).

5.3 References

(1) Hanabusa, K.; Suzuki, M. FOCUS REVIEW Development of Low-Molecular-Weight Gelators and Polymer-Based Gelators. *Polym. J.* **2014**, *46*, 776–782. https://doi.org/10.1038/pj.2014.64.

(2) Fameau, A. L.; Rogers, M. A. The Curious Case of 12-Hydroxystearic Acid — the Dr. Jekyll & Mr. Hyde of Molecular Gelators. *Curr. Opin. Colloid Interface Sci.* **2020**, *45*, 68–82. https://doi.org/10.1016/J.COCIS.2019.12.006.

(3) TachibanaTaro; KambaraHideko. Studies of Helical Aggregates of Molecules. I. Enantiomorphism in the Helical Aggregates of Optically Active 12-Hydroxystearic Acid

and Its Lithium Salt. *http://dx.doi.org/10.1246/bcsj.42.3422* **2006**, *42* (12), 3422–3424. https://doi.org/10.1246/BCSJ.42.3422.

(4) Thierry Brotin; Ralf Utermöhlen; Frédéric Fages; Henri Bouas-Laurent; Jean-Pierre Desvergne. A Novel Small Molecular Luminescent Gelling Agent for Alcohols. *J. Chem. Soc. Chem. Commun.* **1991**, *0* (6), 416–418. https://doi.org/10.1039/C39910000416.

(5) Terech, P.; Weiss, R. G. Low Molecular Mass Gelators of Organic Liquids and the Properties of Their Gels. *Chem. Rev.* **1997**, *97* (8), 3133–3159. https://doi.org/10.1021/cr9700282.

(6) Terech, P.; Everine Friol, S. Rheometry of an Androstanol Steroid Derivative Paramagnetic Organogel. Methodology for a Comparison with a Fatty Acid Organogel. **2007**. https://doi.org/10.1016/j.tet.2007.02.067.

(7) Terech, P.; Ramasseul, R.; Volino, F. Electron Spin Resonance Study of the Gel Formed by a Spin-Labeled Steroid in Cyclohexane and Determination of the Phase Diagram. *J. Colloid Interface Sci.* **1983**, *91* (1), 280–282. https://doi.org/10.1016/0021-9797(83)90334-X.

(8) Y. Li, †; J. F. Holzwarth, † and; C. Bohne*, ‡. Aggregation Dynamics of Sodium Taurodeoxycholate and Sodium Deoxycholate. *Langmuir* **1999**, *16* (4), 2038–2041. https://doi.org/10.1021/LA9903705.

(9) Meier, A. R.; Yehl, J. B.; Eckenroad, K. W.; Manley, G. A.; Strein, T. G.; Rovnyak, D. Stepwise Aggregation of Cholate and Deoxycholate Dictates the Formation and Loss of Surface-Available Chirally Selective Binding Sites. *Langmuir* **2018**, *34* (22), 6489–6501. https://doi.org/10.1021/ACS.LANGMUIR.8B00467.

(10) Zweep, N.; Van Esch, J. H. The Design of Molecular Gelators. https://doi.org/10.1039/9781849737371-00001.

(11) Singh, A.; Auzanneau, F. I.; Rogers, M. A. Advances in Edible Oleogel Technologies – A Decade in Review. *Food Res. Int.* **2017**, *97*, 307–317. https://doi.org/10.1016/J.FOODRES.2017.04.022.

(12) Singh, A.; Auzanneau, F.-I.; Corradini, M. G.; Grover, G.; Weiss, R. G.; Rogers, M. A. Molecular Nuances Governing the Self-Assembly of 1,3:2,4-Dibenzylidene-d-Sorbitol. *Langmuir* **2017**, *33* (41), 10907–10916. https://doi.org/10.1021/ACS.LANGMUIR.7B02191.

(13) Kumar, D. K.; Steed, J. W. Supramolecular Gel Phase Crystallization: Orthogonal Self-Assembly under Non-Equilibrium Conditions. *Chem. Soc. Rev.* **2014**, *43* (7), 2080–2088. https://doi.org/10.1039/c3cs60224a.

(14) Gallant, M.; Viet, M. T. P.; Viet, M. T. P.; Wuest, J. D. Use of Hydrogen Bonds To Control Molecular Aggregation. Association of Dipyridones Joined by Flexible Spacers. *J. Org. Chem.* **1991**, *56* (7), 2284–2286. https://doi.org/10.1021/jo00007a007.

(15) Ducharme, Y.; Wuest, J. D. Use of Hydrogen Bonds to Control Molecular Aggregation. Extensive, Self-Complementary Arrays of Donors and Acceptors. *J. Org. Chem.* **1988**, *53* (24), 5787–5789. https://doi.org/10.1021/jo00259a037.

(16) Jean-Hugues Fournier, 1,†; Thierry Maris, †; James D. Wuest, *,†; Wenzhuo Guo, ‡ and; Elena Galoppini*, ‡. Molecular Tectonics. Use of the Hydrogen Bonding of Boronic Acids To Direct Supramolecular Construction. *J. Am. Chem. Soc.* **2002**, *125* (4), 1002–1006. https://doi.org/10.1021/JA0276772.

(17) Chang, S. K.; Hamilton, A. D. Molecular Recognition of Biologically Interesting Substrates: Synthesis of an Artificial Receptor for Barbiturates Employing Six Hydrogen Bonds. *J. Am. Chem. Soc.* **1988**, *110* (4), 1318–1319.

(18) Mahoney, M. W.; Jorgensen, W. L. A Five-Site Model for Liquid Water and the Reproduction of the Density Anomaly by Rigid, Nonpolarizable Potential Functions. *J. Chem. Phys.* **2000**, *112* (20), 8910. https://doi.org/10.1063/1.481505.

(19) Khalak, Y.; Baumeier, B.; Karttunen, M. Improved General-Purpose Five-Point Model for Water: TIP5P/2018. *J. Chem. Phys.* **2018**, *149* (22), 224507. https://doi.org/10.1063/1.5070137.

(20) Israelachvili, J. Intermolecular and Surface Forces. *Intermol. Surf. Forces* **2011**. https://doi.org/10.1016/C2009-0-21560-1.

(21) Thomas, G. II. Liquid Diffusion Applied to Analysis. *Proc. R. Soc. London* **1862**, *11*, 243–247. https://doi.org/10.1098/RSPL.1860.0048.

(22) D'Urso, E. M.; Fortier, G. New Hydrogel Based on Polyethylene Glycol Cross-Linked with Bovine Serum Albumin. *Biotechnol. Tech. 1994 82* **1994**, *8* (2), 71–76. https://doi.org/10.1007/BF00152843.

(23) Millon, L. E.; Mohammadi, H.; Wan, W. K. Anisotropic Polyvinyl Alcohol Hydrogel for Cardiovascular Applications. *J. Biomed. Mater. Res. Part B Appl. Biomater.* **2006**, *79B*

(2), 305–311. https://doi.org/10.1002/JBM.B.30543.

(24) Jabbari, E.; Nozari, S. Swelling Behavior of Acrylic Acid Hydrogels Prepared by γ-Radiation Crosslinking of Polyacrylic Acid in Aqueous Solution. *Eur. Polym. J.* **2000**, *36* (12), 2685–2692. https://doi.org/10.1016/S0014-3057(00)00044-6.

(25) Yuan, Z.; Lu, W.; Liu, W.; Hao, J. Gel Phase Originating from Molecular Quasi-Crystallization and Nanofiber Growth of Sodium Laurate-Water System. *Soft Matter* **2008**, *4* (8), 1639–1644. https://doi.org/10.1039/b804157a.

(26) Zawko, S. A.; Schmidt, C. E. Assembly of Sodium Soap Fibers and Fibrillar Particles Triggered by Dissolution of Sodium Chloride Crystals. *Soft Matter* **2010**, *6* (14), 3289–3297. https://doi.org/10.1039/c002084b.

(27) Arakawa, H.; Takeda, K.; Higashi, S. L.; Shibata, A.; Kitamura, Y.; Ikeda, M. Self-Assembly and Hydrogel Formation Ability of Fmoc-Dipeptides Comprising α-Methyl-L-Phenylalanine. *Polym. J.* **2020**. https://doi.org/10.1038/s41428-019-0301-5.

(28) Madenci, D.; Egelhaaf, S. U. Self-Assembly in Aqueous Bile Salt Solutions. *Current Opinion in Colloid and Interface Science*. 2010. https://doi.org/10.1016/j.cocis.2009.11.010.

(29) Goldshleger, N. F.; Lobach, A. S.; Baulin, V. E.; Tsivadze, A. Y. Supramolecular Gels Based on Bile Acid Salts. *Russ. Chem. Rev.* **2017**, *86* (4), 269–297. https://doi.org/10.1070/rcr4682.

(30) Di Gregorio, M. C.; Travaglini, L.; Del Giudice, A.; Cautela, J.; Pavel, N. V.; Galantini, L. Bile Salts: Natural Surfactants and Precursors of a Broad Family of Complex Amphiphiles. *Langmuir* **2019**, *35* (21), 6803–6821. https://doi.org/10.1021/acs.langmuir.8b02657.

(31) Zhang, M.; Waldron, K. C.; Zhu, X. X. Formation of Molecular Hydrogels from a Bile Acid Derivative and Selected Carboxylic Acids. *RSC Adv.* **2016**, *6* (42), 35436–35440. https://doi.org/10.1039/c6ra04536g.

(32) Zhang, M.; Ma, Z.; Wang, K.; Zhu, X. X. CO 2 Sequestration by Bile Salt Aqueous Solutions and Formation of Supramolecular Hydrogels. *ACS Sustain. Chem. Eng.* **2019**, *7* (4), 3949–3955. https://doi.org/10.1021/acssuschemeng.8b05112.

(33) Li, G.; Hu, Y.; Sui, J.; Song, A.; Hao, J. Hydrogelation and Crystallization of Sodium Deoxycholate a b c a b C. *88364750*.

(34) La Mesa, C.; Khan, A.; Fontell, K.; Lindman, B. Phase Diagrams and NMR Studies of Some Ternary Sodium Deoxycholate-Surfactant-Water Systems. *J. Colloid Interface Sci.* **1985**, *103* (2), 373–391. https://doi.org/10.1016/0021-9797(85)90116-X.

(35) Karthika, S.; Radhakrishnan, T. K.; Kalaichelvi, P. A Review of Classical and Nonclassical Nucleation Theories. *Cryst. Growth Des.* **2016**, *16* (11), 6663–6681. https://doi.org/10.1021/acs.cgd.6b00794.

(36) Rui Yu; Naibo Lin; Weidong Yu; Yang Liu, X. Crystal Networks in Supramolecular Gels: Formation Kinetics and Mesoscopic Engineering Principles. *CrystEngComm* **2015**, *17* (42), 7986–8010. https://doi.org/10.1039/C5CE00854A.

(37) Sear, R. P. Heterogeneous and Homogeneous Nucleation Compared: Rapid Nucleation on Microscopic Impurities. *J. Phys. Chem. B* **2006**, *110* (10), 4985–4989. https://doi.org/10.1021/jp056377e.

(38) Steed, J. W.; Atwood, J. L. Supramolecular Chemistry: Second Edition. *Supramol. Chem. Second Ed.* **2009**, 1–970. https://doi.org/10.1002/9780470740880.

(39) Hirst, A. R.; Smith, D. K.; Liu, X. Y. Low Molecular Mass Gelators : Design, Self-Assembly, Function. *Top. Curr. Chem.* **2005**, *256*, 237–273. https://doi.org/10.1007/b107178.

(40) Li, J. L.; Liu, X. Y. *Soft Fibrillar Materials: Fabrication and Applications*; John Wiley & Sons, 2013.

(41) Bennema, P. Spiral Growth and Surface Roughening: Developments since Burton, Cabrera and Frank. *J. Cryst. Growth* **1984**, *69* (1), 182–197. https://doi.org/10.1016/0022-0248(84)90027-7.

(42) Rongyao Wang; Xiang-Yang Liu, *; Junying Xiong, and; Li, J. Real-Time Observation of Fiber Network Formation in Molecular Organogel: Supersaturation-Dependent Microstructure and Its Related Rheological Property. *J. Phys. Chem. B* **2006**, *110* (14), 7275–7280. https://doi.org/10.1021/JP054531R.

(43) Rong-Yao Wang, †,‡; Xiang-Yang Liu, *,‡; Janaky Narayanan, ‡; Jun-Ying Xiong, ‡ and; Li‡, J.-L. Architecture of Fiber Network: From Understanding to Engineering of Molecular Gels. *J. Phys. Chem. B* **2006**, *110* (51), 25797–25802. https://doi.org/10.1021/JP065101J.

(44) Kim, J.; Zhang, G.; Shi, M.; Suo, Z. Fracture, Fatigue, and Friction of Polymers in Which

Entanglements Greatly Outnumber Cross-Links. *Science (80-.).* **2021**, *374* (6564), 212–216. https://doi.org/10.1126/SCIENCE.ABG6320.

(45) Lloyd, D. J. The Problem of Gel Structure. *Colloid Chem.* **1926**, *1*, 767–782.

(46) Takahashi, A.; Sakai, M.; Kato, T. Melting Temperature of Thermally Reversible Gel. VI. Effect of Branching on the Sol–Gel Transition of Polyethylene Gels. *Polym. J. 1980 125* **1980**, *12* (5), 335–341. https://doi.org/10.1295/polymj.12.335.

(47) Raghavan, S. R.; Cipriano, B. H. Gel Formation: Phase Diagrams Using Tabletop Rheology and Calorimetry. *Mol. Gels Mater. with Self-Assembled Fibrillar Networks* **2006**, 241–252. https://doi.org/10.1007/1-4020-3689-2_9.

(48) Slone, R. V. Encyclopedia of Polymer Science and Technology; Mark, HF, Ed. John Wiley & Sons: New York 2004.

(49) Miyoshi, E.; Takaya, T.; Nishinari, K. Effects of Salts on the Gel-Sol Transition of Gellan Gum by Differential Scanning Calorimetry and Thermal Scanning Rheology. *Thermochim. Acta* **1995**, *267* (C), 269–287. https://doi.org/10.1016/0040-6031(95)02485-9.

(50) Derkach, S. R.; Ilyin, S. O.; Maklakova, A. A.; Kulichikhin, V. G.; Malkin, A. Y. The Rheology of Gelatin Hydrogels Modified by κ-Carrageenan. *LWT - Food Sci. Technol.* **2015**, *63* (1), 612–619. https://doi.org/10.1016/J.LWT.2015.03.024.

(51) Kiyotake, E. A.; Douglas, A. W.; Thomas, E. E.; Nimmo, S. L.; Detamore, M. S. Development and Quantitative Characterization of the Precursor Rheology of Hyaluronic Acid Hydrogels for Bioprinting. *Acta Biomater.* **2019**, *95*, 176–187. https://doi.org/10.1016/J.ACTBIO.2019.01.041.

(52) Sawatari, C.; Okumura, T.; Matsuo, M. Molecular Weight Dependence on the Morphological Properties of Polyethylene Gels. *Polym. J. 1986 1810* **1986**, *18* (10), 741–758. https://doi.org/10.1295/polymj.18.741.

(53) Venkatesan, R.; Nagarajan, N. R.; Paso, K.; Yi, Y. B.; Sastry, A. M.; Fogler, H. S. The Strength of Paraffin Gels Formed under Static and Flow Conditions. *Chem. Eng. Sci.* **2005**, *60* (13), 3587–3598. https://doi.org/10.1016/J.CES.2005.02.045.

(54) Günther, H. *NMR Spectroscopy: Basic Principles, Concepts and Applications in Chemistry*; John Wiley & Sons, 2013.

(55) Bloembergen, N.; Purcell, E. M.; Pound, R. V. Relaxation Effects in Nuclear Magnetic Resonance Absorption. *Phys. Rev.* **1948**, *73* (7), 679.

https://doi.org/10.1103/PhysRev.73.679.

(56) Murata, Y.; Sugihara, G.; Fukuehlma, K.; Tanaka, M.; Matsushita, K. Study of the Micelle Formation of Sodium Deoxycholate. Concentration Dependence of Carbon-13 Nuclear Magnetic Resonance Chemical Shift. *J. Phys. Chem* **1982**, *86*, 4690–4694.

(57) Bertini, I.; Luchinat, C.; Parigi, G.; Ravera, E. Relaxation. *Solut. NMR Paramagn. Mol.* **2017**, 77–126. https://doi.org/10.1016/B978-0-444-63436-8.00004-1.

(58) Grant, D. M.; Harris, R. K. Encyclopedia of Nuclear Magnetic Resonance, Volume 9, Advances in NMR. *Spectroscopy* **1996**.

(59) Vögeli, B. The Nuclear Overhauser Effect from a Quantitative Perspective. *Prog. Nucl. Magn. Reson. Spectrosc.* **2014**, *78*, 1–46. https://doi.org/10.1016/J.PNMRS.2013.11.001.

(60) Tamesue, S.; Takashima, Y.; Yamaguchi, H.; Shinkai, S.; Harada, A. Photoswitchable Supramolecular Hydrogels Formed by Cyclodextrins and Azobenzene Polymers. *Angew. Chemie Int. Ed.* **2010**, *49* (41), 7461–7464. https://doi.org/10.1002/ANIE.201003567.

(61) Abian, O.; Vega, S.; Neira, J. L.; Velazquez-Campoy, A. High-Throughput Screening for Intrinsically Disordered Proteins by Using Biophysical Methods. *Protein Homeost. Dis.* **2020**, 359–387. https://doi.org/10.1016/B978-0-12-819132-3.00017-8.

(62) Atta-ur-Rahman; Choudhary, M. I.; Atia-tul-Wahab. Nuclear Overhauser Effect. *Solving Probl. with NMR Spectrosc.* **2016**, 227–264. https://doi.org/10.1016/B978-0-12-411589-7.00006-1.

(63) Krishnan, V. Ligand Screening by Saturation-Transfer Difference (STD) NMR Spectroscopy. *Curr. Anal. Chem.* **2005**, *1* (3), 307–320. https://doi.org/10.2174/157341105774573956.

(64) Yan, J.; Kline, A. D.; Mo, H.; Shapiro, M. J.; Zartler, E. R. The Effect of Relaxation on the Epitope Mapping by Saturation Transfer Difference NMR. *J. Magn. Reson.* **2003**, *163* (2), 270–276. https://doi.org/10.1016/S1090-7807(03)00106-X.

(65) Ramalhete, S. M.; Nartowski, K. P.; Sarathchandra, N.; Foster, J. S.; Round, A. N.; Angulo, J.; Lloyd, G. O.; Khimyak, Y. Z. Supramolecular Amino Acid Based Hydrogels: Probing the Contribution of Additive Molecules Using NMR Spectroscopy. *Chem. - A Eur. J.* **2017**, *23* (33). https://doi.org/10.1002/chem.201700793.

(66) Segarra-Maset, M. D.; Escuder, B.; Miravet, J. F. Selective Interaction of Dopamine with the Self-Assembled Fibrillar Network of a Molecular Hydrogel Revealed by STD-NMR.

Chem. - A Eur. J. **2015**, *21* (40), 13925–13929. https://doi.org/10.1002/chem.201502018.

(67) Nonappa; Šaman, D.; Kolehmainen, E. Studies on Supramolecular Gel Formation Using DOSY NMR. *Magn. Reson. Chem.* **2015**, *53* (4), 256–260. https://doi.org/10.1002/MRC.4185.

(68) Šmejkalová, D.; Piccolo, A. Aggregation and Disaggregation of Humic Supramolecular Assemblies by NMR Diffusion Ordered Spectroscopy (DOSY-NMR). *Environ. Sci. Technol.* **2008**, *42* (3), 699–706. https://doi.org/10.1021/es071828p.

(69) Sajid Iqbal; Francisco Rodríguez-LLansola; Beatriu Escuder; F. Miravet, J.; Ingrid Verbruggen; Rudolph Willem. HRMAS 1H NMR as a Tool for the Study of Supramolecular Gels. *Soft Matter* **2010**, *6* (9), 1875–1878. https://doi.org/10.1039/B926785A.

(70) Liu, Y.; Guo, D.-S.; Zhang, H.-Y.; Ding, F.; Chen, K.; Song, H.-B. Supramolecular Assemblies of Sulfonatocalixarenes with Phenanthroline: Factors Governing Capsule Formation versus Bilayer Arrangements. https://doi.org/10.1002/chem.200600668.

(71) BEARDEN, J. A. X-Ray Wavelengths. *Rev. Mod. Phys.* **1967**, *39* (1), 78. https://doi.org/10.1103/RevModPhys.39.78.

(72) Whittig, L. D.; Allardice, W. R. X-Ray Diffraction Techniques. *Methods Soil Anal. Part 1 Phys. Mineral. Methods* **2018**, 331–362. https://doi.org/10.2136/SSSABOOKSER5.1.2ED.C12.

(73) Bunaciu, A. A.; Udriştioiu, E. gabriela; Aboul-Enein, H. Y. X-Ray Diffraction: Instrumentation and Applications. *http://dx.doi.org/10.1080/10408347.2014.949616* **2015**, *45* (4), 289–299. https://doi.org/10.1080/10408347.2014.949616.

(74) Hwang, I.; Jeon, W. S.; Kim, H.-J.; Kim, D.; Kim, H.; Selvapalam, N.; Fujita, N.; Shinkai, S.; Kim, K. Cucurbit[7]Uril: A Simple Macrocyclic, PH-Triggered Hydrogelator Exhibiting Guest-Induced Stimuli-Responsive Behavior. *Angew. Chemie* **2007**, *119* (1–2), 214–217. https://doi.org/10.1002/ANGE.200603149.

(75) Draper, E. R.; Dietrich, B.; McAulay, K.; Brasnett, C.; Abdizadeh, H.; Patmanidis, I.; Marrink, S. J.; Su, H.; Cui, H.; Schweins, R.; Seddon, A.; Adams, D. J. Using Small-Angle Scattering and Contrast Matching to Understand Molecular Packing in Low Molecular Weight Gels. *Matter* **2020**, *2* (3), 764–778. https://doi.org/10.1016/J.MATT.2019.12.028.

(76) Nair, P. *The Bile Acids Chemistry, Physiology, and Metabolism: Volume 1: Chemistry*;

Springer Science & Business Media, 2013.

(77) Bachmann, V.; Kostiuk, B.; Unterweger, D.; Diaz-Satizabal, L.; Ogg, S.; Pukatzki, S. Bile Salts Modulate the Mucin-Activated Type VI Secretion System of Pandemic Vibrio Cholerae. *PLoS Negl. Trop. Dis.* **2015**, *9* (8), e0004031. https://doi.org/10.1371/JOURNAL.PNTD.0004031.

(78) Jia, Y. G.; Yu, Q.; Ma, Z.; Zhang, M.; Zhu, X. X. Tunable Upper Critical Solution Temperatures for Acrylamide Copolymers with Bile Acid Pendants. *Biomacromolecules* **2017**, *18* (8), 2663–2668. https://doi.org/10.1021/ACS.BIOMAC.7B00860/SUPPL_FILE/BM7B00860_SI_001.PDF .

(79) Ma, Z.; Zhu, X. X. Core Cross-Linked Micelles Made of Glycopolymers Bearing Dopamine and Cholic Acid Pendants. *Mol. Pharm.* **2018**, *15* (6), 2348–2354. https://doi.org/10.1021/ACS.MOLPHARMACEUT.8B00205/SUPPL_FILE/MP8B00205_SI_001.PDF.

(80) Gauthier, M. A.; Simard, P.; Zhang, Z.; Zhu, X. X. Bile Acids as Constituents for Dental Composites: In Vitro Cytotoxicity of (Meth)Acrylate and Other Ester Derivatives of Bile Acids. *J. R. Soc. Interface* **2007**, *4* (17), 1145–1150. https://doi.org/10.1098/RSIF.2007.1018.

(81) Gauthier, M. A.; Zhang, Z.; Zhu, X. X. New Dental Composites Containing Multimethacrylate Derivatives of Bile Acids: A Comparative Study with Commercial Monomers. *ACS Appl. Mater. Interfaces* **2009**, *1* (4), 824–832. https://doi.org/10.1021/AM8002395/SUPPL_FILE/AM8002395_SI_001.PDF.

(82) Jia, Y. G.; Zhu, X. X. Nanocomposite Hydrogels of LAPONITE® Mixed with Polymers Bearing Dopamine and Cholic Acid Pendants. *RSC Adv.* **2016**, *6* (27), 23033–23037. https://doi.org/10.1039/c5ra26316f.

(83) Jia, Y. G.; Zhu, X. X. Self-Healing Supramolecular Hydrogel Made of Polymers Bearing Cholic Acid and β-Cyclodextrin Pendants. *Chem. Mater.* **2015**, *27* (1), 387–393. https://doi.org/10.1021/cm5041584.

(84) Jia, Y. G.; Jin, J.; Liu, S.; Ren, L.; Luo, J.; Zhu, X. X. Self-Healing Hydrogels of Low Molecular Weight Poly(Vinyl Alcohol) Assembled by Host-Guest Recognition. *Biomacromolecules* **2018**, *19* (2), 626–632.

https://doi.org/10.1021/ACS.BIOMAC.7B01707/SUPPL_FILE/BM7B01707_SI_001.PDF
.

(85) Zhang, M.; Strandman, S.; Waldron, K. C.; Zhu, X. X. Supramolecular Hydrogelation with Bile Acid Derivatives: Structures, Properties and Applications. *J. Mater. Chem. B* **2016**, *4* (47), 7506–7520. https://doi.org/10.1039/c6tb02270g.

(86) Jia, Y. G.; Zhang, M.; Zhu, X. X. CO2-Switchable Self-Healing Host-Guest Hydrogels. *Macromolecules* **2017**, *50* (24), 9696–9701. https://doi.org/10.1021/ACS.MACROMOL.7B02163/SUPPL_FILE/MA7B02163_SI_001.PDF.

(87) Russell, D. W. THE ENZYMES, REGULATION, AND GENETICS OF BILE ACID SYNTHESIS. **2003**. https://doi.org/10.1146/annurev.biochem.72.121801.161712.

(88) Chiang, J. Y. L. Regulation of Bile Acid Synthesis: Pathways, Nuclear Receptors, and Mechanisms. *J. Hepatol.* **2004**, *40* (3), 539–551. https://doi.org/10.1016/J.JHEP.2003.11.006.

(89) Federici, G. Bile Acids. *Lab. Guid. to Methods Biochem. Genet.* **2017**, 607–664. https://doi.org/10.1007/978-3-540-76698-8_27.

(90) Small, D. M. The Physical Chemistry of Cholanic Acids. *Bile Acids Chem. Physiol. Metab.* **1971**, 249–356. https://doi.org/10.1007/978-1-4757-0647-5_8.

(91) Madenci, D.; Egelhaaf, S. U. Self-Assembly in Aqueous Bile Salt Solutions. *Curr. Opin. Colloid Interface Sci.* **2010**, *15* (1–2), 109–115. https://doi.org/10.1016/j.cocis.2009.11.010.

(92) Paula, S.; Stis, W.; Tuchtenhagen, J.; Blume, A. Thermodynamics of Micelle Formation as a Function of Temperature: A High Sensitivity Titration Calorimetry Study. *J. Phys. Chem* **1995**, *99*, 11742–11751.

(93) Reis, S.; Moutinho, C. G.; Matos, C.; De Castro, B.; Gameiro, P.; Lima, J. L. F. C. Noninvasive Methods to Determine the Critical Micelle Concentration of Some Bile Acid Salts. *Anal. Biochem.* **2004**, *334* (1), 117–126. https://doi.org/10.1016/J.AB.2004.07.017.

(94) Matsuoka, K.; Moroi, Y. Micelle Formation of Sodium Deoxycholate and Sodium Ursodeoxycholate (Part 1). *Biochim. Biophys. Acta - Mol. Cell Biol. Lipids* **2002**, *1580* (2–3), 189–199. https://doi.org/10.1016/S1388-1981(01)00203-7.

(95) Hofmann, A. F.; Small, D. M. Detergent Properties of Bile Salts: Correlation with

Physiological Function. *https://doi.org/10.1146/annurev.me.18.020167.002001* **2003**, *18*, 333–376. https://doi.org/10.1146/ANNUREV.ME.18.020167.002001.

(96) Garidel, P.; Hildebrand, A.; Neubert, R.; Blume, A. Thermodynamic Characterization of Bile Salt Aggregation as a Function of Temperature and Ionic Strength Using Isothermal Titration Calorimetry. *Langmuir* **2000**, *16* (12), 5267–5275. https://doi.org/10.1021/LA9912390.

(97) Carey, M. C.; Small, D. M. Micelle Formation by Bile Salts: Physical-Chemical and Thermodynamic Considerations. *Arch. Intern. Med.* **1972**, *130* (4), 506–527. https://doi.org/10.1001/ARCHINTE.1972.03650040040005.

(98) Norman, A.; Bergman, S.; Bak, T. A.; Varde, E.; Westin, G. The Conductance of Conjugated and Unconjugated Bile Acid Salts in Aqueous Solutions. Bile Acids and Steroids. 80. *Acta Chem. Scand.* **1960**, *14*, 1300–1309. https://doi.org/10.3891/acta.chem.scand.14-1300.

(99) HOFMANN, A. F. THE FUNCTION OF BILE SALTS IN FAT ABSORPTION. THE SOLVENT PROPERTIES OF DILUTE MICELLAR SOLUTIONS OF CONJUGATED BILE SALTS. *Biochem. J.* **1963**, *89* (1), 57–68. https://doi.org/10.1042/BJ0890057.

(100) Hofmann, A. F.; Roda, A. Physicochemical Properties of Bile Acids and Their Relationship to Biological Properties: An Overview of the Problem. *J. Lipid Res.* **1984**, *25* (13), 1477–1489. https://doi.org/10.1016/S0022-2275(20)34421-7.

(101) SMALL, D. M. Size and Structure of Bile Salt Micelles. **1968**, 31–52. https://doi.org/10.1021/ba-1968-0084.ch004.

(102) Waissbluth, O. L.; Morales, M. C.; Bohne, C. Influence of Planarity and Size on Guest Binding with Sodium Cholate Aggregates. *Photochem. Photobiol.* **2006**, *82* (4), 1030–1038. https://doi.org/10.1562/2006-02-14-RA-803.

(103) Ju, C.; Bohne, C. Dynamics of Probe Complexation to Bile Salt Aggregates. *J. Phys. Chem.* **1996**, *100* (9), 3847–3854. https://doi.org/10.1021/JP952657Q.

(104) Kawamura, H.; Murata, Y.; Yamaguchi, T.; Igimi, H.; Tanaka, M.; Sugihara, G.; Kratohvil, J. P. Spin-Label Studies of Bile Salt Micelles. *J. Phys. Chem.* **1989**, *93* (8), 3321–3326. https://doi.org/10.1021/j100345a087.

(105) Madenci, D.; Egelhaaf, S. U. Self-Assembly in Aqueous Bile Salt Solutions. *Curr. Opin. Colloid Interface Sci.* **2010**, *15* (1–2), 109–115.

https://doi.org/10.1016/J.COCIS.2009.11.010.

(106) Campanelli, A. R.; Candeloro De Sanctis, S.; Chiessi, E.; Giglio, E.; Scaramuzza, L.; Sapienza, L.; le Moro, P. A. Sodium Glyco-and Taurodeoxycholate: Possible Helical Models for Conjugated Bile Salt Micelles.

(107) Campanelli, A. R.; Candeloro, S.; Sanctis, D. E.; Giglio, E.; Pavel, N. V.; Quagliata, C. From Crystal to Micelle: A New Approach to the Micellar Structure. *J. Incl. Phenom. Mol. Recognit. Chem.* **1989**, *7*, 391.

(108) Hofmann, A. F.; Mysels, K. J. Bile Acid Solubility and Precipitation in Vitro and in Vivo: The Role of Conjugation, PH, and Ca2+ Ions. *J. Lipid Res.* **1992**, *33* (5), 617–626. https://doi.org/10.1016/S0022-2275(20)41426-9.

(109) Rich, A.; Blow, D. M. Formation of a Helical Steroid Complex. *Nature* **1958**, *182* (4633), 423–426. https://doi.org/10.1038/182423a0.

(110) Blow, D. M.; Rich, A. Studies on the Formation of Helical Deoxycholate Complexes1, 2. *J. Am. Chem. Soc.* **1960**, *82* (14), 3566–3571.

(111) Sobotka, H.; Czeczowiczka, N. The Gelation of Bile Salt Solutions. *J. Colloid Sci.* **1958**, *13* (2), 188–191. https://doi.org/10.1016/0095-8522(58)90024-2.

(112) Kratohvil, J. P.; Hsu, W. P.; Kwok, D. I. How Large Are the Micelles of Di-α-Hydroxy Bile Salts at the Critical Micellization Concentrations in Aqueous Electrolyte Solutions? Results for Sodium Taurodeoxycholate and Sodium Deoxycholate. *Langmuir* **2002**, *2* (2), 256–258. https://doi.org/10.1021/LA00068A026.

(113) Sada, K.; Sugahara, M.; Kato, K.; Miyata, M. Controlled Expansion of a Molecular Cavity in a Steroid Host Compound. *J. Am. Chem. Soc.* **2001**, *123* (19), 4386–4392. https://doi.org/10.1021/JA0038528/SUPPL_FILE/JA0038528.CIF.

(114) Miki, K.; Masui, A.; Kasai, N.; Miyata, M.; Shibakami, M.; Takemoto, K. New Channel-Type Inclusion Compound of Steroidal Bile Acid. Structure of a 1:1 Complex between Cholic Acid and Acetophenone. *J. Am. Chem. Soc.* **1988**, *110* (19), 6594–6596. https://doi.org/10.1021/JA00227A067/SUPPL_FILE/JA00227A067_SI_001.PDF.

(115) Qiao, Y.; Lin, Y.; Wang, Y.; Yang, Z.; Liu, J.; Zhou, J.; Yan, Y.; Huang, J. Metal-Driven Hierarchical Self-Assembled One-Dimensional Nanohelices. *Nano Lett.* **2009**, *9* (12), 4500–4504. https://doi.org/10.1021/NL9028335.

(116) Qiao, Y.; Lin, Y.; Zhang, S.; Huang, J. Lanthanide-Containing Photoluminescent

Materials: From Hybrid Hydrogel to Inorganic Nanotubes. https://doi.org/10.1002/chem.201003255.

(117) Chakrabarty, A.; Maitra, U.; Das, A. D. Metal Cholate Hydrogels: Versatile Supramolecular Systems for Nanoparticle Embedded Soft Hybrid Materials. *J. Mater. Chem.* **2012**, *22* (35), 18268–18274. https://doi.org/10.1039/C2JM34016J.

(118) Qiao, Y.; Wang, Y.; Yang, Z.; Lin, Y.; Huang, J. Self-Templating of Metal-Driven Supramolecular Self-Assembly: A General Approach toward 1D Inorganic Nanotubes. *Chem. Mater.* **2011**, *23* (5), 1182–1187. https://doi.org/10.1021/CM102649Y.

(119) Sada, K.; Sugahara, M.; Kato, K.; Miyata, M. Controlled Expansion of a Molecular Cavity in a Steroid Host Compound. *J. Am. Chem. Soc.* **2001**, *123* (19), 4386–4392. https://doi.org/10.1021/JA0038528/SUPPL_FILE/JA0038528.CIF.

(120) Noponen, V.; Toikkanen, K.; Kalenius, E.; Kuosmanen, R.; Salo, H.; Sievänen, E. Stimuli-Responsive Bile Acid-Based Metallogels Forming in Aqueous Media. *Steroids* **2015**, *97*, 54–61. https://doi.org/10.1016/j.steroids.2014.10.001.

(121) Dukh, M.; Šaman, D.; Kroulík, J.; Černý, I.; Pouzar, V.; Král, V.; Drašar, P. Metal Coordination as a Tool for Controlling the Self-Assembling and Gelation Properties of Novel Type Cholic Amide–Phenanthroline Gelating Agent. *Tetrahedron* **2003**, *59* (23), 4069–4076. https://doi.org/10.1016/S0040-4020(03)00587-8.

(122) Di Gregorio, M. C.; Varenik, M.; Gubitosi, M.; Travaglini, L.; Pavel, N. V.; Jover, A.; Meijide, F.; Regev, O.; Galantini, L. Multi Stimuli Response of a Single Surfactant Presenting a Rich Self-Assembly Behavior. *RSC Adv.* **2015**, *5* (47), 37800–37806. https://doi.org/10.1039/c5ra01394a.

(123) Ryu, E. H.; Ellern, A.; Zhao, Y. High Guest Inclusion in 3β-Amino-7α,12α-Dihydroxycholan-24-Oic Acid Enabled by Charge-Assisted Hydrogen Bonds. *Tetrahedron* **2006**, *62* (29), 6808–6813. https://doi.org/10.1016/J.TET.2006.04.094.

(124) Vázquez Tato, J.; Meijide, F.; Antelo, A.; Alvarez Alcalde, M.; Jover, A.; Galantini, L.; Pavel, N. V. Supramolecular Structures Generated by a P- Tert-Butylphenylamide Derivative of Deoxycholic Acid. from Planar Sheets to Tubular Structures through Helical Ribbons. *Langmuir* **2010**, *26* (11), 7768–7773. https://doi.org/10.1021/LA904548K/SUPPL_FILE/LA904548K_SI_001.PDF.

(125) Travaglini, L.; D'annibale, A.; Schillén, K.; Olsson, U.; Sennato, S.; Pavel, N. V.;

Galantini, L. Amino Acid – Bile Acid Based Molecules: Extremely Narrow Surfactant Nanotubes Formed by a Phenylalanine-Substituted Cholic Acid. *Chem. Commun.* **2012**, *48* (98), 12011–12013. https://doi.org/10.1039/C2CC36030F.

(126) Gubitosi, M.; Travaglini, L.; di Gregorio, M. C.; Pavel, N. V.; Vázquez Tato, J.; Sennato, S.; Olsson, U.; Schillén, K.; Galantini, L. Tailoring Supramolecular Nanotubes by Bile Salt Based Surfactant Mixtures. *Angew. Chemie* **2015**, *127* (24), 7124–7127. https://doi.org/10.1002/ANGE.201500445.

(127) Di Gregorio, M. C.; Severoni, E.; Travaglini, L.; Gubitosi, M.; Sennato, S.; Mura, F.; Redondo-Gómez, C.; Jover, A.; Pavel, N. V.; Galantini, L. Bile Acid Derivative-Based Catanionic Mixtures: Versatile Tools for Superficial Charge Modulation of Supramolecular Lamellae and Nanotubes. *Phys. Chem. Chem. Phys.* **2018**, *20* (28), 18957–18968. https://doi.org/10.1039/c8cp02745e.

(128) Dévédec, F. Le; Fuentealba, D.; Strandman, S.; Bohne, C.; Zhu, X. X. Aggregation Behavior of Pegylated Bile Acid Derivatives. *Langmuir* **2012**, *28* (37), 13431–13440. https://doi.org/10.1021/LA303218Q.

(129) Cunningham, A. J.; Feng, X.; Zhang, H.; Banquy, X.; Chain, J. L.; Zhu, X.-X. Thermoresponsive Properties of Star-Shaped Amphiphilic Block Copolymers with a Cholic Acid Core and Functional Amine Groups. *Mater. Today Commun.* **2021**, *29*, 102816. https://doi.org/10.1016/J.MTCOMM.2021.102816.

(130) Maitra, U.; Mukhopadhyay, S.; Sarkar, A.; Rao, P.; Indi, S. S. Hydrophobic Pockets in a Nonpolymeric Aqueous Gel: Observation of Such a Gelation Process by Color Change. *Angew. Chemie* **2001**, *113* (12), 2341–2343.

(131) Mukhopadhyay, S.; Maitra, U.; Ira; Krishnamoorthy, G.; Schmidt, J.; Talmon, Y. Structure and Dynamics of a Molecular Hydrogel Derived from a Tripodal Cholamide. *J. Am. Chem. Soc.* **2004**, *126* (48), 15905–15914. https://doi.org/10.1021/JA046788T.

(132) Zhao, Y. Spacer-Dependent Folding and Aggregation of Oligocholates in SDS Micelles. *J. Org. Chem.* **2009**, *74* (19), 7470–7480. https://doi.org/10.1021/JO901651H/SUPPL_FILE/JO901651H_SI_001.PDF.

(133) Zhao, Y. Conformation of Oligocholate Foldamers with 4-Aminobutyroyl Spacers. *J. Org. Chem.* **2009**, *74* (2), 834–843. https://doi.org/10.1021/JO802201B/SUPPL_FILE/JO802201B_SI_001.PDF.

(134) Zhao, Y.; Zhong, Z. Oligomeric Cholates: Amphiphilic Foldamers with Nanometer-Sized Hydrophilic Cavities. *J. Am. Chem. Soc.* **2005**, *127* (50), 17894–17901. https://doi.org/10.1021/JA056151P/SUPPL_FILE/JA056151PSI20051026_045259.PDF.

(135) Zhao, Y.; Zhong, Z. Tuning the Sensitivity of a Foldamer-Based Mercury Sensor by Its Folding Energy. *J. Am. Chem. Soc.* **2006**, *128* (31), 9988–9989. https://doi.org/10.1021/JA062001I/SUPPL_FILE/JA062001ISI20060518_014623.PDF.

(136) Gyimesi, J.; Barcza, L. Dimerization: First Step for Micelle Preorganization of Bile Salts. *J. Incl. Phenom. Mol. Recognit. Chem. 1993 152* **1993**, *15* (2), 153–158. https://doi.org/10.1007/BF00710224.

(137) Gouin, S.; Zhu, X. X. Fluorescence and NMR Studies of the Effect of a Bile Acid Dimer on the Micellization of Bile Salts. *Langmuir* **1998**, *14* (15), 4025–4029. https://doi.org/10.1021/LA971155W.

(138) Egelhaaf, S. U.; Schurtenberger, P. Shape Transformations in the Lecithin-Bile Salt System: From Cylinders to Vesicles. *J. Phys. Chem.* **1994**, *98* (34), 8560–8573.

(139) Zhang, M.; Ma, Z.; Wang, K.; Zhu, X. X. CO 2 Sequestration by Bile Salt Aqueous Solutions and Formation of Supramolecular Hydrogels. *ACS Sustain. Chem. Eng.* **2019**, *7* (4), 3949–3955. https://doi.org/10.1021/ACSSUSCHEMENG.8B05112/SUPPL_FILE/SC8B05112_SI_001.PDF.

(140) Zhang, M.; Fives, C.; Waldron, K. C.; Zhu, X. X. Self-Assembly of a Bile Acid Dimer in Aqueous Solutions: From Nanofibers to Nematic Hydrogels. *Langmuir* **2017**, *33* (4), 1084–1089. https://doi.org/10.1021/acs.langmuir.6b04033.

(141) Li, J.-L.; Liu, X.-Y. Architecture of Supramolecular Soft Functional Materials: From Understanding to Micro-/Nanoscale Engineering. *Adv. Funct. Mater.* **2010**, *20* (19), 3196–3216. https://doi.org/10.1002/ADFM.201000744.

(142) Lee, E. C. Y.; Steeno, G.; Wassermann, A. M.; Zhang, L.; Shah, F.; Price, D. A. Amine Promiscuity and Toxicology Analysis. *Bioorg. Med. Chem. Lett.* **2017**, *27* (3), 653–657. https://doi.org/10.1016/J.BMCL.2016.11.085.

(143) Du, X.; Zhou, J.; Xu, B. Supramolecular Hydrogels Made of Basic Biological Building Blocks. *Chem. – An Asian J.* **2014**, *9* (6), 1446–1472. https://doi.org/10.1002/ASIA.201301693.

(144) Ye, E.; Chee, P. L.; Prasad, A.; Fang, X.; Owh, C.; Yeo, V. J. J.; Loh, X. J. Supramolecular Soft Biomaterials for Biomedical Applications. **2015**, 107–125. https://doi.org/10.1007/978-981-287-152-7_5.

(145) Ryan, D. M.; Nilsson, B. L. Self-Assembled Amino Acids and Dipeptides as Noncovalent Hydrogels for Tissue Engineering. *Polym. Chem.* **2011**, *3* (1), 18–33. https://doi.org/10.1039/C1PY00335F.

(146) Wang, H.; Yang, Z. Short- Peptide -Based Molecular Hydrogels: Novel Gelation Strategies and Applications for Tissue Engineering and Drug Delivery. *Nanoscale* **2012**, *4* (17), 5259–5267. https://doi.org/10.1039/C2NR31149F.

(147) Friggeri, A.; Feringa, B. L.; Van Esch, J. Entrapment and Release of Quinoline Derivatives Using a Hydrogel of a Low Molecular Weight Gelator. *J. Control. Release* **2004**, *97* (2), 241–248. https://doi.org/10.1016/J.JCONREL.2004.03.012.

(148) Skilling, K. J.; Citossi, F.; Bradshaw, T. D.; Ashford, M.; Kellam, B.; Marlow, M. Insights into Low Molecular Mass Organic Gelators: A Focus on Drug Delivery and Tissue Engineering Applications. *Soft Matter* **2013**, *10* (2), 237–256. https://doi.org/10.1039/C3SM52244J.

(149) Zhao, X.; Huebsch, N.; Mooney, D. J.; Suo, Z. Stress-Relaxation Behavior in Gels with Ionic and Covalent Crosslinks. *J. Appl. Phys.* **2010**, *107* (6), 063509. https://doi.org/10.1063/1.3343265.

(150) Hashemnejad, S. M.; Kundu, S. Probing Gelation and Rheological Behavior of a Self-Assembled Molecular Gel. *Langmuir* **2017**, *33* (31), 7769–7779. https://doi.org/10.1021/acs.langmuir.7b01531.

(151) Li, J.; Suo, Z.; Vlassak, J. J. Stiff, Strong, and Tough Hydrogels with Good Chemical Stability. *J. Mater. Chem. B* **2014**, *2* (39), 6708–6713. https://doi.org/10.1039/C4TB01194E.

(152) Ito, K. Novel Cross-Linking Concept of Polymer Network: Synthesis, Structure, and Properties of Slide-Ring Gels with Freely Movable Junctions. *Polym. J. 2007 396* **2007**, *39* (6), 489–499. https://doi.org/10.1295/polymj.pj2006239.

(153) Rezaee, M.; Oskuee, R. K.; Nassirli, H.; Malaekeh-Nikouei, B. Progress in the Development of Lipopolyplexes as Efficient Non-Viral Gene Delivery Systems. *J. Control. Release* **2016**, *236*, 1–14. https://doi.org/10.1016/J.JCONREL.2016.06.023.

(154) Wytrwal, M.; Pichon, C. Polyallylamine Derivatives: Novel Nontoxic Transfection Agents. *Methods Mol. Biol.* **2016**, *1445*, 159–174. https://doi.org/10.1007/978-1-4939-3718-9_10.

(155) Kim, Y. H.; Baek, N. S.; Han, Y. H.; Chung, M. A.; Jung, S. D. Enhancement of Neuronal Cell Adhesion by Covalent Binding of Poly-d-Lysine. *J. Neurosci. Methods* **2011**, *202* (1), 38–44. https://doi.org/10.1016/J.JNEUMETH.2011.08.036.

(156) Laurent, N.; Wattiaux-De Coninck, S.; Mihaylova, E.; Leontieva, E.; Warnier-Pirotte, M. T.; Wattiaux, R.; Jadot, M. Uptake by Rat Liver and Intracellular Fate of Plasmid DNA Complexed with Poly-l-Lysine or Poly-d-Lysine. *FEBS Lett.* **1999**, *443* (1), 61–65. https://doi.org/10.1016/S0014-5793(98)01677-9.

(157) Kwoh, D. Y.; Coffin, C. C.; Lollo, C. P.; Jovenal, J.; Banaszczyk, M. G.; Mullen, P.; Phillips, A.; Amini, A.; Fabrycki, J.; Bartholomew, R. M.; Brostoff, S. W.; Carlo, D. J. Stabilization of Poly-l-Lysine/DNA Polyplexes for in Vivo Gene Delivery to the Liver. *Biochim. Biophys. Acta - Gene Struct. Expr.* **1999**, *1444* (2), 171–190. https://doi.org/10.1016/S0167-4781(98)00274-7.

(158) Vermeersch, H.; Remon, J. P. Immunogenicity of Poly-D-Lysine, a Potential Polymeric Drug Carrier. *J. Control. Release* **1994**, *32* (3), 225–229. https://doi.org/10.1016/0168-3659(94)90232-1.

(159) 7.1: Structure of Water - Chemistry LibreTexts https://chem.libretexts.org/Courses/Chippewa_Valley_Technical_College/CVTC_Basic_Chemistry/07%3A_Solutions/7.01%3A_Structure_of_Water (accessed Oct 19, 2021).

(160) Jun-Ying Xiong; Xiang-Yang Liu, *; Jing-Liang Li, and; Vallon, M. W. Architecture of Macromolecular Network of Soft Functional Materials: From Structure to Function. *J. Phys. Chem. B* **2007**, *111* (20), 5558–5563. https://doi.org/10.1021/JP070600L.

(161) Reeder, S. B. Emergence of 3D MR Elastography–Based Quantitative Markers for Diffuse Liver Disease. *https://doi.org/10.1148/radiol.2021211444* **2021**, *301* (1), 163–165. https://doi.org/10.1148/RADIOL.2021211444.

(162) Kulkarni, V. S.; Shaw, C. Rheological Studies. *Essent. Chem. Formul. Semisolid Liq. Dosages* **2016**, 145–182. https://doi.org/10.1016/B978-0-12-801024-2.00009-1.

(163) Wilson, D. I. What Is Rheology? *Eye 2018 322* **2017**, *32* (2), 179–183. https://doi.org/10.1038/eye.2017.267.

(164) Nebot, V. J.; Smith, D. K. *CHAPTER 2. Techniques for the Characterisation of Molecular Gels*; 2013. https://doi.org/10.1039/9781849737371-00030.

(165) Samateh, M.; Pottackal, N.; Manafirasi, S.; Vidyasagar, A.; Maldarelli, C.; John, G. Unravelling the Secret of Seed-Based Gels in Water: The Nanoscale 3D Network Formation. *Sci. Reports 2018 81* **2018**, *8* (1), 1–8. https://doi.org/10.1038/s41598-018-25691-3.

(166) Tachibana, T.; Kambara, H. Enantiomorphism in the Helical Aggregate of Lithium 12-Hydroxystearate. *J. Am. Chem. Soc.* **1965**, *87* (13), 3015–3016. https://doi.org/10.1021/ja01091a046.

(167) Hirst, A. R.; Miravet, J. F.; Escuder, B.; Noirez, L.; Castelletto, V.; Hamley, I. W.; Smith, D. K. Self-Assembly of Two-Component Gels: Stoichiometric Control and Component Selection. *Chem. - A Eur. J.* **2009**, *15* (2), 372–379. https://doi.org/10.1002/chem.200801475.

(168) Schnablegger, H.; Singh, Y. The SAXS Guide: Getting Acquainted with the Principles. *Anton Paar*. A-8054 Graz, Austria: Austria: Anton Paar GmbH 2013, p 124.